Synthesis and Characterization of New Conjugated Polymers for Application in Solar Cells

Mohd Sani Bin Sarjadi

A thesis submitted to
The University of Sheffield
as partial fulfillment for the degree of Doctor of Philosophy

The University Of Sheffield.

October 2014

Declaration

This thesis is submitted for the degree of doctorate of philosophy (PhD) at the University of Sheffield, having been submitted for no other degree. It records the research carried out the University of Sheffield from November 2009 to October 2014. It is entirely my original work, unless where referenced.

Signed:.....  .....

Date:.....**15 OCTOBER 2014**.....

Abstract

Plastic photovoltaic devices based on solution processed conjugated polymers have attracted much attention as potential candidates for the next generation of solar cells. Polymer solar cells based on blends of conjugated polymer donors and molecular acceptors such as PCBM (often referred to as bulk heterojunction solar cells) are attracting a great deal of interest. These systems have potential technological value due to their ease of fabrication and their relatively low production costs. This enabled devices to be produced that have solar power conversion efficiencies approaching 9%. The purpose of this research project is to develop new and more efficient materials for application in this area. A new class of alternating copolymers comprising carbazole units and thieno-thiophene units for application in the area of bulk heterojunction solar cells is presented in this contribution. The polymers were prepared using Suzuki coupling methods. Three main classes of such polymers were prepared. The first class of polymers **P1 - P3** consisted of alternating co-polymers comprising thienothiophene repeat units and either 2,7-linked 9-alkyl carbazole units **P1**, or 2,7-linked-9-alkyl carbazole repeat units with fluorine substituents at their 3,6-positions **P2**, or 2,7-linked-9,9-dioctylfluorene **P3**. The second class of materials consisted of alternating copolymers comprising benzothiadiazole repeat units and 2,7-linked carbazole repeat units flanked by thienothiophene repeat unit with or without fluorine-substituents at the 3,6-positions on the carbazole repeat units (polymers **P4 - P7)**. The third class of materials consisted of alternating donor acceptor conjugated polymers which are similar to the second class of materials but have octyloxy-substituents on the benzothiadiazole repeat units **P8 - P10**. The presence of octyloxy-substituents units on the benzothiadiazole electron accepting units along the polymer chains reduce the intramolecular charge transfer and provides materials with wider band gaps than those of the second class of materials prepared and hence have lower electronic delocalisation. The structures of the polymers have been confirmed by NMR spectroscopy, FT-IR and elemental analysis, and their weight-average molecular weights were estimated using gel permeation chromatography (GPC). The optical and electronic properties of the polymers were investigated by UV-Vis absorption spectroscopy. Cyclic voltammetry measurements were used to investigate their electrochemical properties. The thermal properties of the materials were investigated by thermal gravimetric analysis (TGA) and differential scanning calorimetry (DSC) measurements.

Acknowledgments

First of all I must thank my parents, my wife Siti Normala Marimin and kids; Balqis Humairah and Bilal Haris for their continuous support, prayers, understanding, patience and encouragement not only during my time as a student, but throughout my entire life, this is for you.

I am deeply grateful to my supervisor Dr. Ahmed Iraqi for his guidance throughout my PhD, without his advice and constant support fulfillment of this degree would not have been possible.

I would like to acknowledge all the members of the Iraqi group past and present especially Dr. Hunan Yi, Dr. Harismah Kun, Dr. Noriko, Dr. Abdulaziz, Dr. Abdulqader, Dr. Reedy, Dr. Ryan Rees, Dr. Mohammed, Solyman Al Fifi, Abdulraheem Almalki, Luke Cartwright, Suguru Nakano, Ary R Murad, Ahmed Al-Azzawi and Sulaiman A. Al-Isaee for their invaluable help and time whenever needed.

I am grateful to all my colleagues on F-floor Dr. Paul Bonner, Dr. Adam Ellis, Dr. Georgia Mann, Azrul Zabidi, Kuljit, and Meshari for contributing to a relaxed working environment which often alleviated the inevitable stress associated with being a postgraduate.

I would also like to thank all the admin, secretarial and accounting staff Ms. Elaine Fisher, Ms. Denise Richards, Ms. Louise Brown-Leng, Ms. Rachel Myers, Ms. Elaine Frary for their kind support, Dr. Brian F. Taylor and Ms. Susan Bradshaw for NMR spectra measurements, Ms. Jennifer Louth and Ms. Melanie Hannah for elemental analysis, Mr. Simon Thorpe and Ms. Sharon Spey for mass spectroscopy analysis, Mr. Robert Hanson for GPC, TGA analysia, DSC and spectroscopy/chromatography analysis, Mr. Peter Farran, Mr. Nick Smith, Mr. Daniel Jackson and Mr. Keith Owen from chemical stores and Mr. Richard Wilkinson for the health and safety advice.

Finally, I would like to acknowledge the financial support of the University of Malaysia Sabah and Ministry of Education Malaysia for their financial support over the period of my research.

TABLE OF CONTENTS

TABLE OF FIGURES

TABLE OF TABLES

TABLE OF SCHEMES

Glossary of Abbreviations and Terms

A

A	Electron Acceptor
Acetone-d_6	Deuterated acetone
Alq_3	Tris(8-hydroxyquinoline)aluminium; an electron-transfer
AM 1.5	Air Mass
ATR	Attenuated total reflectance

B

bm	Broad multiple (NMR)
br	Broad (NMR)
t-BuOH	*tert*-Butanol
t-BuLi	*tert*-Butyllithium

C

CB	Conduction band
$CDCl_3$-d_1	Deuterated Chloroform
$CHCl_3$	Chloroform
$C_2D_2Cl_4$	Deuterated 1,1,2,2-Tetrachlorethane
CV	Cyclic voltammetry

D

D	Electron Donor
d	Doublet (NMR)
DCM	Dichloromethane
DMF	N,N-dimethylformamide
DMSO	Dimethyl sulfoxide
DP	Degree of polymerization
DSC	Differencial Scanning Calorimetry

E

E_A	Electron affinity
E_g	Band gap
E_{pa}	Potential of peak anodic current (from CV)
E_{pc}	Potential of peak cathodic current (from CV)
ETL	Electron Transporting Layer
EtOAc	Ethyl Acetate
EtOH	Etahnol
Et_2O	Diethyl ether
eV	Electron volt
EQE	External Quantum Efficiency

F

F_c	Ferrocene
FET	Field-Effect Transistor
FT-IR	Fourier Transform Infra-Red spectroscopy

G

GPC	Gel Permeation Chromatography

H

HOMO	Highest Occupied Molecular Orbital
HPLC	High Performance Liquid Chromatography
HTL	Hole Transporting Layer
Hz	Hertz

I

I_p	Ionisation potential
IR	Infra-Red spectroscopy
ITO	Indium Tin Oxide
IPCE	Incident Photon to Current Efficiency
IQE	Internal Quantum Efficiency
I_{sc}	Short Circuit Voltage

K

KOAc	Potassium acetate

L

LED	Light-Emitting Diode
LUMO	Lowest Unoccupied Molecular Orbital
λ	Wavelength (nm)
LEOFETs	light-emitting organic field effect transistors

M

m	Multiplet (NMR)
M_n	Number average molecular weight
M_w	Weight average molecular weight
MALDI-TOF MS	Matrix Assisted Laser Desorption Ionization-Time of Flight Mass Spectroscopy
M. p.	Melting point
MO	Molecular Orbital Theory

N

NMR	Nuclear Magnetic Resonance
NBS	N-Bromosuccinide

O

OFETs	Organic field-effect transistors
OLED	Organic light emitting diode
OLETs	Organic light-emitting transistors
OSC	Organic Solar Cell
OPV	Organic Photovoltaic

P

P(*o*-tol)$_3$	Tri-*ortho*-tolylphosphine
P_3AT	Poly(3-alkylthiophene)
P_3HS	Poly(3-hexylselenophene)
P_3HT	Poly(3-hexylthiophene)

PA	Polyacetylene
PCBM	1-(3-Methoxycarbonyl)propyl-1-phenyl [6,6]-methanofullerene
PCDTBT	Poly[N-9-heptadecanyl-2,7-carbazole-alt-5,5-(4'-7'-di-2-thienyl-2',1',3'-benzothiadiazole]
PCE	Power Conversion Efficiency
PD	Polydispersity: Pd = M_w/M_n
Pd(dppf)Cl_2	[1,1'-Bis(diphenylphosphino)ferrocene]dichloropalladium (II)
Pd(OAc)$_2$	Palladium (II) acetate
$Pd_2(dba)_3$	Tris(dibenzylidene acetone) dipalladium (0)
PDI	Perylene tetracarboxylicdiimide
PDPyDP	2,5-Bis[2-(4-tert-butylphenyl)-1,3,4-oxadiazol-5-yl]pyridine
PEDOT:PSS	Poly(3,4-ethylenedioxythiophene):Poly(styrenesulfonate)
PL	Photoluminescence
PLEDs	Polymer light emitting diodes
PPh_3	Triphenylphosphine
PPP	Poly(*para*-phenylene)
PPV	Poly(*para*-phenylenevinylene)
PPy	Polypyrrole
PT	Poly(thiophene)
PV	Photovoltaic
PVK	Poly(*N*-vinylcarbazole)

Q

QE	Quantum Efficiency

R

R_f	Retardation factor
RT	Retention time
ROMP	Ring Opening Metathesis Polymerisation

S

s	Singlet (NMR)
I_{sc}	Short Circuit Voltage
STC	Standard Test Condition

T

t	Triplet (NMR)
T_g	Polymer glass-transition temperature (from DSC)
TGA	Thermo-gravimetric analysis
THF	Tetrahydrofuran
TLC	Thin layer chromatography
TMS	Tetramethylsilane
TPD	*N,N'*-diphenyl-*N,N'*-bis(3-methylphenyl)-1,1'-biphenyl-4,4'-diamine

U

UV-Vis	Ultra Violet-visible spectroscopy

V

V_{oc}	Open-Circuit Voltage
V	Volt

CHAPTER 1 - INTRODUCTION

1.1 Conjugated Polymers

Polymer-based solar cells provide potential advantages over mainstream inorganic-based solar cells such as significantly reduced material/fabrication costs, flexible substrates, and lightweight of finished solar cells. [1-6] Conjugated polymers are organic macromolecules which consist of a backbone chain of alternating double- and single carbon-carbon bonds, depending upon the monomer units used to build the polymer. Normally, the conjugated polymer can be arbitrarily divided into three constituting components - the conjugated backbone, the side chains, and the substituents.[5, 7-11] The properties of these polymers depend on the monomer units used.[12, 13] **Figure 1.1** includes the structure of polyacetylene, which is the simplest, commonly studied conjugated polymer and some of the different classes of conjugated polymers.

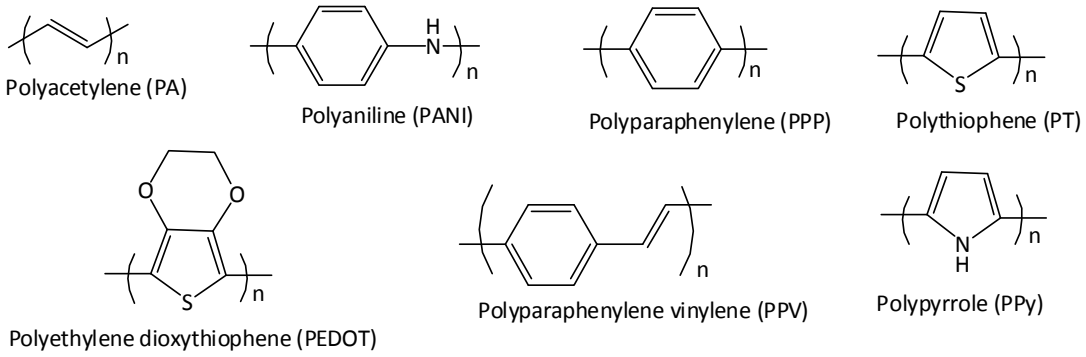

Figure 1.1: Generic structures of some important conjugated polymers.

All conjugated polymers have a backbone of atoms with overlapping sp^2 hybrid orbitals forming σ-bonds.[14] The remaining out-of-plane p_z-orbitals on the carbon atoms overlap with adjoining p_z orbitals to give π-bonds.[15-17] Due to the fact that the p_z-orbitals of the carbon atoms which form the π-orbitals of the alternating double-and single-bonds mesomerise more or less, the single and double bonds become similar, in length as the result of electronic delocalisation. [10, 17-19] While electrons on the σ-bonds are relatively localised the remaining electrons on p_z orbitals (π-bonds) are delocalised along the entire molecule.[11, 18-20]

1.2 Properties of Conjugated Polymers

In the interest of achieving high efficiency in polymer solar cells, [21, 22] the demands at the molecular level is to prepare p-type conjugated polymers that (1) simultaneously possess better conductivity and high hole mobility for efficient charge transport; (2) produce low band gap for a strong and broad absorption spectrum and capture more solar photons; (3) show sufficient solubility to guarantee solution processability and miscibility with an n-type material and (4) are stable and reliable to the green environment.[23-26]

1.2.1 Conductivity of Conjugated Polymers

Conjugated polymers are characterised by a molecular structure that features alternating single and multiple bonds.[12, 20, 27-31] The electronic and physico-chemical characteristics of conjugated macromolecules are not only governed by the nature of the polymer backbone, but also by the intermolecular interactions.[15, 32-35] **Table 1.1** shown the conductivity of several common conjugated polymers in their oxidised states.

The electrical conductivity of conjugated polymers varies widely depending on several factors such as the doping level and synthesis conditions.[36-42] Based on the **Figure 1.2** materials can be classified into three types according to their conducting properties at room temperature: conductors, semiconductors and insulators.[43-46]

Based on these factors, conjugated polymers can be classified into one of the abovementioned types.[9, 20, 21, 47] Possessing different levels of conductivities which expands the scope of their applications.[48-50]

Table 1.1: Conductivity of some conjugated polymers in their oxidized (doped) state.

Structural Formula	Conductive Polymer	Conductivity (S/cm)	Reference
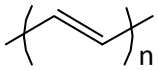	Polyacetylene	10^5	51, 52
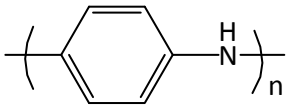	Polyaniline	10	53
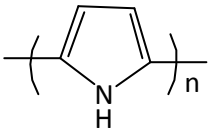	Polypyrrole	600	20, 53-55
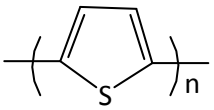	Polythiophene	200	43, 56-60
	Polyparaphenylene	250	61-64
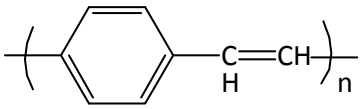	Polyphenylene vinylene	1	65, 66
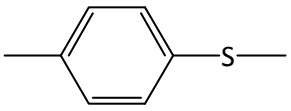	Polyparaphenylene sulphide	20	66-68
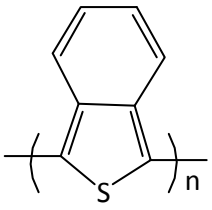	Poly-iso-thanapthene	50	10, 51, 53, 69

Conjugated polymers have delocalised π-electron bonding along the polymer backbone which enables them to transport charge along it.[6, 70-72] One of the most important properties of conjugated polymers is the ability to adjust their conductivity and band gap through the process of doping. Possessing different levels of conductivity expands the scope of applications.[12, 73-75]

However, the structure is not fully delocalised but has an alternating structure of double and single bonds of different lengths. This has the effect of raising the energy of the lowest unoccupied molecular orbital (LUMO) and lowering the energy of the highest occupied molecular orbital (HOMO) to give the band gap E_g.[22, 61, 70, 76-78]

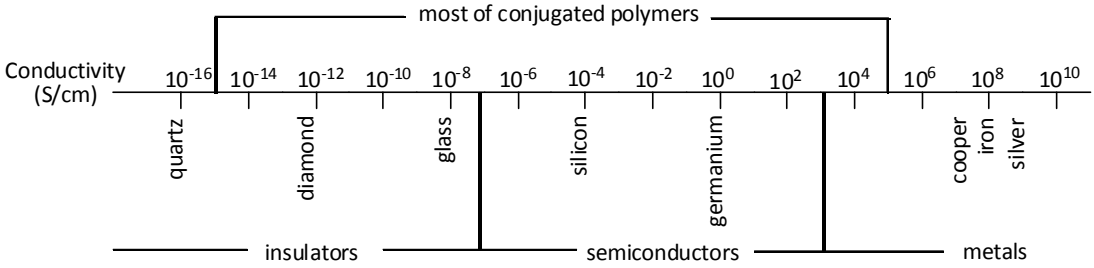

Figure 1.2: The different electrical conductivity in one over Ohm-meter of insulators, semiconductors and metals. [69, 79, 80]

This is a consequence of Peierls transition instability,[46, 81-83] leading to two degenerate states. These states can be degenerate in the case of polyacetylene or non-degenerate in the case of aromatic polymers such as poly(*para*-phenylene) (PPP) or poly*(para*-phenylene vinylene*)* (PPV) [61, 62, 65, 67, 84] as shown in **Figure 1.3**. Therefore, these materials are classed as semiconductors and the band gap is a consequence of this alternating state.

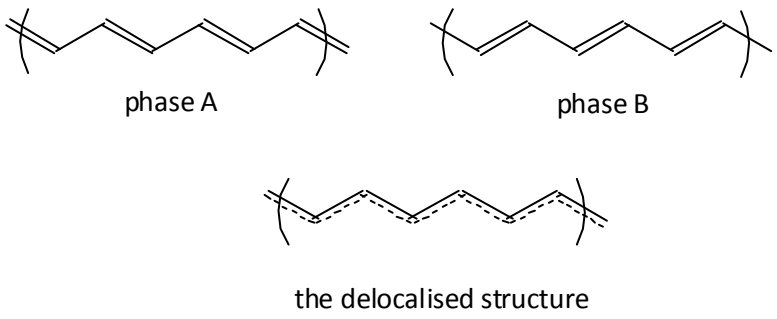

Figure 1.3: Two degenerate ground states of *trans* polyacetylene and its delocalised structure.

In general, inorganic semiconductors are doped in order to increase their conductivity. This is illustrated in **Figure 1.4**. There are two types of doping: n-type and p-type. In n-type doping, the extra electrons provided by the dopant occupy donor levels with lower energy than the lowest unoccupied molecular orbitals (LUMO). Thus in p- type doping, the valence band is no longer completely filled and an acceptor band is formed which enable promotion of electrons.[58, 85]

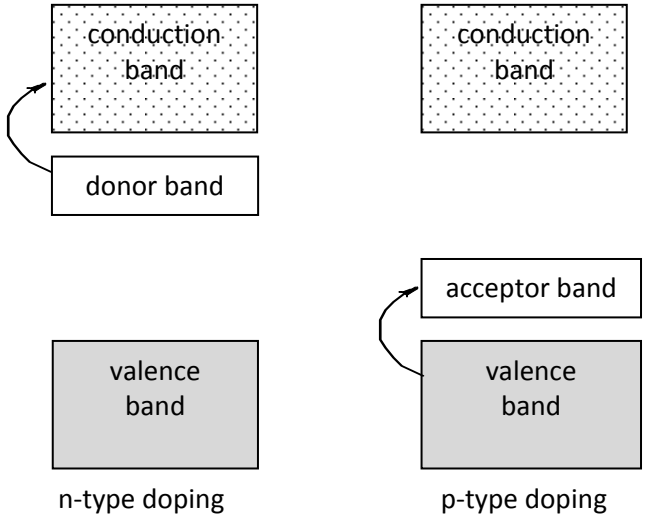

Figure 1.4: Two types (p,n) of doping in inorganic semiconductors.

Conjugated polymers themselves are not conducting in their menthol form, but require doping. Doping of conjugated polymers, either by oxidation or reduction, generates a radical cation or anion known as a polaron.[61, 86-90] Oxidation leads to the promotion of a single electron to a new energy level between the valence and conduction band. **Scheme 1.1** shows the oxidative doping of polyacetylene in order to generate polarons and solitons.[8, 91-93]

Reduction creates a negative polaron with one paired and one unpaired electron at a higher energy.[94, 95] With further oxidation a second radical combines with the first to give a bipolaron which is energetically more favourable than the formation of a second polaron.

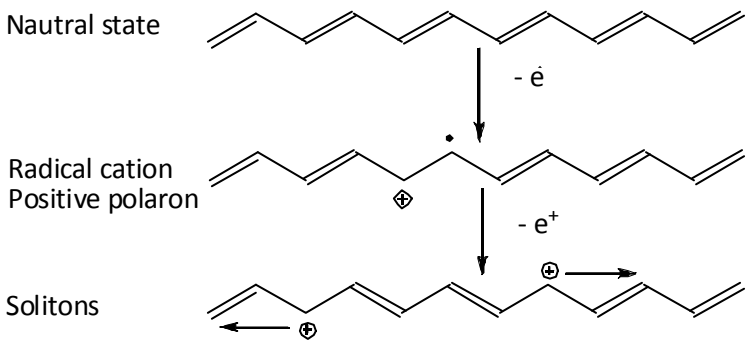

Scheme 1.1: Oxidative doping of polyacetylene to generate polarons and solitons.

Subsequently, conjugated polymers require doping as they are not conducting in their neutral form. Doping of conjugated polymers, either by oxidation or reduction, generates a radical cation or anion known as a polaron.[61, 86-90] Oxidation leads to the promotion of a single electron to a new energy level between the valence and conduction band. **Scheme 1.1** shows the oxidative doping of polyacetylene in order to generate polarons and solitons.

Reduction creates a negative polaron with one paired and one unpaired electron at a higher energy.[94, 95] With further oxidation, a second radical combines with the former to give a bipolaron, which is energetically more favourable than the formation of a second polaron.

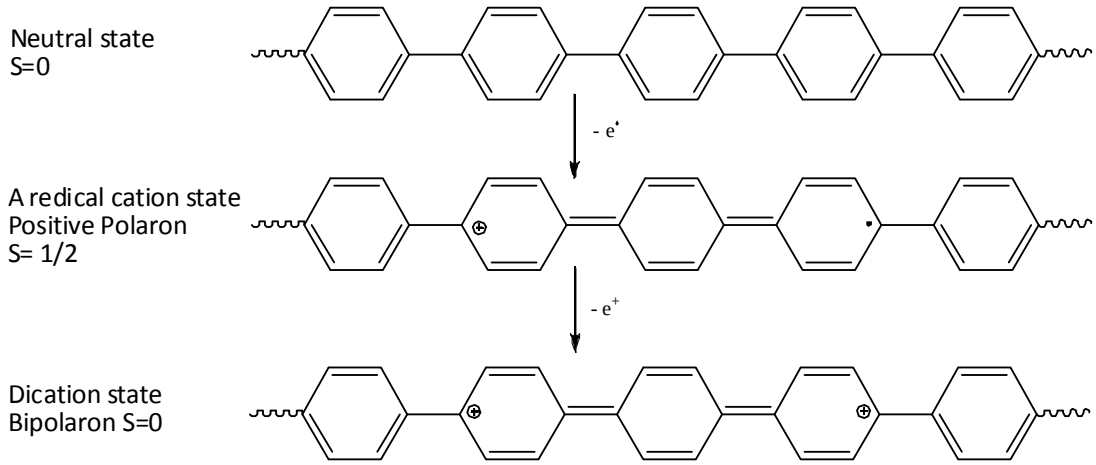

Scheme 1.2: The scheme of oxidative doping of polyparaphenylene to generate polarons and bipolarons.

The polymer is then transformed from a benzenoid structure to the lower energy quinoid structure, resulting in new energy levels, otherwise known as a polaron, and bipolaron by further oxidation. [86] The polaron and bipolaron states acquire new energy bands between the valence band and the conduction band as shown in **Figure 1.5**.

The doping of a conjugated polymer is also possible *via* a potential difference being applied across two electrodes.[58] The anode removes electrons (also known as injecting holes) whilst the cathode injects electrons, creating positive and negative polarons respectively. These then travel in opposite directions along the polymer backbones, conducting the charge.

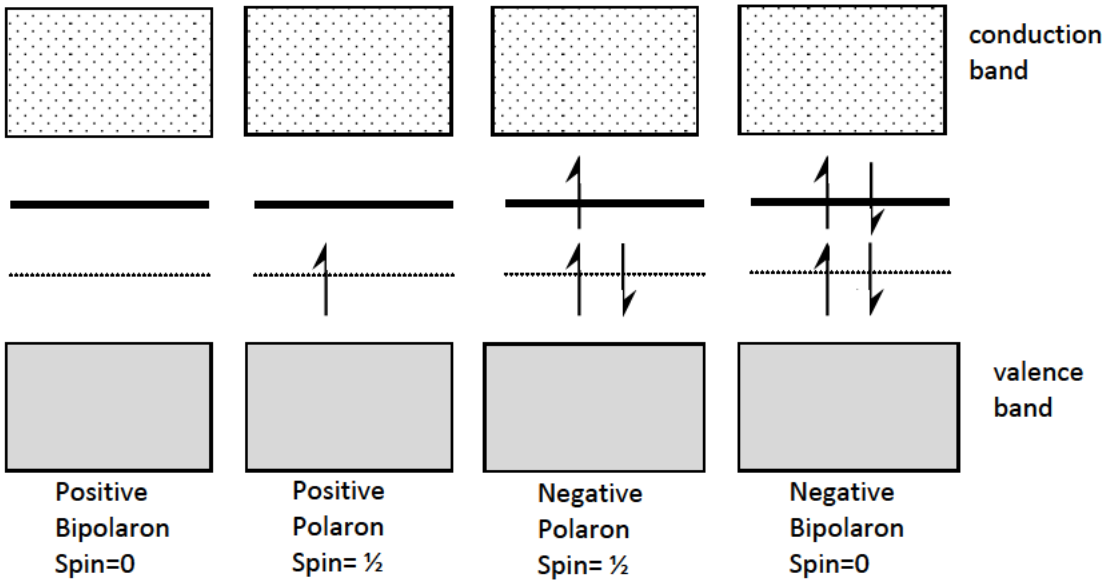

Figure 1.5: Energy level diagram of bipolarons and polarons.

1.2.2 Polymers band gap energy

Electrical conductivity is a direct effect of delocalized chemical bonding. The absence of sp^3 hybridized carbon atoms leads to a situation where the overlap of p-orbitals on successive carbon atoms enables the delocalization of π-electrons along the polymer backbone.[69] The large number of atomic orbitals in the macromolecules translates into a large number of molecular orbitals, which form a energy bands.[97]

These energy bands are a continuum, as represented in metals. It is due to the high density of electronic states with electrons of relatively low binding energy. *Free electrons* can easily redistribute and move easily from atom to atom under an applied electric field, thus rendering the material conducting electrically.[96]

Hückel's theory predicts that in conjugated macromolecules, π-electrons are delocalised in similar fashion over the entire chain. Based on that, one would expect that the electronic properties of a polymer material composed of sufficiently long conjugated chains are also described well by a continuous energy band.

Thus, the electronic properties of conjugated polymers in their neutral state are usually described by a filled valence band (π-band, bonding) formed by the highest occupied molecular orbitals (HOMOs) and an empty conduction band (π*-band, antibonding) formed by the lowest unoccupied molecular orbitals (LUMOs).[7] Conjugated polymers are typically *semi*conductors in their neutral, *undoped* state. The energy difference between the highest occupied and the lowest unoccupied bands is referred to as the band gap (E_g), which is usually not near zero.

The magnitude of the E_g will depend on the molecular structure and arrangement of the polymer's repeat unit and can be tailored via modification of the latter.[7, 15] **Figure 1.6** shows the basic concept of the polymer band gap. In a simple term, E_g of a polymer is defined as the total energy difference between the HOMO and the LUMO, and is usually stated in electronvolt (eV) units.

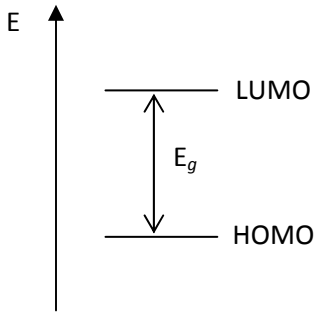

Figure 1.6: Definition of band gap, E_g.

1.2.2.1 Preparation of low band gap polymers

1. Photon energies and current limits

At the core of the Sun, 5 million tons of energy is released every second in the form of γ-rays, which is equivalent to 3.86 x 10^{26} J.[81, 98] The γ-rays make their way to the surface of the sun by absorption and re-emission at lower and lower temperature until they reach the surface, mainly as visible light we observe on earth.[99]

From this point of view, it is of great interest to harvest photons at the longer wavelengths. It should be borne in mind that the energy of the charge carriers generated from longer wavelengths is lower and this limits the voltage difference that the device can produce. Thus, there is an optimum band gap, which is currently subject to discussion for excitonic devices.[44, 65, 100]

Poly(3-hexylthiophene) has a band gap of 650 nm (1.9 eV) and thus only has the possibility to harvest up to 22.4 % of the available photons from sunlight giving a maximum theoretical current density of 14.3 mA cm^{-2}.[101] However, this may increase if the polymer is applied in a bulk heterojunction device, due to the absorption of the acceptor, i.e. phenyl-C_{61}-butyric acid methyl ester (PCBM).[102]

2. Open circuit voltage

In the discussion above, we have shown that lowering the band gap of conjugated polymers allows for absorption of more photons resulting in higher currents that can lead to higher power conversion efficiencies from solar cell devices.[103] The increase in power conversion efficiency is not granted by the current density alone; a high open circuit voltage (V_{OC}) is also needed.[25, 104, 105]. The V_{OC} is defined in the two models as the difference between the HOMO of the donor and the LUMO of the acceptor as shown in **Figure 1.7**.

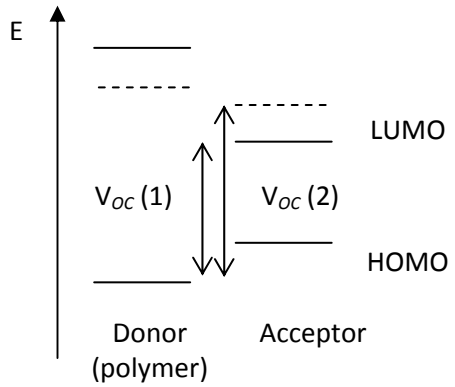

Figure 1.7: The diagram of different HOMO and LUMO in bulk heterojunction device

To increase the V_{OC} from V_{OC} *(1)* to V_{OC} *(2)* and thus the efficiency of the device, we must prepare new low band gap polymer materials, which absorb light with longer wavelengths resulting in more absorption of the photons in the solar spectrum.[36, 106] One of the typical methods to obtain better V_{OC} is by increasing the difference between the HOMO level of the donor and the LUMO of the acceptor.[107]

3. Ideal energy levels

In order to achieve better efficiencies in solar cells an efficient electron transfer from the donor to the acceptor is required which in turn requires an adjustment of the energy levels of these two components in the active layer. As an example, the charge movement is scaled from the donor polymer to the fullerene acceptor. The value of the energy difference α, from the polymer's LUMO to the PCBM's LUMO can be seen clearly in **Figure 1.8.** There is a range of the minimum common value for the V*oc* and it is indicated as energy, β.

In order to gain an efficient charge separation, the range levels of α and β have to be taken into consideration. Large values of V_{OC} could be achieved if the polymer has a large band gap (around 2 eV). Furthermore, the range of the HOMO level of the donor polymer can be tailored when fulfilling the criteria between α, β and ΔE as shown in **Figure 1.8.** The relationship between α, β, ΔE and E_g is given below.

$$\Delta E = E_g - \alpha - \beta.$$

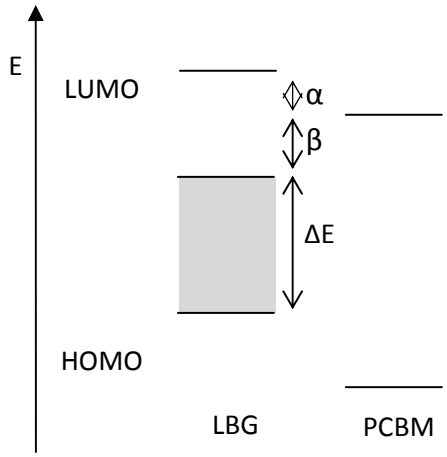

Figure 1.8: Diagram of the bulk heterojunctions with conjugated and PCBM.

4. Low band gap polymer design

There are several factors that influence the band gap of a conjugated polymer material. Among these are intra-chain charge transfer, bond-length alternation, aromaticity, substituents effects, intermolecular interactions and π-conjugation length.[26, 56, 104, 110] The low band gap copolymers reported are often based on thiophene, but other electron-rich aromatic units such as pyrrole, are also found. [26, 36]

By mathematical simulation, it is shown that the electron affinity is higher around the acceptor units compared with the donor units in these types of copolymers. Planarity along the aromatic backbone results in a low band gap, due to a high degree of delocalisation of the π-electrons. In addition, the alternation between single and double bonds along the polymer chain has a tendency to increase the band gap. A reduction of the difference in bond length alternation is achieved by the alternation of donor and acceptor units along the conjugated polymer chain, thus lowering the band gaps.

Another aspect that should be focused upon during the preparation of low band gap conjugated polymers is the total number of single and double bonds in the materials whichhas a high tendency to produce a better band gap. [56, 110]

There are many scenarios affected caused by the non-similarity in the bond length alternation, including the reduction interaction. The presence of the donor and acceptor units on the conjugated polymer leads to the reduction and lowering of the band gaps.

Moreover, existing literature evidently mentions that in order to achieve polymers with low band gaps, the HOMO and LUMO levels must be close to each other as shown in **Figure 1.9.**

Consequently, the donor and the acceptor must have good electronic interactions in order to produce lower band gaps. The main interaction is achieved due to the efficient electron donation from the donor to the electron acceptor unit. Examples of electron withdrawing groups are thiadiazole, CN, NO_2, pyrazines and quinoxalines; all of them are proposed acceptors with better and lower energy levels. Thiophene or pyrrole are examples of electron donors and could increase the HOMO energy level.[36]

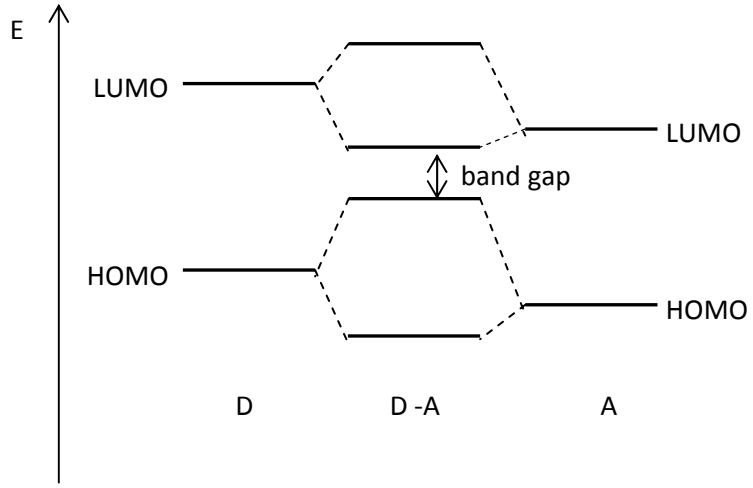

Figure 1.9: Orbital mixing containing alternating donor-acceptor units and the effective method to achieve low band gap.

1.2.3 Solubility of Conjugated Polymers

The band gaps of most conjugated polymers are such that they absorb light in the visible region of the spectrum. The emission color can be tuned to essentially any desired wavelength region by altering the chemical nature of either the polymer backbone or the side groups due to the alternating electron arrangement from the chemical nature.[65, 104]

Conjugated polymers can be used as novel materials in high performance optoelectronic devices such as plastic light-emitting diodes (LEDs) or photovoltaic cells.[100, 103, 111] These are great materials because they are easy to process and practically take less time to prepare.

One of the advantages of conjugated polymers is their rigid structure. However, due to their rigidity, the materials are insoluble in common organic solvents, but they can be converted into soluble polymers through functionalisation with flexible side chains, typically alkyl and/or alkoxy groups. **Figure 1.10** shows four groups of common conjugated polymers which are soluble in some organic solvents.[31, 61, 112, 113]

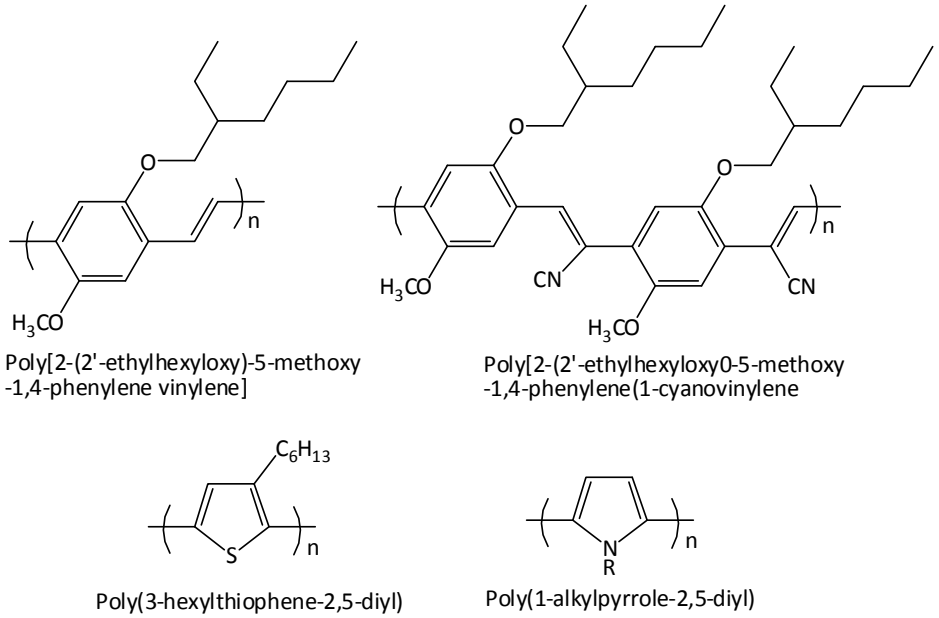

Figure 1.10: Conjugated polymers soluble in common organic solvents.

There are many procedures in order to change the electronic properties of conjugated materials. The nature and bulk of their substituents could alter the packing of the chains of the conjugated polymers films.[65, 114] It has been mentioned in literature that film morphology can be tailored by a few factors which include solvent and concentration effects, the different spin speeds in the deposition of films, and preparation of the films by using Langmuir–Blodgett techniques (layer-by-layer). [12, 31, 65]

Intramolecular charge transfer along the polymer backbone will introduce better carrier transport on the film and simultaneously produces low level reading of luminescence quantum efficiency, which signifies good internal interactions of the conjugated polymers aromatic chains.[115]. The mobility factor and a high value of electron carrier densities are very important aspect in order to produce better emissive excitons during the electrical injection.[116, 117] These will generate a high degree of internal interaction for the device which contains conjugated materials chains. In order to generate good luminescence efficiency, the interchain interaction must be controlled in a minimal value when the exciton is formed and the carrier is recombined. [27, 114]

1.2.4 Stability of Conjugated Polymers

There are two different types of stabilities, extrinsic stability and intrinsic stability, and a number of different factors, which determine the stability of conducting polymers in both types of stability.[61, 95, 118, 119] However, extrinsic stability is related to vulnerability of the polymer to external environmental agents such as oxygen, water vapour and peroxides.[120-122]

This is determined by the susceptibility of charged sites on the polymer chains to outbreak the free radicals, electrophiles and nucleophiles. In this case, the conducting polymer is extrinsically unstable and must be coated by a stable coating for protection.[123] Intrinsic stability is related to stable conductivity level for the polymer and the polymer susceptibility to degradation over time even in oxygen free and dry environment.[110]

This degradation occurs due to irreversible contact between the charge area on the conjugated materials chain and the adjacent neutral π-system of chain or the dopant counter ion, which makes an sp^3 carbon that subsequently breaks the conjugation and decreases the conductivity. Furthermore, intrinsic instability arises when the polymer loses its dopant due to a thermally driven mechanism, where the conformational changes in the backbone of the polymer causes unstable charge sites. This effect is found in alkyl-substituted polythiophenes.[56, 58]

1.3 Organic Photovoltaic Cells

Organic photovoltaic cell materials may be cost effective but they do still have low power conversion energies. [124] The distinct advantages of organic solar cells include economy in the processing on large areas, possible semi-transparency, mechanical flexibility, processability and light weight. [88, 97, 125, 126]

A power conversion efficiency of around 10 % is required in order for organic-based solar cells to be used commercially.[107, 120] The active layers in solar cells normally consists of blends of polymer donors and molecular acceptors in a bulk heterojunction environment, upon mixing conjugated polymers as a source of electrons and fullerenes as electron acceptors.[127]

Major problems are still to be solved with organic photovoltaic cell materials, such as low power conversion efficiency and smaller photocurrent than that of inorganic alternatives.[109, 110] The solar cell field, based on conjugated polymers is subject to strong efforts in both academic and industrial research. The organic photovoltaic cells devices comprise of a thin film layer of organic material sandwiched between two electrodes as shown in **Figure 1.11**. The active layers in theses devices are deposited using wet processing methods such as ink jet printing and spin coating.[96, 128]

The anode typically consists of indium tin oxide (ITO) coated on a glass substrate; the transparency of the two layers allows the light to pass through the device. Cathodes that are typically used are either aluminium or calcium, the cathode allows light to be reflected back into the device to increase its efficiency. The device is finally encapsulated in an inert chamber to prevent oxidation. Like any OLEDs, parameters such as work function, ability to transport charge carriers, stability and overall expense need to be taken into consideration when selecting materials for these purposes.[14, 129]

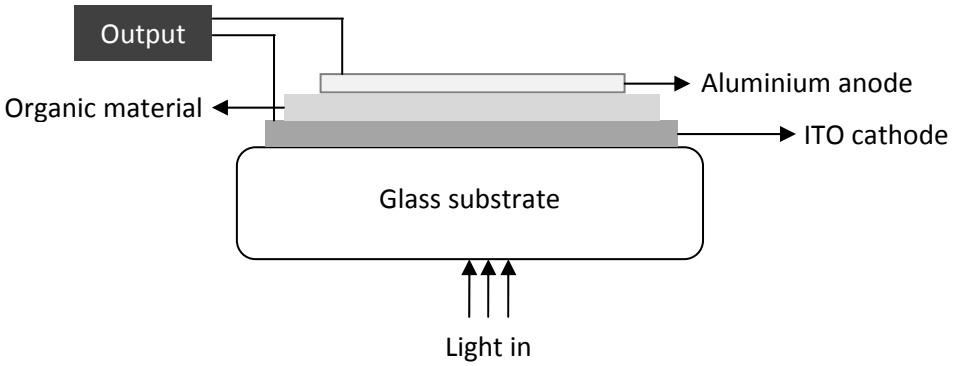

Figure 1.11: Polymer based solar cell.

The cathode typically aluminium or calcium used allows light to be reflected back into the device to increase its efficiency. Finally the device is encapsulated in an inert chamber to prevent oxidation. Like with any OLEDs, parameters such as work function, ability to transport charge carriers, stability and overall expense need to be taken into consideration when selecting materials for these purposes.[14, 129]

1.3.1 Solar Cell Operational Principles

The polymer in the active layer absorbs light and forms an exciton, which then splits into an electron/hole pair. Fullerene which is often used as a molecular acceptor in blends will receive an electron from the excited state level.[130] Furthermore, the fullerene network enables electron movement through a 'hopping' mechanism until the electrons reach the cathode. The holes are transported along the polymers backbone and make their way to the anode. [4, 7, 131] The electrodes are chosen to give an intrinsic field gradient so their work function must differ. The key stages of this photogeneration are explained in the **Figure 1.12**.

The coulomb attraction is a really important subject to discuss in order to enable exciton dissociation to occur successfully. The factor of potential difference between the electrodes and the photogenerated excitons has to be calculated sufficiently, thus generating the absorbed photons and excitons which are radiativity with high non- or photoluminescence (decay geminately). [106, 132]The work functions of the two electrodes used in the OPV device have a crucial role in determining the efficiency of the cell.[15, 124]

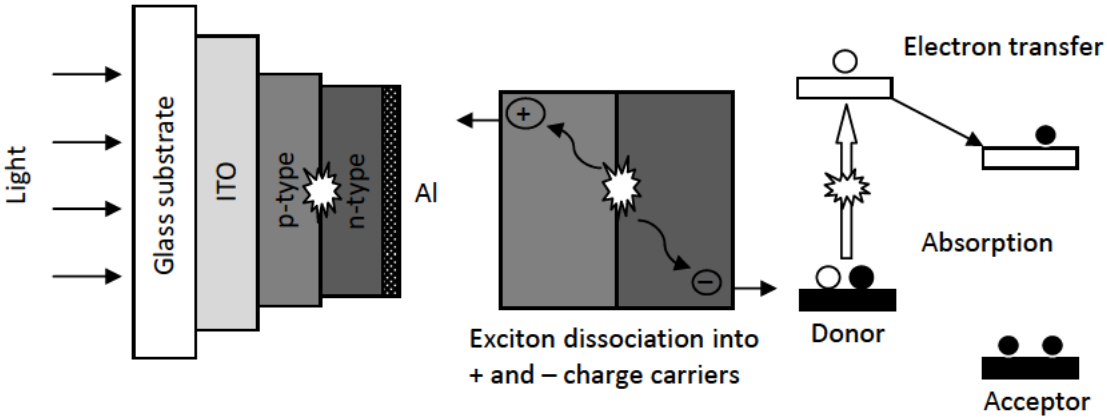

Figure 1.12: Diagram showing the key steps in photocurrent generation.

Generally, cathode terminals use Al and anode terminals use ITO. However, due to operational cell limitations, it is highly insufficient to generate photo-induced charge separation from this working of potential or terminal-function difference,[133] and calcium and PEDOT:PSS are added as extra layers between respectively aluminium and the active layer from the cathode side and ITO and the active layer from the anode side.

In conjunction with a bulk heterojunction, by using the donor acceptor method, improvements can be generated in the device.[86, 134] It is important that the device is encapsulated in an inert atmosphere as any air may cause defects due to oxidation.

1.3.2 Organic Solar Cells vs. Inorganic Solar Cells

There are many differences between organic photovoltaic (OPV) cells and their inorganic counterparts.[135-137] The photo-generated excitation of OPVs generates strongly-bound pairs of charges. This is in strong contrast to inorganic semiconductors in which weaker hole/electron energies hold these charges together. [2, 13, 138]

The range of spectral absorption of OPV materials is generally lower than that of certain inorganic semiconductors used in PV devices such as silicon which has a band gap of about 1.1 eV. However, despite the higher band gap of organic semiconductors used in OPV devices, they have generally much higher molar absorption coefficients which enables their

efficient use with typical active layers of the order of 100 nm. The optical and electronic properties of conjugated polymers are also far superior to those of their inorganic counterparts. [15, 58]

Most organic materials absorb light in the blue and green parts of the electromagnetic spectrum and are less efficient at absorbing in the red and infrared parts of the spectrum. [139] In order to improve the performance of OPV devices, it is important to extend their absorption sensitivity and bandwidth which must be controlled through an increase of their degree of electronic conjugation.

In order to break up the electron-hole pairs upon photogeneration in OPV devices, a powerful driving force such as an electric field should be introduced. It is also vital to overcome the low mobility of the charge carriers in OPV devices.

When the materials have limited absorption of sunlight, the photocurrent generated will also be limited. In addition, temperature is one of the main factors that can affect photocurrent and charge transportation in OPV devices. The thickness of the active layers is also amongst the important factors to control in order to improve the power conversion efficiency of devices.

The factors mentioned above indicate the differences between organic and inorganic based solar cells. In inorganic semiconductors, charge carriers are produced in bulk with holes and electrons not as firmly bound to each other as in organic semiconductors, therefore the charges are easily transported through the built-in electric field. In contrast to organic solar cells, the holes and electron are firmly bound as excitons. However, their separation is complicated due to low dielectric constant of organic semiconductors.[102, 124] The diagram in **Figure 1.13** shows the difference in charge generation between the two systems.

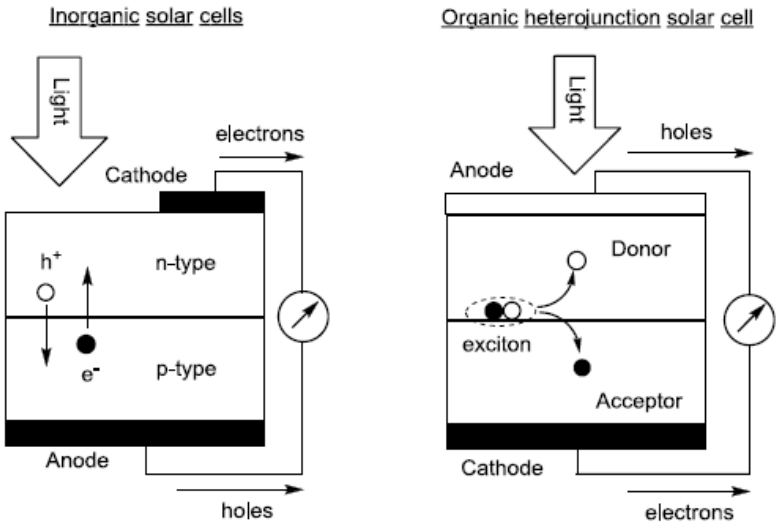

Figure 1.13: Schematic diagram of distribution of excitons on the organic and inorganic solar cells.

1.3.3 Organic Photovoltaic device architectures

Organic compounds have to meet two main criteria to be used in organic solar cells. They have to be able to absorb a good portion of sunlight and thus produce charge carriers, they also have to transport these charges effectively. These two properties are linked to the delocalised π-bond system on these materials and very much linked to their semiconducting properties.[140] The architectures of the three types of active layers used in organic based solar cells are described below.

1.3.4.1 Single layer

The simplest device structure is a layer of organic material sandwiched between two different conducting contacts, typically indium tin oxide (ITO) and a low work function metal such as Al, Ca or Mg as seen in **Figure 1.14**.[141] The difference in work function provides an electric field, which drives separated charge carriers towards the respective contacts (in rough analogy to a *p-i-n* junction in amorphous silicon). This electric field is seldomly sufficient to break up the photogenerated exciton. Instead, the exciton diffuses within the organic layer until it reaches a contact, where it may be broken up to supply separate charges, or recombine.[142]

Since exciton diffusion lengths are short, typically 1-10 nm, exciton diffusion limits charge carrier generation in such device.[69] Photocarrier generation is therefore a function not only of bulk optical absorption, but also of available mechanisms for exciton dissociation.[120] Other loss factors are non-radiative recombination at the interfaces and non-geminate recombination at impurities or trapped charges.

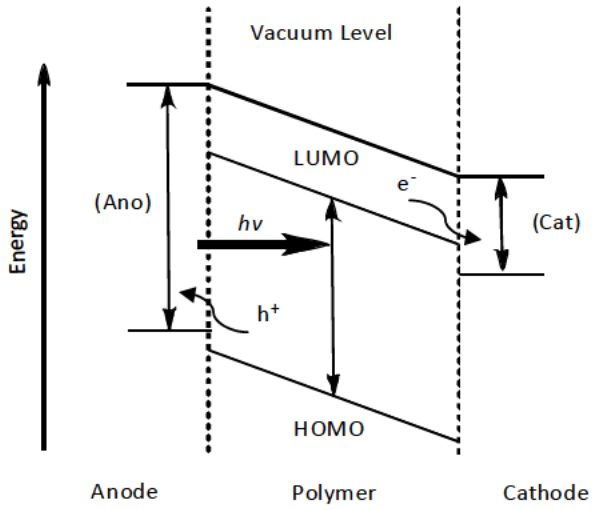

Figure 1.14: The basic function of a single layer organic photovoltaic cells device.

If both the excited state and ground state of the donor material lie at energies sufficiently higher than those of the acceptor material, it is energetically favourable for an exciton reaching the interface to dissociate, leaving a positive polaron on the donor and a negative polaron on the acceptor.[67] For efficient photocurrent generation, charge separation should compete successfully with geminate recombination after a photon absorption event, and transfer to contacts should compete with interfacial recombination.

Quantum efficiencies (QE) is the ratio of electrons delivered to the external circuit per incident photon of a given wavelength, and is the figure of merit in organic photovoltaics.[143] High QE is a necessary, though not sufficient, condition for high photovoltaic efficiency. In organic devices, the value is still far from the values of 80-90 % typical in inorganic solar cells.[65] Single layer solar cells of this type deliver QE of less than

1% and power conversion efficiencies of less than 0.1%. The structure of a single layer organic solar cell is show in **Figure 1.15.**

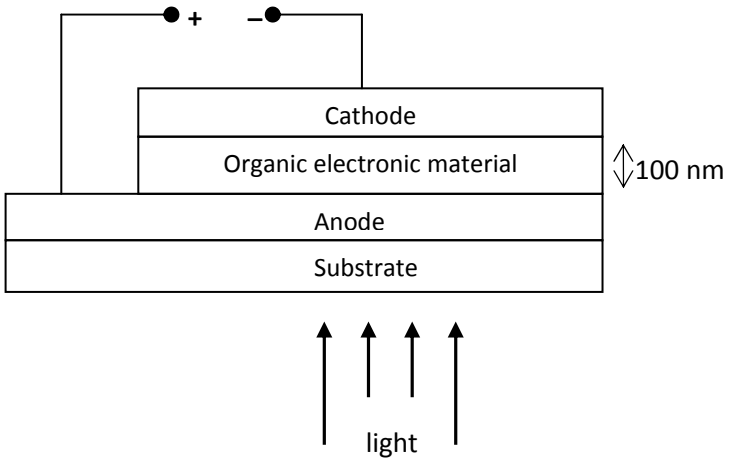

Figure 1.15: Schematic illustration of the structure of a single layer organic solar cell device.

1.3.4.2 Bilayer heterojuction

Most of the developments that have improved the performance of organic photovoltaic devices are based on donor–acceptor heterojunctions. At the interface between two different materials, electrostatic forces result from the differences in electron affinity and ionisation potential.[113]

If both the electron affinity and the ionisation potential are greater in one material (the electron acceptor) than the other (the electron donor), the interfacial electric field drives charge separation as can be seen in **Figure 1.16.**

These local electric fields are strong and may break up the photogenerated excitons provided that the differences in potential energy are larger than the exciton binding energy.[44] In a planar heterojunction, or 'bi-layer' device, the organic donor–acceptor interface separates excitons much more efficiently than the organic–metal interfaces in a single layer device and with very high purity materials, efficient photovoltaic devices may be made.[100]

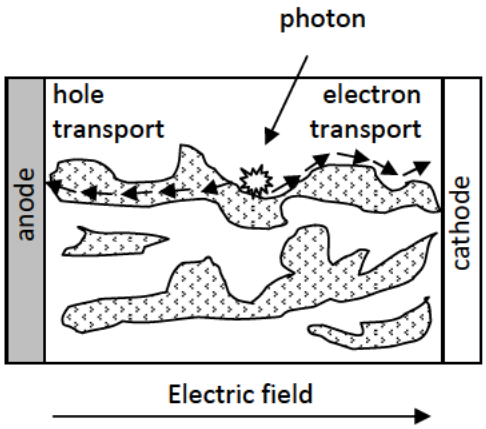

Figure 1.16: Donor and acceptor materials may be blended together to yield a dispersed heterojunction.

If the length scale of the blend is similar to the exciton diffusion length, then the probability that an exciton will reach the interface and dissociate is high. For efficient photocurrent collection, each material must provide a continuous path for the transport of separated charge to the contacts. Isolated domains can trap charges, causing recombination.[44, 86]

A revolutionary development in organic photovoltaics (and photodetectors) came in the mid 1990s with the introduction of a *dispersed* heterojunction, where an electron accepting and an electron donating material are blended together.[144] If the length scale of the blend is similar to the exciton diffusion length, then wherever an exciton is photogenerated in either material, it is likely to diffuse to an interface and break up.

If continuous paths exist in each material from the interface to the respective electrodes, then the separated charge carriers may travel to the contacts and deliver current to the external circuit. This effect was reported independently by several groups and for a blend of two conjugated polymers.

The blend improved quantum efficiencies (QE) to around 6 - 8 % from less than 1 % for either polymer alone.[55, 145] Around the same time, Yu and coworkers[64, 113] reported a QE of 29 % for a blend of the hole transporter, PPV, with a derivative of C60, where the C60 acts as the electron transporting component.[146] **Figure 1.17** shows the structure of a typical bilayer heterojunction polymer solar cell device.

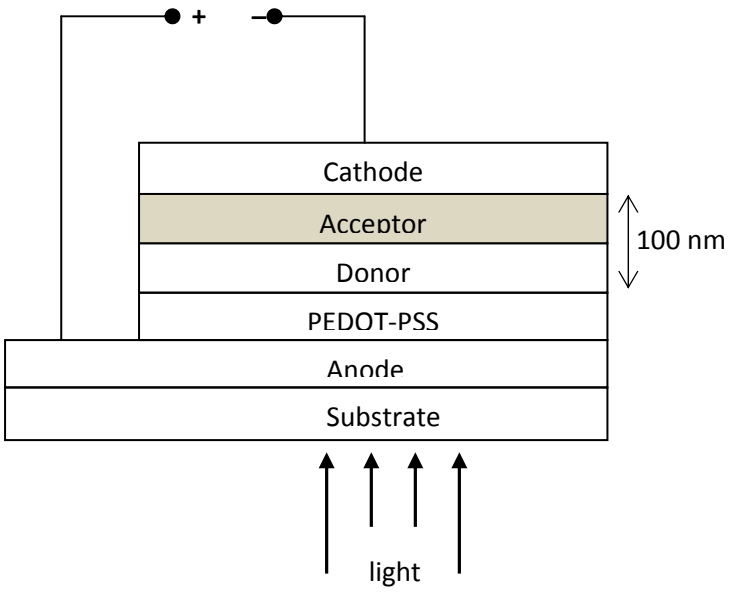

Figure 1.17: Schematic illustration of the structure of a typical bilayer heterojunction polymer solar cell device.

1.3.4.3 Bulk heterojuction

In a complete bulk heterojunction (BHJ) solar cell, the active layer is sandwiched between a transparent anode (typically tin-doped indium oxide, ITO) and a metal cathode.[27, 102, 105] Additionally, a thin layer of poly (3,4-ethylenedioxythiophene)-poly (styrenesulfonate) (PEDOT:PSS) is generally applied in between the ITO and the active layer to improve the electrical contact between the ITO and the active layer and to adjust energy levels as shown in **Figure 1.18.**

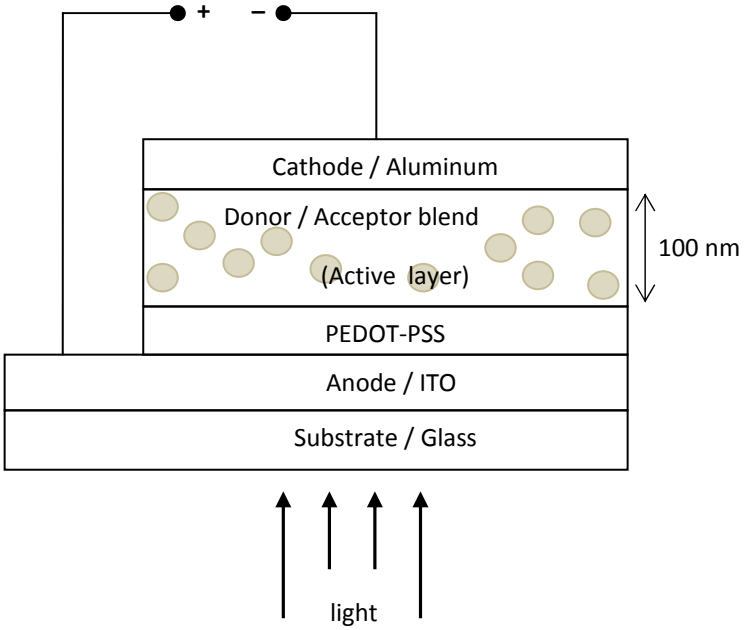

Figure 1.18: Schematic illustration of the structure of a typical bulk-heterojunction polymer solar cell device.

The active layer is sandwiched between two contacts: an indium-tin-oxide electrode coated with a hole transport layer PEDOT:PSS and an aluminium top electrode.

The principles behind the active organic layer in bulk heterojunction photovoltaic cells comprise of combined donor and acceptor blend. When light is absorbed by the active layer, an exciton is generated, and splits into a hole/electron pair, and then an electron is transferred from its excited state to the LUMO of the acceptor.[124]

The added acceptor layer allows a "stepping stone" mechanism to ascend, leading to easier dissociation of the exciton.[12, 147] The whole process is driven by the built in potential of the cell. Dissociation of the exciton leads to free charges, which move to their respective anode (holes) and cathode (electrons). The electrons travel through the fullerene network and the holes move along the donor polymer as indicated in **Figure 1.19**.[127, 148]

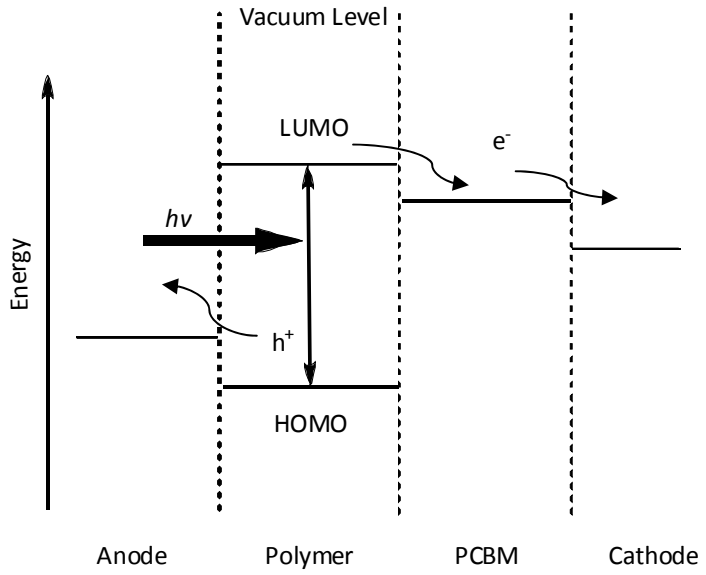

Figure 1.19: How light absorbed by a donor-acceptor bulk heterojunction PV device is converted into electricity.

A strong electric field is required for efficient dissociation to form two separate charges and contribute to the photocurrent efficiency.[149] If the exciton cannot dissociate, it will decay via a radiative or non-radiative pathways, leading to a decrease in the efficiency of the device. As discussed earlier power conversion efficiencies of up to 10.5 % have so far been achieved in OPV devices using tandem cells, and for them to be commercially viable, power conversion efficiencies around 10 % are required.[1, 145, 150, 151]

In order to increase the power conversion efficiency of devices, there are many variables that require consideration, such as the polymer used in the blend.[26] Efficient harvesting of solar energy requires the development of polymers with high absorption coefficients as well as possessing an extended absorption spectral range 350-900 nm to enable photocurrent generation from lower-energy photons.[152, 153]

The interpenetrated network of BHJ offers two advantages: (1) It minimizes the traveling distance of excitons (electron-hole pair generated upon light absorption) to the DONOR/ACCEPTOR (D/A) interface and concurrently maximizes the D/A interfacial area, thereby ensuring the exciton dissociation at the D/A interface to generate maximum free charge carriers; (2) offers charge transport pathways to facilitate the charge collection at

electrodes, completing the conversion of the photon energy to electrical energy, photovoltaic effect.[149, 154-156]

Composite films or bulk heterojunctions of semiconducting polymers and C_{60} derivatives have received considerable attention for photovoltaic energy conversion. The primary step in the operation of such a bulk heterojunction photovoltaic cells is a fast photo induced electron-transfer reaction from the conjugated polymer as a donor to the fullerene as an acceptor.[146, 157-159]

An intimate mixing of the donor and acceptor in the blend and a large donor-acceptor interfacial area in the active layer are required for efficient charge generation because the exciton diffusion length in conjugated polymers is limited to the nanometer scale and electron transfer occurs at the donor-acceptor interface.[94, 110]

1.4 Synthesis of Conjugated polymers

Since the first reports on the polymerization of poly(acetylene) in 1977, conjugated polymers have attracted much attention and have been synthesized through a number of different techniques.[160] The synthetic routes can be divided into three major groups: the oxidative polymerisation routes, metal-catalysed cross-coupling routes and condensation polymerisation routes.[69, 161, 162] There are many ways to prepare conjugated polymers in these majors groups, but some of the most significant methods are discussed in the next section.[160]

1.4.1 Oxidative preparation routes

1.4.1.1 Electrochemical Polymerisation

Electrochemical synthesis can be divided into cathodic and anodic polymerization routes. Anodic polymerisation is most commonly used.[163-165] Anodic polymerisation involves oxidation of monomers in solution leading to precipitates of the polymers as coating on the anode.[166] Electrochemical polymerisation is done in a classical three-electrode cell as shown in **Figure 1.20.**

Electrochemical polymerisation has many advantages, such as the requirement of a small amount of monomer with no catalyst required. The polymer is directly formed as a thin film on the anode where the rate of reaction can be regulated by changing the current at the working electrode. Concurrently, thermodynamics of the system can also be regulated by the potential applied to the working electrode and is a quick method to electro-polymerised materials.[109, 167]

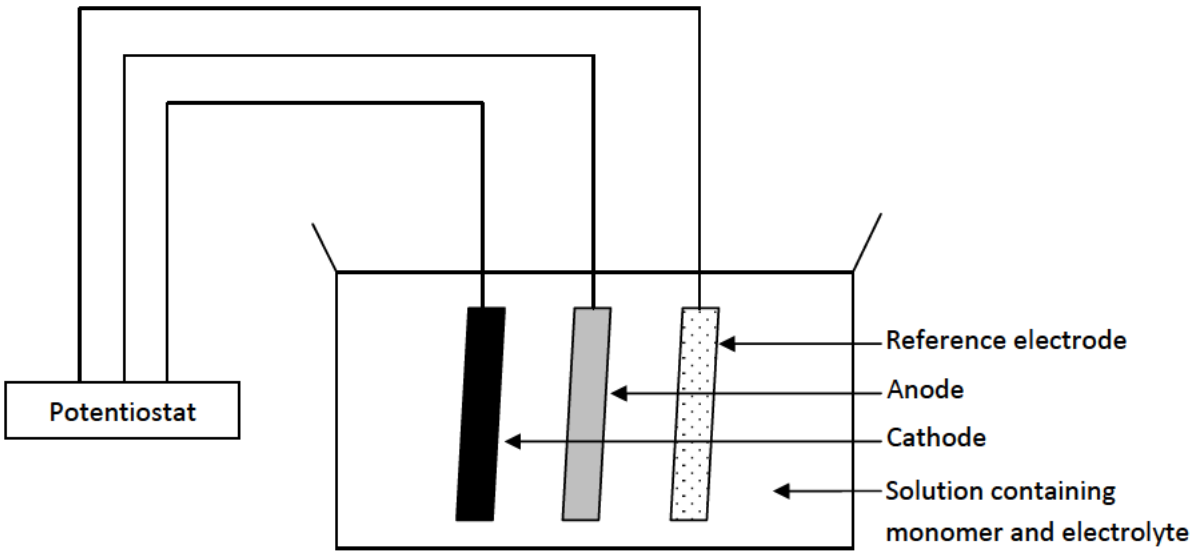

Figure 1.20: Classical three electrode cells.

Oxidative coupling is mainly used for the synthesis of polythiophenes, polypyrroles and polyaniline. The oxidation route can be carried out chemically, for example with ferric chloride to dissolve and oxidise the monomer, or also electrochemically.[106, 168] The schemes for the electrochemical oxidation and chemical oxidation routes are shown in **Scheme 1.3** for the preparation of polypyrrole and polythiophene.

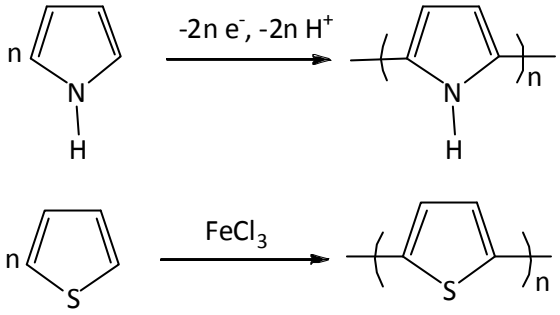

Scheme 1.3: Electrochemical oxidation route and chemical oxidation route.

1.4.2 Metal-catalysed Routes to conjugated polymers

1.4.2.1 Yamamoto Coupling

This method was discovered by Yamamoto *et al.* in 1980.[169] The preparation is illustrated in **Scheme 1.4**. It uses a stoichiometric amount of Ni complexes, starting from dihalides as monomers for the polymerisation. High molecular weight materials can be obtained using the Yamamoto coupling.[169,170] The Yamamoto coupling can be used to prepare many classes of conjugated polymers, such as polycarbazoles, polythiophenes and polyphenylenes. However, high amounts of Ni complex have to be used in this reaction.

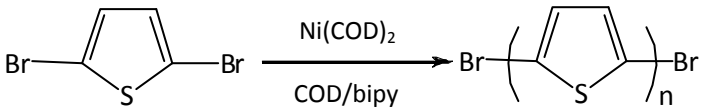

Scheme 1.4: Yamamoto Coupling.

1.4.2.2 Kumada Type Cross-coupling

Bi-functional monomers comprising both halo- and halomagnesio-functionalities are used in these polymerization.[171, 172] Polymerizations are carried out by using a nickel catalyst $Ni(dppp)Cl_2$ (where dppp= diphenyl phosphinopropane). Palladium-based catalysts such as ($Pd(PPh_3)_2Cl_2$) have also been used in this reaction. The mechanism for the Kumada cross-coupling reaction consists of five steps as shown in **Scheme 1.5**.

In the first step, an intermediate diaryl diphosphine nickel intermediate is formed by reaction of a dihalo diphosphine nikel with a Grignard reagent. In step 2, elimination of the dihalo diphosphine nikel creates diphosphine nikel[0] complex, which reacts with an aryl halide to produce halo aryl diphosphine nickel[II] complex as illustrated in Step 3. In step 4 the halo aryl phosphine nickel complex reacts with a Grignard reagent, which results in a diaryl diphosphine nickel complex. The last step is the reductive elimination of the product to complete the cycle.

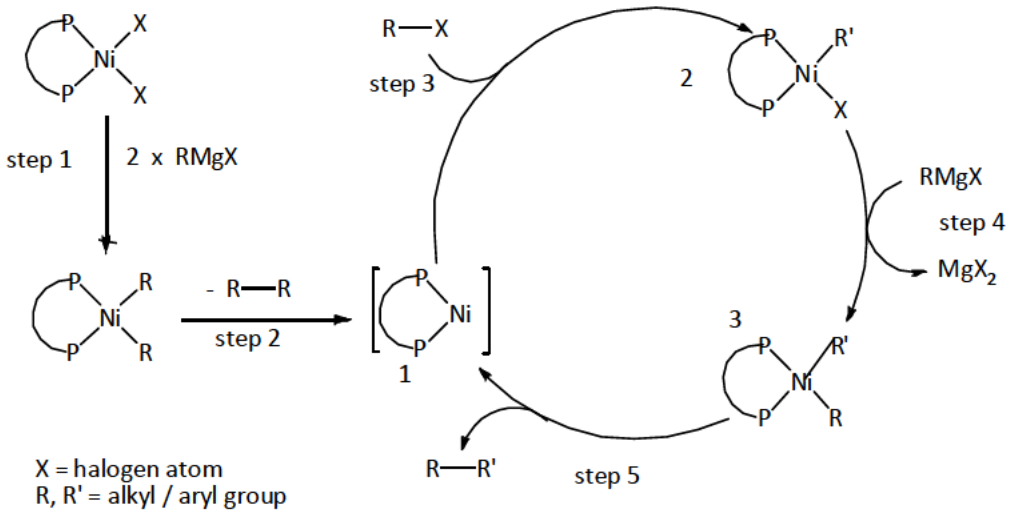

Scheme 1.5: The mechanism of Kumada Cross-coupling reaction.

The phosphine/nickel complex catalyses the cross-coupling of a number of functionalities, for instance alkyl, alkenyl, aryl and hetero aryl Grignard reagents can be readily reacted with aryl, heteroaryl and alkenyl halides. This method can thus be seen to have a wide scope of application.

Alkyl halides also exhibit considerable reactivity, nevertheless give a complex mixture of products. A labile diorgano-nickel complex involving the two organic groups originating from the Grignard reagent and from the organic halide, respectively has been proposed as an intermediate in the reaction.

Based on this method, it is remarkably evident that simple alkyl Grignard reagents with hydrogen-bearing β-carbon atoms react with equal efficiency, considering the great tendency with which transition metal alkyls undergo a β-hydrogen elimination reaction, forming alkenes and metal hydrides.

Although the β-elimination may be responsible for the side products formed during the coupling, an appropriate choice of phosphine ligand for the nickel catalyst minimizes this side reaction. The catalytic activity of the phosphine / nickel complex depends not only on the nature of the phosphine ligand but also on the combination of the Grignard reagent and organic halide.[173]

1.4.2.3 Stille Type Cross-coupling

In these reactions, functional monomers comprising halo- and/or organotin-functionalities are used.[174] The Stille cross-coupling reactions are similar to Kumada-type cross-coupling reactions, apart that organotin-derivatives are used instead of Grignard-derivatives.

The Stille reaction was discovered in 1977 by John K. Stille and co-workers. This type of reaction continues to be exploited in industry, especially in the pharmaceutical industry. The reaction is usually performed under inert atmosphere using dry and degassed solvents. This is because oxygen causes the oxidation of the palladium catalyst and promotes homo coupling of organic stannyl compounds, and these side reactions lead to a decrease in the yield of the cross coupling reaction.[175] As the organic tin compound, a trimethylstannyl or tributylstannyl group is normally attached to the aryl or vinyl group to be functionalised. Although trimethylstannyl compounds show higher reactivity compared to tributylstannyl compounds, the toxicity of the former is about 1000 times higher than that of the latter.[109] Therefore it is better to avoid using trimethylstannyl compounds unless necessary.

Polymerisation is carried out by using a palladium based catalyst such as $Pd(PPh_3)_4$ as shown in **Scheme 1.6**. This method is useful as it yields conjugated polymers with high molecular weights.[160] It is suitable for bi-functional monomers, which have both halo- and organotin- functionalities.

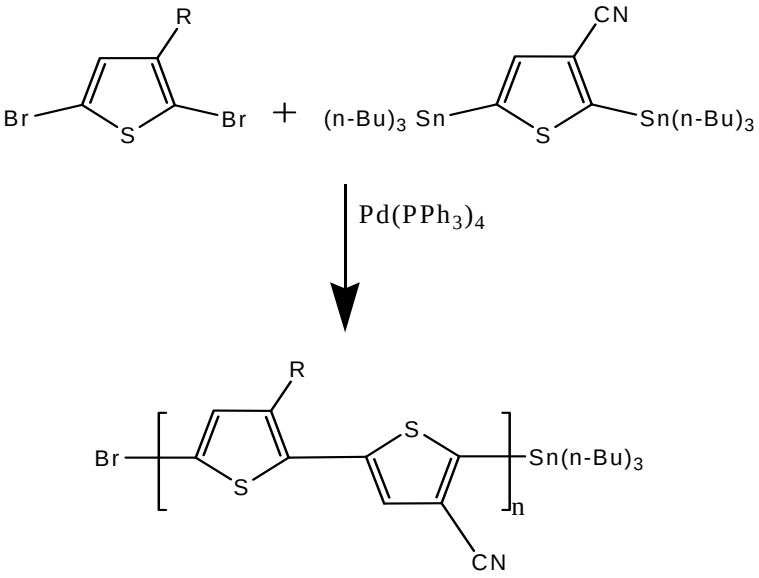

Scheme 1.6: Formation of a conjugated copolymer using the Stille cross-coupling by using $Pd(PPh_3)_3$.

The mechanism of the Stille coupling consists of four steps as shown in **Scheme 1.7**. The first step is an oxidative addition, followed by a trans metalation. The third step is a cis / trans isomerization and finally the final step is a reductive elimination.

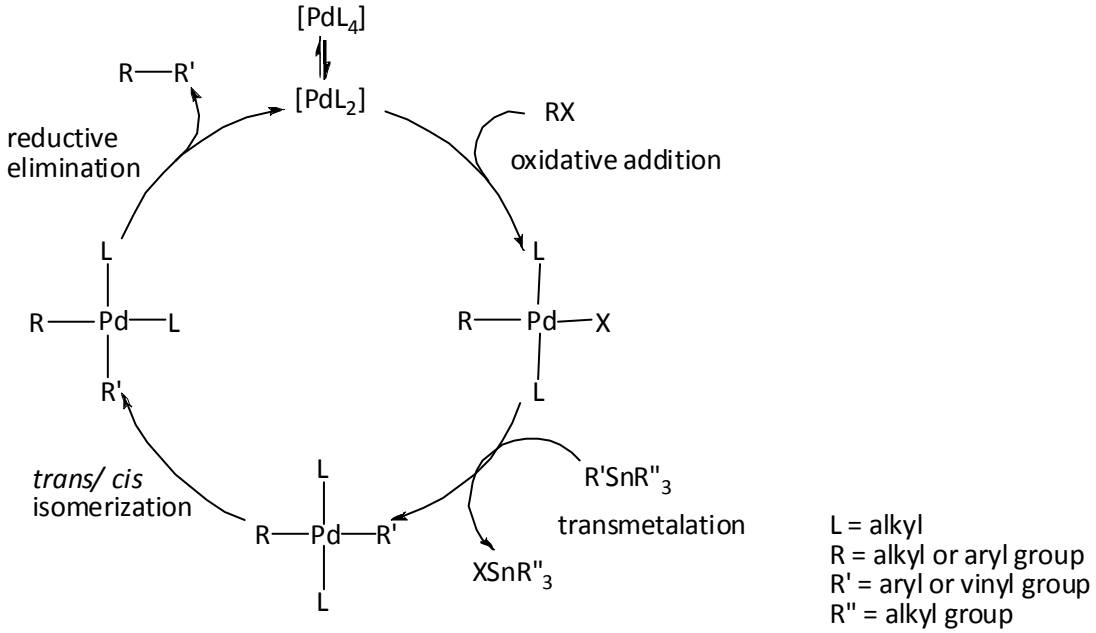

Scheme 1.7: The mechanism of Stille type cross-coupling.

1.4.2.4 Suzuki Type Cross-coupling

The Suzuki cross coupling is the reaction of an aryl- or vinyl-boronic acid/ ester with an aryl- or vinyl-halide catalyzed by a palladium(0) complex.[36, 176] This is a powerful synthetic tool as it represents one of the most valuable methods for carbon-carbon bond formation, not least because of its tolerance of a broad range of functional groups and of its non-toxic bi-products. The boronic acid is also thermally stable and inert to air and water which allows easy handling without special precautions.[169] The presence of a mineral base seems to be fundamental for the success of the cross-coupling reaction.

Polymerisation is carried out by using Palladium catalyzed cross-coupling between an aryl boronic ester or acid derivative with aryl halides as shown in **Scheme 1.8**. Suzuki coupling is widely used to synthesis-conjugated polymers which have many functional groups. In addition, this method is widely used to prepare a wide range of copolymers.[103]

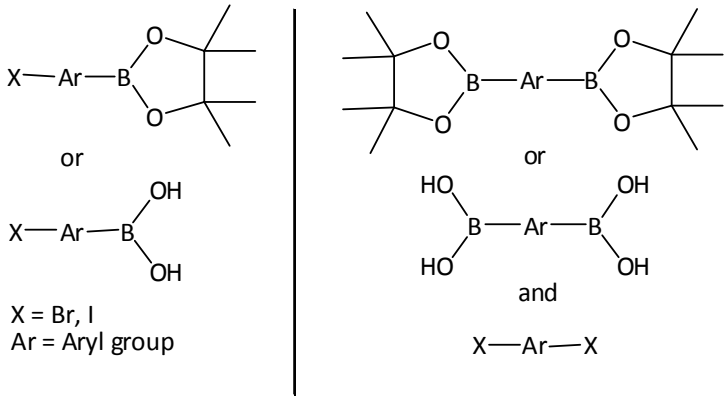

Scheme 1.8: Structure of boronic monomer counterparts used in Suzuki cross-coupling reaction.

The mechanism of the Suzuki reaction is best viewed from the perspective of the palladium catalyst. The first step is the oxidative addition of palladium to the halide to form the organo-palladium species. The reaction with the base leads to a palladium intermediate where the halide is removed from the metal centre. Transmetallation with the boronate complex forms an organopalladium species where two aryl groups are attached to the palladium centre. Reductive elimination of the desired product restores the original palladium catalyst as shown below in **Scheme 1.9**.

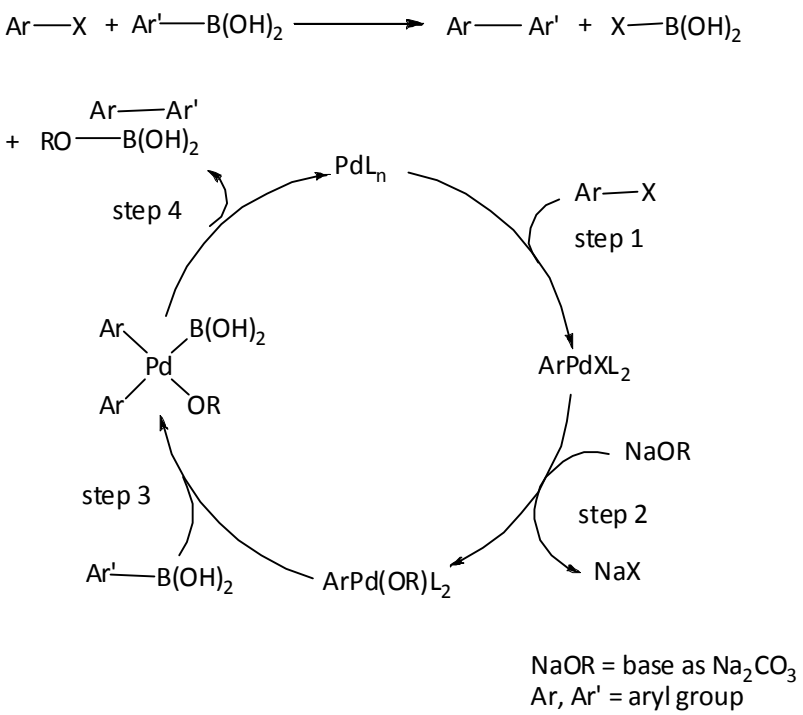

Scheme 1.9: The mechanism of Suzuki Coupling reaction.

One difference between the Suzuki mechanism and that of the Stille Coupling is that the boronic acid must be activated, for example, with a base. This activation of the boron atom enhances the polarisation of the organic ligand, and facilitates transmetallation.

If the starting monomers are substituted with base labile groups (for example, esters), powdered KF could be used instead of other mineral bases leaving base labile groups unaffected by the reaction. Due to the versatility of the Suzuki reaction and the low toxicity of the boronic acid monomers, there is currently a widespread interest in the applications of this reaction, with new developments and refinements being constantly reported.

1.4.3 Condensation polymerization routes

Condensation polymerisation involves interaction of two similar (or different) monomers and generally liberates liquid or gaseous by-products (such as water, hydrochloric acid or nitrogen gas) as seen in **Scheme 1.10.**

Monomers with only one reactive group terminate a growing chain, and thus give polymers with a lower molecular weight. Linear polymers are created using monomers with two reactive end groups and monomers with more than two end groups give three dimensional polymers which are cross-linked.[177]

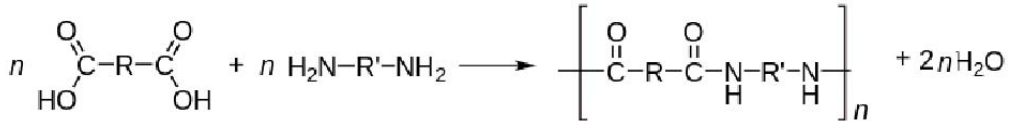

Scheme 1.10: General chemical structure of one type of condensation polymer.

1.5 Background on Carbazole Based Polymers

Carbazole is an aromatic heterocyclic organic compound. It has a tricyclic structure, consisting of two six-membered benzene rings fused on either side of a five-membered nitrogen-containing ring.[86, 178] **Figure 1.21** illustrates the structure.

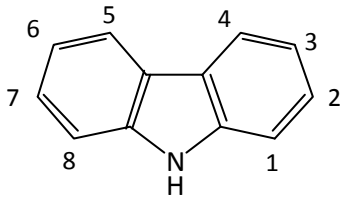

Figure 1.21: Molecule structure of carbazole.

The carbazole monomer contains a rigid biphenyl structure connected at the 9-position by a nitrogen atom.[103] This nitrogen is not oxidised under electrochemical conditions and is easily functionalised with either alkyl or aryl substituents for the purposes of solubility.

Carbazole-based homopolymers have wide energy gaps. Their HOMO and LUMO energy levels can easily be changed through the modification of their side chains. This makes these compounds as ideal candidates in the quest to develop efficient materials for use in photovoltaic cells as well as in LEDs.[14, 100] Polycarbazoles show remarkable thermal stability,

possess much better hole transporting abilities than polyfluorenes, and are thought to be less susceptible to excimer formation as well as being blue emitters, revealing them as promising in the quest for more efficient optoelectronic devices. Structurally, 2,7-linked-carbazole-based materials are more favorable for optoelectronic applications when compared to those where the carbazole repeat units are 3,6-linked as a result of a more extended electronic conjugation. The solubility and processability of these materials is greatly improved through the facile substitution at the remote *N*-position.[83]

1.5.1 Synthetic routes to Polycarbazoles

Suzuki cross-coupling is a suitable method to use in order to synthesize polycarbazoles. This method uses palladium-based reagents as catalyts and displays tolerance to water and to a wide range of functional groups.[36] The Suzuki reaction uses palladium (0) catalysts combining aryl or vinyl groups from boronic esters with aryl or vinyl groups from halides to form carbon-carbon bonds as shown in **Scheme 1.9**.

There are many classes of efficient organic materials that are described for use in optoelectronic devices. Based on the literature, 2,7-linked carbazole based materials have provided encouraging results upon their application in optoelectronic devices.[5, 28, 77, 97]

The features of carbazole-based materials include good hole mobilities as well as good solution processability. They can generate different materials with various HOMO and LUMO energy levels that are stable to process in air. In view of the nature of the carbazole repeat unit which has a rigid ring structure with good electron delocalisation and the possibility to functionalise the nitrogen atom with bulky alkyl chains without affecting the electronic delocalisation on the resulting materials to a great extent,[179] there are many possibilities to use this unit as the electron donor unit in the design of low band gap polymers with alternating electron donor and acceptor repeat units. Indeed, many researchers have used it to develop materials with tailored physical properties for use in solar cells technologies.[8, 150, 180]

CHAPTER 2 - AIMS AND OBJECTIVES

The aims of this project is to prepare new families of highly efficient polymers for PV applications based on carbazole and fluorene monomers with thienothiophene units which should lower their band gap and provide materials with enhanced power conversion efficiencies.[118, 183]

The main objectives of the work are:

(i) To develop new synthetic strategies series of novel conjugated polymers by using carbazole-based, thienothiophenes and benzothiadiazole repeat units with high absorption coefficients and extended absorption spectra suitable for application in solar cells.

(ii) To check the purity of the compounds by using TLC, ^{1}H-NMR, ^{13}C-NMR, as well as other analytical techniques.

(iii) To characterise the physical properties of the polymers and analyse their thermal stability behaviour using TGA, DSC.

(iv) To investigate their photophysical and electronic properties by using UV-Vis spectroscopy and cyclic voltammetry.

Polymers will be synthesised using palladium catalysed Suzuki cross coupling reactions as well as other methods and then will be characterised with many physical techniques, the electronic properties and photophysical properties (band gap, HOMO, LUMO levels) will be investigated using UV/Vis spectroscopy and cyclic voltammetry. The thermal stability and thermal properties will be measured using TGA and DSC.

2.1 Carbazole and fluorene based copolymers containing thienothiophene

In the first copolymer poly(9-(heptadecan-9-yl)-*9H*-carbazole-alt-thieno[3,2-*b*]thiophene) **(P1)**, the carbazole does not have any protecting groups at the 3- and 6-positions, while the carbazole in the second copolymer poly(3,6-difluoro-9-(heptadecan-9-yl)-*9H*-carbazole-*alt*-thieno[3,2-*b*]thiophene) **(P2)** will have fluorine substituents at the 3- and 6- positions as protecting groups, which should lead to more stable polymers against electrochemical

degradation, oxidation and they are also expected to be narrow bandgap polymers.[184] The target copolymers structures **P1** and **P2** are shown in **Figure 2.1**.

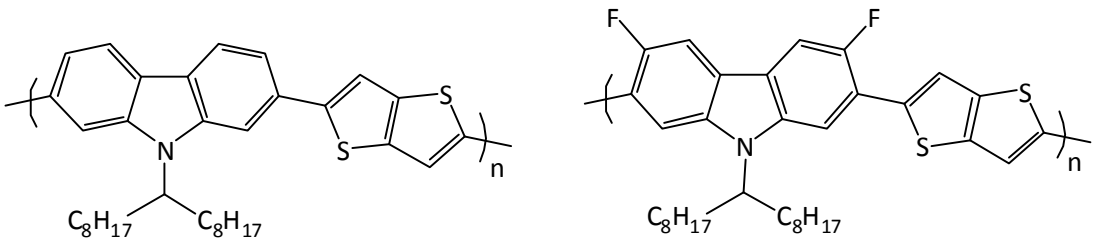

P1 **P2**

Figure 2.1: The target polymers **P1** and **P2**.

In addition, a series of alternating polyfluorene based copolymers with narrow bandgaps have been reported recently in the literature and have exhibited great promise for photovoltaic applications.[27, 88, 185, 186]

A polyfluorene-based co-polymer containing thienothiophene units will also be made.[183] The photophysical and electrical properties of poly (9,9-dioctyl-*9H*-fluorene-alt-thieno[3,2-*b*]thiophene) **(P3)** will be compared to its carbazole analogue **P1** in oder to investigate the effect of changing carbazole repeat units with fluorene units. **Figure 2.2** shows the chemical structure of target copolymer **P3**.

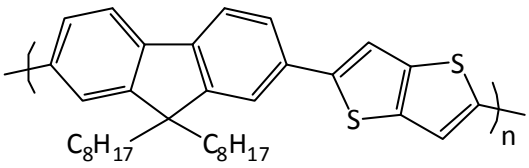

Figure 2.2: The target polymer **P3**.

2.2 Carbazole and fluorene based co-polymers containing thienothiophene and benzothiadiazole units

Poly[N-9'-heptadecanyl-2,7-carbazole-alt-5,5-(4',7'-di-2-thienyl-2',1',3'- benzothiadiazole)] PCDTBT is one of a relatively large type of donor-acceptor polycarbazole copolymers, which exhibit a high efficiency when used as an electron donor polymer in bulk heterojunction solar cells using PCBM as an acceptor.[82, 103, 104] The aim of this project is to synthesise a series of novel copolymers similar to PCDTBT, but where the thiophene units are replaced with thienothiophene units, which should have a lower band gap due to the potential high mobility of the thienothiophene repeat unit.[187] Copolymerization of electron-rich conjugated units and electron-decient conjugated units alternatively is an effective approach to get low band gaps polymers. Electron-rich units have been employed as building blocks in constructing highly efficient photovoltaic polymers for the applications in bulk heterojunction (BHJ) devices. To build conjugated backbones with alternating aromatic structure, i.e. to copolymerize conjugated units with strong aromatic properties, is another effective approach to get low band gaps polymers.

In the first copolymer, poly(9-(heptadecan-9-yl)-*9H*-carbazole-*atl*-4,7-di(thieno[3,2-b]thiophen-2-yl)benzo[*c*] [1,2,5]thiadiazole) **(P4)**, the carbazole does not have any protecting groups at the 3- and 6-positions, while the carbazole in the second copolymer poly(3,6-difluoro-9-(heptadecan-9-yl)-*9H*-carbazole-*atl*-4,7-di(thieno[3,2-*b*]thiophen-2-yl)benzo[*c*][1,2,5]thiadiazole) **(P5)** will have fluorine substituents at the 3- and 6- positions as protecting groups, which should lead to more stable polymers against electrochemical degradation, oxidation and they are also expected to narrow the band gap of the polymers. The target copolymers structures **P4** and **P5** are shown in **Figure 2.3**.

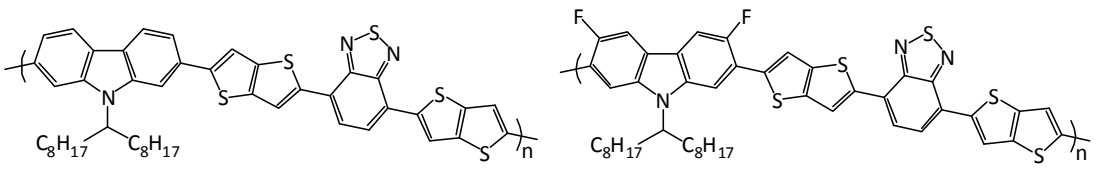

P4 **P5**

Figure 2.3: The target polymers **P4** and **P5**.

The photophysical and electrical properties of polymers **P4** and **P5** will be compared with those of PCDTBT and a fluoro protected polycarbazole PFCDTBT respectively, which have been synthesised by the Iraqi group, to find out the influence of replacing thienothiophene with thienothiophene repeat units and also study the effect of fluorine substituents on the bandgap, the HOMO and LUMO levels of the resulting polymers.[83, 103, 188, 189]

The solubility of polymers **P4** and **P5**, in common solvents is expected to be limited which could influence the purification and processability of the polymers, thus a good solubility is very important to fabricate photovoltaic devices through a solution process. A series of novel alternating copolymers similar to **P4** and **P5**, but where the heptadecane substituents attached at the carbazole units are replaced with longer pentacosane chains, will be made and their properties investigated.

In the first copolymer poly(9-(pentacosan-13-yl)-9H-carbazole-atl-4,7-di(thieno[3,2-b]thiophen-2-yl)benzo[c][1,2,5]thiadiazole) **(P6)**, the carbazole does not have any protecting groups at the 3- and 6-positions, while the carbazole in the second copolymer poly(3,6-difluoro-9-(pentacosan-13-yl)-9H-carbazole-atl-4,7-di(thieno[3,2-b]thiophen-2-yl)benzo[c][1,2,5]thiadiazole) **(P7)** will have fluorine substituents at the 3- and 6- positions as protecting groups, which should lead to more stable polymers against electrochemical degradation, oxidation and they are also expected to be narrow band gap polymers. **Figure 2.4** shows the chemical structures of target copolymers **P6** and **P7**.

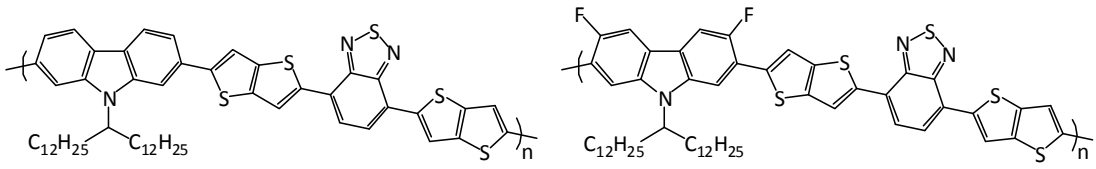

P6 **P7**

Figure 2.4: The target polymers **P6** and **P7**.

2.3 Carbazole and fluorene based copolymers containing thienothiophene and bis-octyloxy substituted benzothiadiazole units

The solubility of high molecular weight PCDTBT and the analogous **P4-P7**, in common solvents is one of the main issues that influence the purification and processability of the polymers, thus a good solubility is very important to fabricate photovoltaic devices through solution processes.

The solubility can be increased by attaching alkyl substituents to the main polymer backbone ideally without affecting the planarity and stability of the polymer, as well as other physical properties.

The aim in this part of the project is to synthesise two novel copolymers similar to polymers **P4** and **P5**, but where the benzothiadiazole units are carrying two octyloxy chains at the 5- and 6-positions to improve the processability and solubility of the resulting polymers.

The photophysical and electrical properties as well as the thermal stability of poly(9-(heptadecan-9-yl)-9H-carbazole-alt-5,6-bis(octyloxy)-4,7-di(thieno[3,2-b]thiophen-2-yl)benzo[c][1,2,5]thiadiazole) **(P8)**, and poly(3,6-difluoro-9-(heptadecan-9-yl)-9H-carbazole-alt-5,6-bis(octyloxy)-4,7-di(thieno[3,2-b]thiophen-2-yl)benzo[c][1,2,5]thiadiazole) (**P9**) will be compared with those of **P4** and **P5**. The structures of **P8** and **P9** are shown in **Figure 2.5.**

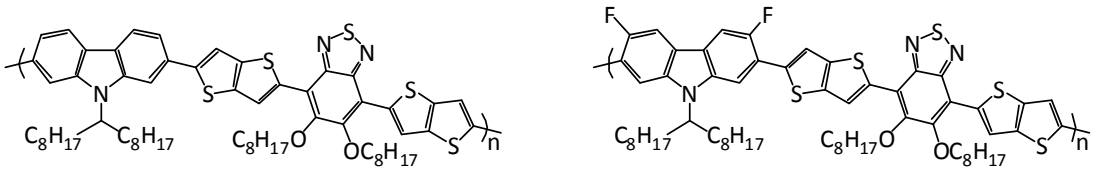

P8 **P9**

Figure 2.5: The target polymer **P8** and **P9**.

A similar polyfluorene-based co-polymer containing thienothiophene units will also be made. Poly(9,9-dioctyl-9H-fluorene-alt-5,6-bis(octyloxy)-4,7-di(thieno[3,2-b]thiophen-2-yl)benzo[c][1,2,5]thiadiazole) **(P10)** will be prepared and its photophysical and electrical

properties compared with those of **P8** and **P9**. **Figure 2.6** shows the chemical structure of target copolymer **P10**.

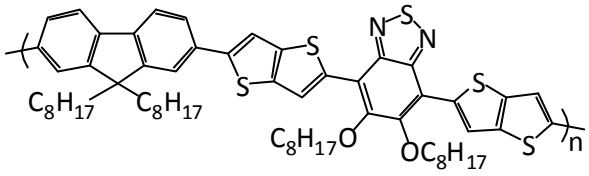

Figure 2.6: The target polymer **P10**.

CHAPTER 3 - EXPERIMENTAL

3.1 Materials

All the starting materials were ordered from commercial suppliers including Sigma-Aldrich, Fisher, Alfa Aesar and Acros Organics. All chemicals were used as received unless stated otherwise.

Dry solvents were used for reactions unless stated otherwise, most of them obtained from Grubbs solvent purification system such as acetonitrile, chloroform, dichloromethane, diethyl ether, dimethylformamide, hexane, methanol, tetrahydrofuran and toluene.

Reagent grade solvents were obtained from internal stores and used for extraction, chromatography and some reactions. Most of the reagents, acids, bases, salts and drying agents were obtained from internal stores. All reactions were carried out in dried glassware and under an inert atmosphere of argon or nitrogen, using Schlenk line techniques.

3.2 Analysis and Characterisation

3.2.1 Thin Layer Chromatography (TLC)

TLC is a chromatographic technique used to separate the components of a mixture using a thin stationary phase supported by an inert backing. It may be performed on the analytical scale as a means of monitoring the progress of a reaction or on the preparative scale to purify small amounts of a compound.

TLC was run on silica-coated aluminium plates. The chromphores were visualised by Spectroline UV light under short wave ultraviolet (254 nm) and long wave ultraviolet (365 nm). In case of absence of chromophores or weakly UV active compounds, TLC was dipped in a solution of *p*-anisaldehyde, and developed by heating. The *p*-anisaldehyde solution consisted of acetic acid (3.80 ml), *p*-anisaldehyde (9.30 ml), H_2SO_4 (12.50 ml), and ethanol (340.00 ml).

3.2.2 Nuclear Magnetic Resonance Spectroscopy (NMR)

NMR is an analytical technique that utilizes magnetic fields to look at magnetic nuclei. These magnetic nuclei absorb and re-emit electromagnetic energy in the presence of the magnetic field. By looking at the peaks in the results spectra the structure of compound can be determined.

All ^{1}H NMR, ^{13}C NMR and ^{19}F NMR spectra were recorded on Bruker AC250 (250 MHz), AMX400 (400 MHz) or DRX500 (500 MHz) NMR spectrometers at 22 °C in chloroform-d_1, DMSO-d_6, acetone-d_6 and 1,1,2,2-trichloroethane-d_2 solutions.

Chemical shifts are reported in ppm relative to internal standard. Observations given are as follows: s (singlet), d (doublet), dd (double doublet), m (multiplet) and b, (broad signal), bm (broad multiplet). Coupling constants are measured in Hz and chemical shifts (or δ) in ppm.

3.2.3 Melting Point Apparatus

The melting point was measured by using a U12802 Gallenkamp MPD350 melting point apparatus.

3.2.4 Fourier Transform - Infra Red Spectroscopy (FT-IR)

In FT-IR, some of the IR radiation is absorbed by the sample and some of IR radiation is passed through (transmitted) the organics sample. Unique molecular fingerprint was represented as result creating of the molecular absorption and transmission.

IR absorption spectra were recorded on the PerkinElmer Spectrum 100 FT-IR spectrometer and on the Nicolet Model 205 FT-IR spectrometer, using the ATR Diamond crystal attachment for solid samples.

3.2.5 Mass Spectrometry (MS)

Matrix-assisted laser desorption/ionization time-of-flight mass spectrometry (MALDI-Tof-MS) spectra were recorded on a Bruker Reflex III in reflection positive-ion mode and with using trans-2-[3-(4-tert-butylphenyl)-2-methyl-2-propenylidene]malononitrile (DCTB) as a matrix. Mass spectra were obtained by the electron impact method (EI) or the chemical ionisation method (CI).

3.2.6 Elemental Analysis

Elemental analyses were carried out by using the Perkin Elmer 2400 CHN Elemental Analyser for CHN analysis, and the Schoniger oxygen flask combustion method for sulphur and halides (anions). The weights submitted for analysis were 10 mg for CHN analysis and 10 mg for the anion analysis.

3.2.7 UV-Visible Absorption Spectroscopy (UV-Vis)

UV-Vis absorption spectra were measured by Hitachi U-2010 Double Beam UV/ Visible Spectrophotometer. The absorbance of monomers and polymers was measured in solution in spectrophotometric grade solvents (toluene or dichloromethane) at ambient temperature using rectangular quartz cuvettes (light path length = 10 mm) purchased from Sigma-Aldrich. Samples of pristine polymer thin films for UV-visible absorption spectra measurements were prepared by dip coating quartz plates into 1 mg cm^{-3} polymer solutions in dichloromethane (HPLC grade); and the measurements were carried out at ambient temperature.

3.2.8 Thermo-Gravimetric Analysis (TGA)

TGA curves were obtained by using the Perkin Elmer Pyris 1 Thermo gravimetric Analyser at a scan rate of 20°C min^{-1} under an inert nitrogen atmosphere. The weights of the samples were ca. 5 mg.

3.2.9 Differential Scanning Calorimetry (DSC)

DSC curves were recorded on the Perkin Elmer Pyris 1 Differential Scanning Calorimeter equipped with Perkin Elmer CCA 7 Subambient Accessory at a scan rate of 10 ºC $minute^{-1}$ under inert nitrogen atmosphere.

3.2.10 Gel Permeation Chromatography Analysis (GPC)

GPC curves were recorded on the equipment consisting of Waters Model 515 HPLC Pump, GILSON Model 234 Autoinjector, MILLIPORE Waters Lambda-Max Model 481 LC Spectrometer, Erma ERC-7512 RI Detector, PLgel 5m 500A Column, and PLgel 10m MIXED-B Column using THF as the eluent at a rate of 1 cm^3 $minute^{-1}$. Polymer solutions in THF (2.5 mg cm^{-3}) were used as samples for GPC analysis. The GPC curves were obtained by the RI-detection method, which was calibrated with a series of polystyrene narrow standards (Polymer Laboratories).

3.2.11 Cyclic Voltammetry (CV)

Cyclic voltammograms (CV) were recorded using a Princeton Applied Research Model 263A Potentiostat/Galvanostat. Measurements were carried out under an inert argon atmosphere at 25 ± 2 °C. Tetrabutylammonium perchlorate ($TBAClO_4$) 10 cm^3 solution in acetonitrile (HPLC) (0.1 mol dm^{-3}) was used as the electrolyte solution.

A three electrode system was used consisting of an Ag/Ag^+ reference electrode (silver wire in 0.01 mol dm^{-3} silver nitrate solution in the electrolyte solution), a platinum working electrode (2 mm-diameter smooth platinum disc, area = 3.14×10^{-2} cm^2), and a platinum counter electrode (platinum wire). Polymer thin films were formed by drop casting 1.0 mm^3 of polymer solutions in dichloromethane (HPLC grade) (1 mg cm^{-3}) onto the working electrode, then dried in air.

Ferrocene was employed as a reference redox system according to IUPAC's recommendation.[190] Polymer thin films were formed by drop-casting 1.0 mm^3 of polymer solutions in dichloromethane (DCM) (analytical reagent, 1 mg cm^{-3}) onto the working electrode and dried in the air.

3.2.12 Purification *via* High Performance Liquid Chromatography (HPLC)

This technique was used because the normal purification methods such as column chromatography and recrystallisation, could not purify the crude product 5,6-bis(octyloxy)-4,7-di(thieno[3,2-*b*]thiophen-2-yl)benzo[*c*][1,2,5]thiadiazole At first, LC-MS analyses were performed using Waters LCT (ES) to identify the mixtures, then using HPLC technique, where the method of purification were developed on a system consisting of Waters 2690 Separation Module, Waters 2487 Dual λ Absorbance Detector and a reversed-phase HPLC column Altima HP C18 HL 5µ (length 150 mm, ID 4.6 mm). The solvent system consisted of 40 to 90 % THF in water over 20 min. The flow rate was 1 ml min^{-1}.

The purification process was carried out by using a preparative HPLC system consisting of Varian ProStar (two pumps, UV-Vis Detector), Varian Automatic Fraction Collector and a reversed-phase HPLC column Altima HP C18 HL 5µ (length 150 mm, ID 22 mm). The samples were prepared as solutions in THF (100 mg cm^{-3}), then (0.475 ml) of the sample solution was injected each time, the flow rate of the mobile phase was (20 ml min^{-1}).

The elution system (mobile phase) consisted of water (A) and THF (B), the following gradient was used: 60 % B for 33 min, then from 60 % to 95 % B for 1 min, then 95 % B for 6 min, then from 95 % to 60 % B for 1 min, then 60 % B for 9 min, the total time was 50 min per one injection. The pure compound was collected between 21 and 29 min.

3.3 Preparation of the Monomers

3.3.1 Heptadecan-9-ol (1)

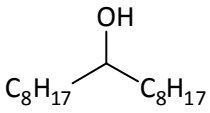

Synthesis of heptadecan-9-ol **(1)** was performed according to the procedure by Blouin et al.[20, 36, 191] Octylmagnesium bromide was firstly prepared by the drop-wise addition of 1-bromooctane (96.57 g, 500 mmol) in THF (155 ml) to a suspension of Mg (13.37 g, 550 mmol) in THF (260 ml). Ethyl formate (12.35 g, 167 mmol) was dissolved in THF (278 ml) and cooled to -78 °C. Octylmagnesium bromide was then added drop wise and stirred overnight at room temperature. Methanol and then a saturated NH_4Cl solution was added to quench the reaction, then extracted with diethyl ether (3 x 300 ml) and washed with a saturated NaCl solution. The organic layer was dried over $MgSO_4$ and solvent removed in *vacuo* to give the product **(1)** as white solid. Yield: 41.9 g (98 %). TLC: R_f = 0.53 in 40-60 petroleum ether/ethyl acetate (10:1). Melting point = 29-32 °C. ^{1}H NMR ($CDCl_3$), (δ_H/ppm): 3.65 (bm, 1H), 1.45 (m, 8H), 1.30 (m, 21H), 0.90 (t, *J* = 7.0 Hz, 6H). ^{13}C NMR ($CDCl_3$), (δ_C/ppm): 72.0, 53.5, 37.5, 31.9, 29.6, 29.3, 25.7, 22.7, 14.1. FT-IR (cm^{-1}): 3306, 2957, 2849, 2873, 2849, 1740. Mass (EI); (m/z): 254 (100 %); (calculated for $C_{17}H_{36}O$: 256.47). Elemental Analysis (%) calculated for $C_{17}H_{36}O$: C, 79.61; H, 14.15. Found: C, 81.11; H, 13.35.

3.3.2 9-Heptadecane-*p*-toluenesulfonate (2)

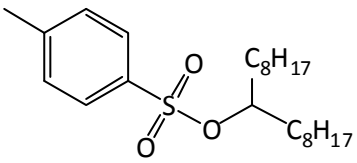

Synthesis of heptadecane-*p*-toluenesulfonate **(2)** was performed according to the procedure by Blouin *et al.*[36, 106] *p*-Toluenesulfonyl chloride (55.63 g, 292 mmol) in DCM (200

ml) was added to heptadecan-9-ol **(1)** (40.98 g, 160 mmol), Et_3N (49.33 g, 68 ml, 487 mmol) and $Me_3N.HCl$ (8.58 g, 0.19 mol) in DCM (200 ml) at 0 °C. The solution was stirred for 90 mins after which H_2O was added and the product extracted with DCM (3 x 300 ml). The organic phase was then washed with H_2O and brine and then dried over Na_2SO_4 the solvent was removed in vacuo to give the product as a low boiling point white solid. The product **(2)** was purified via silica gel column chromatography hexane/ethyl acetate (9:1), white solid. Yield: 70.0 g (88 %). TLC: R_f = 0.45 in hexane/ethyl acetate (9:1). Melting point = 33.5-35 °C. ^{1}H NMR ($CDCl_3$), (δ_H/ppm): 7.81 (d, *J* = 8.0 Hz, 2H), 7.34 (d, *J* = 8.0 Hz, 2H), 4.59-4.51 (m, 1H), 2.46 (s, 3H), 1.67-1.49 (m, 4H), 1.34-1.14 (m, 24H), 0.90 (t, *J* = 7.0 Hz, 6H). ^{13}C NMR ($CDCl_3$), (δ_C/ppm): 144.3, 134.8, 129.6, 127.7, 84.7, 34.1, 31.9, 29.7, 29.4, 29.2, 24.7, 22.7, 21.6, 14.1.FT-IR (cm^{-1}): 2954, 2922, 2851, 1742. Mass (EI); (m/z): 400, 405, 410 (100 %); (calculated for $C_{24}H_{42}O_3S$: 410.65). Elemental Analysis (%) calculated for $C_{24}H_{42}O_3S$: C, 70.19; H, 10.31; O, 11.69; S, 7.81. Found: C, 70.28; H, 10.84; S, 6.88.

3.3.3 4,4'-Dibromo-2,2'-dinitrobiphenyl (3)

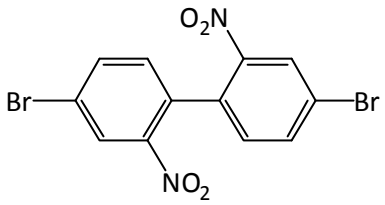

Synthesis of 4,4'-dibromo-2,2'-dinitrobiphenyl **(3)** was conducted using a modified procedure by Dierschke *et al.*[192] In a reaction vessel was placed 1,4-dibromo-2-nitrobenzene (89.30 g, 318 mmol), Cu powder (20.37 g, 321 mmol) and DMF (400 ml). The mixture was then heated at 120 °C for 3 h. The reaction mixture was cooled to ambient temperature, and then toluene (400 ml) was added and the mixture was stirred for a further 1 h at room temperature. The unreacted copper powder was then filtered off and the filtrate washed and extracted with a saturated solution of NaCl (3 × 400 ml). The organic layer was then dried over $MgSO_4$ and the remaining solvent was removed in vacuo. The crude product was then recrystallized from ethanol to afford **(3)** as yellow crystals. Yield: 111.0 g (87 %). TLC: R_f = 0.5 in 40-60 petroleum ether. Melting point: 115-120 °C. ^{1}H NMR ($CDCl_3$), (δ_H/ppm): 8.40 (d, *J* = 2.0 Hz, 2H), 7.85 (dd, *J* = 8.0, 2.0 Hz, 2H), 7.19 (d, *J* = 8.0 Hz, 2H). ^{13}C NMR ($CDCl_3$), (δ_C/ppm): 147.4, 136.7, 132.1, 132.0, 128.1, 122.9. FT-IR (cm^{-1}): 3085, 1780. Mass (EI); (m/z): 400, 402, 404; (calculated for $C_{12}H_6Br_2N_2O_4$: 402). Elemental

Analysis (%) calculated for $C_{12}H_6Br_2N_2O_4$: C, 35.85; H, 1.50; Br, 39.75; N, 6.97. Found: C, 35.95; H, 1.26; Br, 39.93; N, 6.89.

3.3.4 4,4'-Dibromobiphenyl-2,2'-diamine (4)

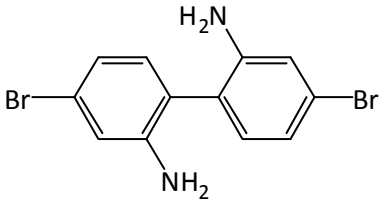

Synthesis of 4,4'-dibromobiphenyl-2,2'-diamine **(4)** was conducted using a modified procedure by Dierschke *et al.*[192] Into a reaction vessel under nitrogen were placed 4,4'-dibromo-2,2'-dinitrobiphenyl **(3)** (46.28 g, 115 mmol), tin powder (-100 mesh) (55.15 g, 465 mmol), ethanol (650 ml) and 32 wt % hydrochloric acid (250 ml). The reaction mixture was refluxed for 90 min. then it was cooled down to room temperature and a further portion of tin powder (55.15 g, 465 mmol) was added. The reaction mixture was then refluxed for a further period of 1 h, then cooled down to room temperature and the un-reacted tin powder filtered off. The resulting filtrate was then poured into a large amount of ice and 10 wt % NaOH aqueous solution (1000 ml). The solution was then extracted with diethyl ether (3 × 500 ml). The extracted diethyl ether solution was then dried over $MgSO_4$ and the solvent evaporated to dryness. The crude product was then re-crystallized from ethanol to afford the product **(4)** as a brown powder. Yield: 29.7 g (75 %). TLC: R_f = 0.29 in 40-60 petroleum ether/ethyl acetate (8:2). Melting point: 162-168 °C. ^{1}H NMR ($CDCl_3$), (δ_H/ppm): 6.99 (d, J = 6.0 Hz, 2H), 6.96 (d, J = 7.0 Hz, 2H), 6.90 (d, J= 8.5 Hz, 2H), 4.51-3.35 (bm, 4H). ^{13}C NMR ($CDCl_3$), (δ_C/ppm): 149.5, 138.2, 132.0, 131.0, 127.2, 121.5. FT-IR (cm^{-1}): 3419, 3390, 3281, 3175, 2159, 2033, 1875, 1627. Mass (EI+): *m/z* 342 (100 %); (calculated for $C_{12}H_{10}Br_2N_2$: 342.03). Elemental Analysis (%) calculated for $C_{12}H_{10}Br_2N_2$: C, 42.14; H, 2.95; Br, 46.72; N, 8.19. Found: C, 43.06; H, 2.69; Br, 44.92; N, 7.89.

3.3.5 2,7-Dibromo-*9H*-carbazole (5)

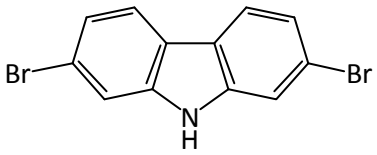

Synthesis of 2,7-dibromo-*9H*-carbazole **(5)** was performed according to the procedure by Blouin *et al.*[36] To 4,4'-dibromobiphenyl-2,2'-diamine **(4)** (20.30 g, 59.40 mmol) was added concentrated phosphoric acid (85 %) (400 ml) and the mixture heated at 190 °C for 24 h. The crude product was filtered and washed with water. The crude product was then solubilised in toluene and the solution filtered through a silica gel plug and dried over $MgSO_4$. The crude product was recrystalised from toluene/hexane (10:1) and was removed *in vacuo* to give a bright brown solid **(5)**. Yield: 17.5 g (91 %). TLC: R_f = 0.71 in 40-60 petroleum ether. Melting point: 245-245 °C. ^{1}H NMR ($CDCl_3$), (δ_H/ppm): 8.07 (s, 1H), 7.90 (d, *J* = 8.32 Hz, 2H), 7.60 (d, *J* = 1.48 Hz, 2H), 7.38 (dd, *J* = 8.32, 1.63 Hz, 2H). ^{13}C NMR ($CDCl_3$), (δ_C/ppm): 140.3, 123.3, 121.8, 121.5, 119.8, 113.8. FT-IR (cm^{-1}): 3828, 3393, 3073, 2511, 2161, 2030, 1891, 1711. Mass (EI); (m/z): 325 (100 %); (calculated for $C_{12}H_7Br_2N$: 325). Elemental Analysis (%) calculated for $C_{12}H_7Br_2N$: C, 44.35; H, 2.17; Br, 49.17; N, 4.31. Found: C, 44.28; H, 1.99; Br, 48.99; N, 4.25.

3.3.6 2,7-Dibromo-9-(heptadecan-9-yl)-*9H*-carbazole (6)

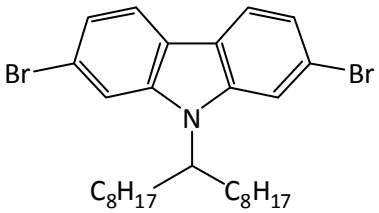

Synthesis of 2,7-dibromo-9-(heptadecan-9-yl)-*9H*-carbazole **(6)** was performed using a modified procedure by Blouin *et al.*[36] 2,7-Dibromo-*9H*-carbazole **(5)** (2.50 g, 7.69 mmol)and grinded KOH (3.00 g, 53.57 mmol) were dissolved in dried DMSO (100 ml). 9-Heptadecane-*p*-toluenesulfonate (**2**) (4.74 g, 11.54 mmol) dissolved in dried THF (20 ml) was added dropwise over 2 h at RT and the reaction was allowed to stir for overnight under nitrogen at temperature 45 °C. After which the reaction was poured onto distilled H_2O (300 ml), and the product extracted with hexane (3 x 300 ml). The combined organic fractions were dried

over $MgSO_4$ and the solvent removed in *vacuo*. The product was purified via silica gel column chromatography pre-absorbed onto silica gel dissolved in DCM and eluted with 40-60 petroleum ether and finally the product was recrytallised from methanol to give the product **(6)** as a white powder. Yield: 3.20 g (74 %). TLC: R_f = 0.72 in 40-60 petroleum ether. Melting point: 135-137 °C. ^{1}H NMR ($CDCl_3$), (δ_H/ppm): 7.90 (dd, *J* = 13.0, 8.5 Hz, 2H), 7.69 (s, 1H), 7.53 (s, 1H), 7.33 (t, *J* = 7.03 Hz, 2H), 4.46-4.37 (m, 1H), 2.25-2.13 (m, 4H), 1.96-1.83 (m, 4H), 1.32-1.04 (m, 18H), 1.03-0.89 (m, 2H), 0.83 (t, *J* = 7.03 Hz, 6H). ^{13}C NMR ($CDCl_3$), (δ_C/ppm): 142.9, 141.4, 139.4, 130.4, 129.9, 123.3, 121. 4, 119.74, 114.5, 113.8, 112.0, 57.0, 33.6, 31.7, 29.1, 26.7, 22.6, 14.1. FT-IR (cm^{-1}): 2951, 2919, 2850, 2158, 2030, 1622. Mass (EI+): *m/z* 561, 563, 565 ($M^{\bullet+}$); (calculated for $C_{29}H_{41}Br_2N$: 563.55). Elemental Analysis (%) calculated for $C_{29}H_{41}Br_2N$: C, 61.82; H, 7.33; Br, 28.36; N, 2.49. Found: C, 61.47; H, 7.28; Br, 28.4; N, 2.45.

3.3.7 9-(Heptadecan-9-yl)-2,7-bis(4,4,5,5-tetramethyl-1,3,2-dioxaborolan-2-yl)-*9H*-carbazole (7)

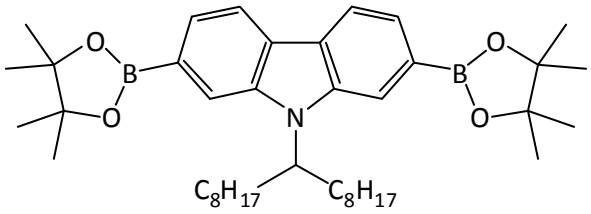

Synthesis of 9-(heptadecan-9-yl)-2,7-bis(4,4,5,5-tetramethyl-1,3,2-dioxaborolan-2-yl)-*9H*-carbazole **(7)** was performed using a modified procedure by Blouin *et al.*[36], Yamato *et al.*[193] and Sonntag *et al.*[194] 2,7-Dibromo-9-(heptadecan-9-yl)-*9H*-carbazole (**6**) (4.70 g, 8.34 mmol), bis(pinacolato)diboron (7.42 g, 29.21 mmol), potassium acetate (4.90 g, 49.93 mmol) and (diphenylphosphino) ferrocene palladium dichloride, $Pd(dppf)Cl_2$ (0.40 g, 0.49 mmol) in DMF (100 ml) was heated to 100 °C for 36 h. The reaction mixture was cooled to room temperature, then poured into H_2O (100 ml) and extracted with diethyl ether (3 × 100 ml). The organic phases were combined, then washed with H_2O (2 × 100 ml) and dried over $MgSO_2$. The crude product was purified *via* recrystallisation, the crude product was dissolved in the minimum amount of acetone and then precipitated in hot methanol which had been ran through a basic column. The product **(7)** was a white solid. Yield: 4.75 g (87 %). TLC: R_f = 0.45 in 40 - 60 petroleum ether/ ethyl acetate (10:1). Melting point: 141-

143°C. ^{1}H NMR ($CDCl_3$), (δ_H/ppm): 8.13 (t, J=8.5 Hz, 2H), 8.02 (S, 1H), 7.89 (S, 1H), 7.66 (d, J=5.5 Hz, 2H), 4.70(t, *J* = 5.0 Hz, 1H), 2.33 (m, 4H), 1.61 (m, 4H), 1.39 (S, 20H), 1.19 (br, 24 H), 0.98 (t, *J* = 6.5 Hz, 6H). ^{13}C NMR ($CDCl_3$), (δ_C/ppm): 142.0, 138.8, 126.4, 126.4, 126.3, 126.3, 126.2, 124.8, 119.8, 120.1, 118.2, 115.5, 83.8, 56.4, 33.9, 29.4, 26.9, 25.0, 22.6, 14.2. Mass (EI+): *m/z* 657; (calculated for $C_{41}H_{65}B_2NO_4$: 657.58). Elemental Analysis (%) calculated for $C_{41}H_{65}B_2NO_4$: C, 74.89; H, 9.96; B, 3.29; N, 2.13; O, 9.73. Found: C, 74.70; H, 10.13; N, 2.20.

3.3.8 Pentacosan-13-ol (8)

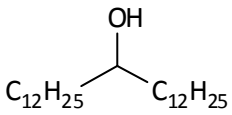

Synthesis of pentacosan-13-ol **(8)** was performed according to the procedure by Ashraf *et al.*[60] Dodecylmagnesium bromide was firstly prepared by the drop-wise addition of 1-bromododecane (125 g, 130 ml, 500 mmol) in THF (155 ml) to a suspension of Mg (13.37 g, 550 mmol) in THF (260 ml) under 0 °C and then the result mixture was heated 66 °C and stirred overnight. Ethyl formate (12.35 g, 167 mmol) was dissolved in THF (278 ml) and cooled to -78 °C. Dodecylmagnesium bromide was then added drop wise and stirred overnight at room temperature. Methanol and then a saturated NH_4Cl solution was added to quench the reaction, then extracted with diethyl ether (3 x 300 ml) and washed with a saturated NaCl solution. The organic layer was dried over $MgSO_4$ and solvent removed in *vacuo* to give the product **(8)** as white solid. Yield: 66.59 g (92 %). TLC: R_f = 0.53 in 40-60 petroleum ether. Melting point: 85-88 °C. ^{1}H NMR ($CDCl_3$), (δ_H/ppm): 3.67-3.50 (m, 1H), 1.44 (s, 1H), 1.28 (s, 44H), 0.90 (t, *J* = 7.0 Hz, 6H). ^{13}C NMR ($CDCl_3$), (δ_C/ppm): 72.0, 37.5, 31.9, 29.7, 29.7, 29.4, 25.7, 22.7, 14.1. FT-IR (cm^{-1}): 3308, 2956, 2914, 2848, 2159, 2022. Mass (EI); (m/z): 369 (100 %); (calculated for $C_{25}H_{52}O$: 368.68). Elemental Analysis (%) calculated for $C_{25}H_{52}O$: C, 81.44; H, 14.22; O, 4.34. Found: C, 81.51; H, 14.91.

3.3.9 Pentacosan-13-yl 4-methylbenzenesulfonate (9)

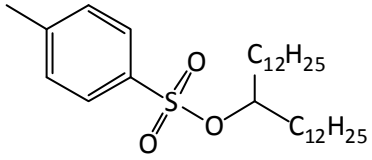

Synthesis of pentacosan-13-yl 4-methylbenzenesulfonate **(9)** was performed according to the procedure by Blouin *et al.*[36, 191] ***p***-Toluenesulfonyl chloride (55.63 g, 292 mmol) in DCM (200 ml) was added to pentacosan-13-ol **(8)** (52.69 g, 160 mmol), Et_3N (49.33 g, 68 ml, 487 mmol) and $Me_3N.HCl$ (8.58 g, 0.19 mol) in DCM (200 ml) at 0 °C. The solution was stirred for 90 mins after which H_2O was added and the product extracted with DCM (3 x 300 ml). The organic phase was then washed with H_2O and brine and then dried over Na_2SO_4 the solvent was removed in vacuo to give the product as a low melting point white solid. The product was purified via silica gel column chromatography 9:1 hexane/ethyl acetateto give **(9)** bright brown solid. Yield: 66.50 g (89 %). TLC: R_f = 0.45 in 40-60 petroleum ether/ethyl acetate (9:1). Melting point: 30-33 °C. ^{1}H NMR ($CDCl_3$), (δ_H/ppm): 7.81 (d, *J* = 8.5 Hz, 2H), 7.34 (d, *J* = 8.0 Hz, 2H), 4.60-4.50 (m, 1H), 2.45 (s, 3H), 1.65-1.48 (m, 4H), 1.23 (d, *J* = 15.5 Hz, 40H), 0.96-0.88 (m, 6H). ^{13}C NMR ($CDCl_3$), (δ_C/ppm): 144.2, 134.9, 129.6, 127.7, 84.6, 34.1, 31.9, 29.4, 24.7, 22.7, 22.6, 21.6, 14.1. FT-IR (cm^{-1}): 2954, 2917, 2849, 2158, 2029. Mass (EI+): *m/z* 545 (MNa^+); (calculated for $C_{32}H_{58}O_3S$: 522.87). Elemental Analysis (%) calculated for $C_{32}H_{58}O_3S$: C, 73.51; H, 11.18; S, 6.13. Found: C, 74.19; H, 11.87; S, 5.90.

3.3.10 2,7-Dibromo-9-(pentacosan-13-yl)-*9H*-carbazole (10)

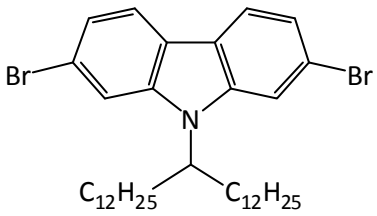

Synthesis of 2,7-dibromo-9-(pentacosan-13-yl)-*9H*-carbazole **(10)** was performed using a modified procedure by Blouin *et al.*[36] In the round bottom flask 2,7-dibromo-*9H*-carbazole **(5)** (5.00 g, 15.38 mmol) and KOH (4.31 g, 76.9 mmol) were dissolved in dried DMSO (100 ml). Pentacosan-13-yl 4-methylbenzenesulfonate **(9)** (12.06 g, 23.08 mmol) dissolved in dried THF (20 ml) was added dropwise over 2 h at temperature 40 °C and the reaction was

allowed to stir for overnight. After which the reaction was poured onto distilled H_2O (300 ml), and the product extracted with hexane (3 x 300 ml). The combined organic fractions were dried over $MgSO_4$ and the solvent removed in *vacuo*. The product was purified via silica gel column chromatography pre-absorbed onto silica gel dissolved in DCM and eluted with petroleum-ether 40-60 to give the product **(10)** as a white crystal. Yield: 7.20 g (69 %). TLC: R_f = 0.78 in 40-60 petroleum ether. Melting point: 58-63 °C. ^{1}H NMR ($CDCl_3$), (δ_H/ppm): 7.92 (q, *J* = 13.5, 8.5 Hz, 2H), 7.72 (s, 1H), 7.56 (s, 1H), 7.35 (t, *J* = 7.0 Hz, 2H), 4.50-4.38 (m, 1H), 2.30-2.13 (m, 4H), 1.99-1.86 (m, 4H), 1.40-1.08 (m, 36H), 0.94-0.83 (m, 6H). ^{13}C NMR ($CDCl_3$), (δ_C/ppm): 144.3, 134.8, 129.6, 127.7, 123.0, 122.3, 121.3, 119.61, 114.5, 114.0, 84.8, 57.0, 34.1, 31.6, 29.3, 24.7, 22.7, 21.6, 14.1. FT-IR (cm^{-1}): 2952, 2917, 2848, 2159, 1864, 1622. Mass (EI+): *m/z* 676.2 (100 %); (calculated for $C_{37}H_{57}Br_2N$: 675.66). Elemental Analysis (%) calculated for $C_{37}H_{57}Br_2N$: C, 65.77; H, 8.50; Br, 23.65; N, 2.07. Found: C, 66.47; H, 9.04; Br, 23.61; N, 1.99.

3.3.11 1,4-Dibromo-2-fluoro-5-nitrobenzene (11)

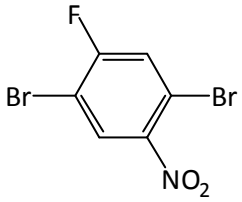

Synthesis of 1,4-dibromo-2-fluoro-5-nitrobenzene **(11)** was performed according to a modified procedure by Kun *et al.*[182, 188] 1,4-Dibromo-2-fluorobenzene (100.00 g, 0.394 mol) was dissolved in a mixture of DCM (300 ml)/trifluoroacetic acid (300 ml)/trifluoroacetic anhydride (150 ml). The solution was cooled using an ice bath to 0 °C and then ammonium nitrate (38.80 g, 0.485 mol) was added slowly with stirring. The mixture was allowed to warm to room temperature and left stirring overnight. Then the reaction was poured onto ice and the product was extracted with DCM (3 x 200 ml). The solution was dried over $MgSO_4$ and solvent removed in *vacuo* to give the crude product as a yellow solid. This was then recrystallised from ethanol and yellow crystals were obtained and dried in vacuo to give **(11)**. Yield: 95.10 g (81 %). TLC: R_f = 0.67 in DCM/hexane (1:1). Melting point: 59.5-62.5 °C. ^{1}H NMR ($CDCl_3$), (δ_H/ppm): 8.21 (d, $J_{H\text{-}F}$ = 6.5 Hz, 1H), 7.56 (d, $^3J_{H\text{-}F}$ = 7.5 Hz, 1H). ^{13}C NMR ($CDCl_3$), (δ_C/ppm): 161.9, 159.3 (d, $J_{C\text{-}F}$ = 258.5 Hz), 146.1, 130.9, 123.0, 122.7 (d, $J_{C\text{-}F}$ = 26.5 Hz), 114.9, 108.8 (d, $J_{C\text{-}F}$ = 23.0 Hz). ^{19}F NMR ($CDCl_3$), (δ_F/ppm): -97.13 (dd, $J_{F\text{-}H}$ = 7.5 Hz). FT-

IR (cm^{-1}): 3091, 3021, 2033, 1760, 1585, 1567, 1526. Mass (EI+): *m/z* 297, 299, 300 (M•+); (calculated for $C_6H_2Br_2FNO_2$: 298.89). Elemental Analysis (%) calculated for $C_6H_2Br_2FNO_2$: C, 24.11; H, 0.67; Br, 53.57; F, 6.36; N, 4.69; O, 10.71. Found: C, 24.15; H, 0.45; N, 4.46; Br, 53.32.

3.3.12 4,4'-dibromo-5,5'-difluoro-2,2'-dinitrobiphenyl (12)

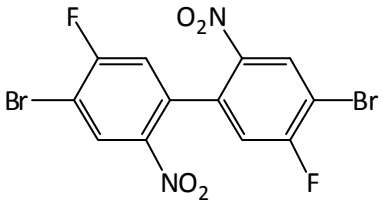

Synthesis of 4,4'-dibromo-5,5'-difluoro-2,2'-dinitrobiphenyl **(12)** was obtained from a modified procedure by Kun *et al.*[182] In a reaction vessel was placed 1,4-dibromo-2-fluoro-5-nitrobenzene **(11)** (95.10 g, 0.318 mol), Cu powder (20.37 g, 0.320 mol) and DMF (400 ml). The mixture was then heated at 120 °C for 3 h. The reaction mixture was cooled to ambient temperature, and then toluene (400 ml) was added and the mixture was stirred for a further 1 h at room temperature. The unreacted copper powder was then filtered off and the filtrate washed and extracted with a saturated solution of NaCl (3 × 400 ml). The organic layer was then dried over $MgSO_4$ and the remaining solvent was removed in vacuo. The crude product was then recrystallized from ethanol to afford 4,4'-dibromo-5,5'-difluoro-2,2'-dinitrobiphenyl **(12)** as yellow crystals. Yield: 110.0 g (79 %). TLC: R_f = 0.56 in 40-60 petroleum ether/ethyl acetate (8:2). Melting point: 114.5-115.2 °C. ^{1}H NMR ($CDCl_3$), (δ_H/ppm): 8.57 (d, J_{H-F} = 6.0 Hz, 2H), 7.09 (d, J_{H-F} = 7.5 Hz, 2H). (Multiple and broad proton peaks are due to the phenomenon of atropisomerism). ^{13}C NMR ($CDCl_3$), (δ_C/ppm): 162.0 (d, J_{C-F} = 258.5 Hz), 159.5, 143.3, 143.0, 135.4, 134.0, 133.9, 130.4, 129.1, 121.3, 119.2 (d, J_{C-F} = 25.5 Hz, 2C), 109.1 (d, J_{C-F} = 23.0 Hz). (Multiple carbon peaks are due to the phenomenon of atropisomerism). ^{19}F NMR ($CDCl_3$), (δ_F/ppm): -95.91 (dd, J_{F-H} = 7.0 Hz). FT-IR (cm^{-1}): 3104, 3071, 2106, 1609, 1564, 1520. Mass (EI+): *m/z* 436, 438, 440 (M•+); (calculated for $C_{12}H_4Br_2F_2N_2O_4$: 437.98). Elemental Analysis (%) calculated for $C_{12}H_4Br_2F_2N_2O_4$: C, 31.43; H, 1.58; Br, 41.82; O, 8.37; S, 16.78. Found: C, 33.32; H, 0.83; N, 6.33; Br, 36.40.

3.3.13 4,4'-Dibromo-5,5'-difluorobiphenyl-2,2'-diamine (13)

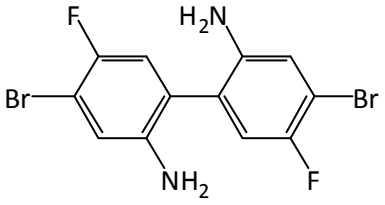

Synthesis of 4,4'-dibromo-5,5'-difluorobiphenyl-2,2'-diamine **(13)** was undertaken following on modified procedure by Kun *et al.*[182] Into a reaction vessel under nitrogen were placed 4,4'-dibromo-5,5'-difluoro-2,2'-dinitrobiphenyl **(12)** (20.00 g, 45.77 mmol), tin powder (-100 mesh) (21.68 g, 182.64 mmol), ethanol (360 ml), and 32 wt % hydrochloric acid (45 ml). The reaction mixture was refluxed for 90 min. then it was cooled down to room temperature and a further portion of tin powder (21.68 g, 182.64 mmol) was added. The reaction mixture was then refluxed for a further period of 1 h, then cooled down to room temperature and the un-reacted tin powder filtered off. The resulting filtrate was then poured into a large amount of ice and 10 wt % NaOH aqueous solution (1000 ml). The solution was then extracted with diethyl ether (3 × 400 ml). The extracted diethyl ether solution was then dried over $MgSO_4$ and the solvent evaporated to dryness. The crude product was then re-crystallized from ethanol to afford the product **(13)** as a pale brown powder. Yield: 15.8 g (92 %). TLC: R_f = 0.45 in 40-60 petroleum ether/ethyl acetate (8:2). Melting point: 162.1-168 °C. ^{1}H NMR ($CDCl_3$), (δ_H/ppm): 7.00 (d, J_{H-F} = 6.0 Hz, 2H), 6.90 (d, $^3J_{H-F}$ = 9.0 Hz, 2H), 3.71 (b, 4H). (Multiple and broad proton peaks are due to the phenomenon of atropisomerism). ^{13}C NMR ($CDCl_3$), (δ_C/ppm): 152.6 (d, J_{C-F} = 238.0 Hz), 150.2, 140.0, 118.7, 116.82(d, J_{C-F} = 23.0 Hz), 108.3 (d, J_{C-F} = 21.5 Hz). (Multiple carbon peaks are due to the phenomenon of atropisomerism). ^{19}F NMR ($CDCl_3$), (δ_F/ppm): -120.83 (dd, J_{F-H} = 5.0 Hz; 3.0 Hz). FT-IR (cm^{-1}): 3407, 3191, 2963, 2159, 2032, 1742, 1620. Mass (EI+): *m/z* 376, 378, 380 (M•+), (calculated for $C_{12}H_8Br_2F_2N_2$: 378.01). Elemental Analysis (%) calculated for $C_{12}H_8Br_2F_2N_2$: C, 38.13; H, 2.13; Br, 42.28; F, 10.05; N, 7.41. Found: C, 38.72; H, 2.04; N, 7.47; Br, 42.34.

3.3.14 2,7-Dibromo-3,6-difluoro-*9H*-carbazole (14)

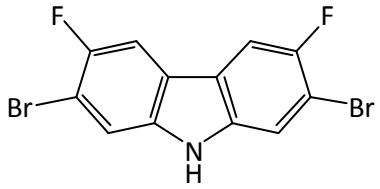

Synthesis of 2,7-dibromo-3,6-difluoro-*9H*-carbazole **(14)** was performed according to the procedure by Kun *et al.*[182] To 4,4-dibromo-5,5-difluoro-biphenyl-2,2-diamine **(13)** (10.00 g, 26.45 mmol) was added concentrated phosphoric acid (85 %) (220 ml) and the mixture heated at 190 °C for 24 h. The crude product was filtered and washed with water. The crude product was then solubilised in toluene and the solution filtered through a silica gel plug and dried over $MgSO_4$. The solvent was removed in vacuo to give a pale orange solid. The crude product was recrystalised from toluene/hexane (10:1) to give the product **(14)** as an ivory powder. Yield: 7.80 g (82 %). TLC: R_f = 0.43 in 40-60 petroleum ether/ethyl acetate (8:2). Melting point: 257.5-261.5 °C. ^{1}H NMR (Acetone-d_6), (δ_H/ppm): 10.7 (br, 1H), 8.1 (d, $J_{H\text{-}F}$ = 10.0 Hz, 2H), 7.86 (d, $J_{H\text{-}F}$ = 6.0 Hz, 2H). ^{13}C NMR (Acetone-d_6), (δ_C/ppm): 206.0, 155.1, 152.8 (d, $J_{C\text{-}F}$ = 234.0 Hz), 138.8, 116.4, 108.11 (d, $J_{C\text{-}F}$ = 21.0 Hz), 68.1, 26.2. ^{19}F NMR (Acetone-d_6), (δ_F/ppm): -119.94 (dd, $J_{F\text{-}H}$ = 15.0 Hz; 3.0 Hz). FT-IR (cm^{-1}): 3453, 3101, 3075, 3043, 2962. Mass (EI); (m/z): 359, 361 (100 %), 362 (M•+).; (calculated for $C_{12}H_5Br_2F_2N$: 360.98). Elemental Analysis (%) calculated for $C_{12}H_5Br_2F_2N$: C, 41.43; H, 1.58; Br, 41.82; O, 8.37; S, 16.78. Found: 40.82; H, 1.50; N, 3.80; Br, 44.33.

3.3.15 2,7-Dibromo-3,6-difluoro-9-(heptadecan-9-yl)-*9H*-carbazole (15)

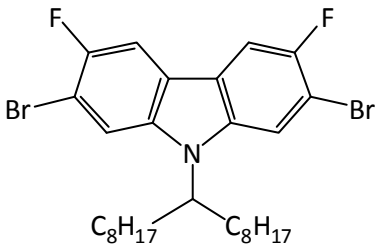

Synthesis of 2,7-dibromo-3,6-difluoro-9-(heptadecan-9-yl)-*9H*-carbazole **(15)** was performed according to a modified procedure by Blouin *et al.*[36] 2,7-Dibromo-3,6-difluoro-*9H*-carbazole **(14)** (4.00 g, 11.08 mmol) and grinded KOH (3.00 g, 53.57 mmol) were

dissolved in dried DMSO (100 ml). 9-Heptadecane *p*-toluenesulfonate **(2)** (7.00 g, 17.05 mmol) dissolved in dried THF (20 ml) was added dropwise over 2 h at room temperature and the reaction was allowed to stir for overnight under nitrogen at temperature 45 °C. After which the reaction was poured onto distilled H_2O (300 ml), and the product extracted with hexane (3 x 300 ml). The combined organic fractions were dried over $MgSO_4$ and the solvent removed in *vacuo*. The product was purified via silica gel column chromatography pre-absorbed onto silica gel dissolved in DCM and eluted with petroleum-ether 40-60 to give the product **(15)** as a white powder. Yield: 5.80 g (87 %). TLC: R_f = 0.48 in 40-60 petroleum ether. Melting point: 55.5 - 58.5 °C. ^{1}H NMR ($CDCl_3$), (δ_H/ppm): 7.73 (bm, 2H), 7.57 (d, J_{H-F} = 4.5 Hz, 2H), 4.39 (m, 1H), 2.19 (bm, 2H), 1.92 (bm, 2H), 1.18 (bm, 20H), 0.95 (bm, 4H), 0.85 (t, J = 7.0 Hz, 6H). ^{13}C NMR ($CDCl_3$), (δ_C/ppm): 154.0 (d, J_{C-F} = 235.0 Hz), 139.5, 135.9, 122.6, 121.3, 115.6, 113.4, 107.4 (bm), 106.9 (d, J_{C-F} = 24.0 Hz), 57.3, 33.5, 31.7, 31.1, 29.2, 29.1, 26.7, 22.6, 14.0. ^{19}F NMR ($CDCl_3$), (δ_F/ppm): -118.83 (d, J_{F-H} = 122.5 Hz, 2F). FT-IR (cm^{-1}): 2920, 2852, 1600, 1570. Mass (EI+): *m/z* 597, 599, 601 (M•+), (calculated for $C_{29}H_{39}Br_2F_2N$: 599.43). Elemental Analysis (%) calculated for $C_{29}H_{39}NF_2Br_2$: C, 58.11; H, 6.56; N, 2.34; Br, 26.66. Found: C, 58.63; H, 6.75; N, 2.24; Br, 26.13.

3.3.16 3,6-Difluoro-9-(heptadecan-9-yl)-2,7-bis(4,4,5,5-tetramethyl-1,3,2-dioxaborolan-2-yl)-*9H*-carbazole (16)

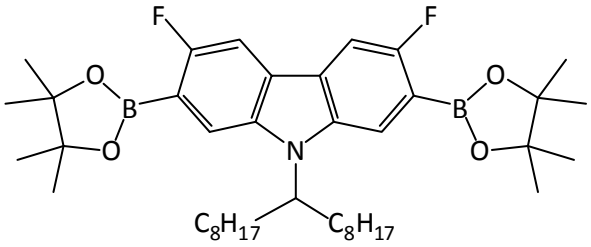

Synthesis of 3,6-difluoro-9-(heptadecan-9-yl)-2,7-bis(4,4,5,5-tetramethyl-1,3,2-dioxaborolan-2-yl)-*9H*-carbazole **(16)** was performed following a modified procedure by Blouin *et al.*[36] A 250 ml one necked flask under nitrogen containing 2,7-dibromo-3,6-difluoro-9-(1-octyl-nonyl)-*9H*-carbazole **(15)** (5.00 g, 8.34 mmol), bis(pinacolato)diboron (7.42 g, 29.21 mmol), potassium acetate (4.90 g, 49.93 mmol) and Pd(dppf)Cl_2 (0.40 g, 0.49 mmol) in DMF (100 ml) was heated to 100 °C for 36 h. The reaction mixture was cooled to room temperature, then poured into H_2O (100 ml) and extracted with diethyl ether (3 ×

100 ml). The organic phases were combined, then washed with H_2O (2 × 100 ml) and dried over $MgSO_2$. The crude product was purified *via* recrystallisation, the crude product was dissolved in the minimum amount of acetone and then precipitated in hot methanol which had been ran through a basic column. The product **(16)** was a light brown solid. Yield: 3.5 g (60 %). Melting point: 138.5-142 °C. ^{1}H NMR ($CDCl_3$), (δ_H/ppm): 7.89 (s, 1H), 7.80-7.71 (m, 1H), 7.67 (d, J_{H-F} = 9.0 Hz, 2H), 4.67-4.56 (m, 1H), 2.36-2.22 (bm, 2H), 2.00-1.87 (m, 2H), 1.59-1.43 (s, 24H), 1.30-1.09 (m, 20H), 1.03-0.91 (m, 4H), 0.84 (t, J = 7.0 Hz, 6H). ^{13}C NMR ($CDCl_3$), (δ_C/ppm): 161.0 (d, J_{C-F} = 294.0 Hz), 157.6 (d, J_{C-F} = 29.5 Hz), 155.7, 139.4, 136.0, 131.8, 128.4, 126.3, 124.8, 119.0, 116.5, 114.2, 106.0 (d, J_{C-F} = 25.0 Hz), 83.9, 56.5, 33.8, 31.8, 29.4, 29.3, 29.2, 26.6, 24.9, 22.6, 14.1. ^{19}F NMR ($CDCl_3$), (δ_F/ppm): -116.33 (d, 2F, J_{F-H} = 100.0 Hz). FT-IR (cm^{-1}): 2924, 2854, 1611, 1569. Mass (EI+): m/z 692 (100 %); (calculated for $C_{41}H_{63}B_2F_2NO_4$: 693.56). Elemental Analysis (%) calculated for $C_{41}H_{63}B_2F_2NO_4$: C, 71.00; H, 9.16; B, 3.32; N, 2.02. Found: C, 71.39; H, 9.25; N, 1.99.

3.3.17 2,7-Dibromo-3,6-difluoro-9-(pentacosan-13-yl)-*9H*-carbazole (17)

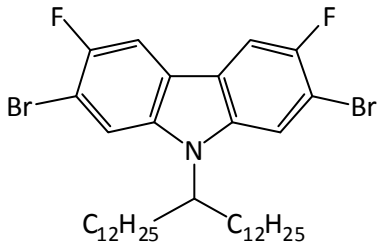

Synthesis of 2,7-dibromo-3,6-difluoro-9-(pentacosan-13-yl)-*9H*-carbazole **(17)** was performed using a modified procedure by Blouin *et al.*[36] In the round bottom flask 2,7-dibromo-3,6-difluoro-*9H*-carbazole **(14)** (3.78 g, 7.69 mmol) and grained flakes KOH (3.00 g, 53.58 mmol) were dissolved in dried DMSO (100 ml). Pentacosan-13-yl 4-methylbenzenesulfonate **(8)** (6.50 g, 11.54 mmol) dissolved in dried THF (20 ml) was added dropwise over 2 h at 40 °C and the reaction was allowed to stir for overnight. After which the reaction was poured onto distilled H_2O (300 ml), and the product extracted with hexane (3 x 300 ml). The combined organic fractions were dried over $MgSO_4$ and the solvent removed in vacuo. The product was purified via silica gel column chromatography pre-absorbed onto silica gel dissolved in DCM and eluted with 40-60 petroleum ether to give the product **(17)** as a bright brown crystal. Yield: 4.0 g (73 %). TLC: R_f = 0.66 in 40-60 petroleum ether. Melting point: 33-35 °C. ^{1}H NMR ($CDCl_3$), (δ_H/ppm): 7.72 (t, J_{H-F} = 10.0 Hz,

2H), 7.54 (d, J_{H-F} = 4.5 Hz, 2H), 4.42-4.32 (m, 1H), 2.22-2.10 (m, 4H), 1.95-1.84 (m, 4H), 1.32-1.07 (m, 34H), 0.99-0.89 (m, 2H), 0.90-0.82 (m, 6H). ^{13}C NMR ($CDCl_3$), (δ_C/ppm): 154.0 (d, J_{C-F} = 239.0 Hz), 139.5, 135.9, 122.6, 121.3, 115.6, 113.4, 106.9 (d, J_{C-F} = 24.0 Hz), 57.3, 33.5, 31.7, 31.1, 29.2, 29.1, 26.7, 22.6, 14.0. ^{19}F NMR ($CDCl_3$), (δ_F/ppm): -118.83 (d, 2F, $_{JH-F}$ = 122.5 Hz). FT-IR (cm^{-1}): 2916, 2848, 2159, 2029, 1600. Mass (EI+): *m/z* 711 (100 %); (calculated for $C_{37}H_{55}Br_2F_2N$: 711.64). Elemental Analysis (%) calculated for $C_{37}H_{55}Br_2F_2N$: C, 62.45; H, 7.79; Br, 22.46; F, 5.34; N, 1.97. Found: C, 62.59; H, 7.84; Br, 22.71; N, 1.91.

3.3.18 3-Bromothiophene-2-carbaldehyde (18)

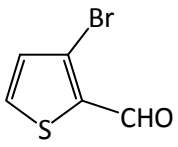

Synthesis of 3-bromothiophene-2-carbaldehyde **(18)** was obtained from a modified procedure by Fuller *et al.*[195] 3-Bromothiophene (20.00 g, 123 mmol) was added dropwise to a stirred solution of lithium diisopropylamide (LDA) [prepared by addition of butyllithium (1.6 mol dm^{-3} in hexane; 76.7 ml, 123 mmol) to diisopropylamine (17.2 ml, 12.42 g, 122.7 mmol)] in tetrahydrofuran (250 ml) at 0 °C and the resulting mixture was stirred for a further 1 h at this temperature prior to addition of 1-formylpiperidine (13.62 ml, 13.88 g, 123 mmol). The mixture was stirred further until TLC analysis indicated that all the starting material had been consumed (24 h) when an excess of 20 % aqueous ammonium chloride (200 ml) was added to it. The product was purified by flash column silica gel chromatography using a mixture of 40-60 petroleum ether/ethyl acetate (9:1). Extraction of the mixture with ether (3 x 100 ml) gave bright yellow oil 3-bromothiophene-2-carbaldehyde **(18).** Yield: 19.85 g (85 %). TLC: R_f = 0.41 in 40-60 petroleum ether/dichloromethane (9:1). Boiling point: 113-115 °C. ^{1}H NMR ($CDCl_3$), (δ_H/ppm): 9.98 (d, J=6.0, 1H), 7.73 (dd, J=6.5 Hz, 1H), 7.16 (d, J=5.0 Hz, 1H). ^{13}C NMR ($CDCl_3$), (δ_C/ppm): 183.1, 137.0, 134.9, 132.1, 120.4. FT-IR (cm^{-1}): 1734. Mass (EI+): *m/z* 189 (100 %), 190 ($M^{\bullet+}$); (calculated for C_5H_3BrOS: 191.05). Elemental analysis (%) calculated for C_5H_3BrOS: C, 31.43; H, 1.58; Br, 41.82; S, 16.78. Found: C, 31.56; H, 1.62; Br: 41.55; S, 16.91.

3.3.19 Ethyl thieno[3,2-b]thiophene-2-carboxylate (19)

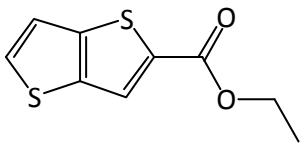

Synthesis of ethyl thieno[3,2-b]thiophene-2-carboxylate **(19)** was obtained according to the procedure by Fuller *et al*.[195] 3-Bromothiophene-2-carbaldehyde **(18)** (13.38 g, 70 mmol) was added to a stirred mixture of ethyl 2-sulfanylacetate (8.42 g, 7.68 ml, 70 mmol), potassium carbonate (13.00 g) and *N*,*N*-dimethylformamide (130 ml) at ambient temperature and the resulting mixture was stirred for a further 72 h under a N_2 atmosphere. Then it was poured into water (150 ml) and extracted with dichloromethane. The combined extracts were dried ($MgSO_4$), filtered and distillation of the solvents under reduced pressure gave the yellow liquid *ester* (**19).** Yield: 13.00 g (81 %). TLC: R_f = 0.44 in petroleum ether/ethyl acetate (9:1). Boiling point: 120-125 °C. ^{1}H NMR ($CDCl_3$), (δ_H/ppm): 8.01 (s, 1H), 7.60 (d, J = 5.5 Hz, 1H), 7.30 (d, J = 5.5 Hz, 1H), 4.40 (q, J = 7.0 Hz, 2H), 1.41 (t, J = 7.0 Hz, 3H).^{13}C NMR ($CDCl_3$), (δ_C/ppm): 162.6, 143.9, 138.7, 135.1, 131.7, 125.6, 119.7, 61.5, 14.4. FT-IR (cm^{-1}): 1707. Mass (EI+): *m/z* 213 (100.0%); (calculated for $C_9H_8O_2S_2$: 212.29). Elemental Analysis (%) calculated for $C_9H_8O_2S_2$: C, 50.92; H, 3.80; S, 30.21. Found: C, 48.26; H, 4.11; S, 28.18.

3.3.20 Thieno[3,2-*b*]thiophene-2-carboxylic acid (20)

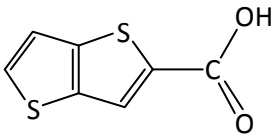

Synthesis of thieno[3,2-*b*]thiophene-2-carboxylic acid **(20)** was obtained from a modified the procedure by Fuller *et al.*[195] A stirred mixture of the ester, ethyl thieno[3,2-*b*]thiophene-2-carboxylate **(19)** (8.50 g, 40 mmol), aqueous lithium hydroxide (1.0 mol dm^{-3}; 85 ml) and THF (85 ml) was heated (100 °C) under reflux with stirring for 3 h (until TLC analysis indicated absence of starting material) when the solvent was distilled off under reduced pressure and concentrated hydrochloric acid (170 ml) was added to the residue. The precipitate was filtered off and washed with water (3 x 150 ml). Then, the toluene (200

ml) was used in order to dry the product. The crude product was obtained after evaporation of the solvents and provided the white solid acid **(20)**. Yield: 6.60 g (89 %). TLC: R_f = 0.6 in petroleum ether:ethyl acetate (9:1). Melting point: 218-220 °C. ^{1}H NMR ($CDCl_3$), (δ_H/ppm): 8.12 (s, 1H), 7.67 (d, J = 5.5 Hz, 1H), 7.34 (d, J = 5.5 Hz, 2H). ^{13}C NMR ($CDCl_3$), (δ_C/ppm): 167.3, 145.2, 138.9, 133.7, 132.6, 127.3, 119.8. FT-IR (cm^{-1}): 1672. Mass (EI+): *m/z* 183 (100 %); (calculated for $C_7H_4O_2S_2$: 184.24). Elemental Analysis (%) calculated for $C_7H_4O_2S_2$: C, 45.63; H, 2.19; S, 34.81. Found: C, 45.08; H, 2.24; S, 33.97.

3.3.21 1,2-Bis(2,2-diethoxyethyl)disulfane (21)

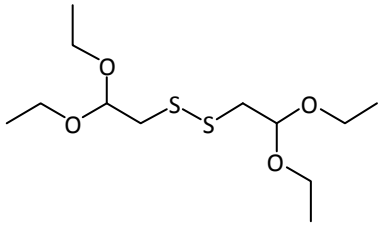

Synthesis of 1,2-bis(2,2-diethoxyethyl)disulfide, **(21)** was obtained from a modified the procedure by Henssler and Matzger.[196] A 5000 ml three necked flask under nitrogen containing sodium sulfide (237.78 g, 0.99 mol), sulfur (39.60 g, 1.23 mol), potassium iodide (9.88 g, 0.06 mol), and 2-bromo-1,1-diethoxyethane (243.38 g, 186 ml, 1.24 mol) were added to stirring ethanol (2000 ml) and heated to reflux overnight. After removing the majority of ethanol by distillation, salts were removed by pouring the residue into a Buchner funnel fitted with filter paper, followed by rinsing with ethyl acetate (3 x 500 ml). The filtrate was washed with water (3 x 300 ml) and then the aqueous layers were combined and extracted with ethyl acetate. The organic layers were combined and washed with brine and then dried over anhydrous Na_2SO_4. The bright crude yellow oily product **(21)** was obtained after filtration and evaporation of solvents. Yield: 260 g, (88 %). TLC: R_f = 0.74 in 40-60 petroleum ether/ethyl acetate (5:1). ^{1}H NMR ($CDCl_3$), (δ_H/ppm): 4.70 (t, J = 5.5 Hz, 2H), 3.71-3.63 (m, 2H), 3.60-3.53 (m, 2H), 2.95 (d, J = 5.5 Hz, 4H), 2.75 (d, J = 5.5 Hz, 4H), 1.31 (t, J = 7.0 Hz, 12H). ^{13}C NMR ($CDCl_3$), (δ_C/ppm): 103.2, 101.5, 62.0, 43.0, 35.6, 15.3.
FT-IR (cm^{-1}): 2975, 2929, 2877. Mass (EI+): *m/z* 299 (100 %); (calculated for $C_{12}H_{26}O_4S_2$: 298.46). Elemental Analysis (%) calculated for $C_{12}H_{26}O_4S_2$: C, 48.29; H, 8.78; S, 21.49. Found: C, 48.04; H, 7.06; S, 19.98.

3.3.22 3-(2,2-diethoxy-ethylsulfanyl)thiophene (22)

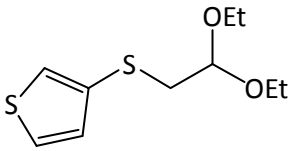

Synthesis of 3-(2,2-diethoxy-ethylsulfanyl)thiophene **(22)** was obtained from a modified procedure by Henssler and Matzger.[196] In a dry flask, 1.7 M *tert*-butyllithium in pentane (88.20 ml, 0.15 mol) was added dropwise to a solution of 3-bromothiophene (12.15 g, 0.075 mol) in ether (500 ml) at -78 °C under a N_2 atmosphere. After stirring for 30 min at this temperature, 1,2-bis(2,2-diethoxyethyl)disulfide **(21)** (22.35 g, 0.075 mol) was added dropwise and the reaction mixture was allowed to warm to room temperature followed by stirring for 10 h. The reaction mixture was quenched with water and the organic layer was washed three times with 1 M aqueous NaOH and then with brine. After drying the organic layer over anhydrous Na_2SO_4 the solvent was removed in *vacuo* to obtain yellow solid **(22).** Yield: 15.14 g (87 %). TLC: R_f = 0.6 in 40-60 petroleum ether. Melting point: 287 - 289 °C. ^{1}H NMR ($CDCl_3$), (δ_H/ppm): 7.32 (dd, J = 5.0, 3.02 Hz, 1H), 7.21 (dd, J = 3.0, 1.28 Hz, 1H), 7.07 (dd, J = 5.0, 1.29 Hz, 1H), 4.72 (t, J = 5.5 Hz, 1H), 3.78-3.62 (m, 4H), 2.97 (d, J = 5.5 Hz, 2H), 1.23 (t, J = 7.0 Hz, 6H). ^{13}C NMR ($CDCl_3$), (δ_C/ppm): 129.8, 126.1, 123.6, 101.5, 62.2, 58.4, 43.0, 38.7, 18.4, 15.1. FT-IR (cm^{-1}): 3101, 2972, 2928, 2880, 2155, 2029, 1974, 1753, 1713, 1665, 1595, 1506. Mass (EI); (m/z): 232 (100 %), 233 ; (calculated for $C_{10}H_{16}O_2S_2$: 232.36). Elemental Analysis (%) calculated for $C_{10}H_{16}O_2S_2$: C, 51.69; H, 6.94; S, 27.60. Found: C, 50.02; H, 6.01; S, 28.22.

3.3.23 Thieno[3,2-*b*]thiophene (23)

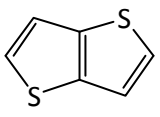

The synthesis of **(23)** was performed using three different methods.

Method 1

Synthesis of thieno[3,2-*b*]thiophene **(23)** was obtained from a modified the procedure by Fuller *et al.*[195] A stirred solution of the acid **(20)** (8.80 g, 48 mmol), copper powder (1.76 g)

and quinoline (80 ml) was heated at 260 °C using a heating-metal. When no further bubbles of carbon dioxide gas could be seen escaping from the mixture (2 h) the reaction mixture was cooled to ambient temperature. TLC analysis confirmed the absence of starting material. Diethyl ether (100 ml) was added to the mixture and most of the quinoline was removed by repeated washing of the resulting solution with hydrochloric acid (1.0 mol dm^{-3}). The crude product did not give a clear spot on TLC. Therefore the purification of the crude product was abandoned.

Method 2

The synthesis of (6) was performed by following a procedure of GooBen *et al.*[197] An oven-dried vessel was charged with **(20)** (1.00 g, 5.43 mmol), Cu_2O (38.84 mg, 0.27 mmol), and 4,7-diphenyl-1,10-phenanthroline (107.6 mg, 0.54 mmol). After purging the vessel with alternating vacuum and nitrogen cycles, a degassed solution of *N*-methyl-2-pyrrolidone (NMP) (8.15 ml) and quinoline (2.72 ml) was added via syringe. The resulting mixture was stirred for 24 h at 170 °C, poured into aqueous HCl (5N, 2.0 ml), and extracted repeatedly with diethyl ether. The combined organic layers were washed with brine, dried over $MgSO_4$ and filtered. The crude product did not give a clear spot on TLC. Therefore the purification of the crude product was abandoned.

Method 3

Synthesis of thieno[3,2-*b*]thiophene **(23)** was obtained from a modified the procedure by Henssler and Matzger.[196] A 100 ml one necked flask under nitrogen containing Anhydrous amberlyst 15 ion exchange resin (11.40 g, 53.52 mmol) was added to a stirring solution of 3-(2,2-diethoxy-ethylsulfanyl)thiophene **(22)** (10.80 g, 46.55 mmol) in ether (250 ml) and the reaction mixture was heated to reflux for 10 h. The solution was then decanted and poured through a buchner funnel fitted with filter paper. Fresh ether was added to the Amberlyst beads and brought to reflux in order to extract the residual product. This solution was combined with the reaction mixture upon decanting through the buchner funnel. After removing the solvent in *vacuo* the residue was purified by column chromatography on silica gel, eluting with 40-60 petroleum ether. Yield: 6.40 g (98 %). TLC: R_f = 0.5 in 40-60 petroleum ether. Melting point: 55-56 °C. ^{1}H NMR ($CDCl_3$), (δ_H/ppm): 7.42 (d, J = 5.0 Hz, 2H), 7.30 (d, J = 5.0 Hz, 2H). ^{13}C NMR ($CDCl_3$), (δ_C/ppm): 139.4, 127.3, 119.4.

FT-IR (cm^{-1}): 3098, 2954, 2922, 2849. Mass (EI+): m/z 140 (100 %), (calculated for $C_6H_4S_2$: 140.23). Elemental analysis (%) calculated for $C_6H_4S_2$: C, 51.39; H, 2.88; S, 45.73. Found: C, 51.35; H, 2.57; S, 45.74.

3.3.24 2,5-Dibromothieno[3,2-*b*]thiophene (24)

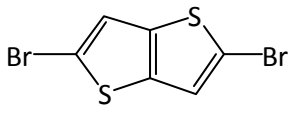

Synthesis of 2,5-dibromothieno[3,2-*b*]thiophene **(24)** was obtained from a modified procedure by Liu *et al*.[198] To a stirred solution of thieno[3,2-*b*]thiophene **(23)** (1.51 g, 10.80 mmol) in a mixture of dichloromethane (25 ml) and acetic acid (12 ml) in a round bottom flask was slowly added NBS (3.84 g, 21.60 mmol) in small portions over a period of 40 min. After the addition, the mixture was stirred at room temperature for 3 h until TLC showed no starting material left. The mixture was washed twice with aqueous $NaHCO_3$ solution (5 %) and three times with water, dried with anhydrous magnesium sulphate, and filtered. The product was recrystallized by ethanol and was obtained after evaporation of the solvent and dried in *vacuo*, resulting **(24)** a white solid. Yield: 3.03 g (94 %). TLC: R_f = 0.64 in 40-60 petroleum ether. Melting point: 124 - 129 °C. ^{1}H: 7.20 (s, 2H). ^{13}C NMR ($CDCl_3$), (δ_C/ppm): 138.3, 121.8, 113.6. FT-IR (cm^{-1}): 3088, 1748, 1619. Mass (EI+): m/z 298 (100 %); (calculated for $C_6H_2Br_2S_2$: 298.02). Elemental Analysis (%) calculated for $C_6H_2Br_2S_2$: C, 24.18; H, 0.68; Br, 53.62; S, 21.52. Found: C, 20.83; H, 0.41; Br, 59.44; S, 11.30.

3.3.25 2-(Tributylstannyl)thieno[3,2-*b*]thiophene (25)

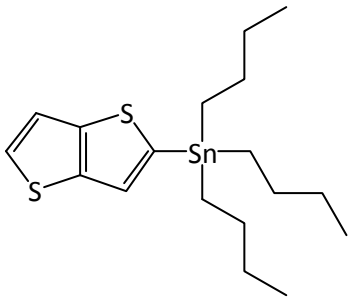

Synthesis of 2-(tributylstannyl)thieno[3,2-*b*]thiophene **(25)** was obtained from a modified procedure by Prim and Kirsch.[161] In a dry flask 2.5 M butyllithium in hexanes (2.86 ml, 7.2 mmol) was added dropwise to a solution of the thieno[3,2-*b*]thiophene **(23)** (1.01 g, 7.2 mmol) in THF (100 ml) at -78 °C under a N_2 atmosphere. After 1 h of stirring at this temperature, neat tributylstannyl chloride (2.33 g, 7.2 mmol) was added dropwise within 2 h. The solution was stirred for overnight and then, the mixture was poured into water and extracted with diethyl ether. The organic layer was washed twice with water and dried and then the solvent removed under reduced pressure and get compound **(25)** as white crystals. Yield: 2.8 g (91 %). TLC: R_f = 0.5 in 40-60 petroleum ether. Melting point: 45-50 °C. ^{1}H NMR ($CDCl_3$), (δ_H/ppm): 7.37 (d, *J* = 5.0 Hz, 1H), 7.26 (d, *J* = 5.0 Hz, 1H), 3.80-3.74 (m, 1H), 1.70-1.55 (m, 6H), 1.44-1.31 (m, 6H), 1.20-1.11 (m, 6H), 0.98-0.85 (m, 9H). ^{13}C NMR ($CDCl_3$), (δ_C/ppm): 143.7, 139.5, 139.0, 125.3, 124.9, 117.3, 66.3, 60.2, 27.5, 27.3, 27.2, 26.2, 25.7, 25.5, 25.4, 24.0, 12.0, 9.3. FT-IR (cm^{-1}): 2918, 2849, 1692, 1648, 1592, 1577, 1466, 1404. Mass (EI+): m/z 430 (100 %); (calculated for $C_{18}H_{30}S_2Sn$: 429.27). Elemental Analysis (%) calculated for $C_{18}H_{30}S_2Sn$: C, 50.36; H, 7.04; S, 14.94; Sn, 27.65. Found: C, 50.25; H, 8.39; S, 8.83.

3.3.26 Trimethyl(thieno[3,2-*b*]thiophen-2-yl)stannane (26)

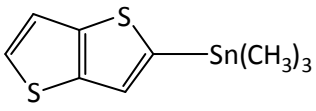

Synthesis of trimethyl(thieno[3,2-*b*]thiophen-2-yl)stannane **(26)** was obtained from a modified procedure by Prim and Kirsch.[161] In a dry flask 1.6 M butyllithium in hexanes (36 ml, 57.60 mmol) was added dropwise to a solution of the thieno[3,2-*b*]thiophene **(23)** (5.00 g, 35.70 mmol) in dried THF (180 ml) at -78 °C under an argon atmosphere and the resulting mixture was stirred for further 30 min at this temperature. Then the 1.0 M solution of trimetylstannyl chloride in hexanes (38.00 ml, 38.00 mmol) was added dropwise to the resulted mixture. The solution was stirred overnight at room temperature. Then, the mixture was poured into water and extracted with diethyl ether. The organic layer was washed twice with water and dried and then the solvent removed under reduced pressure to afford compound **(26)** as white crystals. Yield: 10.68 g (98 %). TLC: R_f = 0.56 in 40-60 petroleum ether. Melting point: 52-56 °C. ^{1}H NMR ($CDCl_3$), (δ_H/ppm): 7.40 (d, *J* = 5.0 Hz,

1H), 7.43 (d, *J* = 5.0 Hz, 1H), 7.3 (s, 1H), 0.55-0.36 (m, 9H). ^{13}C NMR ($CDCl_3$), (δ_C/ppm): 145.2, 141.3, 127.3, 126.4, 119.0, 68.0, 65.9, 25.7, 15.3. FT-IR (cm^{-1}): 3626, 2955, 2921, 2870, 2360, 2338, 1974, 1942, 1505. Mass (EI+): m/z 302, 304 (100 %); (calculated for $C_9H_{12}S_2Sn$: 303.03). Elemental Analysis (%) calculated for $C_9H_{12}S_2Sn$: C, 35.67; H, 3.99; S, 21.16; Sn, 39.17. Found: C, 37.51; H, 3.84; S, 22.57.

3.3.27 1,2-Bis(octyloxy)benzene (27)

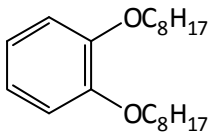

Synthesis of 1,2-bis(octyloxy)benzene **(27)** was obtained from a modified procedure by Petersen *et al*.[199] To a mixture of pyrocatechol (20.00 g, 181.64 mmol), 1-bromooctane (65.64 ml, 1.118 g/ml, 379.97 mmol) and potassium carbonate K_2CO_3 (76.00 g, 549.80 mmol) was added dry DMF (100 ml). Then the mixture was stirred under N_2 overnight at 100 °C. Water (200 ml) was added and the organic layer was separated. The aqueous layer was extracted with DCM (3 x 100 ml) and the combined organic phases were washed with water (5 x 200 ml) to remove DMF. Then it was dried over $MgSO_4$ and the solvent was removed in *vacuo*. The crude product was purified by recrystallisation from methanol to obtain 1,2-bis(octyloxy)benzene **(27)** as white needle crystals. Yield: 58.0 g (95 %). TLC: R_f = 0.61 in 40-60 petroleum ether/ethyl acetate (10:1). Melting point: 24.5-26 °C. ^{1}H NMR ($CDCl_3$), (δ_H/ppm): 6.89 (s, 4H), 4.02 (t, *J* = 7.0 Hz, 4H); 1.88-1.31 (m, 24H); 0.91 (t, *J* = 7.0 Hz, 6H). ^{13}C NMR ($CDCl_3$), (δ_C/ppm): 148.3, 120.0, 113.2, 68.3, 52.4, 30.8, 28.4, 28.3, 25.1, 21.7, 13.1. FT-IR (cm^{-1}): 3064, 2953, 2922, 2870, 2848, 2751, 1593, 1518, 1507. Mass (EI+): m/z 334.0 (100 %); (calculated for $C_{22}H_{38}O_2$: 334.53). Elemental Analysis (%) calculated for $C_{22}H_{38}O_2$: C, 78.99; H, 11.45; O, 9.57. Found: C, 78.11; H, 12.38.

3.3.28 1,2-Dinitro-4,5-bis-octyloxy-benzene (28)

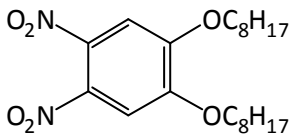

Synthesis of 1,2-dinitro-4,5-bis(octyloxy)benzene **(28)** was obtained from a modified procedure by Petersen *et al*.[199] To a two neck round-bottom flask containing dichloromethane (240 ml), acetic acid (240 ml), and 1,2-bis(octyloxy)benzene **(27)** (20.00 g, 59.78 mmol) cooled to 10 °C was added dropwise 65 % nitric acid (40 ml). The reaction was allowed to warm to room temperature and stirred for 1 h. The mixture was again cooled to 10 °C and 100% nitric acid (80 ml) was added dropwise. The mixture was allowed to warm to room temperature and the mixture was stirred for 40 h. Then, the reaction mixture was poured into ice-water and was extracted with DCM. The combined organic phase was washed with water, saturated $NaHCO_3$, brine and dried over $MgSO_4$. Concentration in vacuum gave the crude yellow solid product that was recrystallized from ethanol. Yield: 23.5 g (93 %). TLC: R_f = 0.52 in 40-60 petroleum ether. Melting point = 86.5-88 °C. ^{1}H NMR ($CDCl_3$), (δ_H/ppm): 7.32 (s, 2H), 4.12 (t, J = 6.5 Hz, 4H), 1.93-1.85 (m, 4H), 1.54-1.46 (m, 4H), 1.44-1.26 (m, 16H), 0.91 (t, J = 7.0 Hz, 6H). ^{13}C NMR ($CDCl_3$), (δ_C/ppm): 151.8, 136.5, 107.9, 70.2, 31.8, 29.2, 28.7, 25.8, 22.6, 14.1. FT-IR (cm^{-1}): 3124, 3071, 2955, 2921, 2853, 2024. Mass (EI); (m/z): 424; (calculated for $C_{22}H_{36}N_2O_6$: 424.53). Elemental Analysis (%) calculated for $C_{22}H_{36}N_2O_6$: C, 62.24; H, 8.55; N, 6.60; O, 22.61. Found: C, 62.19; H, 8.47; N, 6.51.

3.3.29 4,5-Bis(octyloxy)benzene-1,2-diaminium chloride (29)

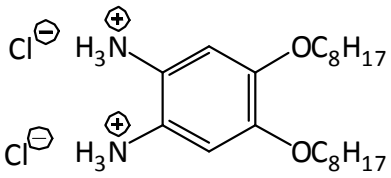

Synthesis of 4,5-bis(octyloxy)benzene-1,2-diaminium chloride **(29)** was obtained from a modified the procedure by Petersen *et al*.[199] A mixture of 1,2-dinitro-4,5-bis(octyloxy)benzene **(28)** (4.00 g, 9.422 mmol) and Sn(II)Cl_2 (14.29g, 75.376 mmol) in ethanol (50 ml) and concentrated HCl (20 ml) was heated to 85 ^{o}C over the night. After cooling to room temperature the product was filtered and washed with water and methanol. Finally it was dried at room temperature under a stream of argon to afford the product as a pale yellow solid which was used directly in the next synthetic step. Yield: 4.0 g (97 %). TLC: R_f = 0.45 in 40-60 petroleum ether. Melting point: 60-65.5 °C. ^{1}H NMR ($CDCl_3$), (δ_H/ppm): 6.71 (s, 2H), 3.84 (t, *J* = 6.0 Hz, 4H), 1.70 - 1.63 (m, 4H), 1.42-1.26 (m, 20H), 0.86 (t, *J* = 6.5 Hz, 6H). ^{13}C NMR ($CDCl_3$), (δ_C/ppm): 145.0, 122.0, 107.9, 69.0, 31.2, 28.7, 25.5,

22.0, 13.8. FT-IR (cm^{-1}): 2918, 2849, 1530, 1499. Mass (EI); 364, 365, 366 (M^+) (m/z): (calculated for $C_{22}H_{42}Cl_4N_2O_2^{2-}$: 508.39). The Cl^- is unable to fly so it was not detected by Mass (EI+) analysis. Elemental Analysis (%) calculated for $C_{22}H_{42}Cl_4N_2O_2^{2-}$: C, 51.97; H, 8.33; Cl, 27.89; N, 5.51. Found: C, 52.10; H, 8.52; N, 5.42; Cl, 15.56.

3.3.30 5,6-Bis(octyloxy)benzo[c][1,2,5]thiadiazole (30)

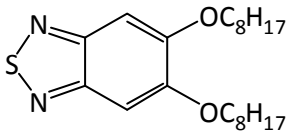

Synthesis of 5,6-bis(octyloxy)benzo[*c*][1,2,5]thiadiazole **(30)** was obtained from a modified the procedure by Petersen *et al*.[199] To a solution of 4,5-bis(octyloxy)benzene-1,2-diammonium chloride **(29)** (4.80 g, 10.97 mmol) and triethylamine Et_3N (122 ml) in dry DCM (122 ml) was added dropwise a solution of thionylchloride (3.80 ml, 30.0 mmol) in dry DCM (12 ml). Then, the reaction mixture was heated to reflux for 6 hours. The mixture was cooled and concentrated then triturated in water for one hour. The crude product was filtered and recrystallised from ethanol to obtain 5,6-bis(octyloxy)benzo[c][1,2,5]thiadiazole **(30)** as a pale brown solid. Yield: 3.7 g (90 %). Melting point: 96-98 °C. ^{1}H NMR ($CDCl_3$), (δ_H/ppm): 7.15 (s, 2H), 4.11 (t, *J* = 6.5 Hz, 4H), 1.98-1.87 (m, 4H), 1.59-1.27 (m, 20H), 0.91 (t, *J* = 7.0 Hz, 6H). ^{13}C NMR ($CDCl_3$), (δ_C/ppm): 154.2, 151.4, 98.4, 69.1, 31.8, 29.3, 29.3, 28.7, 26.0, 22.7, 14.1. FT-IR (cm^{-1}): 3087, 3053, 2956, 2917, 2872, 2849. Mass (EI); (m/z): 394, 393, 392 (100 %); (calculated for $C_{22}H_{36}N_2O_2S$: 392.60). Elemental Analysis (%) calculated for $C_{22}H_{36}N_2O_2S$: C, 67.30; H, 9.24; N, 7.14; S, 8.17. Found: C, 66.23; H, 9.33; N, 7.55; S, 7.87.

3.3.31 4,7-Dibromo-5,6-bis(octyloxy)benzo[*c*][1,2,5]thiadiazole (31)

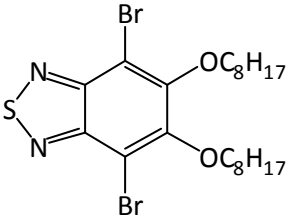

Synthesis of 4,7-dibromo-5,6-bis(octyloxy)benzo[*c*][1,2,5]thiadiazole **(31)** was obtained from a modified procedure by Petersen *et al.*[199] To a solution of 5,6-bis(octyloxy)benzo[*c*][1,2,5]thiadiazole **(30)** (2.50 g, 6.37 mmol) in a mixture of dichloromethane (130 ml) and acetic acid (60 ml) was added bromine (5.0 ml, 97.5 mmol), and the resulting mixture was stirred in the dark for 48 h at room temperature. The mixture was then poured in water (500 ml), extracted with dichloromethane, sequentially washed with water, saturated $NaHCO_3$ (aq), 1M Na_2SO_3 (aq) and the solvents are evaporated under reduced pressure. The crude product was purified by recrystallization from ethanol twice to give fluffy needle-like microcrystals. Yield: 2.90 g (83 %). TLC: R_f = 0.72 in hexane. Melting point = 45.5-47 °C. ^{1}H NMR ($CDCl_3$), (δ_H/ppm): 4.18 (t, *J* = 7.0 Hz, 4H), 1.96 - 1.84 (m, 4H), 1.58-1.31 (m, 20H), 0.91 (t, *J* = 6.5 Hz, 6H). ^{13}C NMR ($CDCl_3$), (δ_C/ppm): 154.5, 150.3, 106.2, 75.1, 31.8, 30.3, 29.4, 29.3, 26.0, 22.7, 14.1. FT-IR (cm^{-1}): 2955, 2922, 2873, 2848, 2159, 2030, 1590. Mass (EI+): (m/z) 550, 551, 552 (M•+); (calculated for $C_{22}H_{34}Br_2N_2O_2S$: 550.39). Elemental Analysis (%): calculated for $C_{22}H_{34}Br_2N_2O_2S$: C, 48.01; H, 6.23; N, 5.09; Br, 29.04; S, 5.83. Found: C, 48.01; H, 6.13; N, 5.07; Br, 29.15; S, 5.98.

3.3.32 5,6-Bis(octyloxy)-4,7-di(thieno[3,2-*b*]thiophen-2-yl)benzo[*c*][1,2,5] thiadiazole (32)

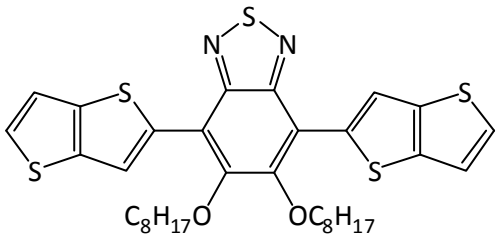

Synthesis of 5,6-bis(octyloxy)-4,7-di(thieno[3,2-*b*]thiophen-2-yl)benzo[*c*][1,2,5]thiadiazole **(32)** was obtained from a modified procedure by Ding *et al.*[152] A mixture of 4,7-dibromo-5,6-bis(octyloxy)benzo[*c*][1,2,5] thiadiazole **(31)** (1.00 g, 1.817 mmol) and trimethyl(thieno[3,2-*b*]thiophen-2-yl)stannane **(26)** (2.11 g, 6.963 mmol) were introduced to a round bottom flask under argon. To the mixture was added toluene (5 ml) and the mixture was degassed. To this mixture was added $Pd(PPh_3)_2Cl_2$ (0.10 g, 0.142 mmol) under an inert argon atmosphere and then degassed and heated to 110 °C for 72 h. The crude product which was purified by open column chromatography on silica and used 40-60 petroleum ether:ethyl acetate: triethylamine (4 : 1 : 0.03) to eluted compound **(32)** as an orange solid. Yield: 1.24 g (84 %). TLC: R_f = 0.74 in 40-60 petroleum ether/ethyl acetate

(9:1). Melting point: 80 - 82 °C. ^{1}H NMR ($CDCl_3$), (δ_H/ppm): 8.86 (s, 2H), 7.50 (d, *J* = 5.0 Hz, 2H), 7.37 (d, *J* = 5.0 Hz, 2H), 4.21 (t, *J* = 7.0 Hz, 4H), 2.06-1.99 (m, 4H), 1.54-1.48 (m, 4H), 1.45-1.26 (m, 16H), 0.98-0.91 (m, 6H). ^{13}C NMR ($CDCl_3$), (δ_C/ppm): 152.0, 150.9, 141.4, 139.3, 136.3, 128.3, 123.0, 119.4, 118.1, 74.7, 31.8, 30.4, 29.5, 29.3, 26.0, 22.7, 14.1. FT-IR (cm^{-1}): 3119, 3079, 3006, 2950, 2915, 2850, 2357, 2319, 1727. Mass (EI+): *m/z* 670, 669, 668 (100 %); (calculated for $C_{34}H_{40}N_2O_2S_5$: 669.01). Elemental Analysis (%) calculated for $C_{34}H_{40}N_2O_2S_5$: C, 61.04; H, 6.03; N, 4.19; O, 4.78; S, 23.96. Found: C, 59.74; H, 5.73; N, 3.91; S, 23.80.

3.3.33 4,7-Bis(5-bromothieno[3,2-*b*]thiophen-2-yl)-5,6-bis(octyloxy)benzo[*c*] [1,2,5] thiadiazole (33)

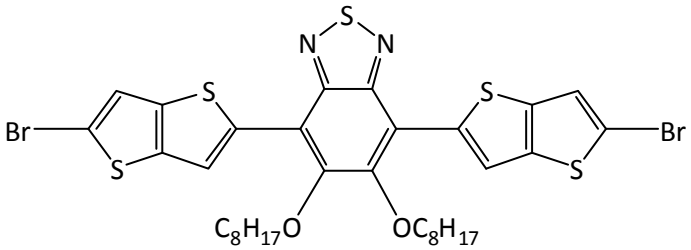

Synthesis of 4,7-bis(5-bromothieno[3,2-*b*]thiophen-2-yl)-5,6-bis(octyloxy)benzo[*c*][1,2,5] thiadiazole **(33)** was obtained from a modified procedure by Ding *et al*.[152] A mixture of 5,6-bis(octyloxy)-4,7-di(thieno[3,2-*b*]thiophen-2-yl)benzo[*c*][1,2,5]thiadiazole **(32)** (618 mg, 0.923 mmol), NBS (337 mg, 1.892 mmol) and chloroform (15 ml) was degassed and stirred in dark for 48 h at room temperature. A further amount of chloroform (10 ml) was added and the mixture stirred for 1 h. The formed precipitate was filtered then washed with water (150 ml) to obtain 4,7-bis(5-bromothieno[3,2-*b*]thiophen-2-yl)-5,6-bis(octyloxy)benzo[*c*][1,2,5] thiadiazole **(33)** as a bright red solid. Yield: 652 mg (85 %). TLC: R_f = 0.5 in 40-60 petroleum ether/toluene (8:2). Melting point: 125-127 °C. ^{1}H NMR ($CDCl_3$), (δ_H/ppm): 8.74 (s, 2H), 7.32 (s, 2H), 4.16 (t, *J* = 7.0 Hz, 4H), 2.03-1.95 (m, 4H), 1.53-1.43 (m, 4H), 1.42-1.27 (m, 16H), 0.93 (t, *J* = 7.0 Hz, 6H). ^{13}C NMR ($CDCl_3$), (δ_C/ppm): 151.8, 150.6, 140.2, 139.5, 135.6, 134.6, 122.2, 117.7, 114.7, 74.8, 31.8, 30.4, 29.5, 29.3, 26.0, 22.7, 14.1. FT-IR (cm^{-1}): 3122, 2917, 2850, 2159, 1972, 1561. Mass (EI+): *m/z* 826 (100 %); (calculated for $C_{34}H_{38}Br_2N_2O_2S_5$: 826.81). Elemental Analysis (%) calculated for $C_{34}H_{38}Br_2N_2O_2S_5$: C, 49.39; H, 4.63; Br, 19.33; N, 3.39; O, 3.87; S, 19.39. Found: C, 48.81; H, 4.61; Br, 19.18; N, 3.31; S, 19.59.

3.3.34 4,7-Dibromobenzo[*c*][1,2,5]thiadiazole (34)

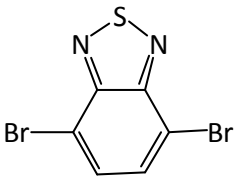

Synthesis of 4,7-dibromobenzo[*c*][1,2,5]thiadiazole **(34)** was obtained from a modified procedure by Edelmann *et al.*[52] A mixture of 2,1,3-benzothiadiazole (20.00 g, 147 mmol) and hydrobromic acid HBr (48 %, 60 ml) was heated under N_2 to 100 °C with stirring before Br_2 (22.60 ml, 440 mmol) was added dropwise over a period of one hour. The product started precipitating then a further amount of HBr (40 ml) was added to facilitate stirring and allowed the mixture to stir under reflux for further 2 hours. The hot reaction mixture was filtered and the precipitate washed with distilled water several time. Then the filtrate was cooled to precipitate further product, filtered and the solid washed with water. The filtrate was poured onto a solution of sodium thiosulphate $Na_2S_2O_3$ (10 % w/w) to destroy the remaining bromine. The obtained orange solid product was recrystallised from ethanol and then recrystallised from a mixture of chloroform/hexane (2:1) to obtain 4,7-dibromo-2,1,3-benzothiadiazole **(34)** as pale yellow solid (needle-like micro-crystals). Yield: 39.5 g (91 %). TLC: R_f = 0.4 in 40-60 petroleum ether. Melting point: 188-191 °C. ^{1}H NMR ($CDCl_3$), (δ_H/ppm): 7.71 (s, 2H). ^{13}C NMR ($CDCl_3$), (δ_C/ppm): 153.1, 132.4, 114.0. FT-IR (cm^{-1}): 3078, 3033, 1857, 1661, 1595. Mass (EI); (m/z): 294 (100 %); (calculated for $C_6H_2Br_2N_2S$: 293.97). Elemental Analysis (%) calculated for $C_6H_2Br_2N_2S$: C, 24.51; H, 0.69; Br, 54.36; N, 9.53; S, 10.91. Found: C, 24.53; H, 0.48, N, 9.35, S 11.04.

3.3.35 4,7-Di(thieno[3,2-*b*]thiophen-2-yl)benzo[*c*][1,2,5]thiadiazole (35)

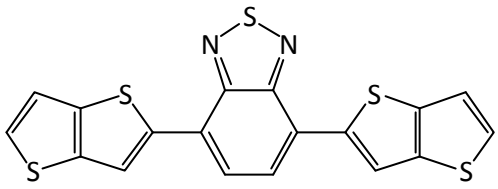

Synthesis of 4,7-di(thieno[3,2-*b*]thiophen-2-yl)benzo[*c*][1,2,5]thiadiazole **(35)** was obtained from a modified procedure by Sun *et al.*[200] A mixture of 4,7-

dibromobenzo[*c*][1,2,5]thiadiazole **(34)** (1.00 g, 3.50 mmol) and trimethyl(thieno[3,2-*b*]thiophen-2-yl)stannane **(26)** (3.09 g, 10.20 mmol) were introduced to a round bottom flask under argon. To the mixture was added toluene (5 ml) and the mixture was degassed. To this mixture was added $Pd(PPh_3)_2Cl_2$ (100 mg, 0.142 mmol) under an inert argon atmosphere and then degassed and heated to 110 °C for 72 h. The crude product was purified by open column chromatography on silica using 40-60 petroleum ether/ethyl acetate/triethylamine (4 : 1 : 0.03) and eluted compound **(35)** was obtained as an orange powder. Yield: 1.20 g (85 %). TLC: R_f = 0.60 in 40-60 petroleum ether/ethyl acetate (4:1). Melting point: 140-144 °C. ^{1}H NMR ($CDCl_3$), (δ_H/ppm): 8.53 (s, 2H), 7.91 (s, 2H), 7.48 (d, *J* = 5.0 Hz, 2H), 7.34 (d, *J* = 5.0 Hz, 2H). ^{13}C NMR ($CDCl_3$), (δ_C/ppm): 154.2, 138.2, 131.2, 129.6, 128.4, 122.8, 121.9, 120.6, 119.6. FT-IR (cm^{-1}): 3073, 2917, 2849, 1568. Mass (EI); (m/z): 412 (100 %); (calculated for $C_{18}H_8N_2S_5$: 412.59). Elemental Analysis (%) calculated for $C_{18}H_8N_2S_5$: C, 52.40; H, 1.95; N, 6.79; S, 38.86. Found: C, 50.40; H, 2.55; N, 7.77; S, 42.01.

3.3.36 4,7-Bis(5-bromothieno[3,2-*b*]thiophen-2-yl)benzo[*c*][1,2,5]thiadiazole (36)

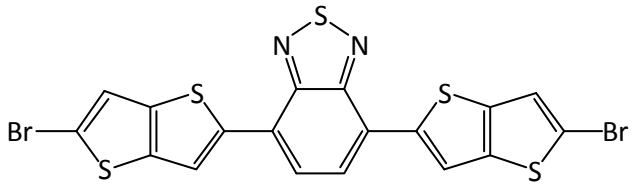

Synthesis of 4,7-bis(5-bromothieno[3,2-*b*]thiophen-2-yl)benzo[*c*][1,2,5]thiadiazole **(36)** was obtained from a modified procedure by Ding *et al.*[152] A mixture of 4,7-di(thieno[3,2-*b*]thiophen-2-yl)benzo[*c*][1,2,5]thiadiazole **(35)** (209 mg, 0.51 mmol), NBS (180 mg, 1.01 mmol) and chloroform (10 ml) was degassed and stirred in dark for 48 h at room temperature. A further amount of chloroform (10 ml) was added and the mixture stirred for 1 h. The formed precipitate was filtered then washed with water (100 ml), ethanol (100 ml), acetone (100 ml) and diethyl ether (100 ml) to obtain insoluble 4,7-bis(5-bromothieno[3,2-*b*]thiophen-2-yl)benzo[*c*][1,2,5]thiadiazole **(36)** as a red solid. Yield: 170 mg (59 %). FT-IR (cm^{-1}): 3092, 2159, 2000, 1851, 1773, 1702. Elemental analysis (%) calculated for $C_{18}H_6Br_2N_2S_5$: C, 37.90; H, 1.06; Br, 28.02; N, 4.91; S, 28.11. Found: C, 39.86; H, 0.94; Br, 26.30; N, 5.07; S, 22.54.

3.3.37 9-(Heptadecan-9-yl)-2,7-di(thieno[3,2-*b*]thiophen-2-yl)-9*H*-carbazole (37)

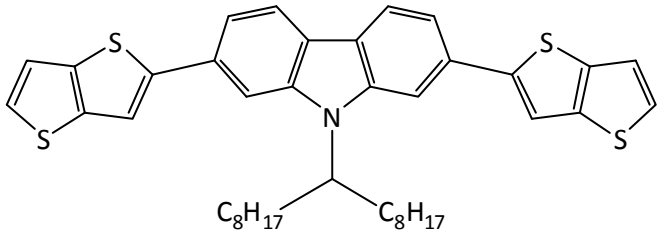

Synthesis of 9-(heptadecan-9-yl)-2,7-di(thieno[3,2-b]thiophen-2-yl)-9H-carbazole **(37)** was obtained from a modified procedure by Kowalski *et al*.[149] A mixture of 2,7-dibromo-9-(heptadecan-9-yl)-*9H*-carbazole **(6)** (1.30 g, 2.32 mmol), trimethyl(thieno[3,2-*b*]thiophen-2-yl)stannane **(26)** (2.11 g, 6.96 mmol), and bis(triphenylphosphine)-palladium(II)dichloride ($Pd(PPh_3)_2Cl_2$) (120 mg, 0.171 mmol) was stirred in toluene (5 ml) under an inert argon atmosphere and then degassed and heated to 110 °C for 72 h. After cooling to room temperature the mixture was poured into water and extracted with dichloromethane. The solution was concentrated by rotary evaporation and the residue was purified via silica gel column chromatography 40-60 petroleum-ether/tolene (10:1). The product was dried in vacuo to give 9-(heptadecan-9-yl)-2,7-di(thieno[3,2-b]thiophen-2-yl)-9H-carbazole **(37)** as a dark yellow oily. Yield: 900 mg (57 %). TLC: R_f = 0.37 in 40-60 petroleum ether/ethyl acetate (10:1). Melting point: 45-47 °C. ^{1}H NMR ($CDCl_3$), (δ_H/ppm): 8.09 (dd, *J* = 11.0, 8.17 Hz, 2H), 7.82 (d, *J* = 6.5 Hz, 1H), 7.66-7.61 (m, 1H), 7.59 (d, *J* = 5.5 Hz, 2H), 7.54 (t, *J* = 7.0 Hz, 2H), 7.38 (d, *J* = 5.0 Hz, 2H), 7.29 (d, *J* = 5.0 Hz, 2H), 4.70-4.58 (m, 1H), 2.45-2.28 (m, 4H), 2.07-1.93 (m, 4H), 1.38-1.00 (m, 18H), 0.91-0.82 (m, 2H), 0.79 (t, *J* = 7.0 Hz, 6H). ^{13}C NMR ($CDCl_3$), (δ_C/ppm): 140.1, 139.3, 127.4, 126.6, 119.5, 117.6, 116.0, 33.8, 31.8, 29.4, 29.3, 29.2, 29.1, 26.8, 22.6, 14.1. FT-IR (cm^{-1}): 3099, 3077, 2920, 2850, 2169, 2025, 1881, 1726, 1621, 1598, 1563. Mass (A.I): 681.4 (calculated for $C_{41}H_{47}NS_4$: 682.08). Elemental Analysis (%) calculated for $C_{41}H_{47}NS_4$: C, 72.20; H, 6.95; N, 2.05; S, 18.80. Found: C, 73.29; H, 7.12; N, 1.89; S, 15.49. UV (nm): λ_{max} (chloroform solution) = 382.5, λ_{max} (thin film) = 398.5.

3.3.38 9-(Pentacosan-13-yl)-2,7-di(thieno[3,2-*b*]thiophen-2-yl)-*9H*-carbazole (38)

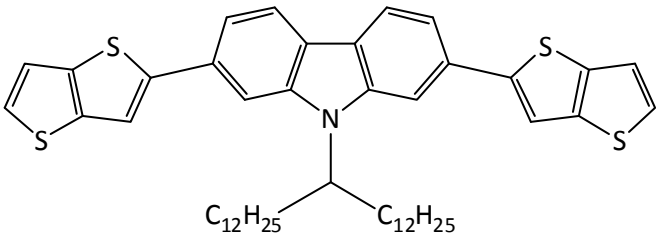

Synthesis of 9-(pentacosan-13-yl)-2,7-di(thieno[3,2-*b*]thiophen-2-yl)-9H-carbazole **(38)** was obtained from a modified procedure by Kowalski *et al.*[149] A mixture of 2,7-dibromo-9-(pentacosan-13-yl)-*9H*-carbazole **(10)** (1.50 g, 2.22 mmol), trimethyl(thieno[3,2-*b*]thiophen-2-yl)stannane **(26)** (2.02 g, 6.66 mmol), and bis(triphenylphosphine)palladium(II)dichloride, $Pd(PPh_3)_2Cl_2$ (100 mg, 0.142 mmol) was stirred in toluene (5 ml) under an inert argon atmosphere and then degassed and heated to 110 °C for 72 h. After cooling to room temperature the mixture was poured into water and extracted with dichloromethane. The solution was concentrated by rotary evaporation and the residue was purified via silica gel column chromatography 40-60 petroleum-ether:tolene (10:1). The product was dried in *vacuo* to give 9-(pentacosan-13-yl)-2,7-di(thieno[3,2-*b*]thiophen-2-yl)-9H-carbazole **(38)** as a orange solid. Yield: 1.70 g (96 %). TLC: R_f = 0.6 in 40-60 petroleum ether/ethyl acetate (10:1). Melting point: 30-35 °C. ^{1}H NMR ($CDCl_3$), (δ_H/ppm): 8.08 (dd, *J* = 11.5, 8.32 Hz, 2H), 7.80 (s, 1H), 7.62 (s, 1H), 7.58 (d, *J* = 6.0 Hz, 2H), 7.52 (d, *J* = 8.0 Hz, 2H), 7.37 (d, *J* = 5.0 Hz, 2H), 7.28 (d, *J* = 5.0 Hz, 2H), 4.67-4.57 (m, 1H), 2.42-2.29 (m, 4H), 2.04-1.91 (m, 4H), 1.33-1.02 (m, 36H), 0.85 (t, *J* = 7.0 Hz, 6H). ^{13}C NMR ($CDCl_3$), (δ_C/ppm): 147.7, 140.1, 138.3, 130.0, 128.3, 126.6, 120.6, 120.6, 119.6, 117.6, 116.2, 115.2, 56.5, 34.7, 33.8, 32.8, 31.9, 30.6, 30.3, 29.6, 29.3, 27.7, 26.8, 22.7, 15.1, 14.1. FT-IR (cm^{-1}): 3083, 2919, 2849, 2159, 2034, 1598, 1562. Mass (EI+): *m/z* 793.6 (100 %); (calculated for $C_{49}H_{63}NS_4$: 794.29). Elemental Analysis (%) calculated for $C_{49}H_{63}NS_4$: C, 74.09; H, 7.99; N, 1.76; S, 16.15. Found: C, 73.56; H, 7.70; N, 1.66; S, 16.09. UV (nm): λ_{max} (chloroform solution) = 376.

3.3.39 3,6-Difluoro-9-(heptadecan-9-yl)-2,7-di(thieno[3,2-b]thiophen-2-yl)-9H-carbazole (39)

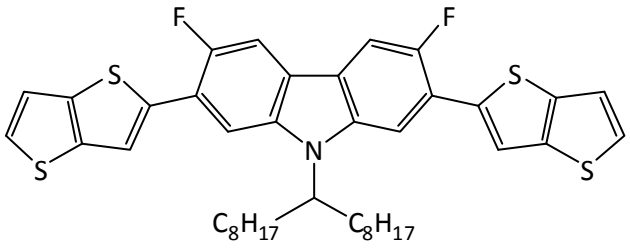

Synthesis of 3,6-difluoro-9-(heptadecan-9-yl)-2,7-di(thieno[3,2-b]thiophen-2-yl)-9H-carbazole **(39)** was obtained from a modified procedure by Kowalski *et al.*[149] A mixture of 2,7-dibromo-3,6-difluoro-9-(heptadecan-9-yl)-9H-carbazole **(15)** (1.33 g, 2.22 mmol), trimethyl(thieno[3,2-*b*]thiophen-2-yl)stannane **(26)** (2.02 g, 6.66 mmol), and bis(triphenylphosphine)-palladium(II)dichloride ($Pd(PPh_3)_2Cl_2$) (100 mg, 0.142 mmol) was stirred in toluene (5 ml) under an inert argon atmosphere and then degassed and heated to 110 °C for 72 h. After cooling to room temperature the mixture was poured into water and extracted with dichloromethane. The solution was concentrated by rotary evaporation and the residue was purified via silica gel column chromatography 40-60 petroleum ether/tolene (10:1). The product was dried in *vacuo* to give 3,6-difluoro-9-(heptadecan-9-yl)-2,7-di(thieno[3,2-b]thiophen-2-yl)-*9H*-carbazole **(39)** as a yellow solid. Yield: 805 mg (50 %). TLC: R_f = 0.35 in 40-60 petroleum ether/toluene (10:1). Melting point: 40-44 °C. ^{1}H NMR ($CDCl_3$), (δ_H/ppm): 7.77 (s, 2H), 7.60 (d, J_{H-F} = 9.0 Hz, 2H), 7.47-7.37 (m, 2H), 7.35-7.30 (m, 2H), 7.27-7.23 (m, 2H), 4.67-4.49 (m, 1H), 2.43-2.24 (m, 4H), 2.06-1.94 (m, 4H), 1.37-1.12 (m, 20H), 0.87-0.77 (m, 6H). (Multiple and broad proton peaks are due to the phenomenon of atropisomerism). ^{13}C NMR ($CDCl_3$), (δ_C/ppm): 155.0, 152.6 (d, J_{C-F} = 237.5 Hz), 140.2, 139.4, 138.2, 127.4, 119.4, 119.0 (d, J_{C-F} = 23.0 Hz), 115.8, 110.6 (d, J_{C-F} = 21.5 Hz), 107.1, 56.8, 31.8, 29.2, 26.7, 23.8, 22.6, 17.5, 14.1. (Multiple carbon peaks are due to the phenomenon of atropisomerism). ^{19}F NMR ($CDCl_3$), (δ_F/ppm): 124.91. FT-IR (cm^{-1}): 3071, 3006, 2920, 2850, 1615, 1568, 1454, 1339. Mass (EI); (m/z): 718 (100 %); (calculated for $C_{41}H_{45}F_2NS_4$: 718.06). Elemental Analysis (%) calculated for $C_{41}H_{45}F_2NS_4$: C, 68.58; H, 6.32; S, 17.86. Found: C, 66.50; H, 7.11; S, 17.07.

3.3.40 3,6-Difluoro-9-(pentacosan-13-yl)-2,7-di(thieno[3,2-b]thiophen-2-yl)-9H-carbazole (40)

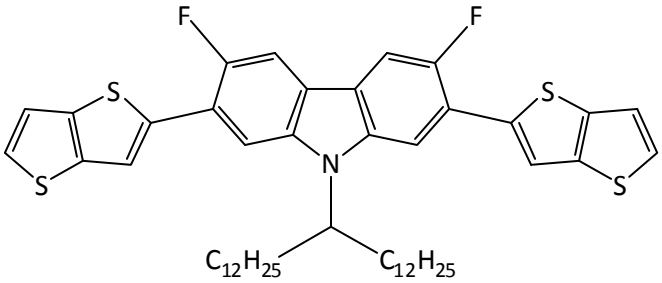

Synthesis of 3,6-difluoro-9-(pentacosan-13-yl)-2,7-di(thieno[3,2-b]thiophen-2-yl)-9H-carbazole **(40)** was obtained from a modified procedure by Kowalski *et al.*[149] A mixture of 2,7-dibromo-3,6-difluoro-9-(pentacosan-13-yl)-*9H*-carbazole **(17)** (1.7 g, 2.22 mmol), trimethyl(thieno[3,2-*b*]thiophen-2-yl)stannane **(26)** (2.02 g, 6.66 mmol), and bis(triphenylphosphine) -palladium(II)dichloride ($Pd(PPh_3)_2Cl_2$) (100 mg, 0.142 mmol) was stirred in toluene (5 ml) under an inert argon atmosphere and then degassed and heated to 110 °C for 72 h. After cooling to room temperature the mixture was poured into water and extracted with dichloromethane. The solution was concentrated by rotary evaporation and the residue was purified via silica gel column chromatography 40-60 petroleum-ether/tolene (10:1). The product was dried in *vacuo* to give 3,6-difluoro-9-(pentacosan-13-yl)-2,7-di(thieno[3,2-*b*]thiophen-2-yl)-*9H*-carbazole **(40)** as a yellow solid. Yield: 900 mg (45 %). TLC: R_f = 0.63 in 40-60 petroleum-ether/toluene (8:2). Melting point: 35-40 °C. ^{1}H NMR ($CDCl_3$), (δ_H/ppm): 7.81-7.72 (m, 2H), 7.55 (d, J_{H-F} = 5.0 Hz, 2H), 7.42 (d, J = 5.0 Hz, 2H), 7.30 (d, J = 5.0 Hz, 2H), 7.18 (d, J = 8.0 Hz, 2H), 4.60-4.48 (m, 1H), 2.33-2.22 (m, 4H), 2.01-1.89 (m, 4H), 1.33-0.85 (m, 36H), 0.85 (t, J = 7.0 Hz, 6H). (Multiple and broad proton peaks are due to the phenomenon of atropisomerism). ^{13}C NMR ($CDCl_3$), (δ_C/ppm): 140.4, 140.2 (d, J_{C-F} = 230.0 Hz), 139.4, 138.9,, 127.5, 119.4, 119.1, 119.0 (d, J_{C-F} = 36.0 Hz), 115.8, 110.6 (d, J_{C-F} = 21.5 Hz), 107.1, 56.8, 33.8, 31.8, 29.3, 26.7, 22.7, 23.8, 22.6, 17.5, 14.1, 14.1. (Multiple carbon peaks are due to the phenomenon of atropisomerism). ^{19}F NMR ($CDCl_3$), (δ_F/ppm): -125.28. FT-IR (cm^{-1}): 3083, 2918, 2849, 1633, 1615, 1564. Mass (EI+): *m/z* 829.5 (100 %) (Calculated for $C_{49}H_{61}F_2NS_4$: 830.27). Elemental Analysis (%) calculated for $C_{49}H_{61}F_2NS_4$: C, 70.88; H, 7.41; F, 4.58; N, 1.69; S, 15.45. Found: C, 70.63; H, 7.36; N, 1.69; S, 14.91. UV (nm): λ_{max} (chloroform solution) = 376.

3.4 Other Compounds Used

3.4.1 9,9-Dioctylfluorene-2,7-diboronic acid bis(1,3-propanediol) ester (41)

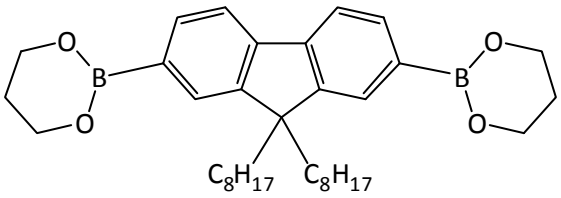

9,9-Dioctylfluorene-2,7-diboronic acid bis(1,3-propanediol) ester was purchased from Sigma-Aldrich.

3.5 Preparation of the Polymers

3.5.1 Poly(9-(heptadecan-9-yl)-*9H*-carbazole-alt-thieno[3,2-*b*]thiophene) (P1)

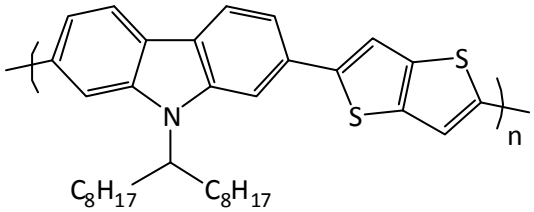

Method 1: Polymerisation in THF using $NaHCO_3$ solution as a base

9-(Heptadecan-9-yl)-2,7-bis(4,4,5,5-tetramethyl-1,3,2-dioxaborolan-2-yl)-*9H*-carbazole **(7)** (0.249 g, 0.379 mmol) and 2,5-dibromothieno[3,2-*b*]thiophene (**24**) (0.113 g, 0.379 mmol) were introduced to a two-necked flask under argon. To the mixture was added THF (8 ml) and a saturated solution of $NaHCO_3$ (2.0 ml, previously degassed). The whole mixture was degassed before addition of $Pd(OAc)_2$ (6.0 mg, 2.68 x 10^{-2} mmol) and tri(o-tolyl)phosphine (16.3 mg, 5.36 x 10^{-2} mmol) and heating to 90 °C for 4 h. The mixture was cooled to room temperature and bromobenzene (0.1 ml, 0.147 g; 0.936 mmol) was added and the mixture degassed and heated to 90 °C for 1 h. The mixture was cooled to room temperature and phenylboronic acid (0.120 g; 0.984 mmol) was added. The mixture was degassed and heated to 90 °C for 3 h. After cooling to room temperature, $CHCl_3$ (200 ml) was added to solubilise the polymer. An ammonium hydroxide solution (28 % in H_2O, 50 ml) was then added and the mixture was stirred overnight. The organic phase was separated and washed

with distilled water (2 x 100 ml). It was then concentrated to about 50 ml in volume and poured into a degassed methanol/water mixture (10:1, v:v, 300 ml). The resulting mixture was then stirred overnight and filtered through a membrane filter. The collected solid was cleaned using a Soxhlet extraction under an inert argon atmosphere with solvents in order methanol (250 ml), acetone (250 ml), hexane (250 ml), and toluene (250 ml). The toluene fraction was concentrated to about 50 ml in volume and then poured into degassed methanol (200 ml). The resulting mixture was stirred overnight and the solid collected by filtration to afford polymer **P1** as a dark red powder. Yield: ~10 mg (no further characterisation).

Method 2: Polymerisation in toluene using 20 % tetraethylammonium hydroxide

A 100 ml one necked flask under argon containing 9-(Heptadecan-9-yl)-2,7-bis(4,4,5,5-tetramethyl-1,3,2-dioxaborolan-2-yl)-*9H*-carbazole **(7)** (0.249 g, 0.379 mmol) and 2,5-dibromothieno[3,2-*b*]thiophene (**24**) (0.1126 g, 0.379 mmol) in dry toluene (8 ml) was degassed. To the mixture 20 % tetraethylammonium hydroxide (2.8 ml, previously degassed 2.5 h) was added and degassed. Then $Pd(OAc)_2$ (11.23 mg, 0.05 mmol) and tri(o-toly)phosphine (38.05 mg, 0.13 mmol) were added, the system was degassed under argon and heated to 90 °C. There was precipitate out of solution after 1 h and the mixture was cooled to room temperature and then bromobenzene (0.10 ml, 0.15 g, 0.94 mmol) was added, degassed and heated to 90 °C for 1 h. Then, the mixture was cooled to room temperature and phenylboronic acid (0.12 g, 0.98 mmol) was added, degassed and heated to 90 °C for 3 h. After cooling to room temperature, $CHCl_3$ (200 ml) was added to solubilise the polymer. An ammonium hydroxide solution (28 % in H_2O, 50 ml) was then added and the mixture was stirred overnight. Then the organic phase was separated and washed with distilled water (2 x 250 ml), concentrated to approximately 50 ml and poured into degassed methanol/water (10:1, v:v, 300 ml). The resulting mixture was then stirred overnight and filtered through a membrane filter. The collected solid was cleaned using a Soxhlet extraction with solvents in order methanol (250 ml), acetone (250 ml), hexane (250 ml), and toluene (250 ml). The toluene fractions were concentrated to approximately 50 ml and then poured into degassed methanol (500 ml), the resulting mixtures stirred overnight and the solid was collected by filtration through a membrane filter. All the fractions of **P1** were dark red powder. Toluene fraction, yield: 65.7 mg (32 %). GPC (1, 2, 4-trichlororbenzene at 100 °C): M_w = 6500, M_n = 2800, PD = 2.3. ^{1}H NMR ($C_2D_2Cl_4$), (δ_H/ppm): 8.18 (d, 2H); 7.84 (d, 2H); 7.80-7.65 (bm, 2H); 7.60-7.45 (bm, 2H); 4.62 (br, 1H); 2.33 (br, 4H); 2.10-1.98 (br, 4H);

1.41 (d, 4H); 1.38-1.01 (bm, 16H); 0.93-0.71 (bm, 6H). FT-IR (cm^{-1}): 3079, 2960, 2923, 2853, 2159, 1981, 1621, 1598, 1561, 1509. Elemental analysis (%) calculated for $C_{35}H_{43}NS_2$: C, 77.58; H, 8.00; N, 2.58; Br, 0.00 Found: C, 76.06; H, 9.01; N, 2.22; Br, 0.00.

3.5.2 Poly(3,6-difluoro-9-(heptadecan-9-yl)-*9H*-carbazole-*alt*-thieno[3,2-*b*]thiophene) (P2)

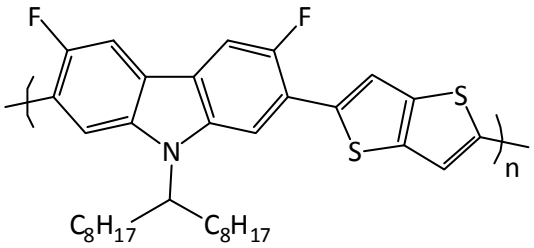

A 100 ml one-necked flask under argon containing 3,6-difluoro-9-(heptadecan-9-yl)-2,7-bis(4,4,5,5-tetramethyl-1,3,2-dioxaborolan-2-yl)-9H-carbazole **(16)** (0.262 g, 0.378 mmol) and 2,5-dibromothieno[3,2-*b*]thiophene **(24)** (0.1126 g, 0.378 mmol) in dry toluene (8.0 ml) was degassed. To the mixture 20 % tetraethylammonium hydroxide (2.8 ml, previously degassed 2.5 h) was added and degassed. Then $Pd(OAc)_2$ (11.2 mg, 0.050 mmol) and tri(o-toly)phosphine (38.05 mg, 0.125 mmol) were added, the system was degassed under argon and heated to 90 °C. There was precipitate out of solution after 1 h and the mixture was cooled to room temperature and then bromobenzene (0.10 ml, 0.15 g, 0.955 mmol) was added, degassed and heated to 90 °C for 1 h. Then, the mixture was cooled to room temperature and phenylboronic acid (0.12 g, 0.984 mmol) was added, degassed and heated to 90 °C for 3 h. After cooling to room temperature, $CHCl_3$ (200 ml) was added to solubilise the polymer. An ammonium hydroxide solution (28 % in H_2O, 50 ml) was then added and the mixture was stirred overnight. Then the organic phase was separated and washed with distilled water (2 x 250 ml), concentrated to approximately 50 ml and poured into degassed methanol/water (10:1, v:v, 300 ml). The resulting mixture was then stirred overnight and filtered through a membrane filter. The collected solid was cleaned using a Soxhlet extraction with solvents in order methanol (250 ml), acetone (250 ml), hexane (250 ml), and toluene (250 ml). The toluene fractions were concentrated to approximately 50 ml and then poured into degassed methanol (500 ml), the resulting mixtures stirred overnight and the solid was collected by filtration through a membrane filter. All the fractions **P2** were dark red powder. Toluene fraction, yield: 131 mg (60 %). GPC (1, 2, 4-trichlororbenzene at 100 °C): M_w = 7 100, M_n = 2 800, PD = 2.4. ^{1}H NMR ($C_2D_2Cl_4$), (δ_H/ppm): 8.15 (d, 2H); 7.80

(d,2H); 7.78-7.60 (bm, 2H); 4.77 (br, 1H), 2.50-2.28 (br, 4H); 2.09-1.92 (br, 4H); 1.42 (bm, 4H); 1.38-0.98 (bm, 16H); 0.84 (br, 6H). FT-IR (cm^{-1}): 2922, 2852, 2184, 1611, 1569, 1527, 1452. Elemental analysis (%) calculated for $C_{35}H_{41}F_2NS_2$: C, 72.75; H, 7.15; N, 2.42; Br, 0.00. Found: C, 74.00; H, 6.55; N, 2.00; Br, 0.00.

3.5.3 Poly(9,9-dioctyl-*9H*-fluorene-alt-thieno[3,2-*b*]thiophene) (P3)

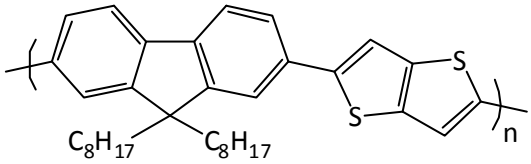

A 100 ml one-necked flask under argon containing 9,9-dioctylfluorene-2,7-diboronic acid bis(1,3-propanediol) ester **(41)** (0.211 g, 0.378 mmol) and 2,5-dibromothieno[3,2-*b*]thiophene **(24)** (0.113 g, 0.378 mmol) in dry toluene (8 ml) was degassed. To the mixture 20 % tetraethylammonium hydroxide (2.8 ml, previously degassed 2.5 h) was added and degassed. Then $Pd(OAc)_2$ (11.23 mg, 0.050 mmol) and tri(o-toly)phosphine (38.05 mg, 0.125 mmol) were added, the system was degassed under argon and heated to 90 °C. There was precipitate out of solution after 1 h and the mixture was cooled to room temperature and then bromobenzene (0.10 ml, 0.15 g, 0.955 mmol) was added, degassed and heated to 90 °C for 1 h. Then, the mixture was cooled to room temperature and phenylboronic acid (0.12 g, 0.984 mmol) was added, degassed and heated to 90 °C for 3 h. After cooling to room temperature, $CHCl_3$ (200 ml) was added to solubilise the polymer. An ammonium hydroxide solution (28 % in H_2O, 50 ml) was then added and the mixture was stirred overnight. Then the organic phase was separated and washed with distilled water (2 x 250 ml), concentrated to approximately 50 ml and poured into degassed methanol/water (10:1, v:v, 300 ml). The resulting mixture was then stirred overnight and filtered through a membrane filter. The collected solid was cleaned using a Soxhlet extraction with solvents in order methanol (250 ml), acetone (250 ml), hexane (250 ml), and toluene (250 ml). The toluene fractions were concentrated to approximately 50 ml and then poured into degassed methanol (500 ml), the resulting mixtures stirred overnight and the solid was collected by filtration through a membrane filter. All the fractions **P3** were dark red powder. Toluene fraction, yield: 107 mg (54 %). GPC (1, 2, 4-trichlororbenzene at 100 °C): M_w = 4600, M_n = 2100, PD = 2.2. ^{1}H NMR ($C_2D_2Cl_4$), (δ_H/ppm): 8.45 (d, 2H); 8.18-8.03 (d, 2H);

7.81-7.68 (bm, 4H); 1.18 (br, 4H); 1.59 (br, 4H); 1.43-1.20 (bm, 20H); 0.82 (br, 6H). FT-IR (cm^{-1}): 3043, 2956, 2923, 2852, 1975, 1623, 1528, 1489, 1462. Elemental analysis (%) calculated for $C_{35}H_{42}S_2$: C, 79.79; H, 8.04; Br, 0.00. Found: C, 80.02; H, 7.55; Br, 0.00.

3.5.4 Poly(9-(heptadecan-9-yl)-*9H*-carbazole-*atl*-4,7-di(thieno[3,2-b]thiophen-2-yl)benzo [*c*][1,2,5]thiadiazole) (P4)

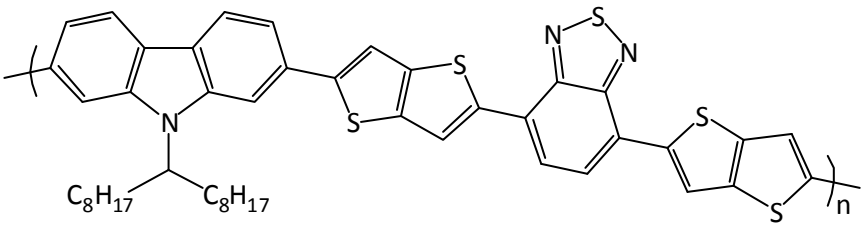

A mixture of 9-(heptadecan-9-yl)-2,7-di(thieno[3,2-*b*]thiophen-2-yl)-*9H*-carbazole **(37)** (164 mg, 0.241 mmol), 4,7-dibromo-2,1,3-benzothiadiazole **(34)** (71 mg, 0.241 mmol), $Pd(OAc)_2$ (2 mg, 8.91 x 10^{-3} mmol) and anhydrous K_2CO_3 (50 mg, 0.362 mmol) was stirred in anhydrous dimethylacetamide, DMAc (3 ml) under an inert argon atmosphere and then degassed and heated to 110 °C for 72 h. The mixture was cooled to room temperature and thiophene (1 ml) was added. It was then degassed and heated to 110 °C for 3 h. After cooling to room temperature, $CHCl_3$ (200 ml) was added to solubilise the polymer. An ammonium hydroxide solution (35 % in H_2O, 50 ml) was then added and the mixture was refluxed overnight. The organic phase was separated and washed with distilled water (2 x 100 ml). It was then concentrated to about 50 ml in volume and added dropwise into a methanol/water mixture (10:1, v/v, 300 ml). The resulting mixture was then stirred overnight and filtered through a membrane filter. The collected solid was cleaned using a Soxhlet extraction under an inert nitrogen atmosphere with methanol (250 ml), acetone (250 ml), hexane (250 ml), toluene (250 ml), chloroform (250 ml) and chlorobenzene (250 ml), respectively. The toluene, chloroform and chlorobenzene fraction was concentrated to about 50 ml and then added dropwise into methanol (250 ml), respectively. The resulting mixture was stirred overnight and the solids collected by filtration to afford polymer **P4** fractions as red powder. Yield: 145.2 mg (74 %). Toluene fraction: (56.9 mg, 29 %), GPC (1, 2, 4-trichlororbenzene at 100 °C): M_w = 10600, M_n = 6200, PD = 1.7. Chloroform fraction: (88.3 mg, 45 %), GPC (1, 2, 4-trichlororbenzene at 100 °C): M_w = 30600, M_n = 13200, PD =

2.3. Due to low yield, no further characterisation for the chlorobenzene fraction. ^{1}H NMR ($C_2D_2Cl_4$), (δ_H/ppm): 8.21 (b, 2H); 7.92 (bm, 2H), 7.61 (d,2H); 7.42 (bm, 2H); 7.21 (d, 2H); 7.09 (b, 2H); 4.81 (b, 1H); 2.28 (b, 4H); 1.91 (b, 4H); 1.20-0.81 (bm, 20H); 0.62 (m, 6H). FT-IR (cm^{-1}): 2962, 2925, 2853, 2121, 1538, 1471, 1455. Elemental analysis (%) calculated for $C_{47}H_{47}N_3S_5$: C, 69.33; H, 5.82; S, 19.69, Br, 0.00. Found: C, 69.33; H, 5.82; S, 19.69, Br, 0.00.

3.5.5 Poly(3,6-difluoro-9-(heptadecan-9-yl)-*9H*-carbazole-*atl*-4,7-di(thieno[3,2-*b*]thiophen-2-yl)benzo[*c*][1,2,5]thiadiazole) (P5)

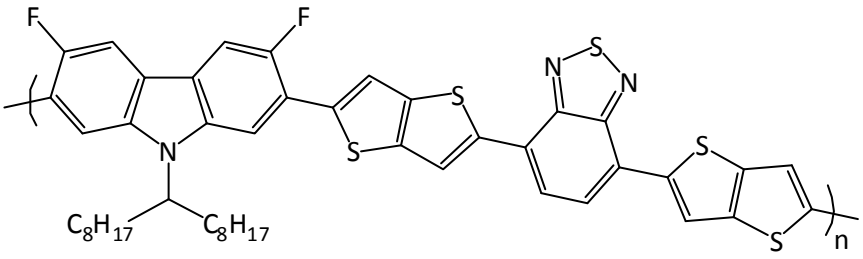

A mixture of 3,6-difluoro-9-(heptadecan-9-yl)-2,7-di(thieno[3,2-*b*]thiophen-2-yl)-9H-carbazole **(39)** (173 mg, 0.241 mmol), 4,7-dibromo-2,1,3-benzothiadiazole **(34)** (71 mg, 0.241 mmol), $Pd(OAc)_2$ (2 mg, 8.91 x 10^{-3} mmol) and anhydrous K_2CO_3 (50 mg, 0.362 mmol) was stirred in anhydrous dimethylacetamide, DMAc (3 ml) under an inert argon atmosphere and then degassed and heated to 110 °C for 72 h. The mixture was cooled to room temperature and thiophene (1 ml) was added. It was then degassed and heated to 110 °C for 3 h. After cooling to room temperature, $CHCl_3$ (200 ml) was added to solubilise the polymer. An ammonium hydroxide solution (35 % in H_2O, 50 ml) was then added and the mixture was refluxed overnight. The organic phase was separated and washed with distilled water (2 x 100 ml). It was then concentrated to about 50 ml in volume and added dropwise into a methanol/water mixture (10:1, v/v, 300 ml). The resulting mixtures were then stirred overnight and filtered through a membrane filter. The collected solid was cleaned using a Soxhlet extraction under an inert nitrogen atmosphere with with methanol (250 ml), acetone (250 ml), hexane (250 ml), toluene (250 ml), chloroform (250 ml) and chlorobenzene (250 ml), respectively.[182] The toluene, chloroform and chlorobenzene fraction was concentrated to about 50 ml and then dropwise into methanol (250 ml). The resulting mixture was stirred overnight and the solids collected by filtration to afford polymer **P5** fraction as red powders. Yield: 139.7 mg (68 %). Toluene fraction: (84.2 mg, 41

%), GPC (1, 2, 4-trichlororbenzene at 100 °C): M_w = 10600, M_n = 6200, PD = 1.7. Chloroform fraction: (55.5 mg, 27 %), GPC (1, 2, 4-trichlororbenzene at 100 °C): M_w = 83400, M_n = 34100, PD = 2.4. Due to low yield, no further characterisation for the chlorobenzene fraction. ^{1}H NMR ($C_2D_2Cl_4$), (δ_H/ppm): 8.38 (b, 2H); 7.64 (b, 2H); 7.39 (b, 2H); 7.23 (b, 2H); 4.58 (b, 1H); 2.22 (b, 4H); 1.98 (b, 4H); 1.64 (b, 4H); 1.43-1.02 (bm, 16H); 0.98-0.64 (bm, 6H). FT-IR (cm^{-1}): 3081, 2950, 2919, 2849, 2155, 2025, 1975, 1615, 1562. Elemental analysis (%) calculated for $C_{47}H_{47}F_2N_3S_5$: C, 66.40; H, 5.33; N, 4.94; Br, 0.00. Found: C, 73.02; H, 7.77; N, 6.65; Br, 0.00.

3.5.6 Poly(9-(pentacosan-13-yl)-*9H*-carbazole-*atl*-4,7-di(thieno[3,2-*b*]thiophen-2-yl)benzo [c][1,2,5]thiadiazole) (P6)

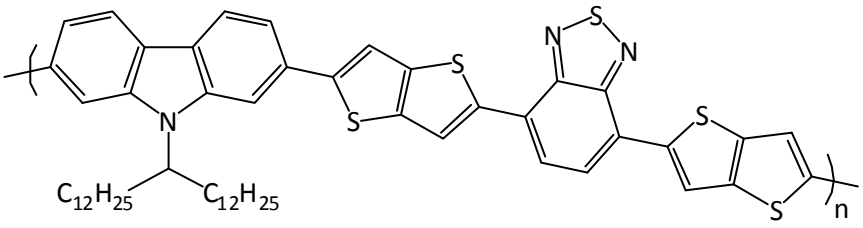

A mixture of 9-(pentacosan-13-yl)-2,7-di(thieno[3,2-*b*]thiophen-2-yl)-*9H*-carbazole **(38)** (250 mg, 0.315 mmol), 4,7-dibromo-2,1,3-benzothiadiazole **(34)** (92.5 mg, 0.315 mmol), $Pd(OAc)_2$ (2.9 mg, 0.013 mmol) and K_2CO_3 (65.2 mg, 0.472 mmol) was stirred in anhydrous dimethylacetamide, DMAc (5 ml) under an inert argon atmosphere and then degassed and heated to 110 °C for 72 h. The mixture was cooled to room temperature and thiophene (1 ml) was added. It was then degassed and heated to 110 °C for 3 h. After cooling to room temperature, $CHCl_3$ (200 ml) was added to solubilise the polymer. An ammonium hydroxide solution (35 % in H_2O, 50 ml) was then added and the mixture was refluxed overnight. The organic phase was separated and washed with distilled water (2 x 100 ml). It was then concentrated to about 50 ml in volume and dropwise into a methanol/water mixture (10:1, v/v, 300 ml). The resulting mixture was then stirred overnight and filtered through a membrane filter. The collected solid was cleaned using a Soxhlet extraction under an inert argon atmosphere with methanol (250 ml), acetone (250 ml), hexane (250 ml), toluene (250 ml), and chloroform (250 ml), respectively. The toluene and chloroform fractions were concentrated to about 50 ml and then poured into methanol (200 ml). The resulting

mixtures was stirred overnight and the solids collected by filtration to afford polymer **P6** fraction as red powders. Due to low yield, no further characterisation for the toluene fraction. Chloroform fraction, yield: 253.9 mg (87 %). GPC (1, 2, 4-trichloror'benzene at 100 °C): M_w = 25100, M_n = 10000, PD = 2.5. ^{1}H NMR ($C_2D_2Cl_4$), (δ_H/ppm):8.41 (bm, 2H); 8.02 (bm, 2H); 7.78 (b, 2H); 7.56 (bm, 2H); 7.35 (d, 2H); 7.22 (d, 2H); 4.56 (b, 1H); 2.23 (b, 4H); 1.93 (b, 4H); 1.57 (bm, 4H); 1.21-0.97 (bm, 32H), 0.77(b, 6H). FT-IR (cm^{-1}): 3075, 2920, 2849, 2515, 2159, 2021, 2029, 2010, 1973, 1624, 1595, 1565, 1498. Elemental analysis (%) calculated for $C_{55}H_{63}N_3S_5$: C, 71.30; H, 6.85; N, 4.54; Br, 0.00. Found: C, 77.11; H, 8.75; N, 6.22; Br, 0.00.

3.5.7 Poly(3,6-difluoro-9-(pentacosan-13-yl)-*9H*-carbazole-*atl*-4,7-di(thieno[3,2-*b*]thiophen-2-yl)benzo[c][1,2,5]thiadiazole) (P7)

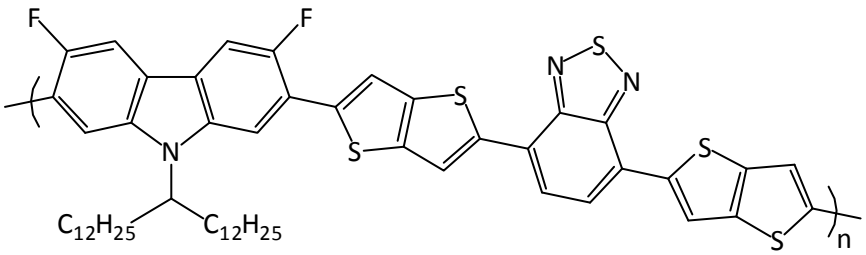

A mixture of 3,6-difluoro-9-(pentacosan-13-yl)-2,7-di(thieno[3,2-*b*]thiophen-2-yl)-*9H*-carbazole **(40)** (200.0 mg, 0.241 mmol), 4,7-dibromo-2,1,3-benzothiadiazole **(34)** (70.8 mg, 0.241 mmol), $Pd(OAc)_2$ (2.1 mg, 9.35 x 10^{-3} mmol) and K_2CO_3 (49.8 mg, 0.360 mmol) was stirred in anhydrous dimethylacetamide, DMAc (3 ml) under an inert argon atmosphere and then degassed and heated to 110 °C for 72 h. The mixture was cooled to room temperature and thiophene (1 ml) was added. It was then degassed and heated to 110 °C for 3 h. After cooling to room temperature, $CHCl_3$ (200 ml) was added to solubilise the polymer. An ammonium hydroxide solution (35 % in H_2O, 50 ml) was then added and the mixture was refluxed overnight. The organic phase was separated and washed with distilled water (2 x 100 ml). it was then concentrated to about 50 ml in volume and dropwise into a methanol/water mixture (10:1, v/v, 300 ml). The resulting mixture was then stirred overnight and filtered through a membrane filter. The collected solid was cleaned using a Soxhlet extraction under an inert argon atmosphere with methanol (250 ml), acetone (250 ml), hexane (250 ml), toluene (250 ml) and chloroform (250 ml), respectively. The toluene

and chloroform fractions were concentrated to about 50 ml and then poured into methanol (200 ml), respectively. The resulting mixtures were stirred overnight and the solids collected by filtration to afford polymer **P7** fractions as red powders. Yield: 151.1 mg (65 %). Toluene fraction: (88.3 mg, 38 %), GPC (1, 2, 4-trichlororbenzene at 100 °C): M_w = 11200, M_n = 4600, PD = 2.4. Chloroform fraction: (62.8 mg, 27 %), GPC (1, 2, 4-trichlororbenzene at 100 °C): M_w = 30600, M_n = 13300, PD = 2.3. ^{1}H NMR ($C_2D_2Cl_4$), (δ_H/ppm): 8.58 (b, 2H); 7.88 (bm, 2H); 7.68 (bm, 2H); 7.38 (d, 2H); 7.22 (d, 2H); 4.52 (b, 1H); 2.32 (b, 4H); 2.04 (b, 4H); 1.42-1.10 (bm, 36H); 0.82 (b, 6H). FT-IR (cm^{-1}): 3105, 3035, 2957, 2920, 2849, 2155, 2033, 1973, 1617, 1565, 1535. Elemental analysis (%) calculated for $C_{55}H_{63}F_2N_3S_5$: C, 68.64; H, 6.39; N, 4.37; Br, 0.00. Found: C, 71.87; H, 9.03; N, 7.00; Br, 0.00.

3.5.8 Poly(9-(heptadecan-9-yl)-*9H*-carbazole-*alt*-5,6-bis(octyloxy)-4,7-di(thieno[3,2-*b*]thiophen-2-yl)benzo[*c*][1,2,5]thiadiazole) (P8)

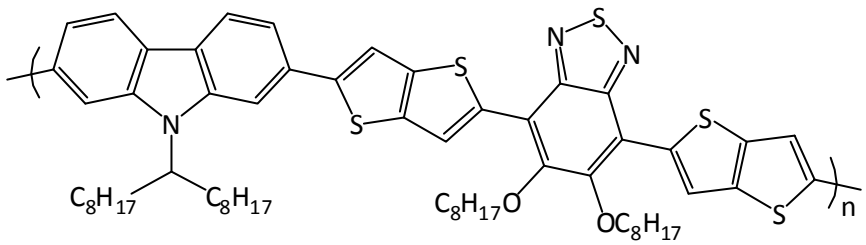

9-(Heptadecan-9-yl)-2,7-bis(4,4,5,5-tetramethyl-1,3,2-dioxaborolan-2-yl)-*9H*-carbazole **(7)** (0.120 g, 0.183 mmol) and 4,7-bis(5-bromothieno[3,2-*b*]thiophen-2-yl)-5,6-bis(octyloxy)benzo [*c*][1,2,5] thiadiazole **(33)** (0.151 g, 0.183 mmol) were introduced to 100 mL round bottom flask under argon. To the mixture was added toluene (5 ml) and the mixture was degassed. Then 20 wt % tetraethyl ammonium hydroxide 20 % (1.0 ml, 1.356 mmol, previously 2.5 h degassed) was added. To this mixture was added $Pd(OAc)_2$ (1.2 mg, 5.3 x 10^{-3} mmol) and tri(*o*-tolyl)phosphine (3.3 mg, 1.08 x 10^{-2} mmol) under an inert argon atmosphere and it was heated to 95 °C for 72 h. The mixture was cooled to room temperature and bromobenzene (0.05 ml, 61.0 mg; 0.3877 mmol) was added. It was then degassed and heated to 90 °C for 1 h. The mixture was cooled to room temperature and phenylboronic acid (50 mg; 0.4076 mmol) was added. The mixture was degassed and heated to 90 °C for 1 h. After cooling to room temperature, $CHCl_3$ (200 ml) was added to

solubilise the polymer. An ammonium hydroxide solution (28 % in H_2O, 50 ml) was then added and the mixture was stirred overnight. The organic phase was separated and washed with distilled water (2 x 100 ml). It was then concentrated to about 50 ml in volume and added drop-wise into a methanol/water mixture (10 : 1, v/v, 300 ml). The resulting mixture was then stirred overnight and filtered through a membrane filter. The collected solid was cleaned using a Soxhlet extraction under an inert argon atmosphere with methanol (250 ml), acetone (250 ml), hexane (250 ml), toluene (250 ml) and chloroform (250 ml), respectively. The toluene and chloroform fractions were concentrated to about 50 ml and then poured into degassed methanol (200 ml). The resulting mixtures were stirred overnight and the solids collected by filtration to afford polymer **P8** fractions as a dark purple powders. Yield: 142.6 mg (73 %). Toluene fraction: (25.4 mg, 13 %), GPC (1, 2, 4-trichlororbenzene at 100 °C): M_w = 20000, M_n = 8500, PD = 2.4. Chloroform fraction: (117.2 mg, 60 %), GPC (1, 2, 4-trichlororbenzene at 100 °C): M_w = 63000, M_n = 27000, PD = 2.3. ^{1}H NMR ($C_2D_2Cl_4$), (δ_H/ppm): 8.78 (d, 2H); 8.09 (b, 2H); 7.88 (b, 2H); 7.74-7.54 (bm, 4H); 4.71 (b, 1H); 4.28 (b, 4H); 2.41 (b, 4H); 2.02 (bm, 4H); 1.58 (b, 4H); 1.38-1.18 (bm, 40H); 1.0-0.85 (bm, 12H). FT-IR (cm^{-1}): 3079, 3009, 2949, 2920, 2851, 2160, 2032, 1977, 1621, 1595, 1562. Elemental analysis (%) calculated for $C_{63}H_{79}N_3O_2S_5$: C, 70.67; H, 7.44; N, 3.92; Br, 0.00. Found: C, 78.00; H, 8.03; N, 4.22; Br, 0.00.

3.5.9 Poly(3,6-difluoro-9-(heptadecan-9-yl)-*9H*-carbazole-*alt*-5,6-bis(octyloxy)-4,7-di(thieno[3,2-*b*]thiophen-2-yl)benzo[c][1,2,5]thiadiazole) (P9)

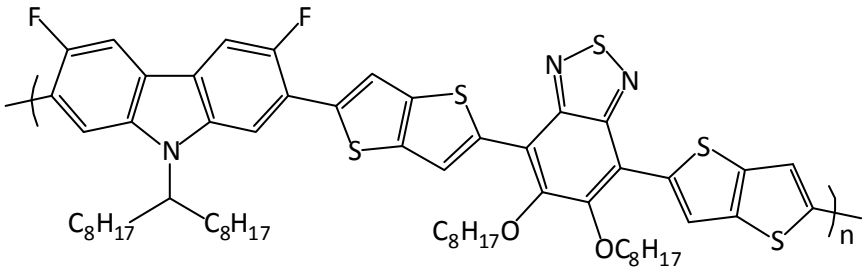

3,6-Difluoro-9-(heptadecan-9-yl)-2,7-bis(4,4,5,5-tetramethyl-1,3,2-dioxaborolan-2-yl)-*9H*-carbazole (**16**) (0.120 g, 0.173 mmol) and 4,7-bis(5-bromothieno[3,2-b]thiophen-2-yl)-5,6-bis(octyloxy)benzo*[c]*[1,2,5]thiadiazole **(33)** (0.1433 g, 0.173 mmol) were introduced to 100 mL round bottom flask under argon. To the mixture was added toluene (5.0 ml) and the

mixture was degassed. Then 20 wt % tetraethyl ammonium hydroxide (1.0 ml, previously degassed) was added. To this mixture was added $Pd(OAc)_2$ (1.2 mg, 4.9 x 10^{-3} mmol) and tri(o-tolyl)phosphine (3.54 mg, 1.2 x 10^{-3} mmol) under an inert argon atmosphere and it was heated to 95 °C for 96 h. The mixture was cooled to room temperature and bromobenzene (0.05 ml, 61 mg; 0.3877 mmol) was added. It was then degassed and heated to 90 °C for 1 h. The mixture was cooled to room temperature and phenylboronic acid (50 mg; 0.4076 mmol) was added. The mixture was degassed and heated to 90 °C for 1 h. After cooling to room temperature, $CHCl_3$ (200 ml) was added to solubilise the polymer. An ammonium hydroxide solution (28% in H_2O, 50 ml) was then added and the mixture was stirred overnight. The organic phase was separated and washed with distilled water (2 x 100 ml). It was then concentrated to about 50 ml in volume and drop-wise into a methanol/water mixture (10: 1, v/v, 300 ml). The resulting mixture was then stirred overnight and filtered through a membrane filter. The collected solid was cleaned using a Soxhlet extraction under an inert argon using a Soxhlet extraction under an inert argon atmosphere with methanol (250 ml), acetone (250 ml), hexane (250 ml), toluene (250 ml) and chloroform (250 ml), respectively. The toluene and chloroform fractions were concentrated to about 50 ml and then poured into degassed methanol (200 ml). The resulting mixture was stirred overnight and the solid collected by filtration to afford polymer **P9** fractions as a dark red powders. Yield: 115.1 mg (60 %). Toluene fraction: (53.7 mg, 28 %), GPC (1, 2, 4-trichlororbenzene at 100 °C): M_w = 4600, M_n = 1900, PD = 2.4. Chloroform fraction: (61.4 mg, 32 %), GPC (1, 2, 4-trichlororbenzene at 100 °C): M_w = 62900, M_n = 26200, PD = 2.4. ^{1}H NMR ($C_2D_2Cl_4$), (δ_H/ppm): 8.72 (d, 2H); 8.62 (d, 2H); 7.72 (bm, 2H); 7.32 (b, 2H); 4.49 (b, 1H); 4.18 (b, 4H); 2.24 (b, 4H); 1.96 (b, 4H); 1.58-1.02 (bm, 44H); 0.91-0.74 (bm, 12H). FT-IR (cm^{-1}): 3113, 2949, 2923, 2949, 2159, 2018, 1977, 1628, 1587, 1565. Elemental analysis (%) calculated for $C_{63}H_{77}F_2N_3O_2S_5$: C, 68.38; H, 7.01; N, 3.80; Br, 0.00. Found: C, 70.10; H, 6.66; N, 3.11; Br, 0.00.

3.5.10 Poly(9,9-dioctyl-*9H*-fluorene-*alt*-5,6-bis(octyloxy)-4,7-di(thieno[3,2-*b*]thiophen-2-yl)benzo[*c*][1,2,5]thiadiazole) (P10)

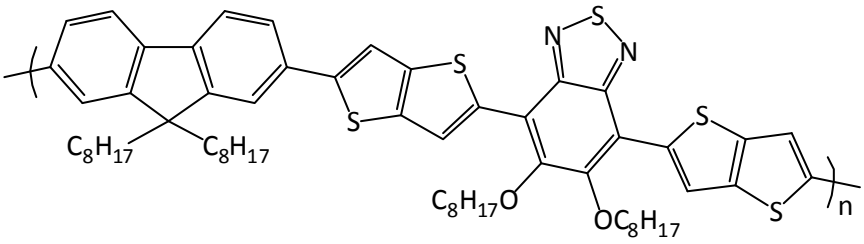

A single-necked flask under argon containing 9,9-dioctylfluorene-2,7-diboronic acid bis(1,3-propanediol) ester **(41)** (0.540 g, 0.968 mmol), 4,7-bis(5-bromothienylthiophen-2-yl)-5,6-bis(octylloxy)benzo[c][1,2,5]thiadiazole **(33)** (0.800 g, 0.968 mmol) was degassed. To the mixture toluene (21 ml) and then tetraethylammonium hydroxide (20% wt, 7.0 ml, degassed) was added and degassed. To this solution $Pd(OAc)_2$ (8.0 mg) and tri(o-tolyl)phosphine (21.7 mg) were added, degassed and heated to 90 ^oC for 48 hours. The mixture was cooled to room temperature and bromobenzene (0.1 ml) were added, degassed and heated 90 ^oC for 1 hour. Again, the mixture was cooled to room temperature and phenylboronic acid (150 mg) was added, degassed and heated to 90 ^oC for 3 hours. After cooling to room temperature, the mixture was dissolved in $CHCl_3$ (300 ml) and to this solution ammonia (200 ml, 35%) was added, heated at reflux temperature for 3 hours, cooled to room temperature. The organic phase was separated then Ethylenediaminetetraacetic acid disodium salt dihydrate (300 mg) was added and stirred overnight. The mixture was washed with distilled water (2 × 200 ml), the organic phase was separated and concentrated to about 50 ml and poured into degassed methanol/water (10:1, 500 ml). The resulting mixture was then stirred overnight and filtered through a membrane filter. The collected solid was cleaned using a Soxhlet extraction with solvents in order methanol (250 ml), acetone (250 ml), hexane (250 ml), and toluene (250 ml). The toluene fraction was concentrated to about 50 ml and then poured into degassed methanol (500 ml). The resulting mixture was stirred overnight and the red powder polymer **P10** was collected by filtration. Toluene fraction, yield: 347.3 mg (34 %). GPC (1, 2, 4-trichlororbenzene at 100 °C): M_w = 20000, M_n = 7600, PD = 2.6. ^1H NMR ($C_2D_2Cl_4$), (δ_H/ppm): 8.77 (d, 2H); 7.81-7.58 (bm, 8H); 4.23 (b, 4H); 2.18-1.89 (bm, 8H); 1.54 (b, 4H); 1.4-1.05 (bm, 40H); 0.98-0.68 (d, 12H). FT-IR (cm^{-1}): 3118, 3081, 3056, 3008, 2953, 2921, 2851, 2158, 2023, 1968, 1887, 1673, 1607, 1563. Elemental analysis (%) calculated for $C_{63}H_{78}N_2O_2S_5$: C, 71.68; H, 7.45; N, 2.65; Br, 0.00. Found: C, 79.01; H, 12.18; N, 4.11; Br, 0.00.

CHAPTER 4 - RESULTS AND DISCUSSION - COMPOUNDS

4.1 Synthesis of heptadecan-9-ol (1)

Synthesis of heptadecan-9-ol **(1)** was performed according to the procedure by Leclerc *et al.*[36]

The crude product was obtained as colourless oil, which then crystallized to a white solid over time in 98 % yield. The preliminary analyses confirmed the purity of crude product, so it was used in the next reaction without purification.[178]

The reaction involves the formation of Grignard reagent at first, which was prepared by reacting magnesium with octylbromide in THF, the reaction was exothermal and ice bath was used to maintain the temperature below 25 °C, the magnesium was inserted between carbon and bromine, resulting in oxidation of magnesium from Mg (0) to Mg (II). The formation of Grignard was observed by consuming the magnesium and turning the solution to milky white over time. In a second step, the formed Grignard solution was added to a solution of ethyl formate in THF at -78 °C, and the mixture allowed to stir overnight at room temperature to obtain the target product **(1)**, then the reaction was quenched by adding methanol and saturated NH_4Cl. The two reactions are shown in **Scheme 4.1**.

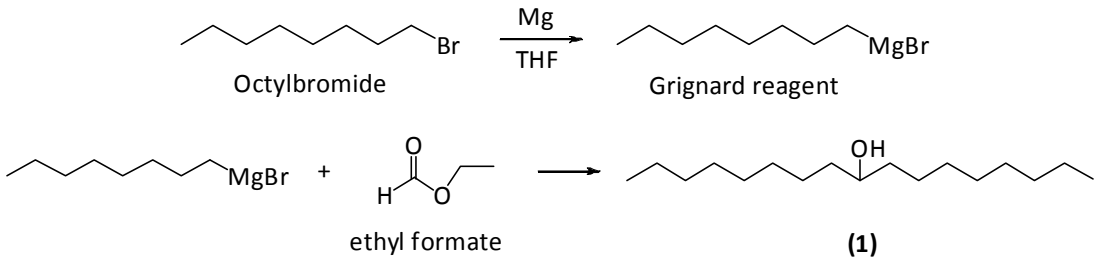

Scheme 4.1: The preparation of the Grignard reagent and the heptadecan-9-ol **(1)**.

The mechanism of Grignard reaction is illustrated in **Scheme 4.2**, at first, Grignard reagent act as a nucleophile, which readily attacks the carbonyl group in ethyl formate, then the carbonyl group reformed, which pushes out the alkoxide group. The formed carbonyl is more reactive than before, therefore, it is subject to another nucleophilic attack by Grignard reagent in a second step, and then a hydrolysis reaction leads to the target product.[171-173]

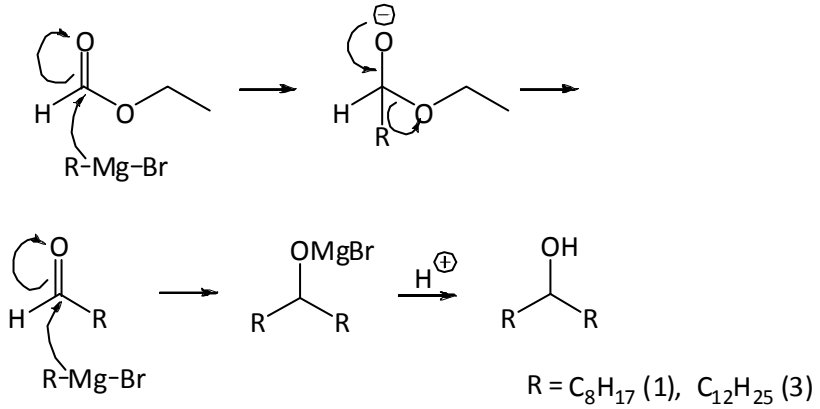

Scheme 4.2: Grignard reaction mechanism for the formation of compound **(1)**.

The purity and the chemical structure of the product **(1)** were confirmed by TLC, the melting point, the mass spectra, elemental analysis, NMR analysis and FT-IR. The product gave a single spot on TLC, and the melting point was 29-32 °C, which was in good agreement with that reported in the literature (28-31 °C).

The mass spectra shows main integer masses for heptadecan-9-ol **(1)**, which is observed at 255. Elemental analysis CHN of **(1)** was in agreement with its proposed structure. The NMR analysis showed the expected peaks as mentioned in the literature.[36]

FT-IR displayed a peak at 3321 cm^{-1} which belongs to the O-H stretching of the hydroxyl group. Also it displayed strong peaks at 2916 cm^{-1}, 2872 cm^{-1} and 2848 cm^{-1}, due to the C-H stretch vibration of alkyl chains.

All analytical results clearly verify that the product was heptadecan-9-ol **(1).**

4.2 Synthesis of 9-heptadecane-*p*-toluenesulfonate (2)

Synthesis of heptadecane-*p*-toluenesulfonate **(2)** was performed according to the procedure by Leclerc *et al.*[36]

Compound **(2)** was prepared by using heptadecan-9-ol **(1)** as starting materials as shown in **Scheme 4.3.** The crude product was purified *via* silica gel column chromatography, eluting with (89 % hexane, 9 % ethylacetate, 2 % Et_3N) to obtain **(2)** as a white solid in 88 % yield.

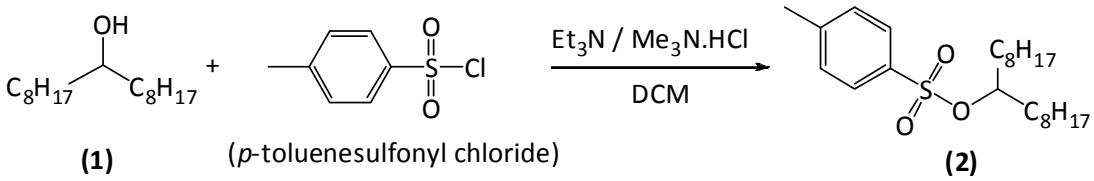

(1) (*p*-toluenesulfonyl chloride) **(2)**

Scheme 4.3: Synthesis of 9-heptadecane p-toluenesulfonate **(2)**.

The product **(2)** was obtained *via* a tosylation method by using p-toluenesulfonyl chloride, trimethylamine hydrochloride as a catalyst in the presence of the base triethylamine. The reaction was carried out at low temperature (5-10 °C) for 90 min, and the reaction mechanism of **(2)** follows the same route as that described for the synthesis of *N*-(1-undecyldodecyl)-*N'*-(6-hexyl-p-toluenesulfonate)perylene-3,4,9,10-tetracarboxylic diimie as shown in **Scheme 4.4**.

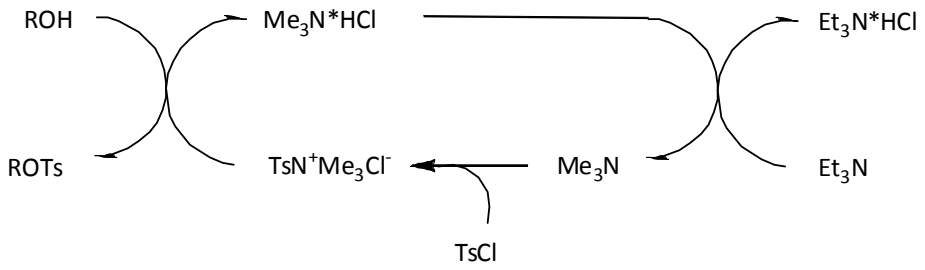

Scheme 4.4: The reaction cycle of the tosylation.

The purity and the chemical structure of product **(2)** were confirmed by TLC, the melting point, the mass spectra, elemental analysis, NMR analysis and FT-IR. The product gave a single spot on TLC, and the melting point was 33.5 °C, which was in good agreement with that reported in the literature (31-32 °C).[36]

The mass spectra shows main integer masses for 9-heptadecane p-toluenesulfonate **(2)** which is observed at 410, and the elemental analysis CHN of **(2)** was in agreement with its proposed structure. The ^{1}H-NMR spectra showed new peaks, two doublet peaks at 7.81 ppm and 7.34 ppm, which corresponded to tosyl group. The multi peaks at 3.60 ppm in previous compound **(1)** was shifted to 4.55 ppm, which belongs to the protons close to the tosyl group. Also a new singlet peak appeared at 2.46 ppm, which corresponded to the methyl of the tosyl group.

The FT-IR of product **(2)** shows on strong peak at 3321 cm^{-1}, which belonged to the O-H stretching of the hydroxyl group in the previous compound **(1)**, has disappeared. Also new peaks were observed as following: at 2954 cm^{-1} belonging to the stretching vibration of the C-H in the aromatic tosyl group, at 1597 and 1566 cm^{-1} belonging to the strechingg vibration of the C-C double bonds in aromatic tosyl group, at 1353 cm^{-1} and 1353 cm^{-1} belonging to the stretching vibration of the (-SO_2) in sulfonate group, at 1021 cm^{-1}, which belongs to the (-S-O-) bonds in sulfonate group.

All analytical results clearly verify and supported that the product was 9-heptadecane p-toluenesulfonate **(2).**

4.3 Synthesis of 4, 4'-dibromo-2,2'-dinitrobiphenyl (3)

Synthesis of 4,4'-dibromo-2,2'-dinitrobiphenyl **(3)** was obtained from a modified the procedure by Dierschke *et al.*[192] and obtained in a 87 % yield.

The product was prepared via a Ullmann coupling reaction of 2,5-dibromonitrobenzene using copper powder in a solution of dimethylformamide as show in **Scheme 4.5**. The reaction was completed after heating the mixture for 2 h at 120 °C, and following work-up to give the isolated product as a pale yellow powder.

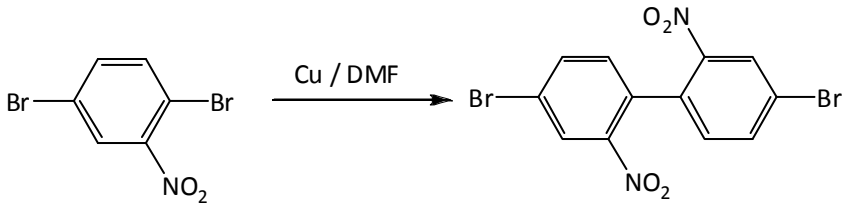

1,4-dibromo-2-nitrobenzene **(3)**

Scheme 4.5: Synthesis of 4,4'-Dibromo-2,2'-dinitrobiphenyl **(3).**

The purity of the product was confirmed by TLC, GC mass spectra, melting point and elemental analysis. The structure of the product was identified by IR absorption, ^{1}H NMR and ^{13}C NMR.

Ullmann coupling reaction proceeds via a two step process as shown in **Scheme 4.6**. This first step is the nucleophilic attack by the copper into the C-Br bond ortho to the nitro group on the benzene ring. The attack is favoured due to the π-orbital stabilization offered by the nitro group functionality. This activating effect of the nitro group ortho to the C - Br bond increases the electropositivity of the aromatic carbon atom at position 1 of the benzene ring, thus facilitating this first step. This is consided to be the rate determining step.

The mechanism of the second step, although not completely clear, proceeds by the copper bromide complex formed on the benzene ring generating a high positive charge due to the copper acting as a Lewis acid hence making the carbon the most nucleophilic. A second molecule of 2,5-dibromonitrobezene attacks at this position on the carbon ring and the coupling takes place producing copper (II) bromide as a side product.

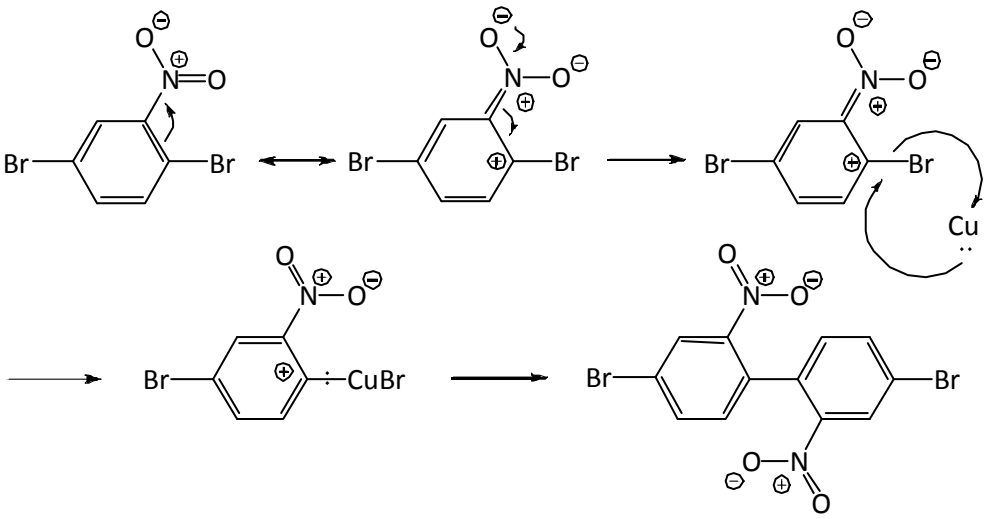

Scheme 4.6: Mechanism of Ullmann coupling reaction forming 4,4'-dibromo-2,2'dinitro biphenyl **(3)**.

The purity of the product was confirmed by a single peak by GC with a retention time of 14.7 min. The masses for 4,4'-dibromo-2,2'-dinitrobiphenyl at 400, 420 and 404 in a 1:2:1 ratio as expected due to ^{79}Br and ^{81}Br isotopes. The melting point of the product was 147-149 °C and was in agreement with reports from literature.[192]

The product was subjected to elemental analysis, for the compound $C_{12}H_6Br_2N_2O_4$ we calculated the expected percentage for the comprising elements to be: C, 35.85; H, 1.50;

Br, 39.75; N, 6.97 %; from analysis we obtained: C, 35.95; H, 1.26; Br, 39.93; N, 6.89 %; which fell into agreement to calculations.

The structure of the product was confirmed by FT-IR spectrum giving peaks at 3071 cm^{-1} and 2850 cm^{-1} as the C-H stretch followed by 1925 cm^{-1}, 1860 cm^{-1}, 1786 cm^{-1} and 1780 cm^{-1} which can be designated to the combination or overtone vibrations of the out-of-plane deformation vibrations of the C-H bonds of the 1, 2,4-trisubstituted benzene ring. Also the bands 1620 cm^{-1}, 1554 cm^{-1}, 1528 cm^{-1} and 1464 cm^{-1} can be donated to C=C for the aromatic rings. The peaks arising at 1528 cm^{-1}, 1341 cm^{-1}, are related to the stretching vibrations of the ar-NO_2 groups and a peak at 865 cm^{-1} stretching vibrations of the C-N bond. Finally the peak at 729 cm^{-1} can be linked to the stretching vibrations of the C-Br bonds.

Based on the ^{1}H-NMR spectrum compound **(3)** identifies the product with 3 distinct signals equal in intensity. The signal at δ 8.37 ppm is linked to the protons assigned on the ring system, which is a singlet due to no coupling with a near by proton. There are protons shown signals at δ 7.17 ppm and δ 7.83 ppm respectively as doublets due close proximity of coupling with one another.

The ^{13}C-NMR gave five peaks on the spectrum which have been estimated to the following positions of the compound δ 147 (2C), δ 138 (2C), δ 132 (4C) and 6, δ 128 (2C) and δ 123 (2C). These peaks are in well agreement with the structure of 4,4’-dibromo-2,2’-dinitrobiphenyl. Since carbons all have the diffrence magnetic moment, it might expect all carbon atoms to give resonance signals at the individual field / frequency values.

All analytical results clearly verify that the product was 4,4’-dibromo-2,2’-dinitrobiphenyl **(3).**

4.4 Synthesis of 2,2'-diamino-4,4'-dibromobiphenyl (4)

Synthesis of 2,2'-diamino-4,4'-dibromobiphenyl **(4)** was obtained from a modified the procedure by Dierschke *et al.*[192]

The product was obtained *via* a reduction reaction of 2,2'-diamino-4,4'-dibromobiphenyl **(4)** using tin powder in a solution mixture of ethanol (HPLC grade) and hydrochloride (conc.), as shown in **Scheme 4.7**. The reaction was complete after heating the mixture for 2 hs at 90 °C to produce a homogeneous solution, and following work-up to give the isolated product as an ivory yellow crystalline solid.

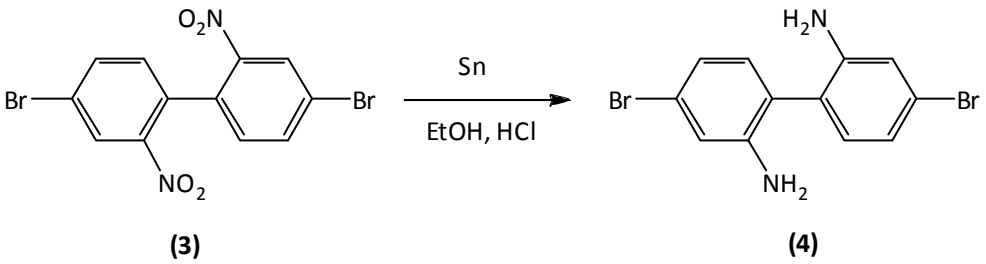

(3) **(4)**

Scheme 4.7: Synthesis of 2,2'-diamino-4,4'-dibromobiphenyl **(4)**.

The purity of the product was confirmed by TLC, GC mass spectra, melting point and elemental analysis. The structure of the product was identified by IR absorption, ^{1}H-NMR and ^{13}C-NMR.

This reaction is considered to be carried out in two parts, the first being the reduction reaction followed by the basification of the mixture in the work-up. The reaction mixture was heterogeneous at first and as the reaction proceeded the tin powder was consumes and the mixture became clearer. This can be considered to occur due to the increased solubility of the product as an amine salt in acidic condition. After 1 h all the tin powder had been consumed, however, the mixture was still heterogeneous probably because the reaction had not reached completion.

After addition of a further portion of tin powder and refluxing for a further period of 1 h the mixture became a homogeneous yellow solution along with a solid lump of excess tin powder. At this point the reaction was considered to have gone to completion and was cooled to room temperature and the tin powder was filtered off. The filtrate was then basifield by pouring onto ice and aqueous sodium hydroxide solution. This produced a fine white suspension probably due a complex formed with the tin. This was filtered off with the aid of Celite® filter gel and the filtrate was then extracted with diethyl ether. The product was obtained as a pale yellow powder.

The reduction of the nitro group to the amine group can be considered to take place mechanistically as follows. The reaction occurs under an acid solution to help formulate a protonated amine. The subsequent treatment with base generates the amine.

$$2ArNO_2 + 3Sn + 12H^+ \longrightarrow 2ArNH_2 + 4H_2O + 3Sn^{4+}$$

Equation 4.1. Reduction of 4,4'-dibromo-2,2'-dinitrobiphenyl **(3)** forming 2,2'-diamine-4,4'-dibromobiphenyl **(4)**.

The purity of the product was confirmed by a single peak by GC with a retention time of 14.6 minutes. The mass spectra showed main integer masses for 2,2'-diamine-4,4'-dibromobiphenyl **(4)** at 340, 342, and 344 in a 1:2:1 ratio as expected due to ^{79}Br and ^{81}Br isotopes.

The melting point of the product was 101-103 °C and was in agreement with reports from literature.[192] The product was subjected to elemental analysis, for the compound $C_{12}H_{10}Br_2N_2$ we calculated the expected percentage for the comprising elements to be: C, 42.14; H, 2.95; Br, 46.72; N, 8.19. %; from analysis we obtained: C, 43.06; H, 2.69; Br, 44.92; N, 7.89. %; which was close to the agreement in calculations.

The structure of the product was confirmed by its IR spectrum giving peaks at 3396 cm^{-1}, 3289 cm^{-1}, 3186 cm^{-1} stretching vibrations of the -NH_2 groups. In reassurance we have lost peaks arising at 1528 cm^{-1}, 1341 cm^{-1} which were related to the stretching vibrations of the Ar-NO_2 groups. The peak at 3073 cm^{-1} as the C-H stretch followed by 1881 cm^{-1}, 1866 cm^{-1}, 1694 $cm^{-1}$and 1639 cm^{-1} which can be designated to the combination or overtone vibrations of the out-of-plane deformation vibrations of the C-H bonds of the 1,2,4-trisubstituted benzene ring. Also the bands 1579 cm^{-1}, 1558 cm^{-1}, 1491 cm^{-1} and 1474 cm^{-1} can be donated to C=C for the aromatic rings. Peaks at 931 cm^{-1}, to 554 cm^{-1} out-of-plane deformation vibrations of the C-NH_2 bonds, and finally the peak at 739 cm^{-1} can be linked to the stretching vibrations of the C-Br bonds.

The ^1H-NMR spectrum identifies the product with 3 distinct signals in the spectrum. The signal at δ 7.0 ppm is linked to the protons assigned on the ring system, which is a singlet due to no coupling with the near proton; a change in chemical shift can be noted from the

transformation of the nitro group to the amine. The protons give rise to the signal at δ 6.97-6.82 ppm as a multiplet due close proximity of coupling with one another and the effect of the amine groups on the chemical shifts. This leaves a broad peak at δ 3.70 ppm which is assigned to the protons within the amine group.

The ^{13}C-NMR gave six peaks on the spectrum which have been estimated to the following positions of the compound δ 145 (2C), δ 132 (2C), δ 123 (2C), δ 122 (2C), δ 119 (2C) and δ 118 (2C). These peaks are in well agreement with the structure of 2,2'-diamine-4,4'-dibromobiphenyl **(4)**.

All these analytical results clearly verify that the proposed product was 2,2'-diamine-4,4'-dibromobiphenyl **(4)**.

4.5 Synthesis of 2,7-dibromo-*9H*-carbazole (5)

Synthesis of 2,7-dibromo-*9H*-carbazole **(5)** was obtained in a 87 % yield and performed according to the procedure by Blouin *et al.*[36]

The product was prepared via a Nazarov cyclization reaction as shown in **Scheme 4.8**. The reaction proceeded by ring closure of the amine groups of 2,2'-diamine-4,4'-dibromobiphenyl **(4)** using phosphoric acid at 180 °C as shown in **Scheme 4.8**. The reaction was complete after heating the mixture for 24 h, following work-up was isolated the product as an orange crystalline solid. The purity of the product was confirmed by TLC, GC mass spectra, melting point and elemental analysis. The structure of the product was identified by IR absorption, ^{1}H NMR and ^{13}C NMR.

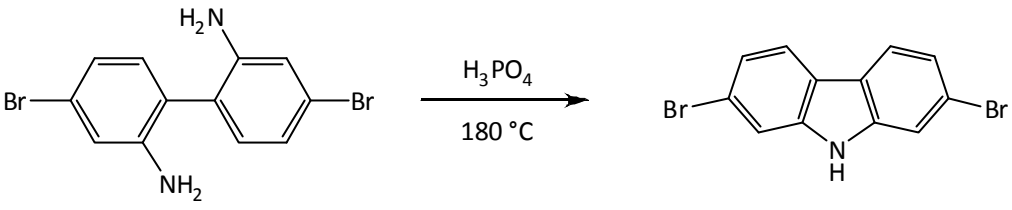

(4) **(5)**

Scheme 4.8: Synthesis of 2,7-dibromo-9H-carbazole **(5)**.

The mechanism of this cyclisation reaction is not fully understood, attempts have been carried out to formulate a mechanism for this process, like that of the reaction of 2,2'-diamino-4,4'-dibromobiphenyl in the presence of aqueous hydrochloric acid carried out by Tauber but in this reaction the reagents and conditions were contrasting and would clearly not work under the basic which was applied.

It can be assumed that the reaction mechanism is achieved through a two step process, the first of which would be the protonation of the amino group to $-NH_3^+$ which would develop a leaving group and the secondary amino group $-NH_2$ acts as a nucleophile. The second step would likely be a intermolecular cyclisation reaction to yield the product. The key step of the reaction mechanism involves a cationic 4π-electrocyclic ring closure as shown in **Scheme 4.9.**

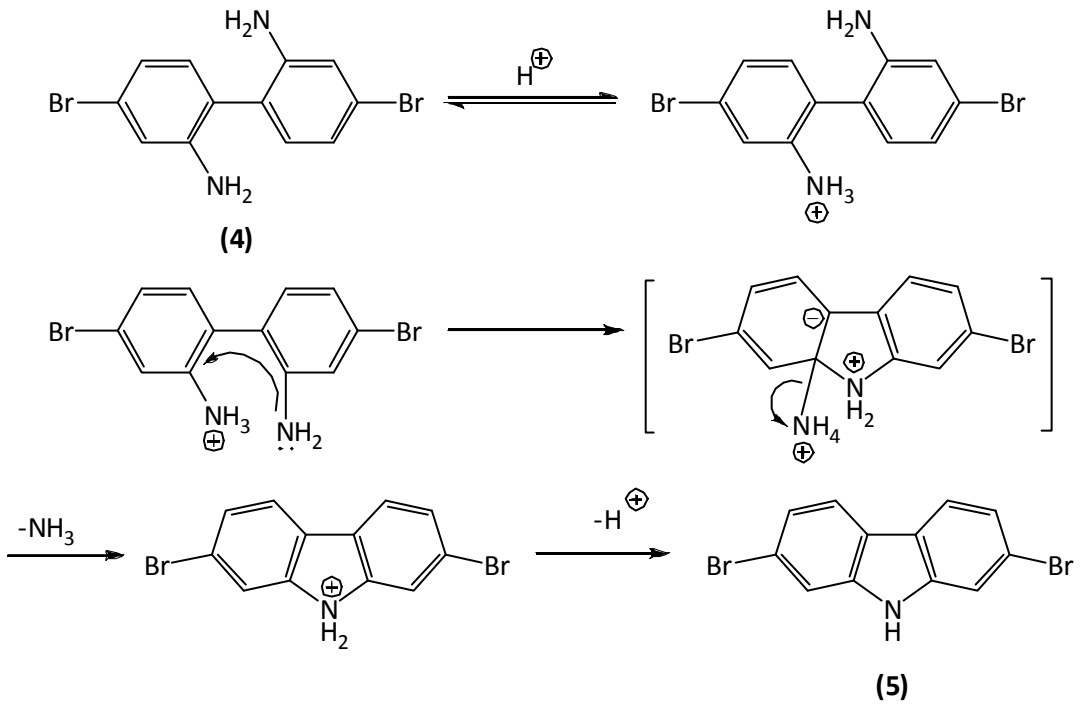

Scheme 4.9: Mechanism of formation of 2,7-dibromo-9H-carbazole **(5)**.

The purity of the product was confirmed by a single peak by GC with a retention time of 15.0 minutes. The mass spectra showed main integer masses for 2,7-dibromo-9H-carbazole **(5)** at 323, 325, and 327 in a 1:2:1 ratio as expected due to ^{79}Br and ^{81}Br isotopes. The melting point of the product was 217-220 °C and was in agreement with reports from literature.[36]

The product was subjected to elemental analysis, for the compound $C_{12}H_7Br_2N$ we calculated the expected percentage for the comprising elements to be : C, 44.35; H, 2.17; Br, 49.17; N, 4.31. %; from analysis we obtained: C, 44.28; H, 1.99; Br, 48.99; N, 4.25. .%; which fell into close agreement to calculations.

The structure of the product was confirmed by IR spectrum giving peaks at 3400 cm^{-1} and 3100 cm^{-1} stretching vibrations of the tertiary –NH groups. The peak at 3074 cm^{-1} relates to the C-H stretch followed by 1889 cm^{-1} and 1705 cm^{-1}, 897 cm^{-1}, 861 cm^{-1}, 805 cm^{-1}, which can be designated to the combination or overtone vibrations of the out-of-plane deformation vibrations of the C-H bonds of the carbazole ring. The peaks arising at 1625 cm^{-1}, 1600 cm^{-1}, 1481 cm^{-1}, 1461 cm^{-1}, 1448 cm^{-1}, 1424 cm^{-1}, stretching vibrations due to C=C bonds of the carbazole ring, also the band at 1241 cm^{-1}, can be donated to C-N on the carbazole ring. Finally the peak at 732 cm^{-1} can be linked to the stretching vibrations of the C-Br bonds.

The ^{1}H-NMR spectrum identifies the product with 4 signals in the spectra. The broad signals at δ 8.00 ppm is linked to the proton 9H on the carbazole ring system. It is the single proton from the attaching tertiary amine with an integral half that of the aromatic carbazole. The next signal is that arising at δ 7.85 ppm which is a doublet in relation to protons. The next set is a singlet at δ 7.45 ppm due to no coupling with near protons. The protons signal also give rise to the signal at δ 7.25 ppm as a doublet.

The ^{13}C-NMR gave six peaks on the spectrum which have been estimated to the following positions of the compound δ 142 (2C), δ 124 (2C), δ 123 (2C), δ 122 (2C), δ 120 (2C) and δ 115 (2C). These peaks are in well agreement with the structure of 2,7-dibromo-9H-carbazole **(5)**.

These analytical results clearly verify that the product was 2,7-dibromo-9H-carbazole **(5)**.

4.6 Synthesis of 2,7-dibromo-9-(heptadecan-9-yl)-*9H*-carbazole (6)

Synthesis of 2,7-dibromo-9-(heptadecan-9-yl)-*9H*-carbazole **(6)** was performed using a modified procedure by Leclerc *et al.*[36]

The crude product was purified *via* silica gel coloumn chromatography pre-absorbed onto silica gel dissolved in DCM and eluting with 40-60 petroleum ether, and then recrystallised from methanol to obtain pure product as white powder in 74 %. The alkylation reaction was carried out at room temperature overnight in DMSO as solvent as seen in **Scheme 4.10.** The KOH was ground and used in excess (1.5 equivalent) to push the reaction towards the product. Then the reaction mixture was poured onto water and extracted with hexane.

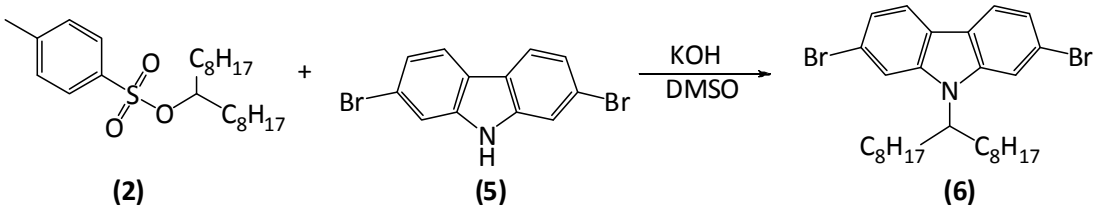

(2) **(5)** **(6)**

Scheme 4.10: Synthesis of 2,7-dibromo-9-(heptadecan-9-yl)-*9H*-carbazole **(6).**

Based on the **Scheme 4.11** the reaction follows a nucleophilic substitution, at first the amine group –NH on the carbazole is deprotonated by the strong base KOH, then the formed ion on nitrogen attacks the carbon close to the tosyl group and gives the desired product. The toyslate group is a good leaving group due to stabilization of negative charge on tosyl group, which also prevent the tosyl group from working as a nucleophile in a reverse reaction.

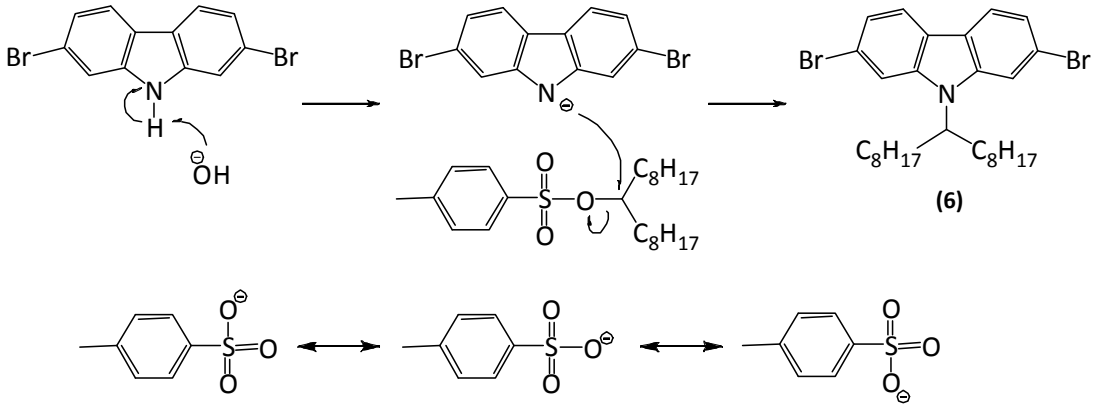

Scheme 4.11: Mechanism of the tosyl group from working as a nucleophile in reverse reaction for forming 2,7-dibromo-9-(heptadecan-9-yl)-*9H*-carbazole **(6)**.

The purity and the chemical structure of the product **(6)** were confirmed by TLC, mass spectra, elemental analysis, NMR analysis and FT-IR. The product gave a single spot on TLC.

The mass spectra shows main integer masses at 561, 563 and 565 in 1:2:1 ratio as expected due to the presence of two bromine isotopes (^{81}Br and ^{79}Br). Elemental analysis CHN of **(6)** was in agreement with its proposed structure.

All analytical results clearly verify and that the proposed product was 2,7-dibromo-9-(heptadecan-9-yl)-*9H*-carbazole **(6).** The ^{1}H-NMR spectra showed broad doublet peaks at 7.75 ppm and 7.57 ppm, which belong to the aromatic protons, the atropisomerism phenomenon is the reason for arising those broad peaks, and it arises from the restricted rotation around a single bond. Also this phenomenon resulted in multiple peaks observed in the ^{13}C NMR spectra in the aromatic region from 155 ppm to 106 ppm.

The FT-IR of the product showed that peak, which corresponded to –NH group at 3451 cm^{-1} in the compound **(5)** has disappeared, and all peaks that corresponded to tosyl group in the compound **(2)** also disappeared.

4.7 Synthesis of 9-(heptadecan-9-yl)-2,7-bis(4,4,5,5-tetramethyl-1,3,2-dioxaborolan-2-yl)-*9H*-carbazole (7)

Synthesis of 9-(heptadecan-9-yl)-2,7-bis(4,4,5,5-tetramethyl-1,3,2-dioxaborolan-2-yl)-*9H*-carbazole **(7)** was synthesized using a modified procedure by Jo *et al.* [201] Blouin *et al.*[36], Yamato *et al.*[193] and Sonntag *et al.*[194] as shown in **Scheme 4.12**.

The product was obtained via recrystallisation as a light brown powder in 87 % yield

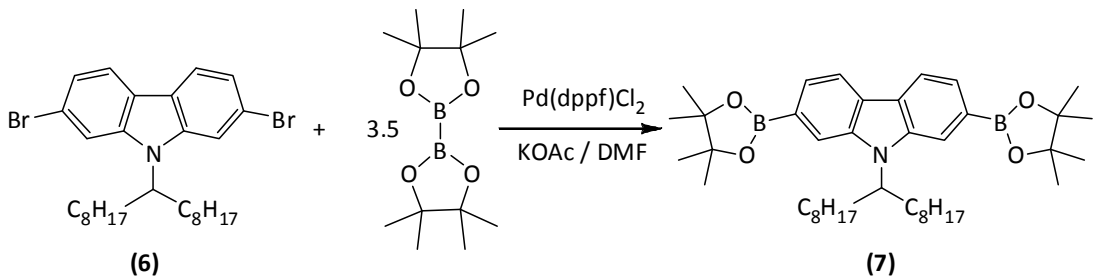

(6) **(7)**

Scheme 4.12: Synthesis of N-(heptadecan-9-yl)-2,7-bis(4,4,5,5-tetramethyl-1,3,2-dioxaborolan -2-yl)-*9H*-carbazole **(7).**

The reaction was performed in dry DMF at 100 °C for 36 h, in the presence of excess amount of bis(pinacolato)diboron to prevent the formation of oligomers, potassium acetate as the base and the [1,1'-bis(diphenylphosphino)ferrocene]dichloropalladium(II) [Pd(dppf)Cl_2] as the reaction catalyst. After completing the reaction, the water was added and then the product extracted with diethyl ether.

The crude product was purified via recrystallisation from methanol, which was passed through a column of basic alumina to remove catalyst residues. Basic alumina was used as the formed boronic ester is very sensitive for degradation in the presence of acids; the crude product was dissolved in a small amount of acetone before precipitating in hot methanol.

The reaction mechanism shown in **Scheme 4.13** follows the Suzuki cross coupling mechanism, Miyaura *et al.*[202] proposed a mechanism for transformation of arylhalides to arylboronic ester using bis(pinacolato)diboron as a reagent, this mechanism involves oxidative addition of the [Pd(dppf)Cl_2] at first step, then the bromide group on the palladium is displaced by the acetate, which leads to the tetra coordinate palladium(II) complex, then transmetalation takes place with bis(pinacolato)diboron, and then a reductive elimination to obtain the product arylboronic ester with [Pd(dppf)].

The purity and chemical structure of product **(7)** were confirmed by Elemental analysis CHN, which was in good agreement with its proposed structure, the mass spectra show a peak with main integer mass at 657.

The ^{1}H-NMR displayed three broad peaks at 7.89 ppm, 7.80-7.71 ppm and 7.67 ppm which belong to the aromatic proton; the broad peaks arise from the atropisomerism phenomenon as shown in **Figure 4.1.** The ^{13}C NMR showed multiple peaks in aromatic region, which is also a result of the atropisomerism phenomenon.

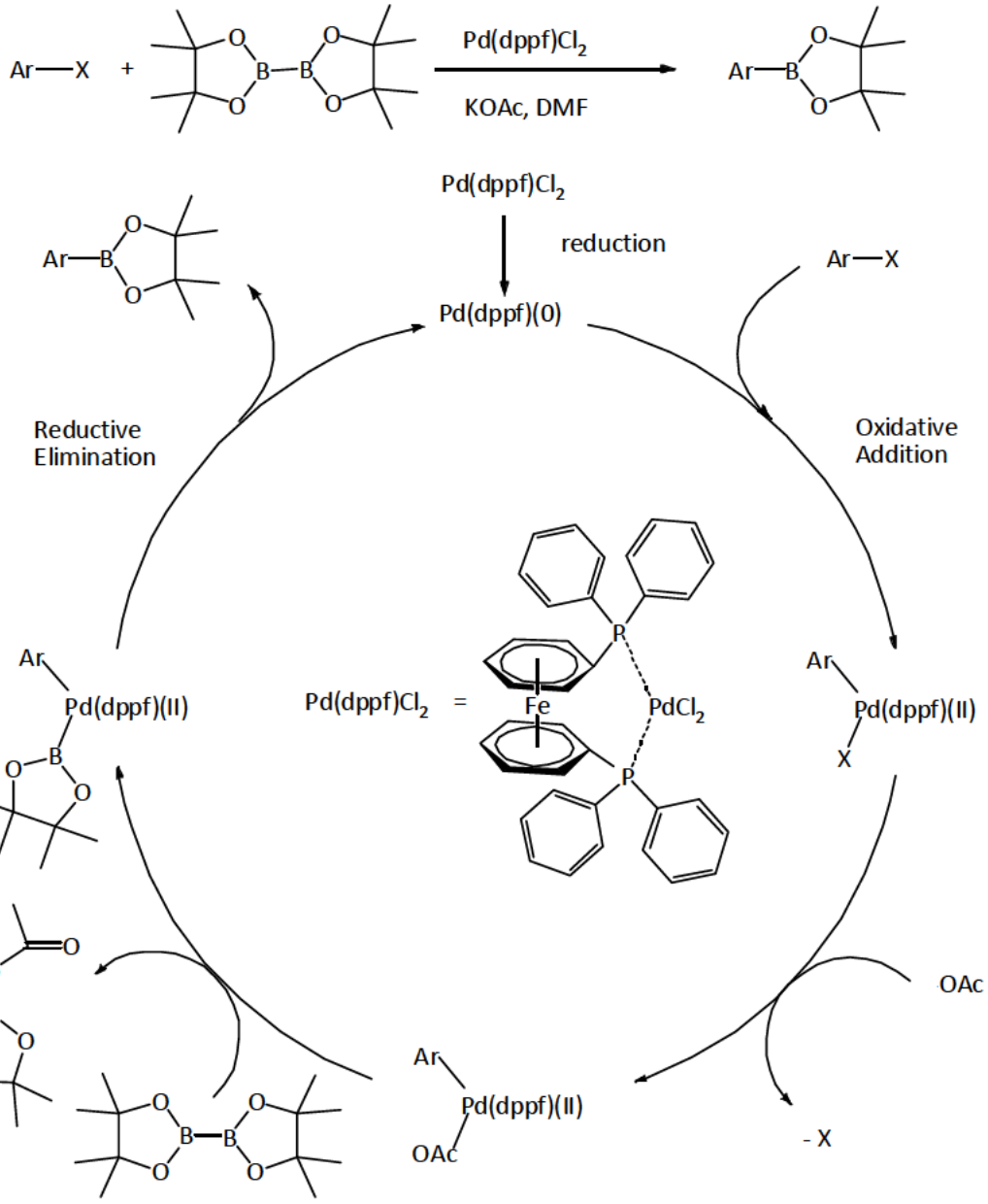

Scheme 4.13: Mechanism of the proposed reaction mechanism for preparing arylboronic esters.

The FT-IR spectra showed absorption band at 1389 cm^{-1} and 1330 cm^{-1} corresponding to the stretching vibration of the B-O bond, one band at 1138 cm^{-1} which corresponds to the B-C stretching. Also a band at 1089 cm^{-1}, which corresponded to the C-Br stretching in the compound **(6)**, has disappeared.

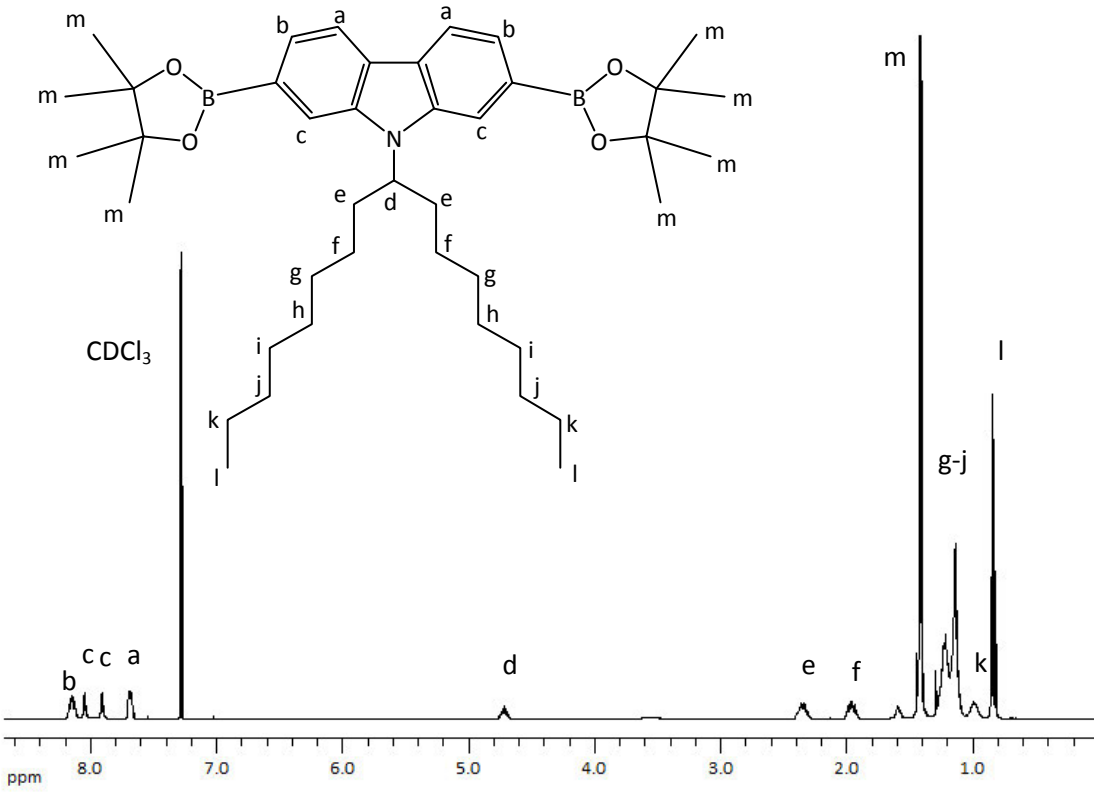

Figure 4.1: ^{1}H-NMR of monomer 9-(heptadecan-9-yl)-2,7-bis(4,4,5,5-tetramethyl-1,3,2-dioxaborolan-2-yl)-*9H*-carbazole **(7)** in $CDCl_3$.

All analytical results clearly verify and proposed that the product was 9-(heptadecan-9-yl)-2,7-bis(4,4,5,5-tetramethyl-1,3,2-dioxaborolan-2-yl)-*9H*-carbazole **(7).**

4.8 Synthesis of pentacosan-13-ol (8)

Synthesis of pentacosan-13-ol **(8)** was performed according to the procedure by Leclerc *et al.*[36]

The crude product was obtained as colourless oil, which then crystallized to a white solid over time in 92 % yield. The preliminary analyses confirmed the purity of crude product, so

it was used in the next reaction without purification. The reaction mechanism for this reaction is the same as that proposed for the preparation of **(1)**.

The purity and the chemical structure of the pentacosan-13-ol **(8)** were confirmed by TLC, the melting point, the mass spectra, elemental analysis, NMR analysis and FT-IR. The product gave a single spot on TLC, and the melting point was 85 88 °C.[36]

The mass spectra shows main integer masses for pentacosan-13-ol **(8)**, which is observed at 369. Elemental analysis CHN of **(8)** was in agreement with its proposed structure. The NMR analysis showed the expected peaks as mentioned in the literature. FT-IR displayed a peak at 3308 cm^{-1} which belongs to the O-H stretching of the hydroxyl group. Also it displayed strong peaks at 2956, 2914 and 2848 cm^{-1}, due to the C-H stretch vibration of alkyl chains.

All analytical results clearly verify and that the proposed product was pentacosan-13-ol **(8).**

4.9 Synthesis of pentacosan-13-yl 4-methylbenzenesulfonate (9)

Synthesis of pentacosan-13-yl 4-methylbenzenesulfonate **(9)** was performed according to the procedure by Leclerc *et al.*[36]

Compound **(9)** was prepared by using pentacosan-13-ol **(8)** as starting materials as shown in **Scheme 4.14.** The product was purified *via* silica gel column chromatography, eluting with (89 % hexane, 9 % ethylacetate, 2 % Et_3N) to obtain **(9)** as a white solid in 89 % yield.

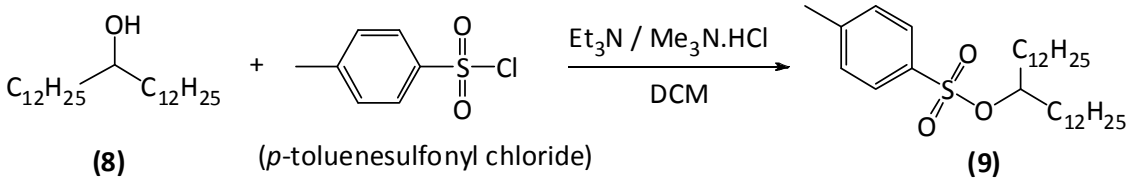

(8) (*p*-toluenesulfonyl chloride) **(9)**

Scheme 4.14: Synthesis of pentacosan-13-yl 4-methylbenzenesulfonate **(9)**.

The product **(9)** was obtained *via* a tosylation method by using *p*-toluenesulfonyl chloride, trimethylamine hydrochloride as a catalyst in the presence of the base triethylamine. The

reaction was carried out at low temperature (5-10 °C) for 90 min, and the reaction mechanism of **(9)** follows the same route as that described for the synthesis of **(2)**.

The purity and the chemical structure of the product **(9)** were confirmed by TLC, the melting point, the mass spectra, elemental analysis, NMR analysis and FT-IR. The product gave a single spot on TLC, and the melting point was 30-33 °C, which was in good agreement with that reported in the literature (31-32 °C).[36]

The mass spectra shows main integer masses for pentacosan-13-yl 4-methylbenzenesulfonate **(9)** which is observed at 545, and the elemental analysis CHN of **(9)** was in agreement with its proposed structure.

The ^{1}H-NMR spectra showed new peaks, two doublet peaks at 7.98 ppm and 7.81 ppm, which corresponded to tosyl group. The multi peaks at 3.60 ppm in previous compound **(8)** was shifted to 4.50 ppm, which belongs to the protons close to the tosyl group. Also a new singlet peak appeared at 2.46 ppm, which corresponded to the methyl of the tosyl group.

The FT-IR of the product **(9)** shows that the strong peak at 3321 cm^{-1}, which belonged to the O-H stretching of the hydroxyl group in the previous compound **(8)**, has disappeared. Also new peaks were observed as following: at 2954 cm^{-1} belonging to the stretching vibration of the C-H in the aromatic tosyl group, at 1597 and 1566 cm^{-1} belonging to the strechingg vibration of the C-C double bonds in aromatic tosyl group, at 1353 cm^{-1} and 1353 cm^{-1} belonging to the stretching vibration of the (-SO_2) in sulfonate group, at 1021 cm^{-1}, which belongs to the (-S-O-) bonds in sulfonate group.

All analytical results clearly verify and that the proposed product was pentacosan-13-yl 4-methylbenzenesulfonate **(9).**

4.10 Synthesis of 2,7-dibromo-9-(pentacosan-13-yl)-*9H*-carbazole (10)

Synthesis of 2,7-dibromo-9-(pentacosan-13-yl)-*9H*-carbazole **(10)** was performed using a modified procedure by Leclerc *et al.*[36]

The crude product was purified *via* silica gel coloumn chromatography pre-absorbed onto silica gel dissolved in DCM and eluting with 40-60 petroleum ether, and then recrystallised from methanol to obtain pure product as white powder in 69 %.

The alkylation reaction was carried out at room temperature overnight in DMSO as solvent as seen in **Scheme 4.15.** The KOH was ground and used in excess (1.5 equivalent) to push the reaction towards the product. Then the reaction mixture was poured onto water and extracted with hexane.

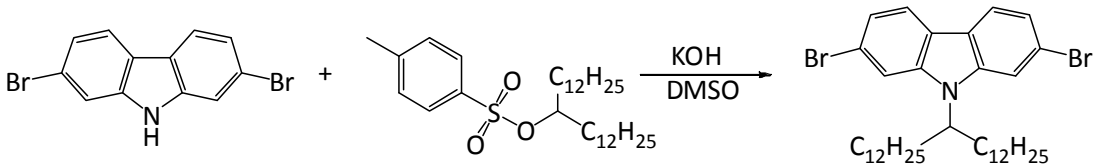

(5) **(9)** **(10)**

Scheme 4.15: Synthesis of 2,7-dibromo-9-(pentacosan-13-yl)-9H-carbazole **(10).**

The reaction follow is the same mechanisms that for the preparation of compound **(6)**. The purity and the chemical structure of the product **(10)** were confirmed by TLC, mass spectra, elemental analysis, NMR analysis and FT-IR. The product gave a single spot on TLC. The mass spectra shows main integer masses at 673, 675 and 677 in 1:2:1 ratio as expected due to the presence of two bromine isotopes (^{81}Br and ^{79}Br). Elemental analysis CHN of **(10)** was in agreement with its proposed structure.

The ^{1}H-NMR spectra showed broad doublet peaks at 7.75 ppm and 7.57 ppm, which belong to the aromatic protons, the atropisomerism phenomenon is the reason for arising those broad peaks, and it arises from the restricted rotation around a single bond. Also this phenomenon resulted in multiple peaks observed in the ^{13}C NMR spectra in the aromatic region from 155 ppm to 106 ppm. The FT-IR of the product showed that peak, which corresponded to –NH group at 3451 cm^{-1} in the compound **(5)** has disappeared, and all peaks that corresponded to tosyl group in the compound **(9)** also disappeared.

All analytical results clearly verify and that the proposed product was 2,7-dibromo-9-(pentacosan-13-yl)-9H-carbazole **(10)**.

4.11 Synthesis of 1,4-dibromo-2-fluoro-5-nitrobenzene (11)

Synthesis of 1,4-dibromo-2-fluoro-5-nitrobenzene **(11)** was obtained from a modified procedure by Kun *et al.*[182] and Choy *et al.*[203]

The product was obtained *via* recrystalisation from ethanol as a yellow solid with a high yield of 87 %. The starting material used in the beginning of the reaction was 1,4-bromo-2-fluorobenzene as shown in **Scheme 4.16**.

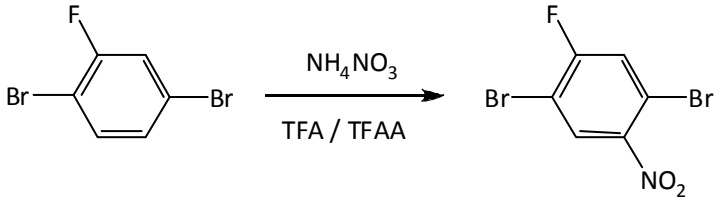

1,4-dibromo-2-fluorobenzene **(11)**

Scheme 4.16: Synthesis of 1,4-dibromo-2-fluoro-5-nitrobenzene **(11)**.

The reaction was carried out in the presence of trifluoroacetic acid, trifluoroacetic anhydride as a catalyst, and ammonium nitrate as a source of nitro- group. At first, ammonium nitrate combines with trifluoroacetic anhydride to form a nitronium cation (NO_2^+), which then attacks the aromatic ring in an electrophilic substitution reaction. **Scheme 4.17** shows the two steps mechanism of the reaction.

The reaction was carried out at room temperature and allowed to stir overnight, then the mixture poured onto ice and the product was extracted with DCM. The purity and structure of the product was confirmed by ^{1}H-NMR, ^{13}C-NMR, mass spectra, elemental analysis, FT-IR and TLC (R_f=0.73).

The ^{1}H-NMR spectra shows two doublet peaks at 8.21 ppm and 7.56 ppm for the aromatic protons. The ^{13}C-NMR spectra show six peaks, three of them are singlet at 130.9, 114.9 and 114.9 ppm, the other three are doublet at 160.6, 122.9 and 108.9 ppm, which are related to carbons that are close to the fluorine atom, because the coupling between carbon and fluorine (spin ½) is very strong.

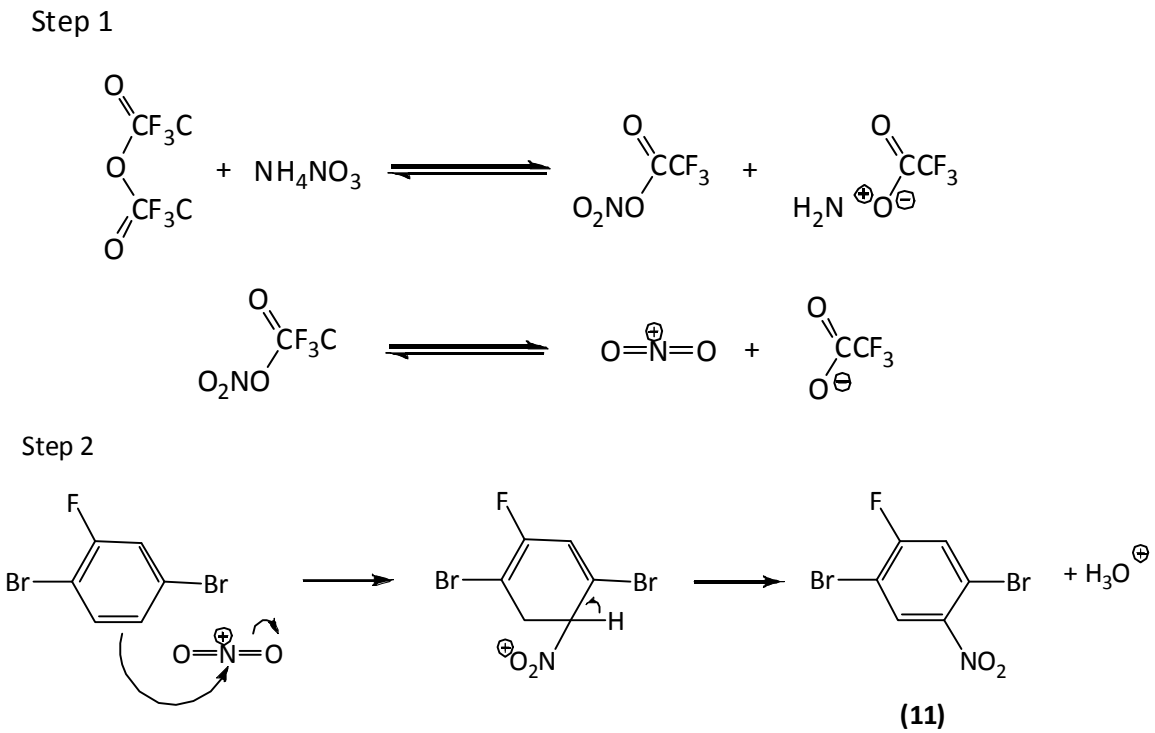

Scheme 4.17: The formation of nitronium ion and then electrophilic substitution reaction to form 1,4-dibromo-2-fluoro-5-nitrobenzene **(11)**.

The mass spectra shows main integer masses for 1,4-dibromo-2-fluoro-5-nitrobenzene **(11)**, which are observed at 297, 299 and 301 in 1:2:1 ratio as expected because of presence of two bromine isotopes (^{79}Br and ^{81}Br). The melting point was 59.5 °C, which was in good agreement with literature values.[203] The CHN elemental analysis also was well consistent with the proposed structure.

The FT-IR of the product displays two bands at 1567 cm^{-1} and 1345 cm^{-1}, which belong to the stretching vibration (asymmetrical and symmetrical) of the aromatic nitro group. A band at 1249 cm^{-1} is related to the stretching vibration of the C-F bond and another band at 1066 cm^{-1} belongs to the stretching vibration of the C-Br bond.

Also, from FT-IR spectra, the C-H stretching vibration band appears at 3021 cm^{-1} and 1585 cm^{-1}, the C-C stretching vibration band appears at 1526 cm^{-1} and 1463 cm^{-1}.

All analytical results clearly verify and proposed that the product was 1,4-dibromo-2-fluoro-5-nitrobenzene **(11)**.

4.12 Synthesis of 4,4'-dibromo-5,5'-difluoro-2,2'-dinitrobiphenyl (12)

Synthesis of 4,4'-dibromo-5,5'-difluoro-2,2'-dinitrobiphenyl **(12)** was obtained from a modified procedure by Kun *et al.*[182]

The product was obtained via recrystalisation from ethanol as a yellow in 71 % yield. The product was obtained by an Ullmann coupling reaction, which was carried out in dry DMF at 120 °C for 3 h as shown in **Scheme 4.18**. After completing the reaction, toluene was added and unreacted Cu was filtered off, then the solvent was removed before recrystallising the product from ethanol, and then analysis by TLC which gave a single spot.

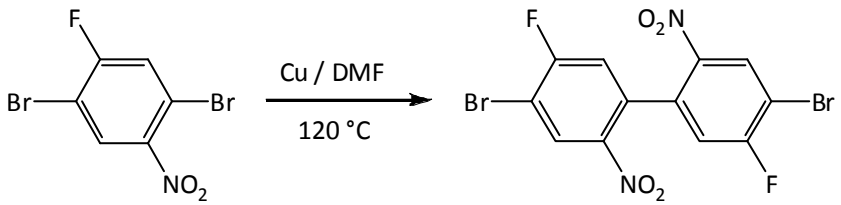

(11) **(12)**

Scheme 4.18: Synthesis of 4,4'-dibromo-5,5'-difluoro-2,2'-dinitrobiphenyl **(12)**.

The mechanism of this reaction is similar to that proposed for the formation of **(3)**. The purity and structure of product was confirmed by TLC, the mass spectra, melting point, elemental analysis, NMR analysis and FT-IR. The mass spectra shows main integer masses for 4,4-dibromo-5,5-difloro-2,2-dinitro-biphenyl **(11)**, which observed at 436, 438 and 440 in 1:2:1 ratio as expected due to the presence of two bromine isotopes (^{79}Br and ^{81}Br). The melting point was 115.5-116.7 C, which was in good agreement with literature values.[182] Elemental analysis CHN of (II) was also in agreement with proposed structure.

The ^{1}H NMR spectra showed two dublets in the aromatic region at 8.57 ppm and 7.09 ppm. The ^{13}C NMR spectra showed six peaks, three of them are singlet at 142.9, 134.0 and 131.1 ppm, the other three are triplets at 161.7, 118.3 and 110.4 ppm, which related to the

carbons that are close to fluorine atom, because the coupling between carbon and fluorine (spin ½) is very strong.

The FT-IR of the product displays two bands at 1520 cm^{-1} and 1335 cm^{-1}, which belong to the stretching vibration (asymmetrical and symmetrical) of the aromatic nitro group. A band at 1288 cm^{-1} is related to the stretching vibration of the C-F bond and another band at 1065 cm^{-1} belongs to the stretching vibration of the C-Br bond. Also, from IR spectra, the C-H stretching vibration band appears at 3071 cm^{-1} and 1489 cm^{-1}, the C-C stretching vibration band appears at 1564 cm^{-1} and 1463 cm^{-1}.

All analytical results clearly verify and that the proposed product was 4,4'-dibromo-5,5'-difluoro-2,2'-dinitrobiphenyl **(12)**.

4.13 Synthesis of 4,4'-dibromo-5,5'-difluorobiphenyl-2,2'-diamine (13)

4,4-Dibromo-5,5-difluoro-biphenyl-2,2-diamine **(13)** was prepared according to a modified procedure by Yamato *et al.*[193] and Kun *et al*.[182], through reduction of compound **(12)** by using tin powder in a mixture of ethanol and HCl, as shown in **Scheme 4.19**. The product was obtained via recrystallisation from ethanol as a pale brown powder in 94 % yield.

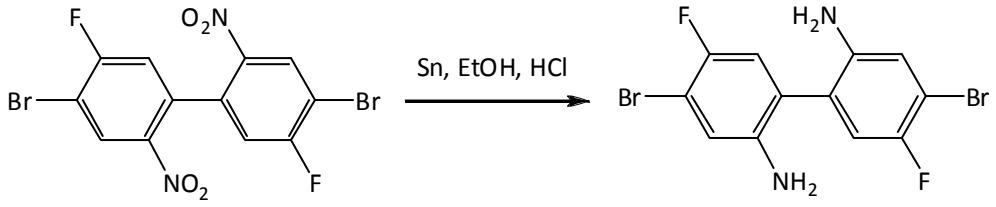

(12) **(13)**

Scheme 4.19: Synthesis of 4,4-dibromo-5,5-difluoro-biphenyl-2,2-diamine **(13)**.

The reduction reaction of 4,4-dibromo-5,5-difluoro-biphenyl-2,2-diamine **(13)** was carried out in presence of HCl and tin, which was added in two portions during the reaction, the reaction mixture was heated to reflux for 150 min to produce a homogenous solution, and then cooled to room temperature and the unreacted tin was filtered off. The mechanism of reaction is thought to proceed are similar monomer to that described for the formation of

(4). The purity and the chemical structure of product 4,4-dibromo-5,5-difluoro-biphenyl-2,2-diamine **(13)** were confirmed by TLC, the melting point, the mass spectra, elemental analysis, NMR analysis and FT-IR.

The product gave a single spot on TLC, and the melting point was 163-168, which is lower than starting material, where the nitro-nitro interaction is stronger than N-H hydrogen-bonding, and it was in good agreement with that reported in the literature. [182]

The mass spectra shows main integer masses for 4,4-dibromo-5,5-difluoro-biphenyl-2,2-diamine **(13)**, which are observed at 376, 378 and 380 in 1:2:1 ratio as expected due to the presence of two bromine isotope (^{81}Br and ^{79}Br). Elemental analysis CHN of 4,4-dibromo-5,5-difluoro-biphenyl-2,2-diamine **(13),** gave satisfactory results.

The ^{1}H-NMR spectra showed a new broad peak at 3.67 ppm corresponding to the amine groups. It also showed two doublets in the aromatic region at 6.99 ppm and 6.90 ppm. The ^{13}C NMR spectra showed six peaks, three of them are singlet at 140.9, 122.9 and 119.8 ppm, the other three are doublets at 152.4, 117.9 and 109.4 ppm, which are related to the carbons close to fluorine atom.

The FT-IR of the product displays two band at 3309 cm^{-1} and 1622 cm^{-1}, which belong to the stretching and bending vibration of the N-H group. A band at 1056 cm^{-1} is related to the stretching vibration of the C-N bond and another band at 1163 cm^{-1} belongs to the stretching vibration of the C-Br bond. The C-H stretching vibration band appears at 3191 cm^{-1} and 1483 cm^{-1}.

All analytical results clearly verify and that the proposed product was 4,4-dibromo-5,5-difluoro-biphenyl-2,2-diamine **(13)**.

4.14 Synthesis of 2,7-dibromo-3,6-difluoro-*9H*-carbazole (14)

Synthesis of 2,7-dibromo-3,6-difluoro-*9H*-carbazole **(14)** was prepared according to a modified procedure by Sonntag *et al.*[194] and Kun *et al.*[182]

Compound **(14)** was prepared by using 4,4-dibromo-5,5-difluoro-biphenyl-2,2-diamine **(13)** as starting materials as shown in **Scheme 4.20.** The product was obtained by recrystallisation from a mixture of toluene/hexane (10:1) as an ivory powder in 73 % yield.

The cyclisation reaction was carried out by heating the starting material 2,7-dibromo-3,6-difluoro-*9H*-carbazole **(14)** in concentrated phosphoric acid at 180 °C for 24 h, then the crude product was filtered and washed with water several times to remove the acid and then solubilised in toluene and the solution filtered through a silica gel plug to remove brown residue traces from the product.

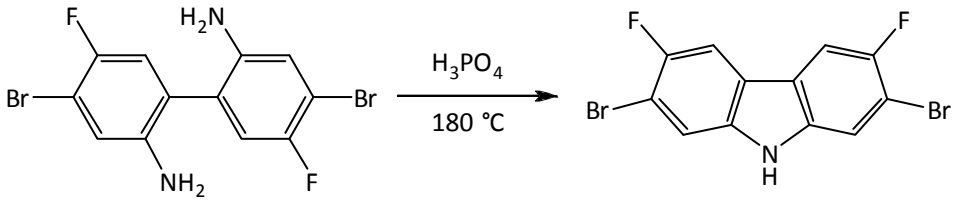

(13) **(14)**

Scheme 4.20: Synthesis of 2,7-dibromo-3,6-difluoro-9H-carbazole **(14)**.

The mechanism of this reaction is similar to that for the formation of **(5)**. The purity and the chemical structure of the product **(14)** were confirmed by TLC, the melting point, the mass spectra, elemental analysis, NMR analysis and FT-IR. The product gave a single spot on TLC, and the melting point was 348 °C, which was in good agreement with that reported in the literature (340-346 °C).[194]

The mass spectra shows main integer masses for 2,7-dibromo-3,6-difluoro-*9H*-carbazole **(14)**, which are observed at 359, 361 and 363 in 1:2:1 ratio as expected due to the presence of two bromine isotopes (^{81}Br and ^{79}Br). Elemental analysis CHN of 2,7-dibromo-3,6-difluoro-*9H*-carbazole **(14)** was in agreement with proposed structure.

The ^{1}H-NMR spectra showed a new broad peak at 10.63 ppm corresponding to the amine groups (-NH). Meanwhile the broad peak at 3.67 ppm corresponding to the amine groups (-NH_2) of the compound 2,7-dibromo-3,6-difluoro-*9H*-carbazole **(14)** disappeared; It also showed two doublets in the aromatic region at 8.07 ppm and 7.83 ppm.

The ^{13}C-NMR spectra showed six peaks, four of them are singlet at 138.7, 123.1, 116.4 and 108.2 ppm; the other three are doublets at 153.9 and 107.9 ppm, which are related to the carbons close to the fluorine atom.

The FT-IR of the product display a new strong absorption peak at 3451 cm^{-1}, which belong to the stretching vibration of the –NH group. A band at 1205 cm^{-1} is related to the stretching vibration of thee C-N bond and another band at 1151 cm^{-1} belongs to the stretching vibration of the C-Br bond. The C-H stretching vibration band appears at 3042 cm^{-1} and 1477 cm^{-1}. The peaks that belonged to –NH_2 in starting material 2,7-dibromo-3,6-difluoro-*9H*-carbazole **(14)** at 3309 cm^{-1} and 1622 cm^{-1} has disappeared.

All analytical results clearly verify that the proposed product was 2,7-dibromo-3,6-difluoro-9H-carbazole **(14)**.

4.15 Synthesis of 2,7-dibromo-3,6-difluoro-9-(heptadecan-9-yl)-*9H*-carbazole (15)

Synthesis of 2,7-dibromo-3,6-difluoro-9-(heptadecan-9-yl)-*9H*-carbazole **(15)** was performed using a modified procedure by Leclerc *et al.*[36]

The crude product was purified *via* silica gel coloumn chromatography pre-absorbed onto silica gel dissolved in DCM and eluting with 40-60 petroleum ether, and then recrystallised from methanol to obtain pure product as white powder in 87 %. The alkylation reaction was carried out at room temperature overnight in DMSO as solvent as seen in **Scheme 4.28.** The KOH was ground and used in excess (1.5 equivalent) to push the reaction towards the product. Then the reaction mixture was poured onto water and extracted with hexane.

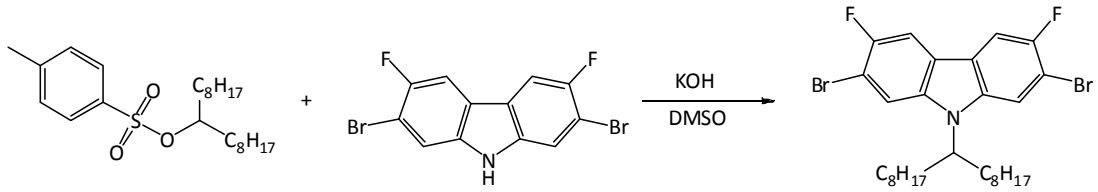

(2) **(14)** **(15)**

Scheme 4.21: Synthesis of 2,7-dibromo-3,6-difluoro-9-(1-octyl-nonyl)-*9H*-carbazole **(15)**.

The mechanism of the reaction is similar to that for the formation of (6). The purity and the chemical structure of the product **(15)** were confirmed by TLC, mass spectra, elemental analysis, NMR analysis and FT-IR. The product gave a single spot on TLC. The mass spectra shows main integer masses at 597, 599 and 601 in 1:2:1 ratio as expected due to the presence of two bromine isotopes (^{79}Br and ^{81}Br). Elemental analysis CHN of **(15)** was in agreement with its proposed structure.

All analytical results clearly verify that the product was 2,7-dibromo-3,6-difluoro-9-(1-octyl-nonyl)-*9H*-carbazole **(15)**. The ^{1}H-NMR spectra showed broad doublet peaks at 7.73 ppm and 7.57 ppm, which belong to the aromatic protons, the atropisomerism phenomenon is the reason for arising those broad peaks, and it arises from the restricted rotation around a single bond. Also this phenomenon resulted in multiple peaks observed in the ^{13}C NMR spectra in the aromatic region from 155 ppm to 106 ppm.

The FT-IR of the product showed that peak, which corresponded to –NH group at 3451 cm^{-1} in the compound **(14)** has disappeared, and all peaks that corresponded to tosyl group in the compound **(2)** also disappeared.

4.16 Synthesis of 3,6-difluoro-9-(heptadecan-9-yl)-2,7-bis(4,4,5,5-tetramethyl-1,3,2-dioxaborolan-2-yl)-*9H*-carbazole (16)

Synthesis of 3,6-difluoro-9-(heptadecan-9-yl)-2,7-bis(4,4,5,5-tetramethyl-1,3,2-dioxaborolan-2-yl)-*9H*-carbazole **(16)** was synthesized using a modified procedure by Jo *et al.*[201] as shown in **Scheme 4.22**. The product was obtained via recrystallisation as a light brown powder in 60 % yield.

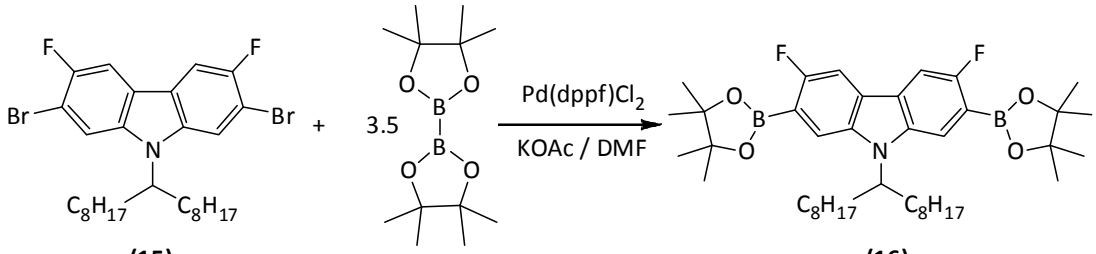

(15) **(16)**

Scheme 4.22: Synthesis of 3,6-difluoro-9-(heptadecan-9-yl)-2,7-bis(4,4,5,5-tetra methyl-1,3,2-dioxaborolan-2-yl)-*9H*-carbazole **(16).**

The reaction was performed in dry DMF at 100 °C for 36 h, in the presence of excess amount of bis(pinacolato)diboron to prevent the formation of oligomers, potassium acetate as the base and the [1,1'-bis(diphenylphosphino)ferrocene]dichloropalladium(II) [Pd(dppf)Cl_2] as the reaction catalyst. After completing the reaction, the water was added and then the product extracted with diethyl ether.

The crude product was purified via recrystallisation from methanol, which was passed through a column of basic alumina to remove catalyst residues. Basic alumina was used as the formed boronic ester is very sensitive for degradation in the presence of acids; the crude product was dissolved in a small amount of acetone before precipitating in hot methanol.

The reaction mechanism is similar to that for the formation of **(7)**. The purity and chemical structure of product **(16)** were confirmed by Elemental analysis CHN, which was in good agreement with its proposed structure, the mass spectra show a peak with main integer mass at 693.

The ^{1}H-NMR displayed three broad peaks at 8.89 ppm, 7.80-7.71 ppm and 7.67 ppm which belong to the aromatic proton; the broad peaks arise from the atropisomerism phenomenon as shown in **Figure 4.2.** The ^{13}C NMR showed multiple peaks in aromatic region, which is also a result of the atropisomerism phenomenon.

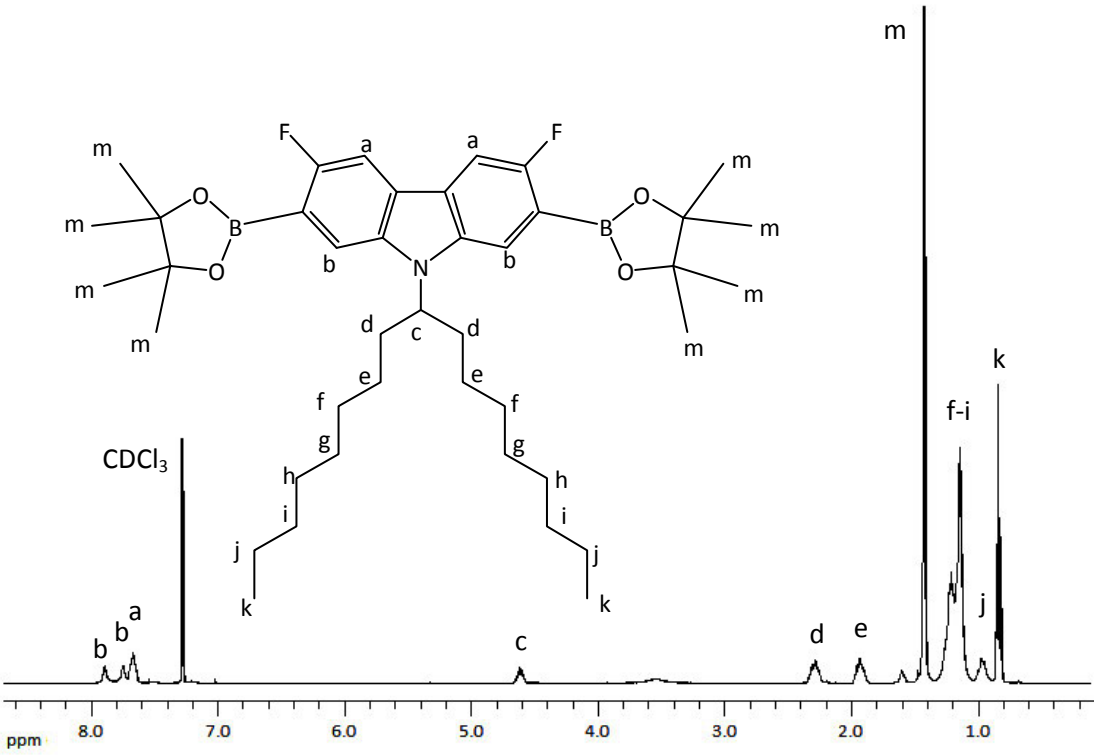

Figure 4.2: ^{1}H-NMR of monomer 3,6-difluoro-9-(heptadecan-9-yl)-2,7-bis(4,4,5,5-tetra methyl-1,3,2-dioxaborolan-2-yl)-*9H*-carbazole **(16)** in $CDCl_3$**.**

The FT-IR spectra showed absorption band at 1389 cm^{-1} and 1330 cm^{-1} corresponding to the stretching vibration of the B-O bond, one band at 1138 cm^{-1} which corresponds to the B-C stretching. Also a band at 1089 cm^{-1}, which corresponded to the C-Br stretching in the compound **(15)**, has disappeared.

All analytical results clearly verify that the proposed product was 3,6-difluoro-9-(heptadecan-9-yl)-2,7-bis(4,4,5,5-tetra methyl-1,3,2-dioxaborolan-2-yl)-*9H*-carbazole **(16).**

4.17 Synthesis of 2,7-dibromo-3,6-difluoro-9-(pentacosan-13-yl)-*9H*-carbazole (17)

Synthesis of 2,7-dibromo-3,6-difluoro-9-(pentacosan-13-yl)-*9H*-carbazole **(17)** was performed using a modified procedure by Leclerc *et al.*[36]

The crude product was purified *via* silica gel coloumn chromatography pre-absorbed onto silica gel dissolved in DCM and eluting with 40-60 petroleum ether, and then recrystallised from methanol to obtain pure product as white powder in 73 %.

The alkylation reaction was carried out at room temperature overnight in DMSO as solvent as seen in **Scheme 4.23.** The KOH was ground and used in excess (1.5 equivalent) to push the reaction towards the product. Then the reaction mixture was poured onto water and extracted with hexane.

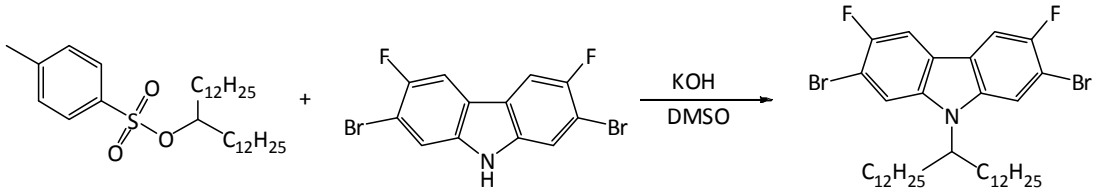

(9) **(14)** **(17)**

Scheme 4.23: Synthesis of 2,7-dibromo-3,6-difluoro-9-(pentacosan-13-yl)-*9H*-carbazole **(17).**

The mechanism of the reaction is similar to that for the formation of **(6)**. The purity and the chemical structure of the product **(17)** were confirmed by TLC, mass spectra, elemental analysis, NMR analysis and FT-IR. The product gave a single spot on TLC. The mass spectra shows main integer masses at 561, 563 and 565 in 1:2:1 ratio as expected due to the presence of two bromine isotopes (^{81}Br and ^{79}Br). Elemental analysis CHN of **(17)** was in agreement with its proposed structure.

The ^{1}H-NMR spectra showed broad doublet peaks at 7.72 ppm and 7.54 ppm, which belong to the aromatic protons, the atropisomerism phenomenon is the reason for arising those broad peaks, and it arises from the restricted rotation around a single bond. Also this phenomenon resulted in multiple peaks observed in the ^{13}C NMR spectra in the aromatic region from 153 ppm to 106 ppm.

The FT-IR of the product showed that peak, which corresponded to –NH group at 3451 cm^{-1} in the compound **(14)** has disappeared, and all peaks that corresponded to tosyl group in the compound **(9)** also disappeared.

All analytical results clearly verify that the proposed product was 2,7-dibromo-3,6-difluoro-9-(pentacosan-13-yl)-*9H*-carbazole **(17).**

4.18 Synthesis of 3-bromothiophene-2-carbaldehyde (18)

Synthesis of 3-bromothiophene-2-carbaldehyde **(18)** was obtained from a modified procedure by Fuller *et al.*[195]

The crude product was purified by flash column silica gel chromatography using a mixture of 40-60 petroleum ether/ethyl acetate (9:1) to obtain **(18)** as a bright yellow oil in **85 %**.

Compound **(18)** was prepared using 3-bromothiophene as starting material and reacted with 1-formylpiperidine as shown in **Scheme 4.24.**

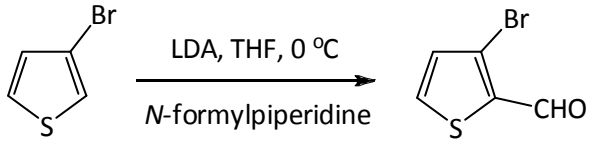

3-Bromothiophene **(18)**

Scheme 4.24: Synthesis of 3-bromothiophene-2-carbaldehyde **(18)**.

The reaction was refluxed for 24 h under basic conditions by using lithium diisopropylamide solution. The purity and the chemical structure of the product **(18)** were confirmed by TLC, which gave a single spot, and boiling point: 113-115 °C.[195] The mass spectra which show multi main masses at 189, elemental analysis C_5H_3BrOS which was in agreement with the proposed structure, NMR analysis and FT-IR.

The ^{1}H-NMR displayed three broad peaks at 9.98 ppm, 7.73 ppm and 7.16 ppm which belong to the protons of the thiophene and aldehyde proton**.** The FT-IR spectrum showed absorption bands at 1734 cm^{-1} are assigned C=O stretch at the thiophene aldehyde substitute.[187]

All analytical results clearly verify that the proposed product was 3-bromothiophene-2-carbaldehyde **(18)**.

4.19 Synthesis of ethyl thieno[3,2-*b*]thiophene-2-carboxylate (19)

Synthesis of ethyl thieno[3,2-b]thiophene-2-carboxylate **(19)** was obtained according to the procedure by Fuller *et al*.[195]

The crude product was extracted with dichloromethane to obtain **(19)** as a bright yellow liquid in **81 %**. Compound **(19)** was prepared by using 3-bromothiophene-2-carbaldehyde **(18)** as starting material and reacted with ethyl 2-sulfanylacetate as shown in **Scheme 4.25.**

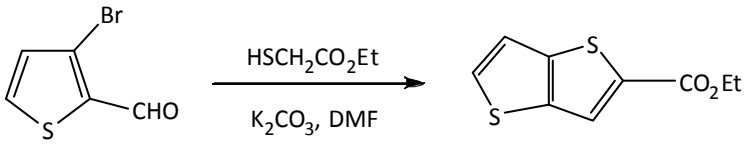

(18) **(19)**

Scheme 4.25: Synthesis of ethyl thieno[3,2-*b*]thiophene-2-carboxylate **(19)**.

The reaction was stirred under ambient temperature within 72 h under a N_2 atmosphere. The purity and the chemical structure of the product **(19)** were confirmed by TLC, which gave a single spot, and boiling point: 120-125 °C.[195] The mass spectra which show multi main masses at 213, elemental analysis $C_9H_8O_2S_2$ which was in agreement with the proposed structure, NMR analysis and FT-IR.

The ^{1}H-NMR displayed three broad peaks at 8.01 ppm, 7.60 ppm and 7.30ppm which belong to the protons of the thienothiophene. The FT-IR spectrum showed absorption bands at 1707 cm^{-1} are assigned C=O stretch at the thiophene.

All analytical results clearly verify that the proposed product was ethyl thieno[3,2-*b*]thiophene-2-carboxylate **(19)**.

4.20 Synthesis of thieno[3,2-*b*]thiophene-2-carboxylic acid (20)

Synthesis of thieno[3,2-*b*]thiophene-2-carboxylic acid **(20)** was obtained from a modified procedure by Fuller *et al.*[195]

The crude product was extracted with dichloromethane to obtain **(20)** as a white solid acid in 89 %. Compound **(20)** was prepared by using ethyl thieno[3,2-*b*]thiophene-2-carboxylate **(19)** as starting materials as shown in **Scheme 4.26.**

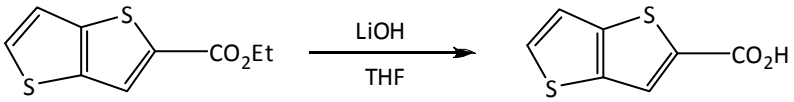

(19) **(20)**

Scheme 4.26: Synthesis of thieno[3,2-*b*]thiophene-2-carboxylic acid **(20).**

The reaction was refluxed in THF over 3 h under a N_2 atmosphere. The purity and the chemical structure of the product **(20)** were confirmed by TLC, which gave a single spot, and melting point: 218-220 °C.[195]

The mass spectra which show multi main masses at 213, elemental analysis $C_7H_4O_2S_2$ which was in agreement with the proposed structure, NMR analysis and FT-IR. The ^{1}H-NMR displayed three broad peaks at 8.12 ppm, 7.67 ppm and 7.34 ppm which belong to the protons of the thienothiophene**.** The FT-IR spectrum showed absorption bands at 1672 cm^{-1} are assigned C=O stretch of the carboxyl group on the thienothiophene.
All analytical results clearly verify that the product was thieno[3,2-*b*]thiophene-2-carboxylic acid **(20)**.

4.21 Synthesis of 1,2-bis(2,2-diethoxyethyl)disulfane (21)

Synthesis of 1,2-bis(2,2-diethoxyethyl)disulfide, **(21)** was obtained from a modified procedure by Parham and Wynberg. [204]

The crude product was extracted with ethyl acetate to obtain **(21)** a yellow oily product in 88 %. Compound **(21)** was prepared by using 2-bromo-1,1-diethoxyethane as starting material as shown in **Scheme 4.27.**

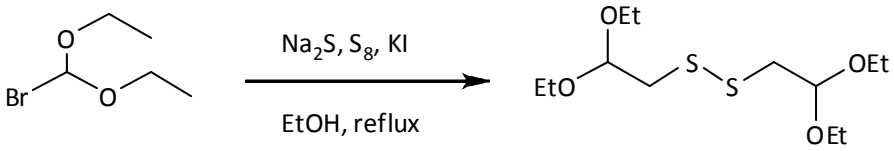

2-bromo-1,1-diethoxyethane **(21)**

Scheme 4.27: Synthesis of 1,2-bis(2,2-diethoxyethyl)disulfide, **(21).**

The reaction mixture was refluxed in ethanol overnight under a N_2 atmosphere. The purity and the chemical structure of product **(21)** were confirmed by TLC, which gave a single spot, and melting point: 106-108 °C.[204] The mass spectra which show multi main masses at 299, elemental analysis $C_{12}H_{26}O_4S_2$ which was in agreement with the proposed structure, NMR analysis and FT-IR.

The ^{1}H-NMR displayed three broad peaks at 4.70 ppm, 3.67 ppm and 2.95 ppm which belong to the protons of the alkyl group**.** The FT-IR spectrum showed absorption bands at 2975 cm^{-1}, 2929 cm^{-1}, 2877 cm^{-1} are assigned C-H stretch at the alkyl group.

All analytical results clearly verify that the product was 1,2-bis(2,2-diethoxyethyl)disulfide, **(21).**

4.22 Synthesis of 3-(2,2-diethoxy-ethylsulfanyl)thiophene (22)

Synthesis of 3-(2,2-diethoxy-ethylsulfanyl)thiophene **(22)** was obtained from a modified procedure by Henssler and Matzger.[196]

The crude product was extracted with ethyl acetate and obtain compound **(22)** as a light yellow oil in **87 %**. Compound **(22)** was prepared by using a mixture of 3-bromothiophene as starting material as shown in **Scheme 4.28.**

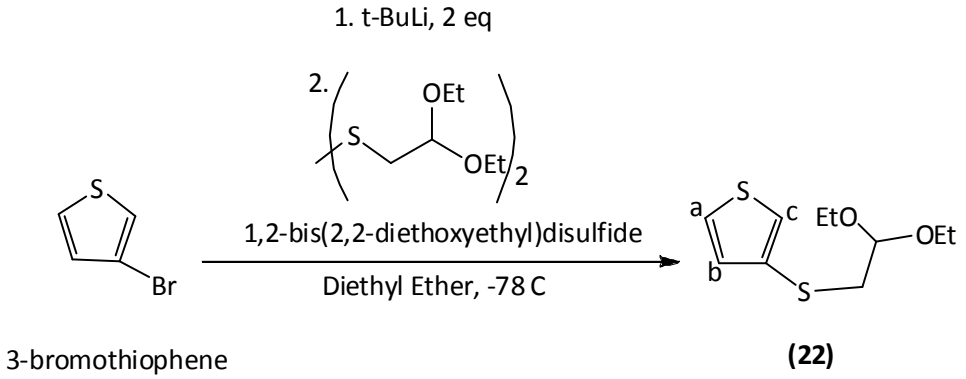

3-bromothiophene **(22)**

Scheme 4.28: Synthesis of 3-(2,2-diethoxy-ethylsulfanyl)thiophene **(22).**

The reaction was performed at room temperature in the dark in 10 h, then the crude product extracted with ethyl acetate. The purity and the chemical structure of the product **(22)** were confirmed by TLC, which gave a single spot, the melting point was 287- 89 °C,[196] the mass spectra which show multi main masses at 232, elemental analysis $C_{10}H_{16}O_2S_2$ which was in agreement with the proposed structure, NMR analysis and FT-IR.

The ^{1}H-NMR displayed three broad peaks at 7.32 ppm (position a), 7.21 ppm (position b) and 7.07 ppm (position c) which belong to the protons of the thienothiophene**.** The FT-IR spectrum showed absorption bands at 3101 cm^{-1}, 2972 cm^{-1}, 2928 cm^{-1} and 2880 cm^{-1} which falls in relation to aromatic thienothiophene groups =C–H stretch. The characteristic peaks at 2029 cm^{-1}, 1974 cm^{-1}, 1713 cm^{-1}, 1753 cm^{-1} and 1665 cm^{-1} are assigned to the alkyl stretching frequencies of the methylene groups.

All analytical results clearly verify that the product was 3-(2,2-diethoxy-ethylsulfanyl)thiophene **(22).**

4.23 Synthesis of thieno[3,2-*b*]thiophene (23)

The synthesis of **(23)** was performed using three different methods from Fuller *et al.*[195], GooBen *et al.*[197] and Henssler and Matzger.[196]

However, the crude products obtained by using Fuller *et al.*[195] and GooBen *et al.*[197] method were difficult to purified.

Based on Henssler and Matzger.[196] the crude product was purified by column chromatography on silica gel, eluting with 40-60 petroleum ether to obtain **(23)** as a white solid in **98 %**.

Compound **(23)** was prepared by using 3-(2,2-diethoxy-ethylsulfanyl)thiophene **(22)** as starting materials as shown in **Scheme 4.29.**

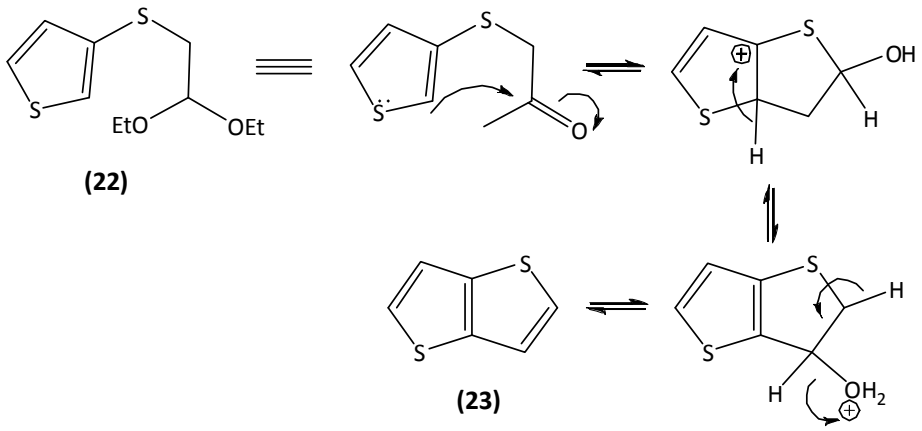

Scheme 4.29: Mechanism of thieno[3,2-*b*]thiophene **(23)** by using anhydrous amberlyst 15 ion exchange resin, ether.

The reaction mixture was refluxed in ether over 10 h with anhydrous amberlyst 15 ion exchange resins. The purity and the chemical structure of the product **(23)** were confirmed by TLC, which gave a single spot, and melting point: 55-56 °C.[197] The mass spectra which show multi main masses at 140, elemental analysis $C_6H_4S_2$ which was in agreement with the proposed structure, NMR analysis and FT-IR.

The ^{1}H-NMR displayed three broad peaks at 9.98 ppm, 7.73 ppm and 7.16 ppm which belong to the protons of the thienothiophene**.** The FT-IR spectrum showed absorption bands at 3098 cm^{-1}, 2954 cm^{-1}, 2922 $cm^{-1}$and 2849 $cm^{-1}$are assigned =C-H stretch at the

thienothiophene. All analytical results clearly verify that the product was thieno[3,2-*b*]thiophene **(23).**

4.24 Synthesis of 2,5-dibromothieno[3,2-*b*]thiophene (24)

Synthesis of 2,5-dibromothieno[3,2-*b*]thiophene **(24)** was obtained from a modified procedure by Liu *et al*.[198]

The crude product was recrystallized by ethanol and obtained as a white solid in **94 %**. Compound **(24)** was prepared by using thieno[3,2-*b*]thiophene **(23)** and NBS as starting materials as shown in **Scheme 4.30.**

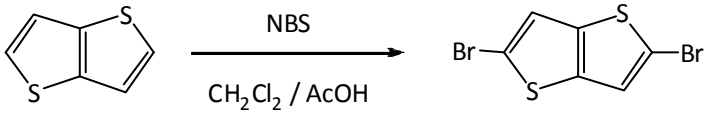

(23) **(24)**

Scheme 4.30: Synthesis of 2,5-dibromothieno[3,2-*b*]thiophene **(24).**

The reaction was performed at room temperature for 48 h in the dark. The mechanism of the reaction proceeds as depicted in the **Scheme 4.41**.

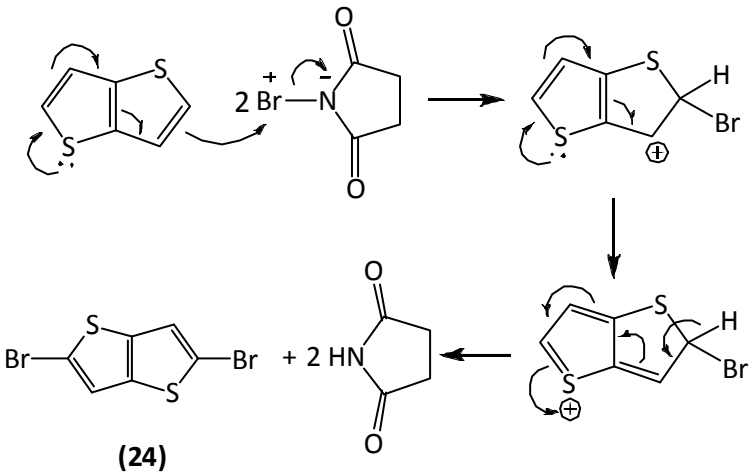

(24)

Scheme 4.31: Mechanism of the bromination reaction of 2,5-dibromothieno[3,2-*b*]thiophene **(24)** using NBS.

The purity and the chemical structure of the product **(24)** were confirmed by TLC, which gave a single spot, and melting point: 124 - 129°C. The mass spectra which show multi main masses at 298, elemental analysis $C_6H_2Br_2S_2$ which was in agreement with the proposed structure, NMR analysis and FT-IR.

The ^{1}H-NMR displayed singlet peak at 7.20 ppm which belong to the two protons on the thienothiophene in a symmetrical position as shown in **Figure 4.3.** The FT-IR spectrum showed absorption bands at 3088 cm^{-1} which falls in relation to aromatic thienothiophene groups =C–H stretch.

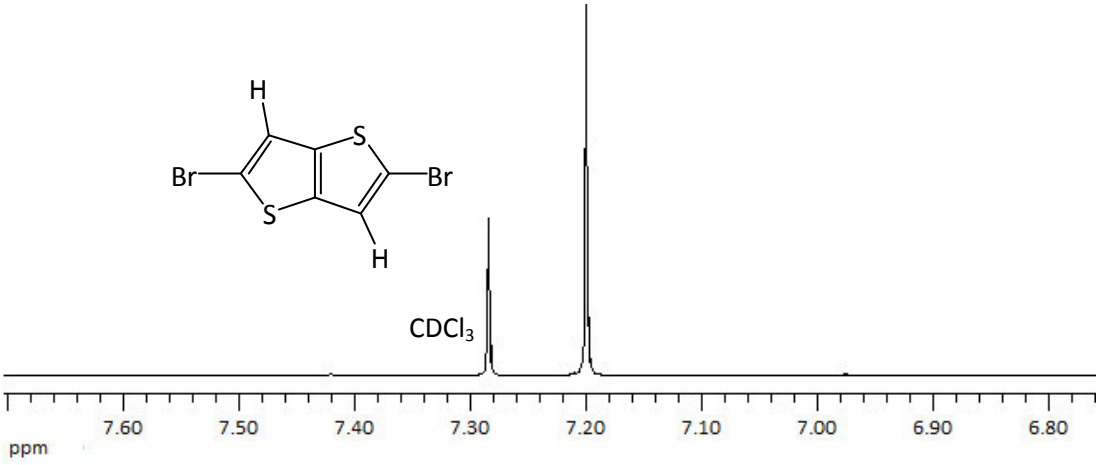

Figure 4.3: ^{1}H-NMR 2,5-dibromothieno[3,2-b]thiophene **(24)** in $CDCl_3$ (7.28 ppm).

All analytical results clearly verify that the product was 2,5-dibromothieno[3,2-b]thiophene **(24).**

4.25 Synthesis of 2-(tributylstannyl)thieno[3,2-*b*]thiophene (25)

2-(Tributylstannyl)thieno[3,2-*b*]thiophene **(25)** was prepared according to a modified procedure by Torun *et al*[205]. The product was purified via silica gel column chromatography, eluting with 98 % hexane and 2 % Et_3N to obtain **(25)** as a colourless oil in 90 % yield.

The first step of the reaction involves the formation of the anion of thienothiophene by adding (0.9 eq) BuLi drop wise at -78 °C, which deprotonates thienothiophene to give a yellow solution. The second step involves adding tri-n-butyltin chloride to quench the reaction and form the compound **(25)** as shown in **Scheme 4.32**.

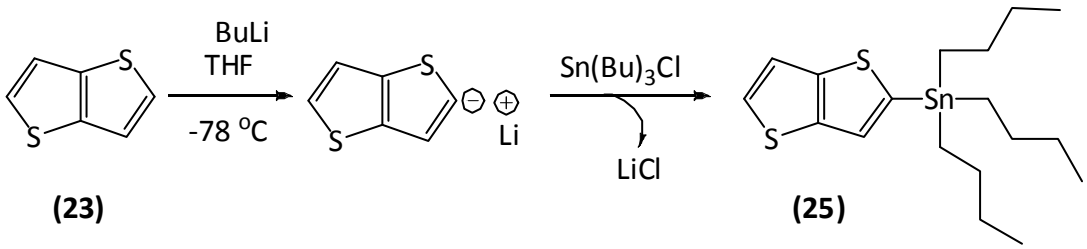

Scheme 4.32: The reaction mechanism of the formation of compound **(25)**.

The crude product was purified by column chromatography using a mixture of hexane and 2 % of triethylamine as a base to neutralize the acidity from the silica gel, and then the mixture used as eluent to avoid decomposition of the product.

The purity and the chemical structure were confirmed by TLC, which presented on spot of the product, elemental analysis CH was in agreement of the proposed structure and the mass spectra show multi main integer masses at 417, 418, 419, 420, 421 as expected due to the presence of tin (^{116}Sn, ^{118}Sn and ^{120}Sn) isotopes.

Also the purity of the product was confirmed by ^{1}H NMR and ^{13}C NMR. The FT-IR spectra showed broad absorption band at 686 cm^{-1} and 628 cm^{-1} which to the stretching vibration of the C-Sn, the band at 516 cm^{-1}, 508 cm^{-1} and 500 cm^{-1} correspond to the stretching vibration of the C-Sn.

All analytical results clearly verify and proposed that the product was 2-(tributylstannyl)thieno[3,2-*b*]thiophene **(25).**

4.26 Synthesis of trimethyl(thieno[3,2-*b*]thiophen-2-yl)stannane (26)

Trimethyl(thieno[3,2-*b*]thiophen-2-yl)stannane **(26)** was prepared according to a modified procedure by Torun *et al.* [205] The product was purified via silica gel column chromatography, eluting with 98 % hexane and 2 % Et_3N to obtain **(26)** as colourless crystal in 98 % yield. The first step of the reaction involves the formation of the anion of thieno[3,2-*b*]thiophene by adding (0.9 eq) BuLi drop wise at -78 °C, which deprotonates thieno[3,2-*b*]thiophene to give a yellow solution. The second step involves adding tri-n-butyltin chloride to quench the reaction and form the compound **(26)** as shown in **Scheme 4.43** trimethylstannyl chloride

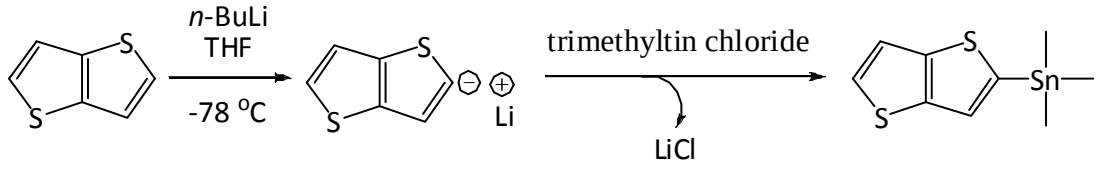

(23) **(26)**

Scheme 4.33: The reaction of the formation of compound trimethyl(thieno[3,2-*b*]thiophen-2-yl)stannane **(26)**.

The crude product was purified by column chromatography using a mixture of hexane and 2 % of triethylamine as a base to neutralize the acidity from the silica gel, and then the mixture used as eluent to avoid decomposition of the product.

The purity and the chemical structure of the product trimethyl(thieno[3,2-*b*]thiophen-2-yl)stannane **(26)** were confirmed by TLC, the melting point, the mass spectra, elemental analysis, NMR analysis and FT-IR. The product gave a single spot on TLC, which presented on spot of the product, elemental analysis CH was in agreement of the proposed structure and the mass spectra show multi main integer masses at 417, 418, 419, 420, 421 as expected due to the presence of tin (^{116}Sn, ^{118}Sn and ^{120}Sn) isotopes.

Also the purity of the product was confirmed by ^{1}H NMR and ^{13}C NMR. The FT-IR spectra showed broad absorption band at 686 cm^{-1} and 628 cm^{-1} which to the stretching vibration of the C-Sn, the band at 516 cm^{-1}, 508 cm^{-1} and 500 cm^{-1} correspond to the stretching vibration of the C-Sn.

All analytical results clearly verify and proposed that the product was trimethyl(thieno[3,2-*b*]thiophen-2-yl)stannane **(26)**.

4.27 Synthesis of 1,2-bis(octyloxy)benzene (27)

Synthesis of 1,2-bis(octyloxy)benzene **(27)** was obtained from a modified procedure by Petersen *et al*.[199] The product was obtained via recrystallisation from methanol as a white needle crystals in 81 % yield as shown in **Scheme 4.34**.

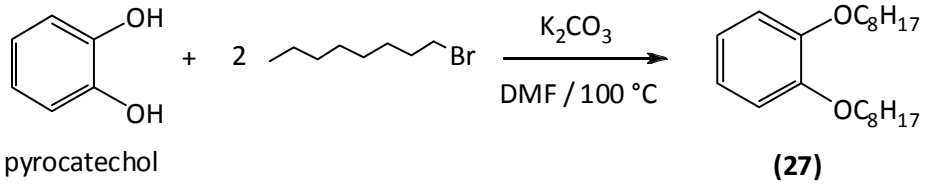

Scheme 4.34: Preparation of 1,2-bis(octyloxy)benzene **(27)**.

The reaction was performed in DMF at 100 °C overnight in the presence of potassium carbonate K_2CO_3 as a base, with excess 1-bromooctane to push the reaction towards the product. The mechanism of the reaction proceeds via nucleophilic substitution (SN2), at first the base deprotonates the hydroxyl groups, which can then work as a nucleophile and attack 1-bromooctane to form the product as shown in **Scheme 4.35**.

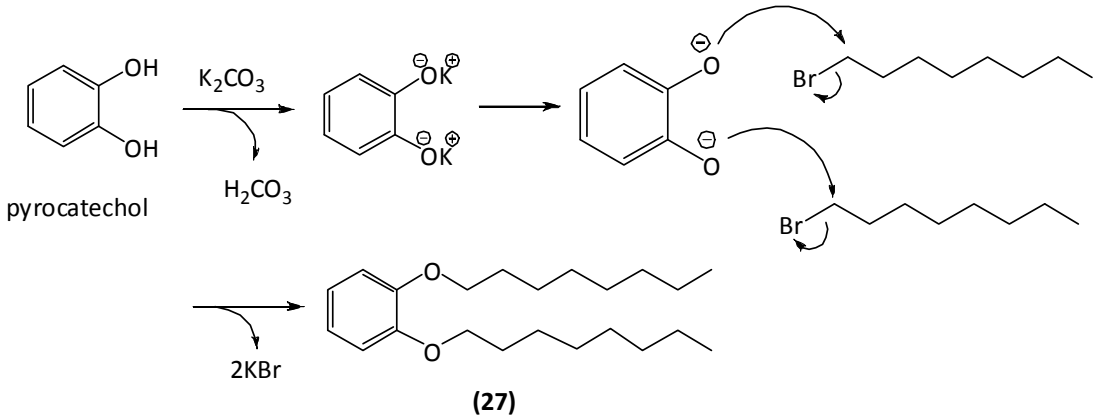

Scheme 4.35: Mechanism of reaction via nucleophilic substitution.

The purity of the product 1,2-bis(octyloxy)benzene **(27)** was confirmed by ^{1}H NMR. It displayed a singlet peak at 6.89 ppm corresponding to the four protons on the ring and the expected peaks which correspond to protons from the two alkyl chains and elemental analysis CH which was in agreement with the proposed structure and the mass spectra which show a main integer mass at 334. The melting point of the product was 24.5-26 °C in close agreement with reported values in the literature (24-24.5 °C).[199]

The FT-IR spectra did not show any absorption band between 3100-3700 cm^{-1} belong to the stretching vibration of the OH, which confirmed the conversion of hydroxyl groups to the target product.

All analytical results clearly verify that the product was 1,2-bis(octyloxy)benzene **(27).**

4.28 Synthesis of 1,2-dinitro-4,5-bis-octyloxy-benzene (28)

Synthesis of 1,2-dinitro-4,5-bis(octyloxy)benzene **(28)** was obtained from a modified procedure by Petersen *et al*.[199]

The product was obtained *via* recrystallisation from ethanol as yellow crystals in 87 % yield as shown in **Scheme 4.36**.

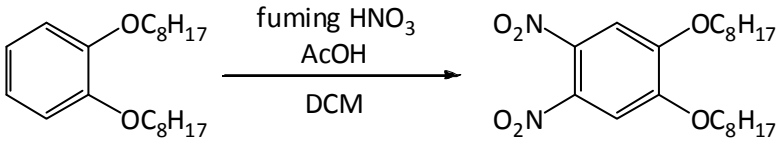

(27) **(28)**

Scheme 4.36: Synthesis of 1,2-dinitro-4,5-bis(octyloxy)benzene **(28)**.

The reaction was carried out in the presence of nitric acid 65 %, fuming nitric acid and acetic acid, the mixture was stirred at room temperature for 40 h. The mechanism of the reaction proceeds in two steps; at first, nitronium cation (NO2+) was generated by reacting nitric acid with acetic acid, which then attacks the aromatic ring in an electrophilic aromatic

substitution reaction. The attacks occurs at 4- and 5- potions on the aromatic ring, which are in the para-positions to the octyloxy groups**. Scheme 4.37** shows the two steps of reaction.

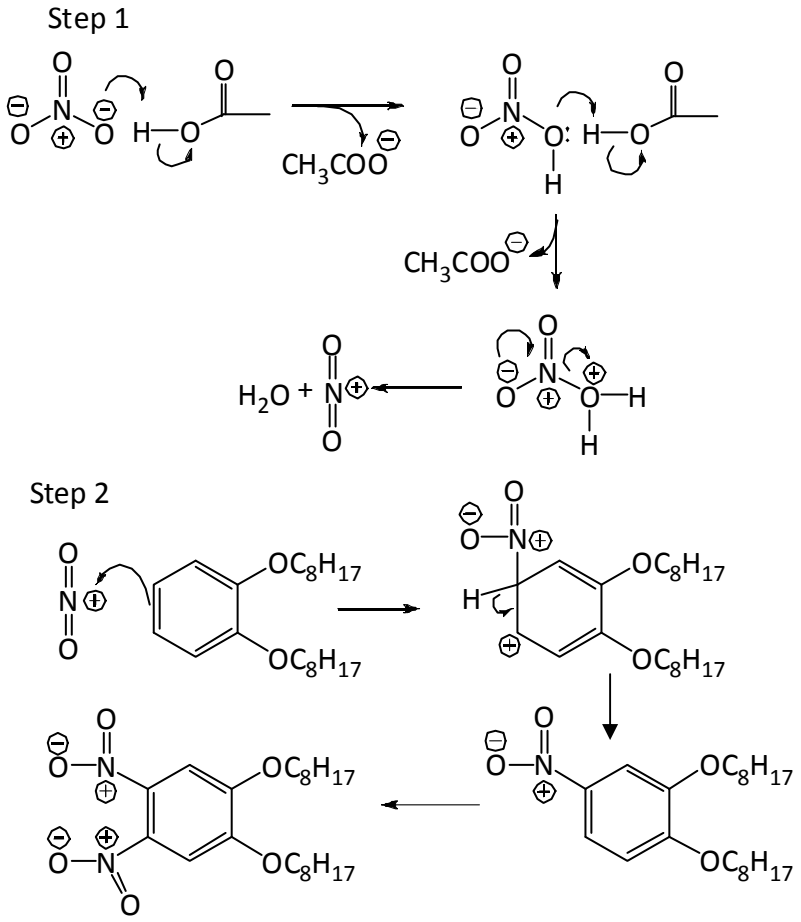

Scheme 4.37: Mechanism of the nitration reaction of compound **(28)**.

The purity and the chemical structure were confirmed by elemental analysis CHN which was in agreement with the proposed structure and the mass spectra show main integer mass at 424. The melting point of the product was 86.5-88 °C in close agreement with reported values in the literature, 87-87.5 °C.[199]

The purity of the product was also confirmed by ^{1}H-NMR and ^{13}C-NMR spectra, which presented the expected peaks. The FT-IR spectra showed a new strong absorption band at 1526 cm^{-1} and 1587 cm^{-1} belonging to the stretching vibration of the nitro groups.

All analytical results clearly verify that the product was 1,2-dinitro-4,5-bis(octyloxy)benzene **(28)**.

4.29 Synthesis of 4,5-bis(octyloxy)benzene-1,2-diaminium chloride (29)

Synthesis of 4,5-bis(octyloxy)benzene-1,2-diaminium chloride **(29)** was obtained from a modified procedure by Helgesen *at al.*[199] 4,5-Bis(octyloxy)benzene-1,2-diammonium chloride **(29)** was synthesis according to the procedure of Helgesen *at al.*[199] The product was obtained as a white powder in 87 % yield and was used directly in the next reaction without purification, due to the instability of the product **(Scheme 4.38)**.

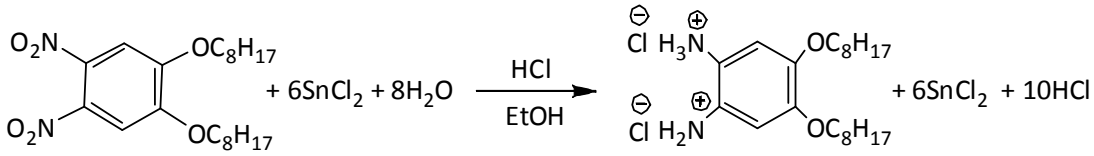

(28) **(29)**

Scheme 4.38: Synthesis of 4,5-bis(octyloxy)benzene-1,2-diammonium chloride **(29)**.

The reaction was carried out in ethanol at 85 °C overnight in the presence of HCl. During the first 1 h of the reaction, the solution changed its colour from yellow to white. Then the reaction mixture was cooled to room temperature and the formed white precipitate was filtered before it was washed with water to remove acid residues and then methanol to remove water. Finally it was dried under a N_2 stream and used directly in the next reaction.

The purity and the chemical structure of the product were confirmed by elemental analysis CHNCl which was in agreement with the proposed structure and the mass spectra shows two main integer masses at 363 and 464, the Cl^- is unable to fly so it was not detected by mass (El^+) analysis. The purity of the product also was confirmed by the ^1H NMR and ^{13}C NMR spectra, which presented the expected peaks.

All analytical results clearly verify that the product was 4,5-bis(octyloxy)benzene-1,2-diammonium chloride **(29)**.

4.30 Synthesis of 5,6-bis(octyloxy)benzo[*c*][1,2,5]thiadiazole (30)

5,6-Bis(octyloxy)benzo[*c*][1,2,5]thiadiazole (30) was synthesized according to a modified procedure of Bouffard *et al*.[206] The product was obtained via recrystallisation from ethanol as brown powder in 90 % yield as shown **Scheme 4.39**.

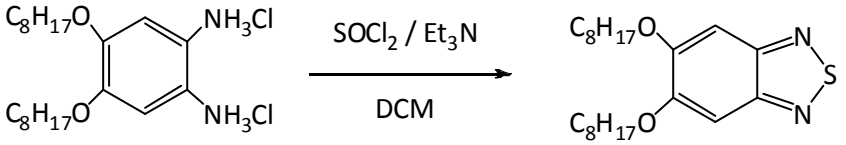

(29) **(30)**

Scheme 4.39: Synthesis of 5,6-bis(octyloxy)benzo[c][1,2,5]thiadiazole **(30)**.

The reaction was performed at reflux for 6 h, in the presence of triethylamine Et_3N, which removes the hydrogen chloride generated by combining with it to form the salt triethylamine hydrochloride. The amine groups act as nucleophiles then, the cyclization occurs and the target product formed after a water molecule is removed from the product as shown **Scheme 4.40.**

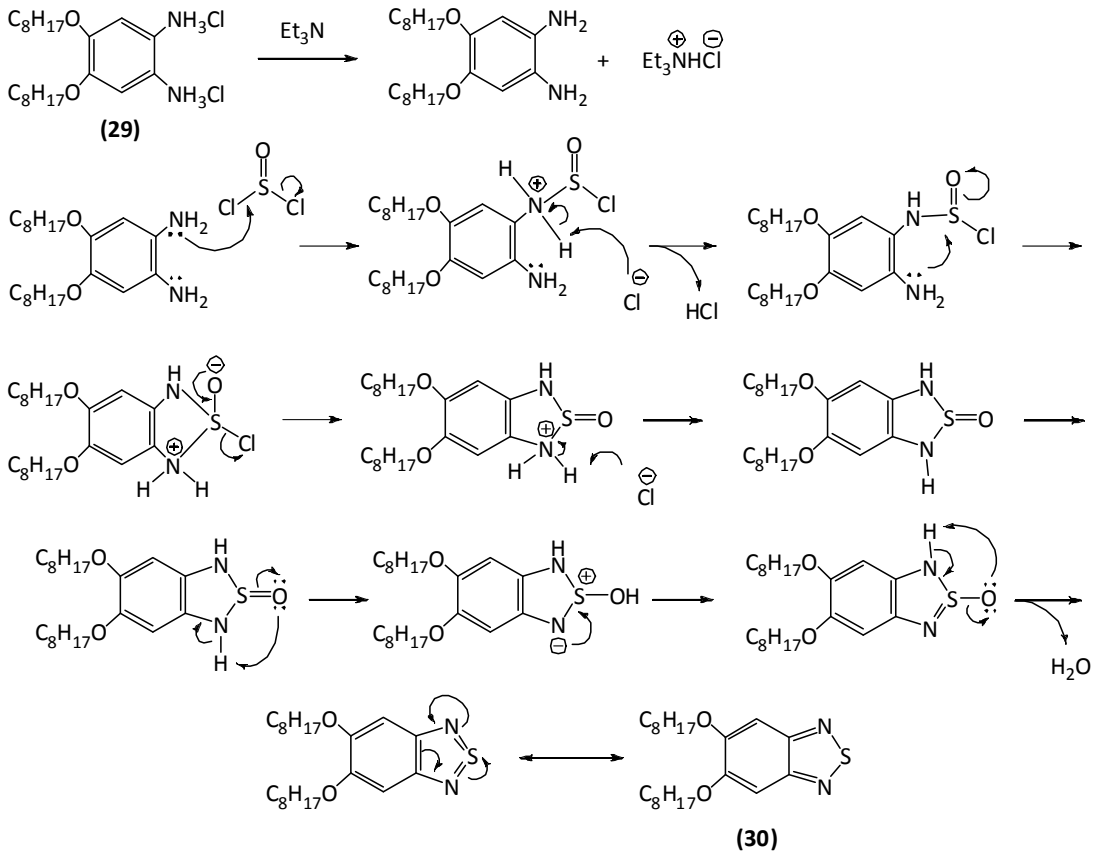

Scheme 4.40: Mechanism to synthesis 5,6-bis(octyloxy)benzo[c][1,2,5]thiadiazole **(30).**

The purity and the chemical structure of product **(30)** were confirmed by TLC, the melting point, the mass spectra, elemental analysis, NMR analysis and FT-IR. The product gave a single spot on TLC, and the melting point of the product was 97.5-98 °C in close agreement with reported values in the literature 97.1-97.5 °C.[199] The purity of the product was also confirmed by the ^{1}H NMR and ^{13}C NMR spectra, which presented the expected peaks.

All analytical results clearly verify that the product was 5,6-bis(octyloxy)benzo[c][1,2,5]thiadiazole **(30).**

4.31 Synthesis of 4,7-dibromo-5,6-bis(octyloxy)benzo[*c*][1,2,5]thiadiazole (31)

Synthesis of 4,7-dibromo-5,6-bis(octyloxy)benzo[*c*][1,2,5]thiadiazole **(31)** was obtained from a modified procedure by Petersen *et al*.[199]

Compound **(31)** was prepared by using 5,6-bis(octyloxy)benzo[c][1,2,5]thiadiazole **(30)** as starting materials as shown in **Scheme 4.41.**

The product was obtained via recrystallisation from ethanol and through silica flash gel column chromatography, eluting with 100 % hexane to obtain **(31)** as an off-white powder in 83 **%** yield.

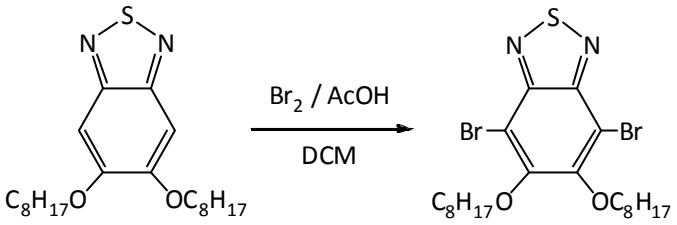

(30) **(31)**

Scheme 4.41: Synthesis of 4,7-dibromo-5,6-bis(octyloxy)benzo*[c]*[1,2,5]thiadiazole **(31)**.

The reaction was carried out in the presence of acetic acid at room temperature for 48 h in the dark, and mechanism of the reaction illustrated in **Scheme 4.42.**

The reaction was performed in hydrobromic acid, which was heated to 100 °C before adding bromine drop-wise over a period of 1 h, and then the mixture was allowed to stir for 2 h at 100 °C. The crude product was recrystallised from ethanol at first, but TLC displayed unreacted bromine, therefore further recrystallisation was carried out from chloroform / hexane (2:1) to remove the bromine.

The reaction mechanism is illustrated in **Scheme 4.42**, the reaction proceeds through electrophilic aromatic substitution, which is selective for the 4- and 7-positions because of the activating nature of the alkoxy groups on the ortho-positions.

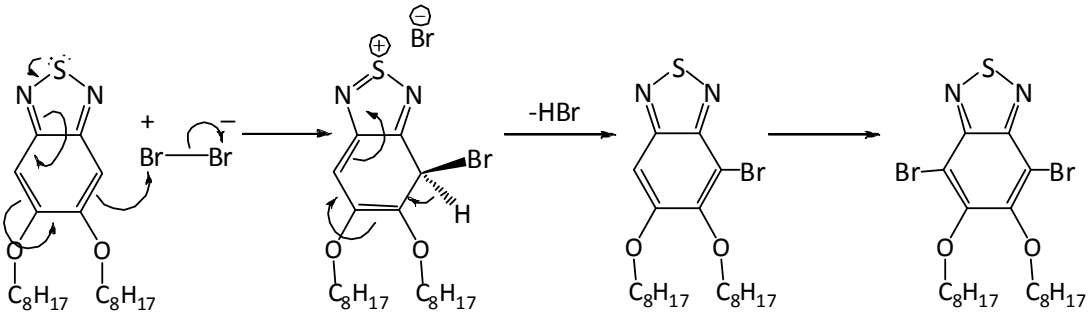

Scheme 4.42: Mechanism of bromination of 4,7-dibromo-5,6-bis(octyloxy)benzo[c][1,2,5]thiadiazole **(31)**.

The purity and the chemical structure of the product were confirmed by elemental analysis CHNBr which was in agreement with the proposed structure and the mass spectra shows three main integer masses at 548, 550 and 552, in 1:2:1 ratio as expexted due to the presence of two bromine isotopes (^{79}Br and^{81}Br). The melting point of the product was 45.5 - 46.5 °C in close agreement with reported values in the literature (44.5-45.6 °C).[199]

The purity of the product was also confirmed by its ^{1}H NMR spectra, which displayed no peaks of the product in the aromatic region. The FT-IR spectra showed absorption bands at 1057 cm^{-1} and 1028 cm^{-1} corresponding to the stretching vibration of the C-Br.

All analytical results clearly verify that the proposed product was 4,7-dibromo-5,6-bis(octyloxy)benzo[c][1,2,5]thiadiazole **(31)**.

4.32 Synthesis of 5,6-bis(octyloxy)-4,7-di(thieno[3,2-*b*]thiophen-2-yl)benzo[*c*][1,2,5]thiadiazole (32)

Synthesis of 5,6-bis(octyloxy)-4,7-di(thieno[3,2-*b*]thiophen-2-yl)benzo[*c*][1,2,5]thiadiazole **(32)** was obtained from a modified procedure by Ding *et al.*[152]

The crude product was purified via silica gel column chromatography, eluting with 40-60 petroleum ether:ethyl acetate: triethylamine (4 : 1 : 0.03) to obtain **(32)** as an orange oil in **84 %**.

Compound **(32)** was prepared by using 4,7-dibromo-5,6-bis(octyloxy)benzo[*c*][1,2,5] thiadiazole **(31)** and trimethyl(thieno[3,2-*b*]thiophen-2-yl)stannane **(26)** as starting materials as shown in **Scheme 4.43.**

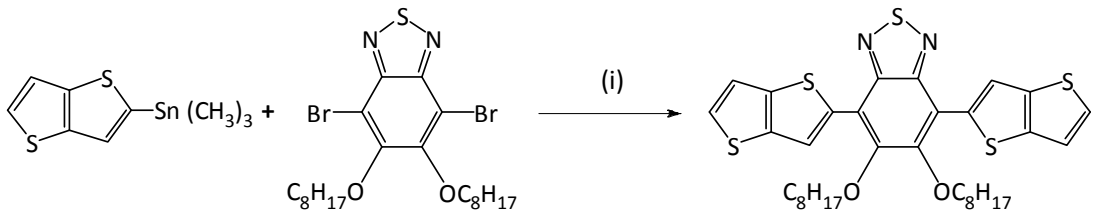

(26) **(31)** **(32)**

Scheme 4.43: Synthesis of 5,6-bis(octyloxy)-4,7-di(thieno[3,2-*b*]thiophen-2-yl)benzo[*c*][1,2,5]thiadiazole **(32).** (i) $Pd(OAc)_2$, $P(o\text{-}tol)_3$ and toluene.

The procedure involves using $Pd(OAc)_2$ and tri-o-tolylphosphine as catalyst, which is commonly used in Stille reactions. The reaction was performed at high temperature 110 °C in the dark, then the crude product purified by column chromatography.

The purity and the chemical structure of the product **(32)** were confirmed by TLC, which gave a single spot, the melting point was 80-82 °C,[152] the mass spectra which show multi main masses at 670, 669 and 668, elemental analysis $C_{34}H_{40}N_2O_2S_5$ which was in agreement with the proposed structure, NMR analysis and FT-IR.

The ^{1}H-NMR displayed three broad peaks at 8.86 ppm, 7.50 ppm and 7.37 ppm which belong to the protons of the thienothiophene**.** The FT-IR spectrum showed absorption

bands at 3119 cm^{-1}, 3079 cm^{-1} and 3077 cm^{-1} which falls in relation to aromatic thienothiophene groups =C–H stretch. The characteristic peaks at 2950 cm^{-1}, 2915 cm^{-1} and 2850 cm^{-1} are assigned to the alkyl stretching frequencies of the methylene groups.

All analytical results clearly verify that the product was 5,6-bis(octyloxy)-4,7-di(thieno[3,2-*b*]thiophen-2-yl)benzo[*c*][1,2,5]thiadiazole **(32).**

4.33 Synthesis of 4,7-bis(5-bromothieno[3,2-*b*]thiophen-2-yl)-5,6-bis(octyloxy)benzo[*c*][1,2,5]thiadiazole (33)

Synthesis of 4,7-bis(5-bromothieno[3,2-*b*]thiophen-2-yl)-5,6-bis(octyloxy)benzo[*c*][1,2,5]thiadiazole **(33)** was obtained from a modified procedure by Ding *et al*.[152]

The crude product was purified via silica gel column chromatography, eluting with hexane:DCM: triethylamine (9 : 0.7 : 0.03) to obtain **(33)** as an orange oil in 85 % as shown in **Scheme 4.44.**

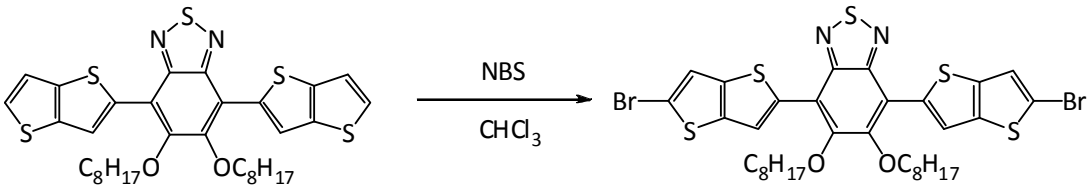

(32) **(33)**

Scheme 4.44: Synthesis of 4,7-bis(5-bromothieno[3,2-*b*]thiophen-2-yl)-5,6-bis(octyloxy)benzo[*c*][1,2,5]thiadiazole **(33)**.

The reaction was performed at room temperature for 48 h in the dark, then the crude product purified by column chromatography. The mechanism of the reaction proceeds as depicted in the **Scheme 4.45.**

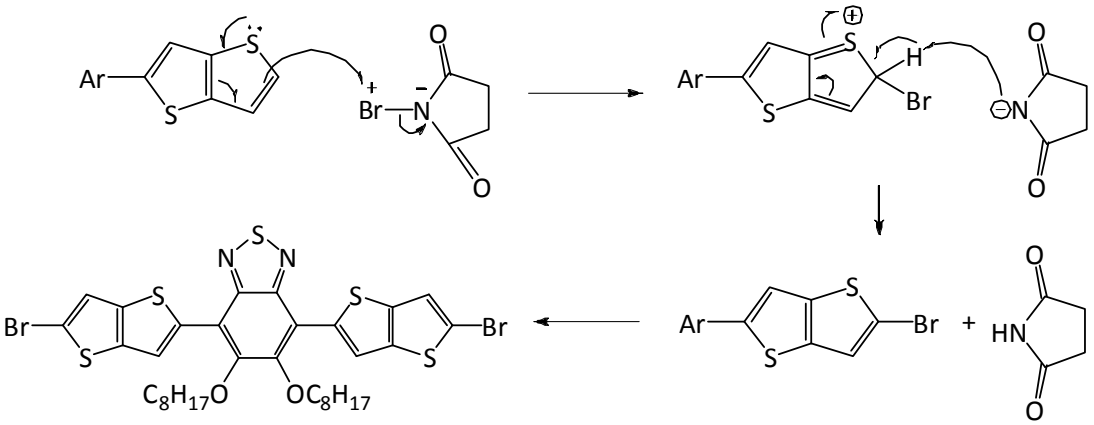

(33)

Scheme 4.45: Mechanism of the bromination reaction of 4,7-bis(5-bromothieno[3,2-*b*]thiophen-2-yl)-5,6-bis(octyloxy)benzo[*c*][1,2,5]thiadiazole **(33)** using NBS.

The ^{1}H NMR spectrum displayed two singlets peaks at 8.74 ppm and 7.32 ppm, which correspond to protons of the thienothiophene as shown in **Figure 4.4**.

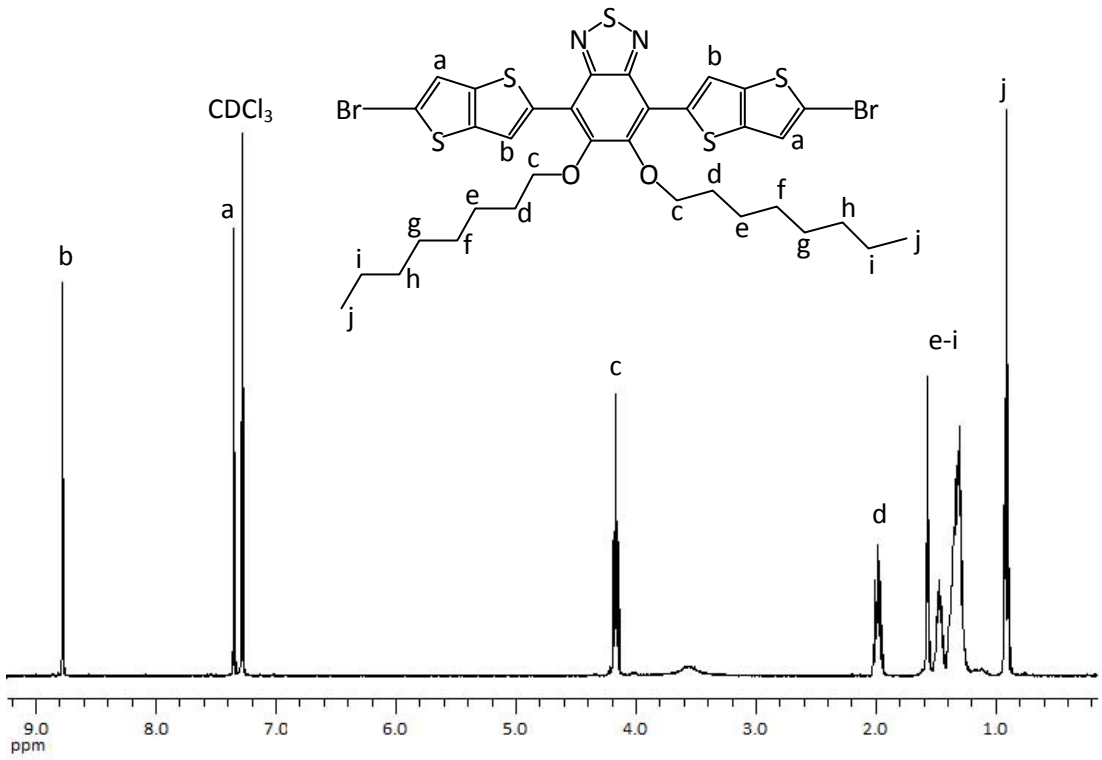

Figure 4.4: ^{1}H-NMR of monomer 4,7-bis(5-bromothieno[3,2-b]thiophen-2-yl)-5,6-bis(octyloxy)benzo[*c*][1,2,5]thiadiazole **(33)** in $CDCl_3$.

All analytical results clearly verify that the product was 4,7-bis(5-bromothieno[3,2-b]thiophen-2-yl)-5,6-bis(octyloxy)benzo[*c*][1,2,5]thiadiazole **(33).**

4.34 Synthesis of 4,7-dibromobenzo[*c*][1,2,5]thiadiazole (34)

Synthesis of 4,7-dibromobenzo[*c*][1,2,5]thiadiazole **(34)** was obtained from a modified the procedure by Edelmann *et al*.[52]

Compound **(34)** was prepared by using 2,1,3-benzothiadiazole as starting materials as shown in **Scheme 4.46.**

The product was obtained via recrystallisation from ethanol and then from chloroform / hexane (2:1) as off-white needle crystals in 99 % yield**.**

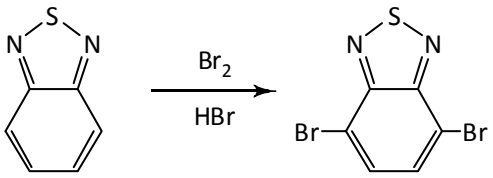

2,1,3-benzothiadiazole **(34)**

Scheme 4.46: Synthesis of 4,7-dibromo-2,1,3-benzothiadiazole **(34)**.

The reaction was performed in hydrobromic acid, which was heated to 100 °C before adding bromine drop-wise over a period of 1 h, and then the mixture was allowed to stir for 2 h at 100 °C. The crude product was recrystallised from ethanol at first, but TLC displayed unreacted bromine, therefore further recrystallisation was carried out from chloroform / hexane (2:1) to remove the bromine.

The reaction mechanism is illustrated in **Scheme 4.47**, the reaction proceeds through electrophilic aromatic substitution, which is selective for the 4- and 7-positions because of the activating nature of imine groups on the fused ring. Also a small amount of tris or tetrakis bromine substitutions on the 5- and 6- position are expected, because the activating nature of the neighbouring bromine substituents.

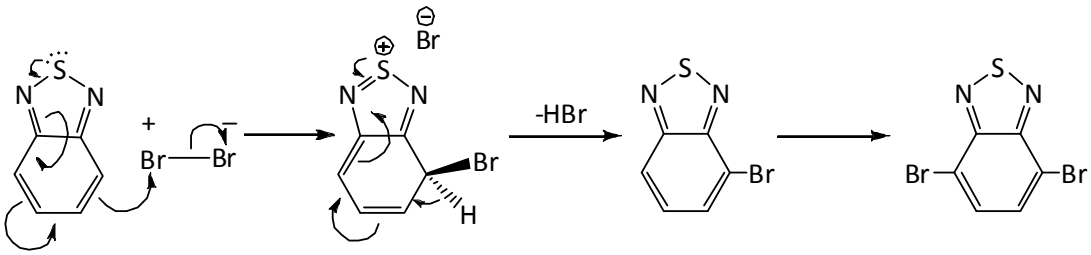

Scheme 4.47: Bromination mechanism of 4,7-dibromo-2,1,3-benzothiadiazole **(34).**

The purity and the chemical structure of the product 4,7-dibromo-2,1,3-benzothiadiazole **(34)** were confirmed by elemental analysis CHNBr, which was in good agreement with the proposed structure. The melting point was 186 °C, which is in agreement with that reported in the literature.[52]

The mass spectra show main integer masses at 292, 294 and 296 in 1:2:1 ratio as expected due to the presence of two bromine isotopes (^{81}Br and ^{79}Br). The ^{1}H-NMR spectra showed a singlet peak at 7.76 ppm corresponding to the two protons on positions 5 and 6 of the ring. The FT-IR spectra of product 4,7-dibromo-2,1,3-benzothiadiazole **(34)** showed a new band at 1080 cm^{-1} belonging to the stretching vibration of the C-Br bond.

The ^{1}H-NMR displayed singlet peak at 7.74 ppm which belong to the two protons on the benzothiadiazole in a symmetrical position as shown in **Figure 4.5.**

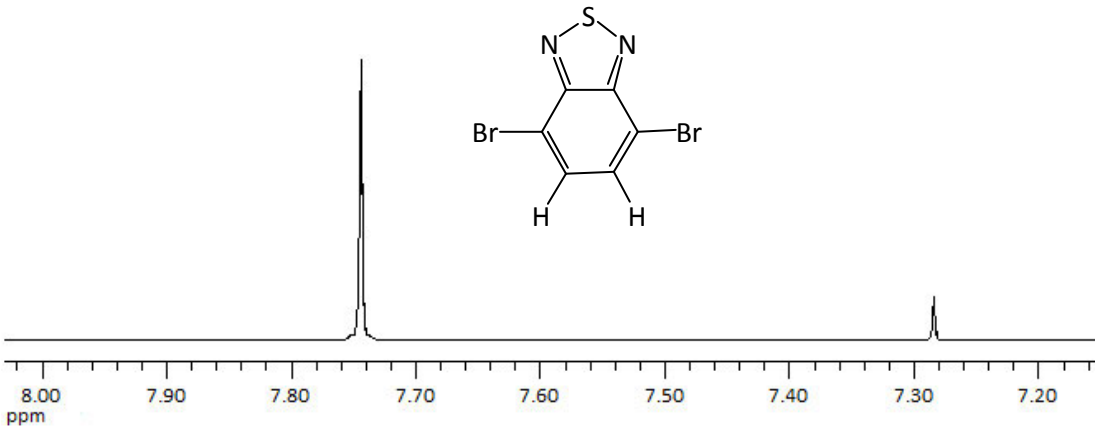

Figure 4.5: ^{1}H NMR spectrum of 4,7-dibromobenzo[*c*][1,2,5]thiadiazole **(34).**

All analytical results clearly verify that the product was 4,7-dibromobenzo[*c*][1,2,5]thiadiazole **(34).**

4.35 Synthesis of 4,7-di(thieno[3,2-*b*]thiophen-2-yl)benzo[*c*][1,2,5]thiadiazole (35)

Synthesis of 4,7-di(thieno[3,2-*b*]thiophen-2-yl)benzo[*c*][1,2,5]thiadiazole **(35)** was obtained from a modified procedure by Sun *et al.*[200]

The crude product was purified by open column chromatography on silica using 40-60 petroleum ether/ethyl acetate/triethylamine (4 : 1 : 0.03) and eluted compound **(35)** as an orange powder in **85 %**. Compound **(35)** was prepared by using a mixture of trimethyl(thieno[3,2-*b*]thiophen-2-yl)stannane **(26)** and 4,7-dibromobenzo[*c*][1,2,5]thiadiazole **(34)** as starting materials as shown in **Scheme 4.58.**

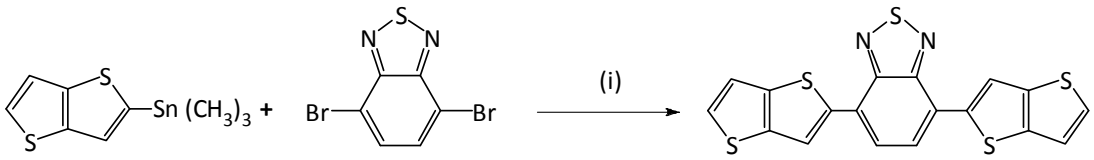

(26) **(34)** **(35)**

Scheme 4.48: Synthesis of 4,7-di(thieno[3,2-*b*]thiophen-2-yl)benzo[*c*][1,2,5]thiadiazole **(35).** (i) $Pd(OAc)_2$, $P(o\text{-}tol)_3$ and toluene.

The procedure involves using $Pd(OAc)_2$ and tri-o-tolylphosphine as catalyst, which is commonly used in Stille reactions. The reaction was performed at high temperature 110 °C in the dark over 72 h, then the crude product purified by column chromatography. The purity and the chemical structure of the product **(35)** were confirmed by TLC, which gave a single spot, the melting point was 140-144 °C, the mass spectra which show multi main masses at 412, elemental analysis $C_{18}H_8N_2S_5$ which was in agreement with the proposed structure.

The ^{1}H-NMR displayed three broad peaks at 8.53 ppm corresponding to protons on the benzothiadiazole, 7.91 ppm, 7.48 ppm and 7.34 ppm which belong to the protons of the thienothiophene**.** The FT-IR spectrum showed absorption bands at 3119 cm^{-1}, 3079 cm^{-1} and 3073 cm^{-1} which falls in relation to aromatic thienothiophene groups =C–H stretch.

All analytical results clearly verify that the product was 4,7-di(thieno[3,2-*b*]thiophen-2-yl)benzo[*c*][1,2,5]thiadiazole **(35).**

4.36 Synthesis of 4,7-bis(5-bromothieno[3,2-*b*]thiophen-2-yl)benzo[*c*][1,2,5]thiadiazole (36)

Synthesis of 4,7-bis(5-bromothieno[3,2-*b*]thiophen-2-yl)benzo[*c*][1,2,5]thiadiazole **(36)** was obtained from a modified procedure by Ding *et al.*[152]

The crude product was obtained as insoluble red solid in all organic solvents in 59 % as shown in **Scheme 4.58.**

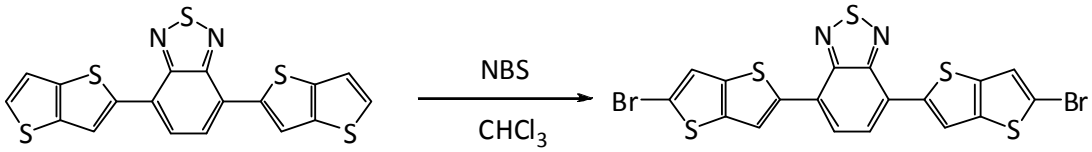

(35) **(36)**

Scheme 4.49: Synthesis of 4,7-bis(5-bromothieno[3,2-*b*]thiophen-2-yl)benzo[*c*][1,2,5] thiadiazole **(36)**.

Given the problems associated with the solubility of this monomer. It was then decided to explore the target polymers having benzothiadiazole repeat units linked by thienothiophene repeat units. Attachment of thienothiophene units on the carbazole units which have alkyl-solubilizing groups followed by a direct arylation polymerization route hence used as a method towards preparing these polymers.

4.37 Synthesis of 9-(heptadecan-9-yl)-2,7-di(thieno[3,2-*b*]thiophen-2-yl)-*9H*-carbazole (37)

Synthesis of 9-(heptadecan-9-yl)-2,7-di(thieno[3,2-b]thiophen-2-yl)-*9H*-carbazole **(37)** was obtained from a modified procedure by Kowalski *et al.*[149]

The crude product was purified *via* preparative HPLC to obtain **(37)** as a yellow solid in 57 %**.** Compound **(37)** was prepared by using 2,7-dibromo-9-(heptadecan-9-yl)-*9H*-carbazole **(6)** and trimethyl(thieno[3,2-*b*]thiophen-2-yl)stannane **(26)** as starting materials as shown in **Scheme 4.50.**

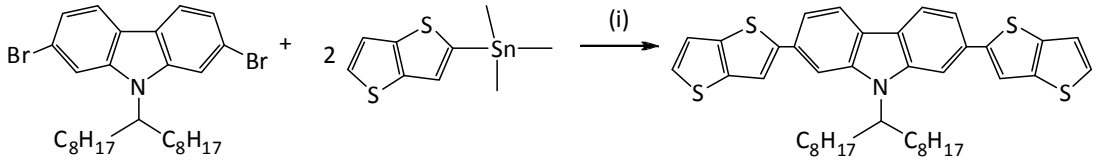

(6) **(26)** **(37)**

Scheme 4.50: Synthesis of 9-(heptadecan-9-yl)-2,7-di(thieno[3,2-b]thiophen-2-yl)-*9H*-carbazole **(37)**. (i) Bis(triphenylphosphine)-palladium(II)dichloride, ($Pd(PPh_3)_2Cl_2$) and toluene/110 °C.

The reaction was performed at high temperature 110 °C in the dark, then the crude product was purified via preparative HPLC, which was performed by using a reversed-phase column chromatography, the elution system (mobile phase) consisted of water (**A**) and THF (**B**), the following gradient was used: 60 % B for 1 min, then from 60 % to 95 % B for 9 min, then 95 % B for 5 min, then from 95 % to 60 % B for 5 min, then 60 % B for 10 min, the total time was 30 min per injection. The pure compound was collected between 7.50 to 7.89 min to afford the product.

The purity and the chemical structure of the product **(37)** were confirmed by TLC, which gave a single spot, the melting point was 45-47 °C, the mass spectra which show multi main masses at 681.4, elemental analysis $C_{41}H_{47}NS_4$ which was in agreement with the proposed structure, NMR analysis and FT-IR.

The ^{1}H-NMR displayed three broad peaks at 8.09 ppm, 7.82 ppm and 7.66 ppm which belong to the aromatic proton for the carbazole and three doublet peaks at 7.59 ppm, 7.54 ppm and 7.29 ppm correspond to protons of the thienothiophene as shown in **Figure 4.6.** The FT-IR spectrum showed absorption bands at 3099 cm^{-1} and 3077 cm^{-1} which falls in relation to aromatic benzene groups =C–H stretch. The characteristic peaks at 2920 cm^{-1} and 2850 cm^{-1} are assigned to the alkyl stretching frequencies of the methylene groups.

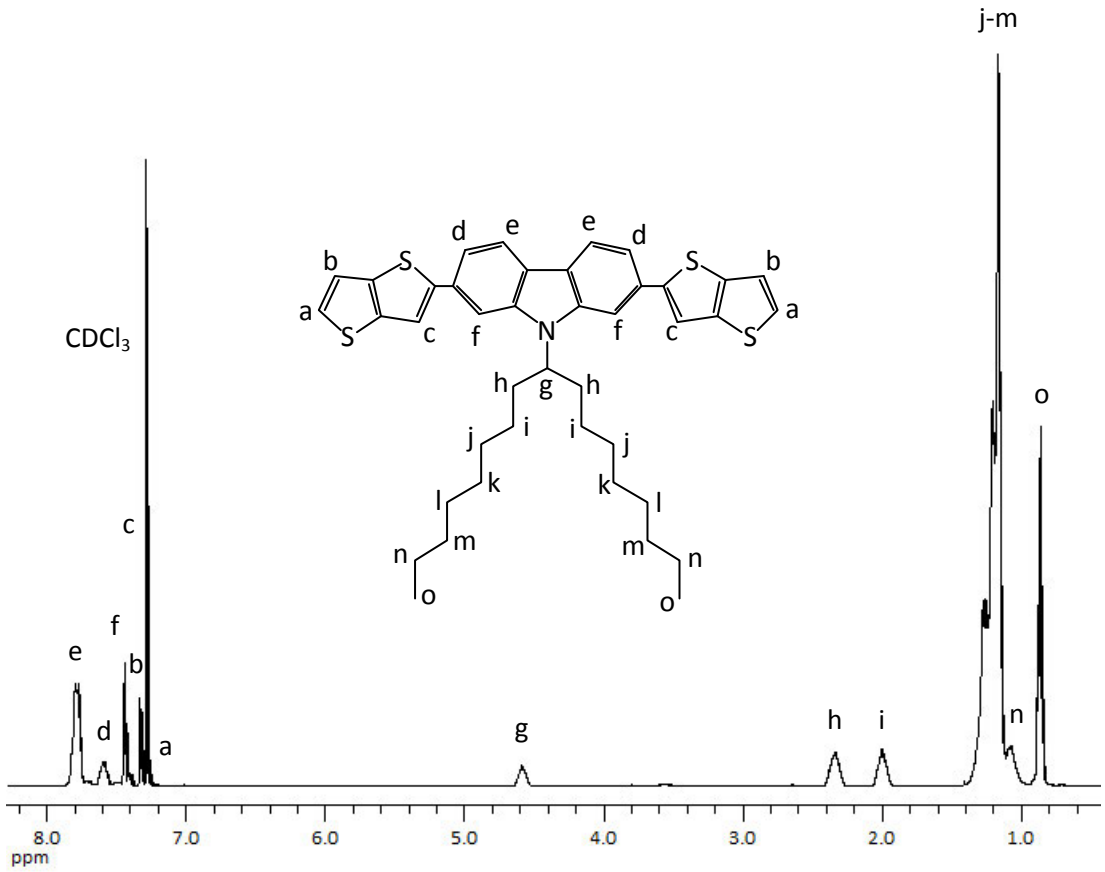

Figure 4.6: ^{1}H NMR of monomer 9-(heptadecan-9-yl)-2,7-di(thieno[3,2-*b*]thiophen-2-yl)-*9H*-carbazole **(37)** in $CDCl_3$.

All analytical results clearly verify that the product was 9-(heptadecan-9-yl)-2,7-di(thieno[3,2-*b*]thiophen-2-yl)-*9H*-carbazole **(37)**.

4.38 Synthesis of 9-(pentacosan-13-yl)-2,7-di(thieno[3,2-*b*]thiophen-2-yl)-*9H*-carbazole (38)

Synthesis of 9-(pentacosan-13-yl)-2,7-di(thieno[3,2-*b*]thiophen-2-yl)-*9H*-carbazole **(38)** was obtained from a modified the procedure by Kowalski *et al.*[149]

The crude product was purified *via* preparative HPLC to obtain **(38)** as a yellow solid in 96 %. Compound **(38)** was prepared by using 2,7-dibromo-9-(pentacosan-13-yl)-*9H*-carbazole **(10)** and trimethyl(thieno[3,2-*b*]thiophen-2-yl)stannane **(26)** as starting materials as shown in **Scheme 4.51.**

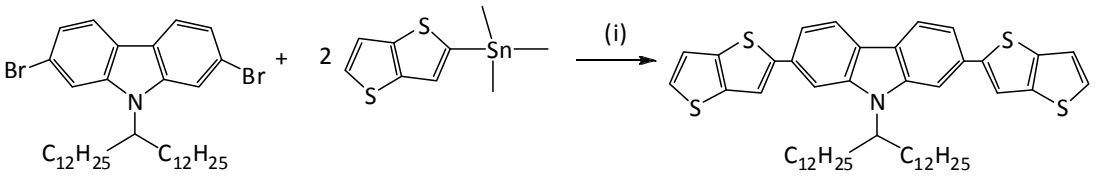

(10) **(26)** **(38)**

Scheme 4.51: Synthesis of 9-(pentacosan-13-yl)-2,7-di(thieno[3,2-*b*]thiophen-2-yl)-*9H*-carbazole **(38)**. (i) Bis(triphenylphosphine)-palladium(II)dichloride, ($Pd(PPh_3)_2Cl_2$) and toluene/110 °C.

The reaction was performed at high temperature 110 °C in the dark, then the crude product purified by column chromatography. The crude product **38** was purified via preparative HPLC, which was performed by using a reversed-phase column, the elution system (mobile phase) consisted of water (**A**) and THF (**B**), the following isocratic was used 25 % A and 75 % B and the total time was 20 min per injection. The pure compound was collected between 10.50 to 11.30 min to afford product.

The purity and the chemical structure of the product **(38)** were confirmed by TLC, which gave a single spot, the melting point was 30-35 °C, the mass spectra which show multi main masses at 793.6, elemental analysis $C_{49}H_{63}NS_4$ which was in agreement with the proposed structure, NMR analysis and FT-IR.

The ^{1}H-NMR displayed three broad peaks at 8.08 ppm, 7.80 ppm and 7.62 ppm which belong to the aromatic proton for the carbazole and three doublet peaks at 7.58 ppm, 7.52 ppm and 7.37 ppm correspond to protons of the thienothiophene as shown in **Figure 4.7.** The FT-IR spectrum showed absorption bands at 3083 cm^{-1} which falls in relation to aromatic benzene groups =C–H stretch. The characteristic peaks at 2919 cm^{-1} and 2849 cm^{-1} are assigned to the alkyl stretching frequencies of the methylene groups.

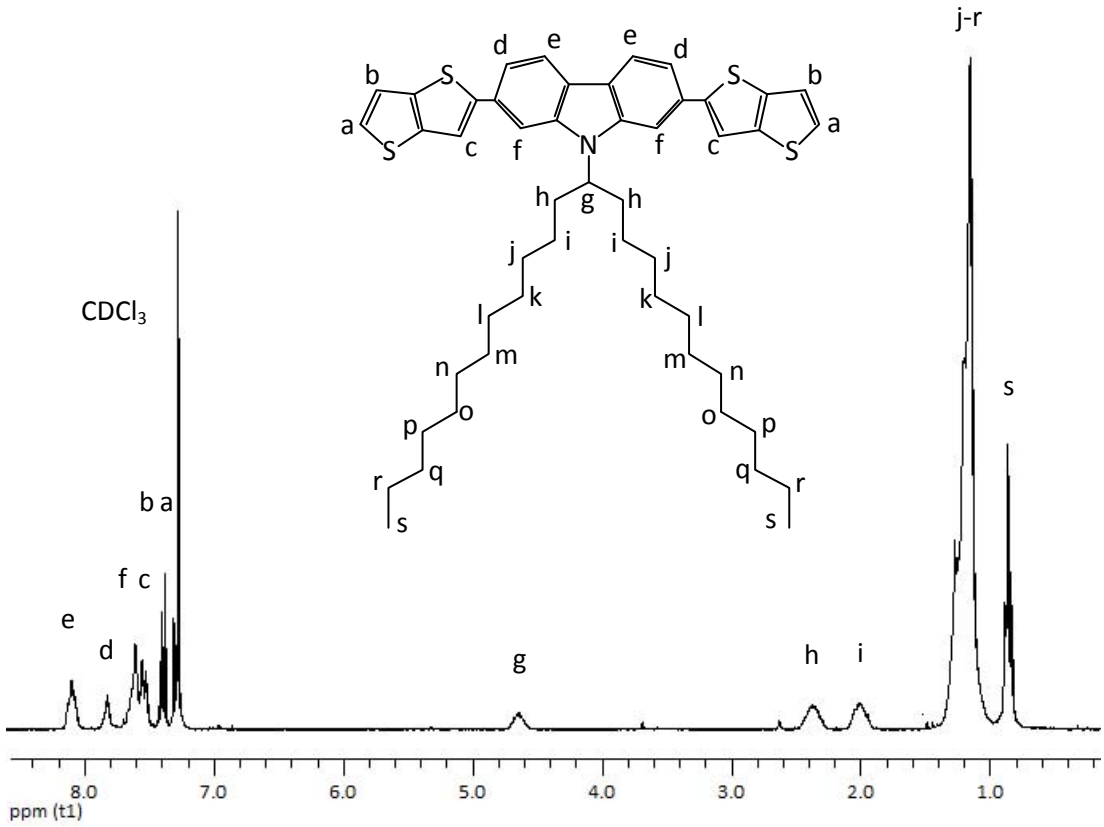

Figure 4.7: ^{1}H NMR of monomer 9-(pentacosan-13-yl)-2,7-di(thieno[3,2-*b*]thiophen-2-yl)-*9H*-carbazole **(38)** in $CDCl_3$.

All analytical results clearly verify and proposed that the product was 9-(pentacosan-13-yl)-2,7-di(thieno[3,2-*b*]thiophen-2-yl)-*9H*-carbazole **(38)**.

4.39 Synthesis of 3,6-difluoro-9-(heptadecan-9-yl)-2,7-di(thieno[3,2-*b*]thiophen-2-yl)-*9H*-carbazole (39)

Synthesis of 3,6-difluoro-9-(heptadecan-9-yl)-2,7-di(thieno[3,2-b]thiophen-2-yl)-*9H*-carbazole **(39)** was obtained from a modified procedure by Kowalski *et al.*[149]

The crude product was purified via silica gel column chromatography, eluting with 40-60 petroleum-ether: tolene (10:1) to obtain **(39)** as yellow solid in 50 %. Compound **(39)** was prepared by using 2,7-dibromo-3,6-difluoro-9-(heptadecan-9-yl)-*9H*-carbazole **(15)** and trimethyl(thieno[3,2-*b*]thiophen-2-yl)stannane **(26)** as starting materials as shown in **Scheme 4.52.**

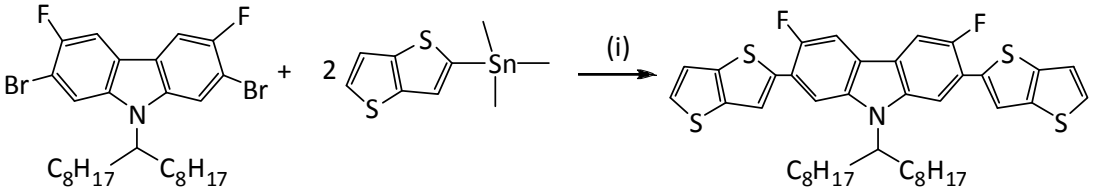

(15) **(26)** **(39)**

Scheme 4.52: Synthesis of 3,6-difluoro-9-(heptadecan-9-yl)-2,7-di(thieno[3,2-b]thiophen-2-yl)-*9H*-carbazole **(39)**. (i) Bis(triphenylphosphine)-palladium(II)dichloride, ($Pd(PPh_3)_2Cl_2$) and toluene/110 °C.

The reaction was performed at high temperature 110 °C in the dark, then the crude product purified by column chromatography. The purity and the chemical structure of the product **(39)** were confirmed by TLC, which gave a single spot, the melting point was 40-44 °C, the mass spectra which show multi main masses at 718, elemental analysis $C_{41}H_{45}F_2NS_4$ which was in agreement with the proposed structure, NMR analysis and FT-IR.

The ^{1}H-NMR displayed three broad peaks between 7.77 ppm and 7.60 ppm which belong to the aromatic proton of the carbazole ring and three doublet peaks at 7.35 ppm, 7.27 ppm which and 7.47 ppm correspond to protons of the thienothiophene as shown in **Figure 4.8.** The FT-IR spectrum showed absorption bands at 3083 cm^{-1} which falls in relation to aromatic benzene groups =C–H stretch. The characteristic peaks at 2918 cm^{-1} and 2849 cm^{-1} are assigned to the alkyl stretching frequencies of the methylene groups.

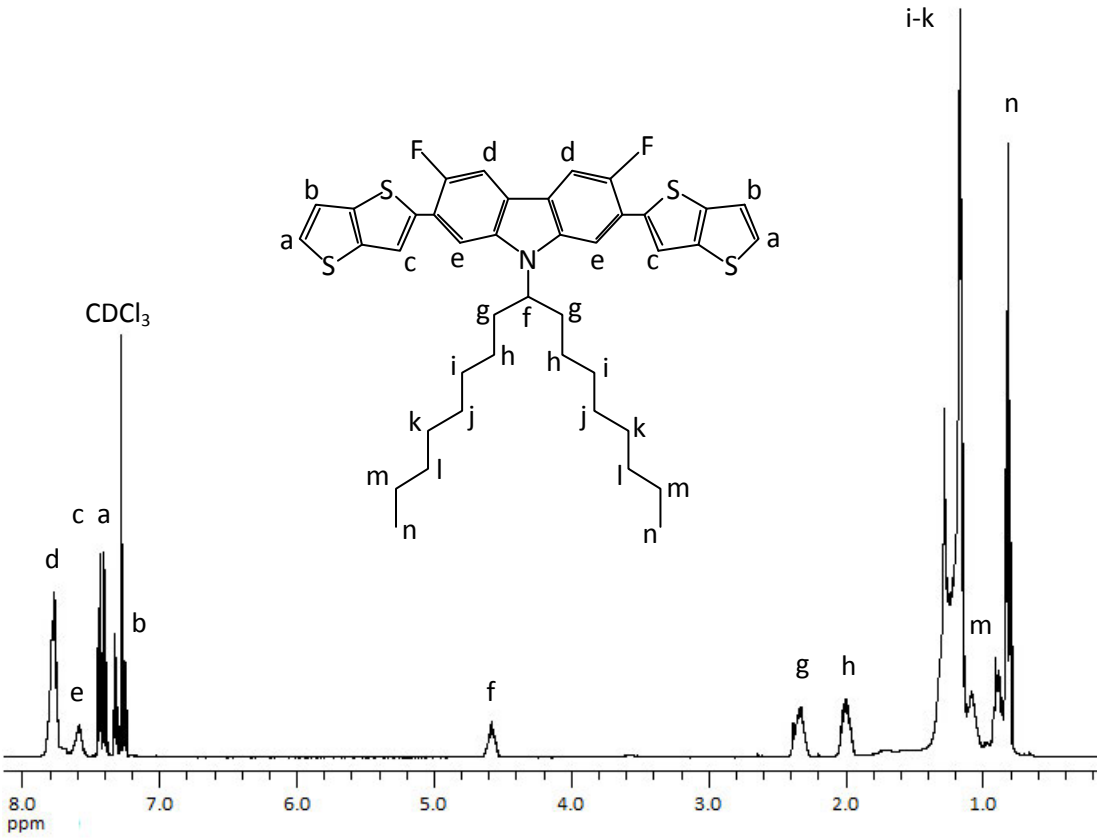

Figure 4.8: ^{1}H-NMR of monomer 3,6-difluoro-9-(heptadecan-9-yl)-2,7-di(thieno[3,2-*b*]thiophen-2-yl)-*9H*-carbazole **(39)** in $CDCl_3$.

Compound **(39)** was prepared in similar fashion. All analytical results clearly verify and proposed that the product was 3,6-difluoro-9-(heptadecan-9-yl)-2,7-di(thieno[3,2-*b*]thiophen-2-yl)-*9H*-carbazole **(39)**.

4.40 Synthesis of 3,6-difluoro-9-(pentacosan-13-yl)-2,7-di(thieno[3,2-*b*]thiophen-2-yl)-*9H*-carbazole (40)

Synthesis of 3,6-difluoro-9-(pentacosan-13-yl)-2,7-di(thieno[3,2-b]thiophen-2-yl)-9H-carbazole **(40)** was performed according to a modified the procedure by Kowalski *et al.*[149]

The crude product was purified via silica gel column chromatography, eluting with 40-60 petroleum-ether: tolene (10:1) to obtain (40) as yellow solid in 45 %. Compound (40) was prepared by using 2,7-dibromo-3,6-difluoro-9-(pentacosan-13-yl)-*9H*-carbazole **(17)** and trimethyl(thieno[3,2-*b*]thiophen-2-yl)stannane **(26)** as starting materials as shown in **Scheme 4.53.**

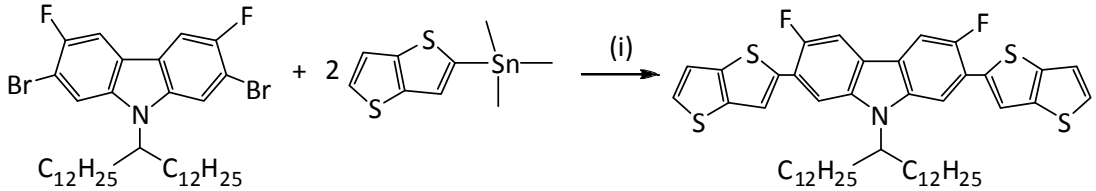

(17) **(26)** **(40)**

Scheme 4.53: Synthesis of 3,6-difluoro-9-(pentacosan-13-yl)-2,7-di(thieno[3,2-*b*]thiophen-2-yl)-*9H*-carbazole **(40)**. (i) Bis(triphenylphosphine)-palladium(II)dichloride, ($Pd(PPh_3)_2Cl_2$) and toluene/110 °C.

The reaction was performed at high temperature 110 °C in the dark, then the crude product purified by column chromatography. The purity and the chemical structure of the product **(40)** were confirmed by TLC, which gave a single spot, the melting point was 35-40 °C, the mass spectra which show multi main masses at 829.5, elemental analysis results were in agreement with the proposed structure. The ^{1}H-NMR displayed two broad peaks at 7.81 ppm and 7.55 ppm which belong to the aromatic proton for the carbazole and three doublet peaks at 7.42 ppm, 7.30 ppm and 7.18 ppm correspond to protons of the thienothiophene as shown in **Figure 4.9.**

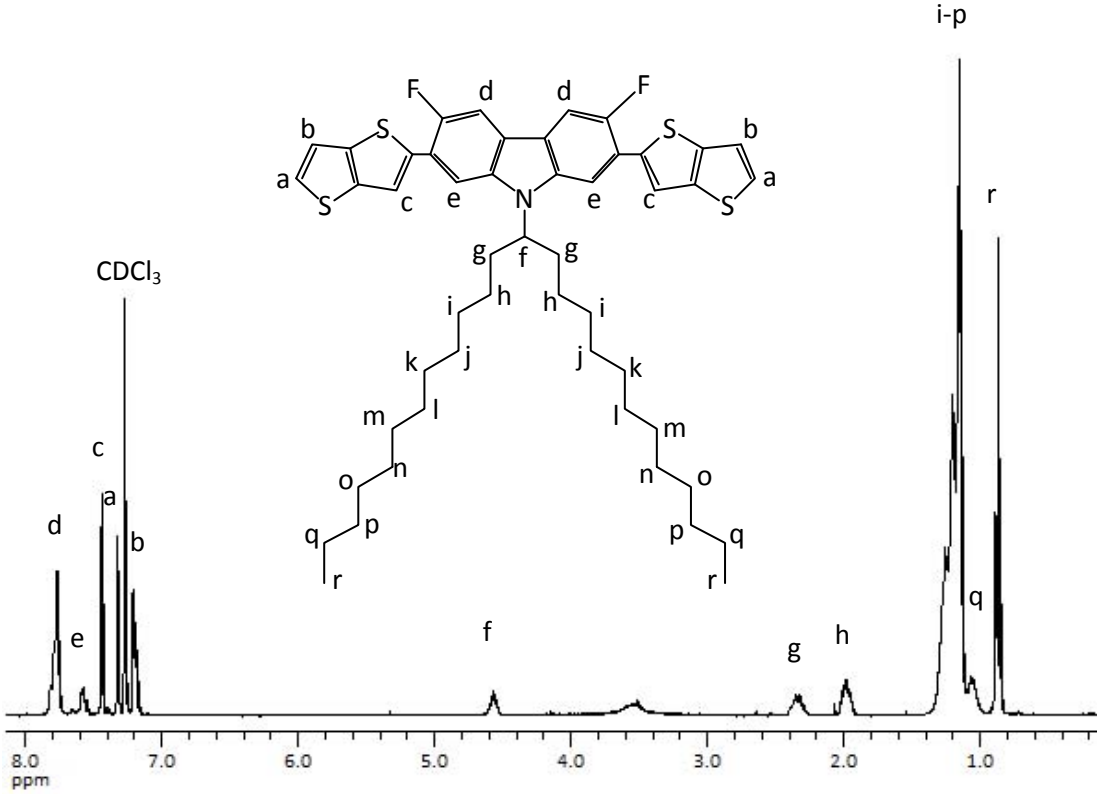

Figure 4.9: ^{1}H NMR of monomer 3,6-difluoro-9-(pentacosan-13-yl)-2,7-di(thieno[3,2-*b*]thiophen-2-yl)-*9H*-carbazole **(40)** in $CDCl_3$.

The FT-IR spectrum showed absorption bands at 3083 cm^{-1} which falls in relation to aromatic benzene groups =C–H stretch. The characteristic peaks at 2918 cm^{-1} and 2849 cm^{-1} are assigned to the alkyl stretching frequencies of the methylene groups.

All analytical results clearly verify and proposed that the product was 3,6-difluoro-9-(pentacosan-13-yl)-2,7-di(thieno[3,2-*b*]thiophen-2-yl)-*9H*-carbazole **(40)**.

CHAPTER 5 - RESULTS AND DISCUSSION - POLYMERS

5.1 The thienothiophene-based Copolymer: P1, P2 and P3

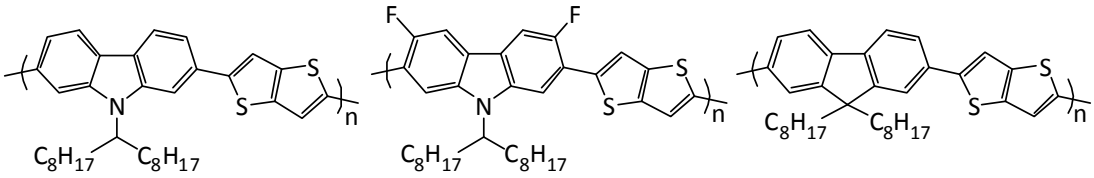

P1 **P2** **P3**

Figure 5.1: Structure of copolymers **P1**, **P2** and **P3**.

5.1.1 Synthesis of P1, P2 and P3

Figure 5.1 shows a series of copolymers, two of them are carbazole based, poly(9-(heptadecan-9-yl)-*9H*-carbazole-*alt*-thieno[3,2-*b*]thiophene) **(P1)** and poly(3,6-difluoro-9-(heptadecan-9-yl)-*9H*-carbazole-*alt*-thieno[3,2-*b*]thiophene) **(P2)**, and one is fluorene based poly(9,9-dioctyl-*9H*-fluorene-*alt*-thieno[3,2-*b*]thiophene) **(P3)**. All of them contain the same thienothiophene-based repeat units. All syntheses of copolymers were performed using a modified procedure by Iraqi *et al.*[103] These polymers were chosen due to similarities in their composition with polymers made previously by the Iraqi group, and also in the literature.[82, 83, 86, 189]

These copolymers were synthesized using Suzuki cross coupling reactions, in the presence of $Pd(OAc)_2$ and tri(o-tolyl)phosphine (1:2) as catalysts.[147, 182] A proposed mechanism for the polymerization is shown in **Scheme 5.1**. The first step involves an oxidative addition of palladium (0) to the aryl bromide to form a palladium (II). The second step involves reaction with the base to produce an intermediate complex, which in the third step forms the organopalladium via transmetallation with the boronic ester in the second monomer. Finally, the polymer is obtained by reductive elimination, which restores the original palladium (0) and then the catalytic cycle starts again.[167] The polymerization of **P1-P3** was performed twice in different conditions, the first one was carried out in THF as solvent and $NaHCO_3$ as base, in the second polymerization, toluene was used as solvent and tetraethylammonium hydroxide as base, due to the high boiling point of toluene, the average molecular weights of the polymers obtained from this polymerization was higher than those from the first polymerization.

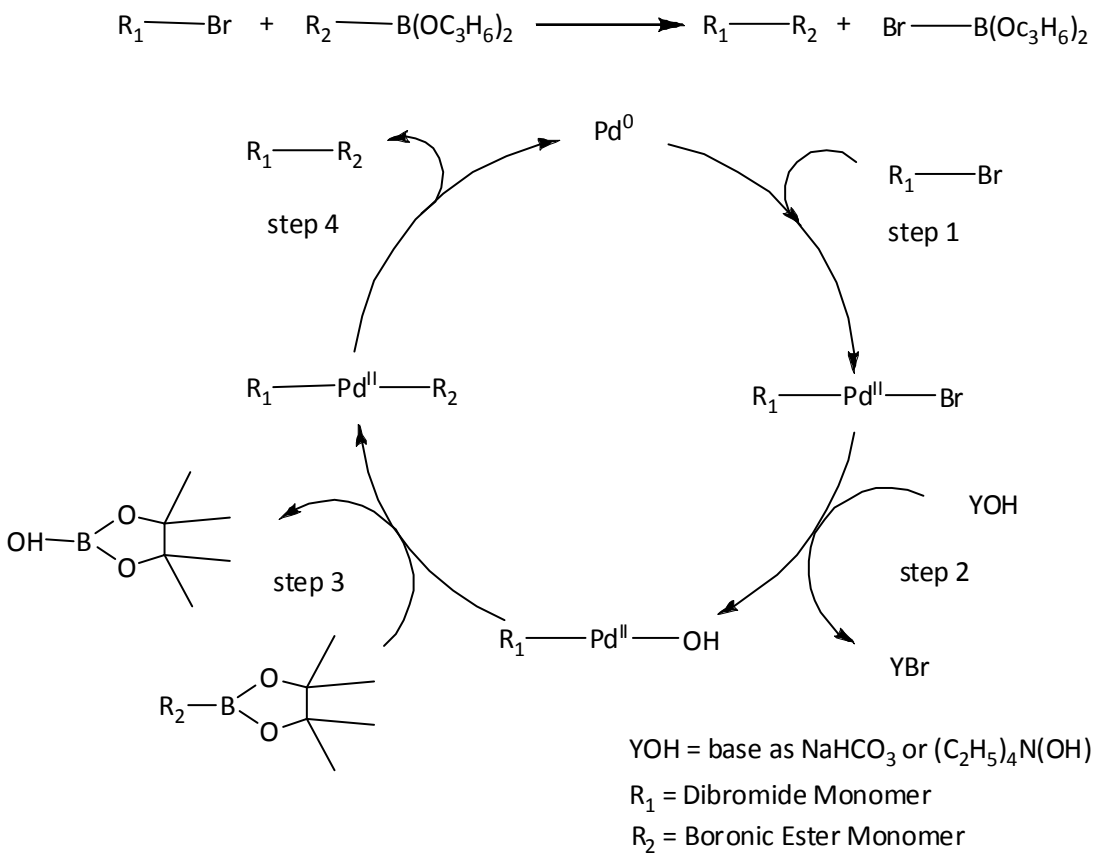

Scheme 5.1: The catalytic cycle of Suzuki cross coupling reaction for polymerization of polymers **P1-P3**.

All polymerizations were performed under argon in degassed systems, and they were stopped when the solutions became too viscous. Then another portion of solvent was added to solubilise the formed polymers, and then the end-capping reagents (bromobenzene and phenyl boronic acid) could be added to the polymer solutions to increase the stability of the polymer in device operation and to remove bromine and boronic ester end groups from the polymer. Then the polymer solutions were stirred with ammonia to remove catalyst remnants and other impurities.

To remove further palladium impurities, oligomers and unreacted monomers, all the crude polymers were purified using several steps. After washing the polymers solutions with water to remove the ammonia and then concertrating the solutions to approximately 50 ml, the polymers were precipitated in methanol to remove end-capping reagents, organic palladium species and unreacted comonomers.

The obtained crude polymers were then collected through filtration on micropore membranes then transferred to fiber glass thimbles and cleaned with different solvents using a Soxhlet apparatus. The first solvent was methanol to remove the palladium residues from the copolymer, followed by acetone and hexane, to clean off the low molecular weight oligomers. Then the purified polymers were extracted with toluene, chloroform and chlorobenzene and the solutions precipitated separately in methanol to obtain the different fractions of polymers as dark purple powders. The elemental analysis of all fractions did not show any traces of bromine and gave satisfactory results.

5.1.2 Nuclear Magnetic Resonance (NMR) spectroscopy analysis of P1, P2 and P3

^{1}H-NMR studies conducted at 100 °C in 1,1,2,2-tetrachloroethane-d_2 ($C_2D_2Cl_4$) on **P1** confirmed its assigned structure. The ^{1}H-NMR spectrum of **P1** is shown in **Figure 5.2**, it reveals in the aromatic region the protons of the carbazole hydrogen with multiplet signal at 8.10 ppm, 7.78 ppm and 7.53 ppm assigned to protons a, b and c respectively.

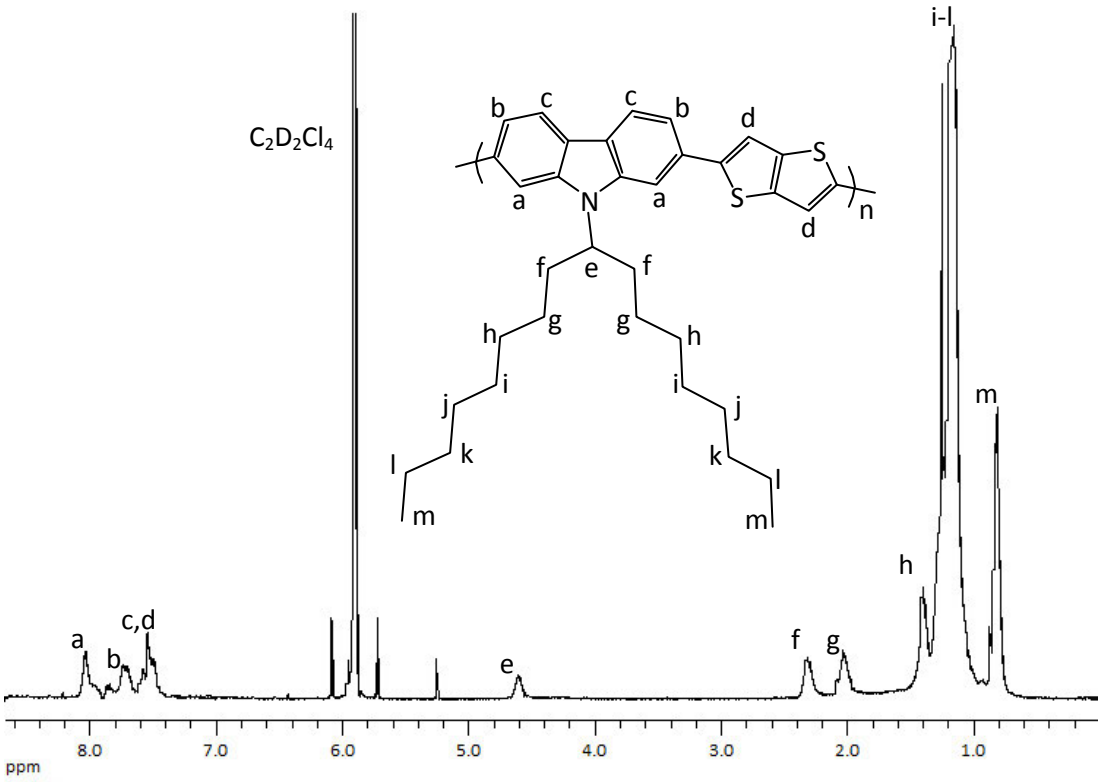

Figure 5.2: The ^{1}H-NMR spectrum of **P1** in $C_2D_2Cl_4$ at 100 °C.

The two protons on the thienothiophene repeat units are observed at broad peak 7.53 ppm. The broad peak at 4.61 ppm corresponds to the proton on the carbon atom at position e. Other peaks correspond to alkyl chains which are connected to carbazole units.

^{1}H-NMR studies conducted at 100 °C in 1,1,2,2-tetrachloroethane-d_2 on **P2** confirmed its assigned structure. The ^{1}H-NMR spectrum of P2 is shown in **Figure 5.3**, it reveals in the aromatic region proton on the carbazole units with multiplet signal at 8.18 ppm and 7.78 ppm assigned to protons a and b respectively.

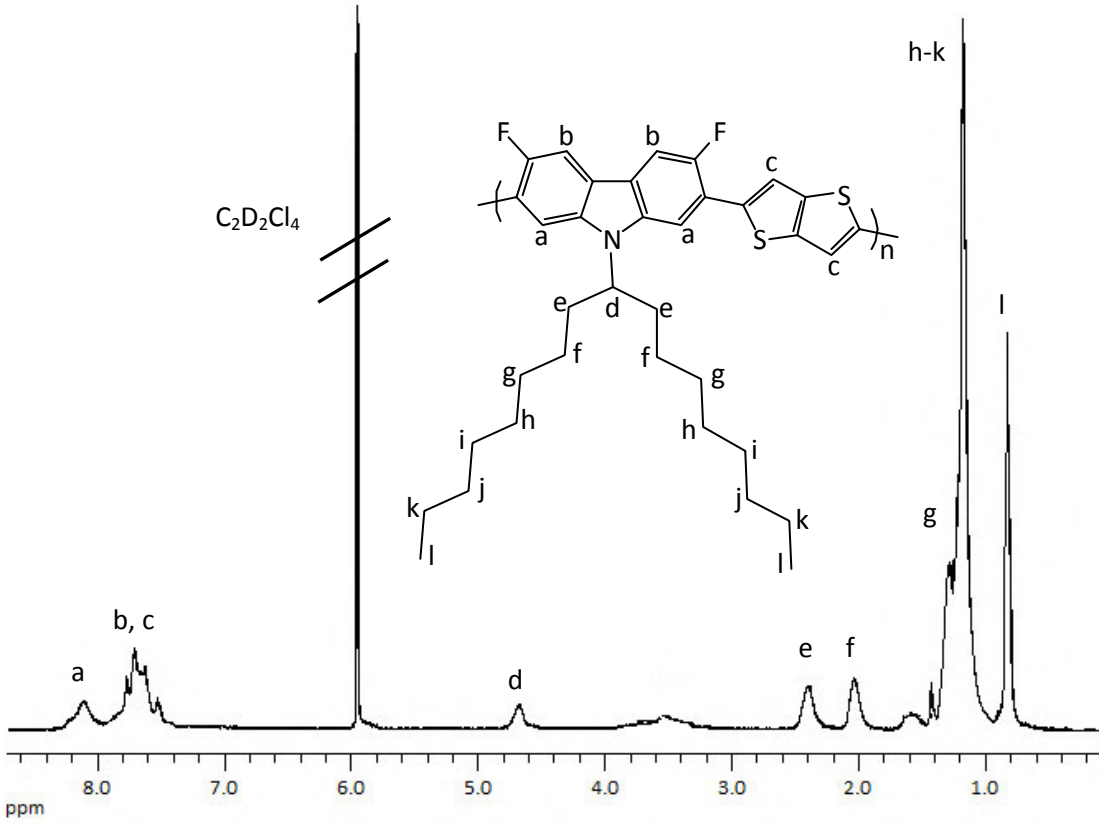

Figure 5.3: The ^{1}H-NMR spectra of **P2** in $C_2D_2Cl_4$ at 100 °C.

The two protons on the thienothiophene repeat units are observed at broad peak 7.78 ppm and overlap with the carbazole proton at position b. The broad peak at 4.77 ppm corresponds to the proton on the carbon atom at position d. Other peaks correspond to alkyl chains which are connected to carbazole units.

^{1}H-NMR studies conducted at 100 °C in 1,1,2,2-tetrachloroethane-d_2 on **P3** confirmed its assigned structure. The ^{1}H-NMR spectrum of **P3** is shown in **Figure 5.4**, it reveals in the aromatic region the proton of the fluorene hydrogen with multiplet signal at 8.51 ppm, 8.19 ppm and 7.83 ppm assigned to protons a, b and c respectively.

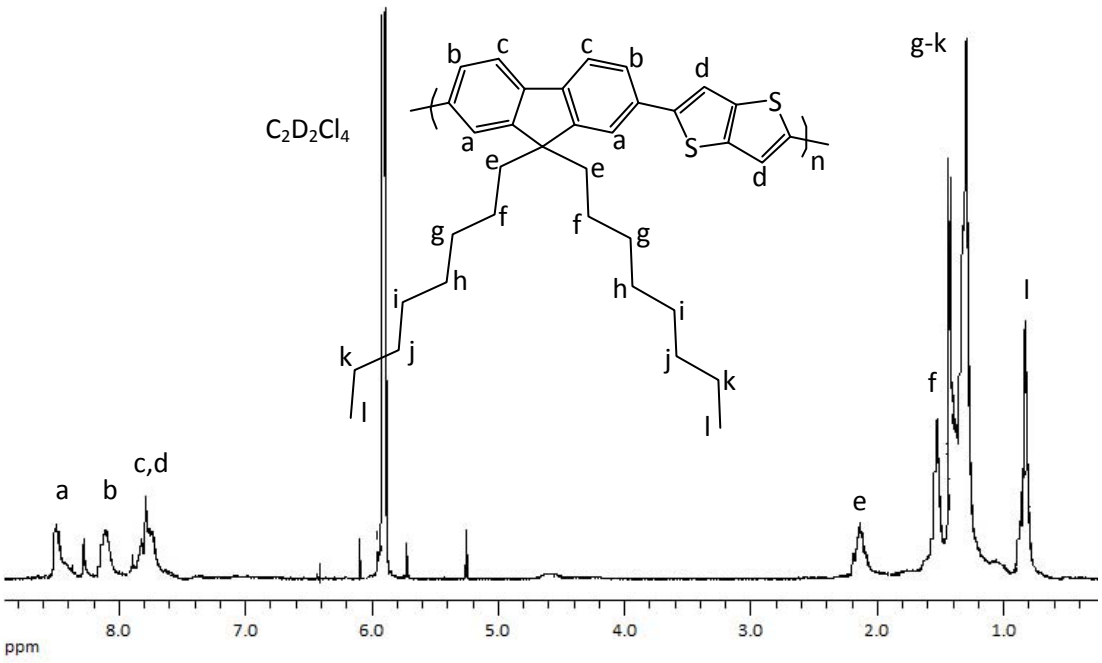

Figure 5.4: The ^{1}H-NMR spectra of **P3** in $C_2D_2Cl_4$ at 100 °C.

The two protons on the thienothiophene repeat units are observed at broad peak 7.83 ppm and overlap with the fluorene proton at position c. Other peaks correspond to alkyl chains which are connected to fluorene units.

5.1.3 Infrared spectroscopy (FT-IR) analysis of P1, P2 and P3

The IR spectrum of **P1** was fairly similar patterns to those of its constituent monomers with some assignments of different bands/peaks. It can be seen the characterizing peak at 3083 cm^{-1} which falls in relation to aromatic benzene groups =C–H stretch. The characteristic peaks at 2961 cm^{-1} and 2853 cm^{-1} are assigned to the alkyl stretching frequencies of the methylene groups.

The characteristic overtones are seen from about 2000-1665 cm^{-1}. The assignment of different peaks compare to monomer **(7)** was observed at 1463 cm^{-1}, 1410 cm^{-1} and 1260 cm^{-1} and it has a mixture of peaks related to the combination bands and also the deformations bands of the aromatic -CH groups and methylene -CH_2- groups.

The peak originally at 1037cm^{-1}, attributed to $C_{aromatic}$-Br linkage in the spectrum of monomer **(24)** disappeared. And also peaks at 1327 cm^{-1} and 1296 cm^{-1} (B-O stretch), and 1140 cm^{-1} (B-C stretch) presents in the spectrum of **(7)** did also disappear from the spectrum of **P1** due to the consumption of the corresponding functional groups in the Suzuki cross-coupling reaction.

The IR spectrum of the **P2** was fairly similar patterns to those of its constituent monomers with some assignments of different bands/peaks. It can be seen the characterizing peak at 3094 cm^{-1} which falls in relation to aromatic benzene groups =C–H stretch. The characteristic peaks at 2960 cm^{-1}, 2923 cm^{-1} and 2852 cm^{-1} are assigned to the alkyl stretching frequencies of the methylene groups.

The characteristic overtones are seen from about 2161-1665 cm^{-1}. The assignment of different peaks compare to monomer **(16)** was observed at 1455 cm^{-1}, 1431 cm^{-1} and 1335 cm^{-1} and its has a mixture of peaks related to the combination bands and also the deformations bands of the aromatic –CH groups and methylene –CH_2- groups. Peaks at 1258 cm^{-1} are characteristic to the C-N bond and a peak at 1079 cm^{-1} and 1017 cm^{-1} is assigned to the C-F bonds.

The peak originally at 1037cm^{-1}, attributed to $C_{aromatic}$-Br linkage in the spectrum of monomer **(24)** disappeared. And also peaks at 1327 cm^{-1} and 1296 cm^{-1} (B-O stretch), and 1140 cm^{-1} (B-C stretch) present in the spectrum of (**16**) did also disappear from the spectrum of **P2** due to the consumption of the corresponding functional groups in the Suzuki cross-coupling reaction.

The IR spectrum of the **P3** has fairly similar patterns to those of its constituent monomers with some assignments of different bands/peaks. The character peak in relation to aromatic benzene groups =C–H stretch can seen at 3085 cm^{-1}. The characteristic peaks at 2959 cm^{-1}, 2920 cm^{-1} and 2850 cm^{-1} are assigned to the alkyl stretching frequencies of the methylene groups.

The characteristic overtones are seen from about 2170-1721 cm^{-1}. The assignment of different peaks compare to monomer **(41)** was observed at 1499 cm^{-1}, 1453 cm^{-1} and 1335

cm^{-1} and its has a mixture of peaks related to the combination bands and also the deformations bands of the aromatic –CH groups and methylene $–CH_2-$ groups.

The peak originally at $1037cm^{-1}$, attributed to $C_{aromatic}$-Br linkage in the spectrum of monomer **(24)** disappeared. And also peaks at 1327 cm^{-1} and 1296 cm^{-1} (B-O stretch), and 1140 cm^{-1} (B-C stretch) present in the spectrum of **(41)** did also disappear from the spectrum of **P3** due to the consumption of the corresponding functional groups in the Suzuki cross-coupling reaction.

5.1.4 Gel Permeation Chromatography (GPC) analysis of P1, P2 and P3

The yields quoted for the polymers in **Table 5.1** are the yields after Soxhlet extraction of the polymers. Analysis of the polymers was conducted on the highest molecular weight fractions which will be used in the actual photovoltaic devices. Gel permeation chromatography measurements were taken in 1, 2, 4-trichlororbenzene (TCB) at 100 °C as at lower temperatures it was not possible to solubilise all the higher molecular weight polymer fractions to obtain the true molecular weights. GPC results from the polymerization for polymers **P1, P2** and **P3** by using polystyrene standards are shown in **Table 5.1**.

Table 5.1: GPC data of **P1, P2** and **P3.**

Polymer	Yield (%)	M_w	M_n	PDI
P1	32	6500	2800	2.3
P2	60	7100	2900	2.4
P3	54	4600	2100	2.2

Polymer **P1** was obtained as a red solid in 32 % yield. GPC analysis of chloroform fraction of polymer **P1** gave an M_w = 6500 and M_n = 2800 with a polydispersity of 2.3.

Polymer **P2** was obtained as a red solid in 60 % yield. GPC analysis of chloroform fraction of polymer **P2** gave an M_w = 7100 and M_n = 2900 with a polydispersity of 2.4.

Polymer **P3** was also obtained as a red solid in 54 % yield. GPC analysis of chloroform fraction of polymer **P3** gave an M_w = 4600 and M_n = 2100 with a polydispersity of 2.2.

Based on the **Table 5.1**, polydispersity of **P3** is lower than polymers **P1** and **P2**. It is due to the rich alternating electron along their backbone which is presence from carbazole and fluorine linked compare with the limited alternating electron in fluorine in **P3** as the compound backbone.

5.1.5 Elemental analysis of P1, P2 and P3

Elemental analysis was used to check if a sample is consistent with a given molecular formula by using qualitative analysis technique. **Table 5.2** shows no bromine content, indicating that the terminal groups were end-capped in polymers **P1, P2** and **P3**. The elemental analysis of the other elements of polymers **P1, P2** and **P3** did also give a satisfactory agreement with their proposed structure.

Table 5.2: Elemental analysis data of **P1, P2** and **P3**.

Polymers	Formula Weight	Molecule Weight		Elemental analysis (%)			
				C	H	N	Br
P1	$(C_{35}H_{43}NS_2)_n$	$(541.86)_n$	Calculated	77.58	8.00	2.58	0
			Found	76.06	9.01	2.22	0
P2	$(C_{35}H_{41}F_2NS_2)_n$	$(577.84)_n$	Calculated	72.75	7.15	2.42	0
			Found	74.00	6.55	2.00	0
P3	$(C_{35}H_{42}S_2)_n$	$(526.84)_n$	Calculated	79.79	8.04	-	0
			Found	80.02	7.55	-	0

* n = repeating unit

5.1.6 UV-Visible absorption spectroscopy (UV-Vis) analysis of P1, P2 and P3

The UV-Visible absorption spectra of the polymers were measured in chloroform and in solid state as thin films. The optical band gaps were calculated from the onset of absorption of the polymers in the solid state, the results of these studies are summarized in **Table 5.3**.

Table 5.3: UV-Vis data of **P1**, **P2** and **P3**.

Polymers	λ_{max} Solution (nm)	λ_{max} Thin film (nm)	λ Onset Abs. (nm)	E_g Optical (eV)
P1	435	442	505	2.46
P2	405	419	525	2.36
P3	395	400	503	2.47

Figure 5.5 shows the absorption spectra of **P1** in solution (chloroform) and in the solid state. Polymer **P1** displays a maximum absorption in solution at λ_{max} = 435 nm. The electronic spectra of polymer **P1** in the solid state display similar features to those in solution with a λ_{max} = 442 nm with a shoulder peak at 505 nm, indicating more extended electronic conjugation in films than in solution. The optical band gap of polymer **P1** as determined from the onset of its absorption spectra in the solid state and has a value E_g = 2.46 eV.

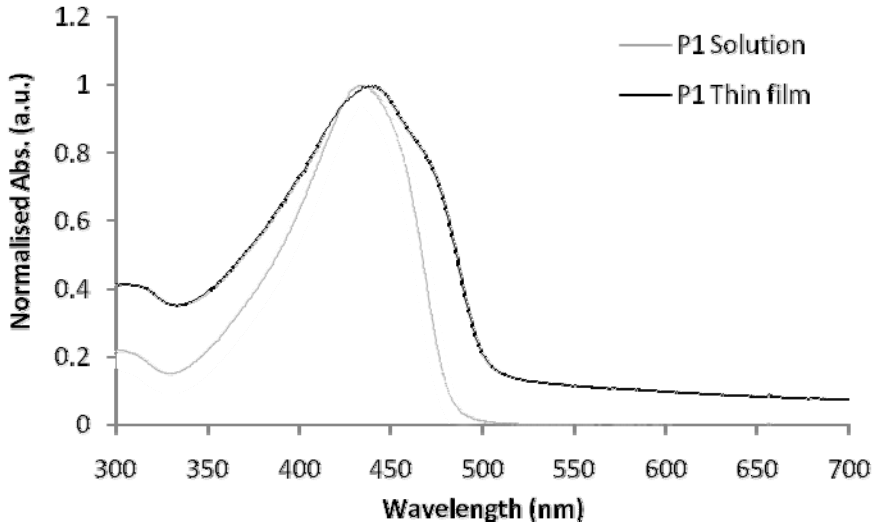

Figure 5.5: Normalised UV-Vis spectra of **P1** in chloroform solution (grey line) and a thin film (black line).

Figure 5.6 shows the absorption spectra of **P2** in solution (chloroform) and in the solid state. Polymer **P2** displays a maximum absorption in solution at λ_{max} = 405 nm with a shoulder absorption band at 511 nm. The shoulder absorption peak can be explained by the existence of segments of more extended electronic conjugation along the polymer chains.

The electronic spectra of polymer **P2** in the solid state display similar features to those in solution with a λ_{max} = 419 nm and a shoulder peak at 525 nm, indicating more extended electronic delocalization in **P2** as on films.

The optical band gap of polymer **P2** as determined from the onset of its absorption spectra in the solid state has a value E_g = 2.36 eV. The presence of fluorine substitutes at the 3,6-position of carbazole repeat units on **P2** has led into a monomer band gap in the polymer when it is composed to that of the equivalent polymer without fluorine substituent **P1**. This indicates the present of fluorine interactions of **P2** with neighboring sulfur or hydrogen atoms of the thienothiophene repeat units along the polymer backbone.

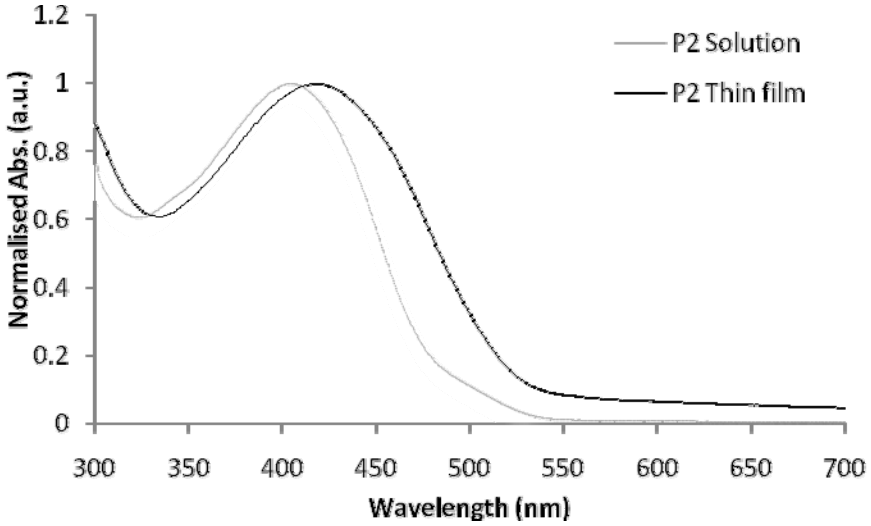

Figure 5.6: Normalised UV-Vis spectra of **P2** in chloroform (grey line) and a thin film (black line).

Figure 5.7 shows the absorption spectra of **P3** in solution (chloroform) and in the solid state. Polymer **P3** displays a maximum absorption in solution at λ_{max} = 395 nm. The electronic spectra of polymer **P3** in the solid state display similar features to those in solution with a λ_{max} = 400 nm. The optical band gap of polymer **P3** as determined from the

onset of its absorption spectra in the solid state has a value E_g = 2.47 eV. The indicating similar electronic properties between the polymers with little differences in their electronic delocalization or simple change of carbazole to fluorene repeat units.

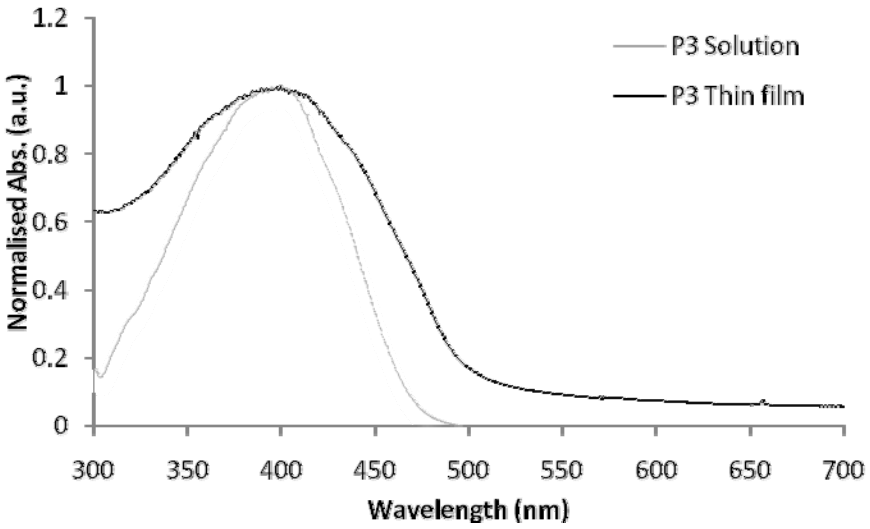

Figure 5.7: Normalised UV-Vis spectra of **P3** in chloroform (grey line) and a thin film (black line).

5.1.7 Cyclic Voltammetry (CV) analysis of P1, P2 and P3

Investigations of the electrochemical properties of polymers **P1, P2** and **P3** were also undertaken in cyclic voltammetry (CV) performed on drop-cast polymer films in acetonitrile with tetrabutylammonium perchlorate as the electrolyte. The LUMO level and the HOMO level were calculated from the onset reduction and oxidation respectively. Then, the electrochemical band gap (E_g) can be calculated from the difference between them. The cyclic voltammogram of the polymers **P1, P2** and **P3** are shown in **Figure 5.8**.

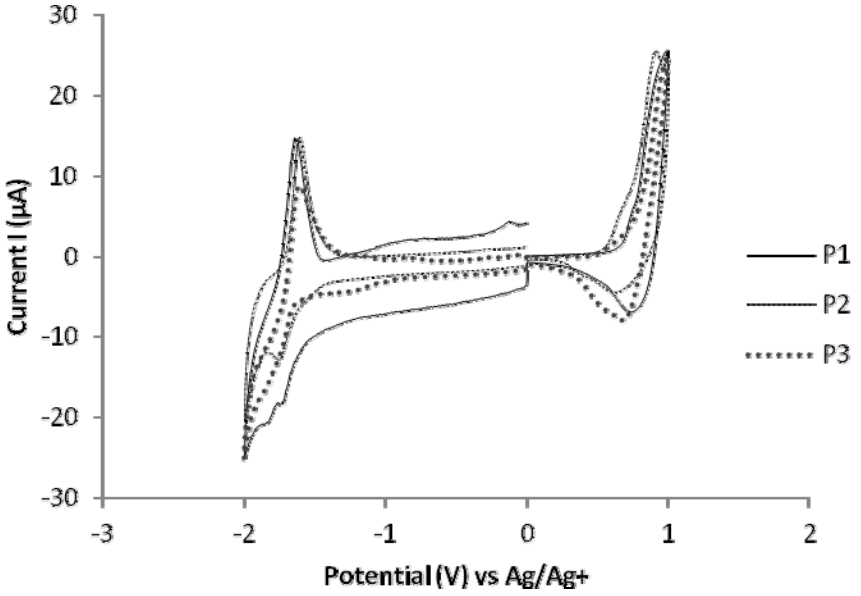

Figure 5.8: Normalised cyclic voltammogram of **P1**, **P2** and **P3**.

All values were taken relative to the reference electrode Ag/Ag+, on the basis that the energy level of the ferrocene/ ferrocenium is 4.8 eV below the vacuum level and oxidation occurs at 0.082 V data from the spectra were adjusted to give the polymers relative to these values.[207]

Polymer **P1** exhibits an oxidation wave at E_{pa} = 0.98 V and a reduction wave at E_{pa} = -1.65 V, and their associated reduction and oxidation waves at E_{pc} = 0.74 V and E_{pc} = -1.76 V, respectively. From the onset of oxidation (0.65 V) and the onset of reduction (-1.53 V), the HOMO level is at -5.45 eV and the LUMO level is at -3.27 eV for the polymer backbone (on the basis that ferrocene/ferrocenium has an IP of 4.8 eV below the vacuum level and the oxidation occurs at 0.082 V relative to Ag/Ag^+), therefore the electrochemical band gap of the polymer is 2.18 eV. Polymer **P2** exhibits an oxidation wave at E_{pa} = 1.10 V and a reduction wave at E_{pa} = -1.65 V, and their associated reduction and oxidation waves at E_{pc} = 0.75 V and E_{pc} = -1.74 V, respectively. From the onset of oxidation (0.70 V) and the onset of reduction (-1.63 V), the HOMO level is at -5.50 eV and the LUMO level is at -3.17 eV for the polymer backbone (on the basis that ferrocene/ferrocenium has an IP of 4.8 eV below the vacuum level and the oxidation occurs at 0.082 V relative to Ag/Ag^+), therefore the electrochemical band gap of the polymer is 2.33 eV.

Polymer **P3** exhibits an oxidation wave at E_{pa} = 1.17 V and a reduction wave at E_{pa} = -1.62 V, and their associated reduction and oxidation waves at E_{pc} = 0.82 V and E_{pc} = -1.77 V, respectively. From the onset of oxidation (0.84 V) and the onset of reduction (-1.60 V), the HOMO level is at -5.64 eV and the LUMO level is at -3.20 eV for the polymer backbone (on the basis that ferrocene/ferrocenium has an IP of 4.8 eV below the vacuum level and the oxidation occurs at 0.082 V relative to Ag/Ag^+), therefore the electrochemical band gap of the polymer is 2.44 eV as shown in **Table 5.4.**

Table 5.4: Voltammetry results and band gaps of **P1**, **P2** and **P3.**

Polymers	*E*onset, $_{ox}$ (V)[a)]	*E*onset, $_{red}$ (V) [a)]	HOMO (eV)	LUMO (eV)	Band gap (eV)
P1	0.65	-1.53	-5.45	-3.27	2.18
P2	0.70	-1.63	-5.50	-3.17	2.33
P3	0.84	-1.60	-5.64	-3.20	2.44

[a)] *vs*. Ag/Ag^+

The band gap **P3** is higher compare to **P1** and **P2**. It is due to associated reduction and oxidation waves the polymers **P1** and **P2** with fluorine substituents has or more extended electronic delocalisation. These results also point to the presence of interactions between the fluorine substituents on carbazole repeat units on **P2**.

5.1.8 Thermogravimetric Analysis (TGA) of P1, P2 and P3

The thermal stability of **P1, P2** and **P3** were investigated in this study. The thermogram of **P1, P2** and **P3** is shown in **Figure 5.9** and the details of the TGA results are shown in **Table 5.5**.

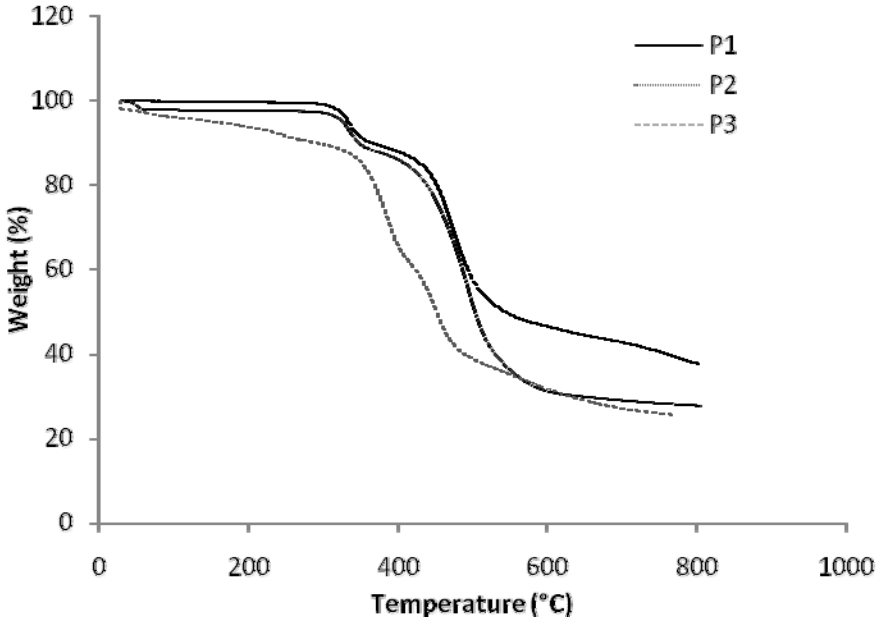

Figure 5.9: The TGA thermogram of **P1**, **P2** and **P3**.

Figure 5.9 shows the TGA curves for of the thermal degradation of the polymer **P1**, the onset of the degradation occurs at 318 °C, the onset of second degradation is 430 °C with a weight loss of 73.1 %. The percentage of residual weight 26.9 % is consistent with percentage weight of the polymer backbone.

The TGA analysis confirms that the polymer has high thermal stability up to 380 °C. Thermal gravimetry analysis measurements revealed the remarkable stability of the polymer up to 430 °C, which indicated that these polymers are thermally very stable. The subsequent degradation and weight loss of the polymer beyond 430 °C was proportional to the mass of its a alkyl-group substituents. The polymer did not show any further weight loss up to a temperature of 800 °C.

Figure 5.9 shows the TGA curves for of the thermal degradation of the polymer **P2**, the onset of the degradation occurs at 311 °C, the onset of second degradation is 432 °C with a weight loss of 72.9 %. The percentage of residual weight 27.1 % is consistent with percentage weight of PDI units and polymer backbone.

The TGA analysis confirms that the polymer has high thermal stability up to 380 °C. Thermal gravimetry analysis measurements revealed the remarkable stability of the polymer up to 432 °C, which indicated that these polymers are thermally very stable. The subsequent

degradation and weight loss of the polymer beyond 432 °C was proportional to the mass of its a alkyl-group substituents. The polymer did not show any further weight loss up to a temperature of 800 °C.

Based on the thermogram as shows in the **Figure 5.9** TGA curves of the thermal degradation of the polymer **P3**, the onset of the degradation occurs at 291 °C, the onset of second degradation is 425 °C with a weight loss of 72 %. The percentage of residual weight 28 % is consistent with percentage weight of PDI units and polymer backbone.

The TGA analysis confirms that the polymer has high thermal stability up to 380 °C. Thermal gravimetry analysis measurements revealed the remarkable stability of the polymer up to 425 °C, which indicated that these polymers are thermally very stable. The subsequent degradation and weight loss of the polymer beyond 425 °C was proportional to the mass of its a alkyl-group substituents. The polymer did not show any further weight loss up to a temperature of 800 °C.

5.1.9 Differential Scanning Calorimetry (DSC) analysis of P1, P2 and P3

Table 5.5 summarises the results from the thermo gravimetric analysis (TGA) and the differential scanning calorimetry (DSC). In applications that can experience temperature extremes, it is important to know what will happen when these polymers are exposed to variants in temperature and how they will affect the mechanical behaviour of the polymer.

Table 5.5: The TGA and DSC data of **P1, P2** and **P3**.

Polymers	TGA Analysis			DSC Analysis
	Onset degradation temp. / °C		Weight loss at 800 °C (wt. %)	T_g / °C
	1^{st} degradation	2^{nd} degradation		
P1	318	430	73.1	70
P2	311	432	72.9	78
P3	291	425	72.0	76

The glass transition (T_g) is obtained from the DSC trace and it is a function of polymer backbone flexibility. The polymers were subjected to a first heating run, cooling run followed by further heating run, at the scan rate 10 °C/ min, and when no T_g was seen, 20 up to 100 °C/ min rates was applied. The glass transitions (T_g) value were estimated and obtained from the first scans as broad peaks, they were above 50 °C indicating that all polymers have good tolerance to the stages required in making devices. Based on the table the T_g of **P1, P2** and **P3** were 70 °C, 78 °C and 76 °C, respectively. All the T_g results of the polymers are similar to each other, due to the present of thienothiophene, which provide more flexibility for the polymer backbones.

5.2 Thienothiophene-benzothiadiazole-based Copolymers: P4, P5, P6 and P7

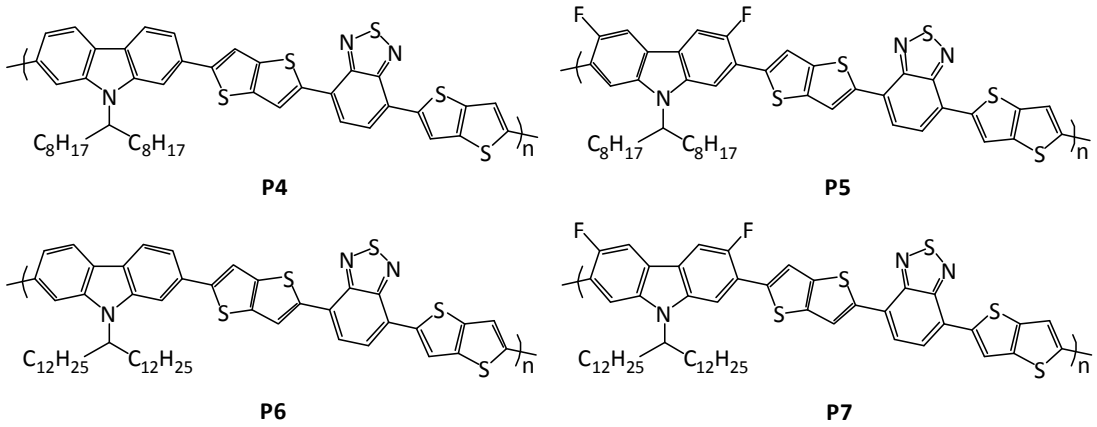

Figure 5.10: Structures of copolymers **P4, P5, P6** and **P7**.

5.2.1 Synthesis of P4, P5, P6 and P7

Figure 5.10 shows a series of carbazole-based copolymers, two of them have heptadecanyl substituent, poly(9-(heptadecan-9-yl)-*9H*-carbazole-*atl*-4,7-di(thieno[3,2-b]thiophen-2-yl)benzo [*c*][1,2,5]thiadiazole) **(P4)**, poly(3,6-difluoro-9-(heptadecan-9-yl)-*9H*-carbazole-*atl*-4,7-di(thieno[3,2-*b*]thiophen -2-yl)benzo[*c*][1,2,5]thiadiazole) **(P5),** and the other two have pentacosanyl substituents, poly(9-(pentacosan-13-yl)-*9H*-carbazole-*atl*-4,7-di(thieno[3,2-*b*]thiophen-2-yl)benzo [c][1,2,5]thiadiazole) **(P6)** and poly(3,6-difluoro-9-(pentacosan-13-yl)-*9H*-carbazole-*atl*-4,7-di(thieno[3,2-*b*]thiophen-2-yl)benzo[c][1,2,5]thia diazole) **(P7)**. All of them contain the same thienothiophene-benzothiadiazole-based repeat units.

While Suzuki coupling has been widely used to prepare conjugated polymers in view of its high efficiency and also of the purity of the resulting polymers made using this method, it was difficult to prepare polymers **P4-P7** using this approach. This was mainly due problems associated with the l solubility **(36)** of one of the intermediate required to prepare such polymers as shown **Scheme 5.2** below.

Original synthetic method proposed to prepare polymers **P4**-**P7** using the Suzuki coupling reaction.

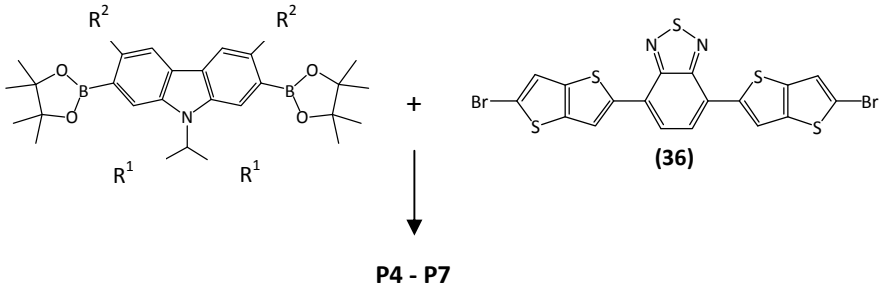

Alternative method used to prepare **P4 - P7** using the arylation reaction:

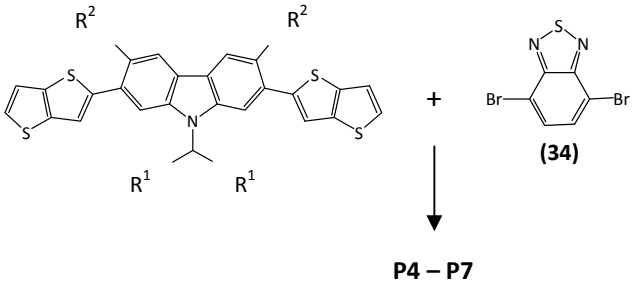

Scheme 5.2: Synthetic routes to **P4-P7**.

Syntheses of all copolymers were performed using a modified procedure by literatures.[149] Reaction were carried out at 110 °C using $Pd(OAc)_2$ as the catalyst and K_2CO_3 (1.5 equiv) in DMAc (10 mL).[208]

5.2.2 Nuclear Magnetic Resonance (NMR) spectroscopy analysis of P4, P5, P6 and P7

^{1}H-NMR studies conducted at 100 °C in 1,1,2,2-tetrachloroethane-d_2 ($C_2D_2Cl_4$) on **P4** confirmed its assigned structure. The ^{1}H-NMR spectrum of **P4** is shown in **Figure 5.11**, it reveals in the aromatic region the proton of the carbazole hydrogen with multiplet signal at 8.23 ppm, 7.97 ppm and 7.69 ppm assigned to protons a, b and c respectively.

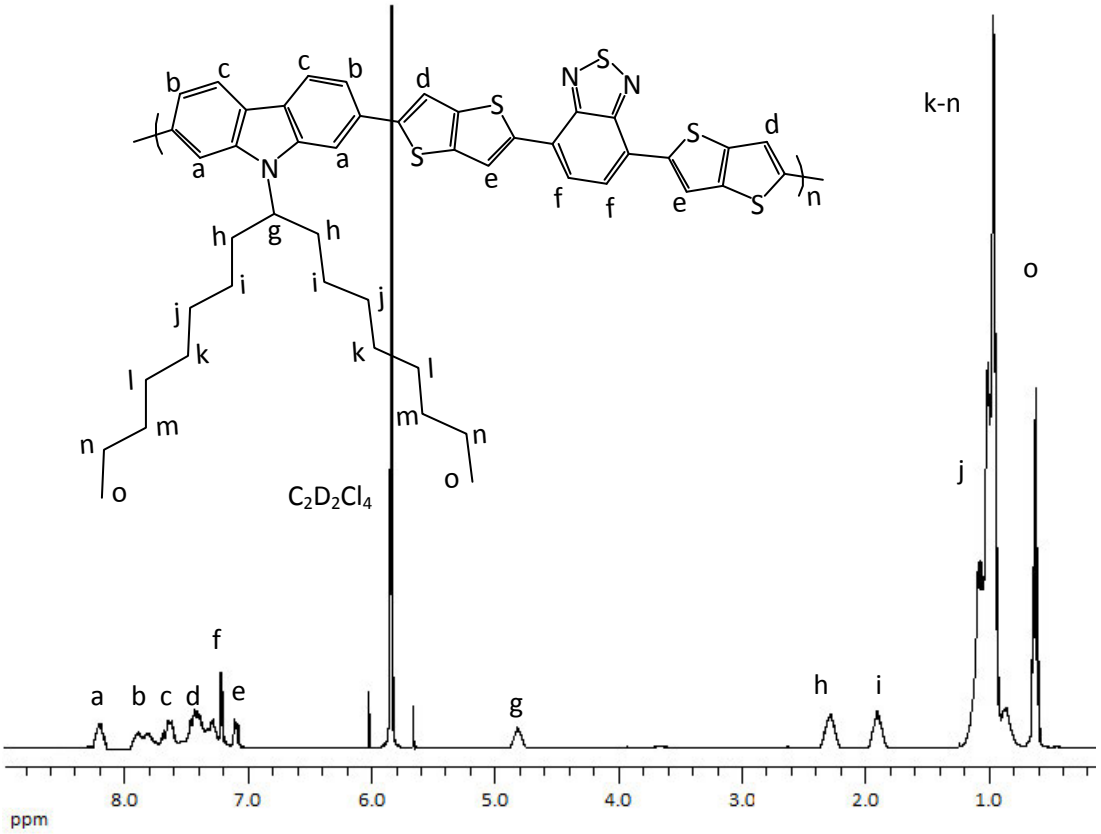

Figure 5.11: The ^{1}H-NMR spectra of **P4** in $C_2D_2Cl_4$ at 100 °C.

The two protons on the thienothiophene repeat units are observed at broad peak 7.42 ppm and 7.16 ppm assigned to protons d and e respectively. The broad peak at 4.81 ppm corresponds to the proton on the carbon atom at position g. Other peaks correspond to alkyl chains which are connected to carbazole units.

^{1}H-NMR studies conducted at 100 °C in 1,1,2,2-tetrachloroethane-d_2 on **P5** confirmed its assigned structure. The ^{1}H-NMR spectrum of **P5** is shown in **Figure 5.12**, it reveals in the aromatic region the proton of the carbazole hydrogen with multiplet signal at 8.43 ppm, and 7.77 ppm assigned to protons a and b respectively.

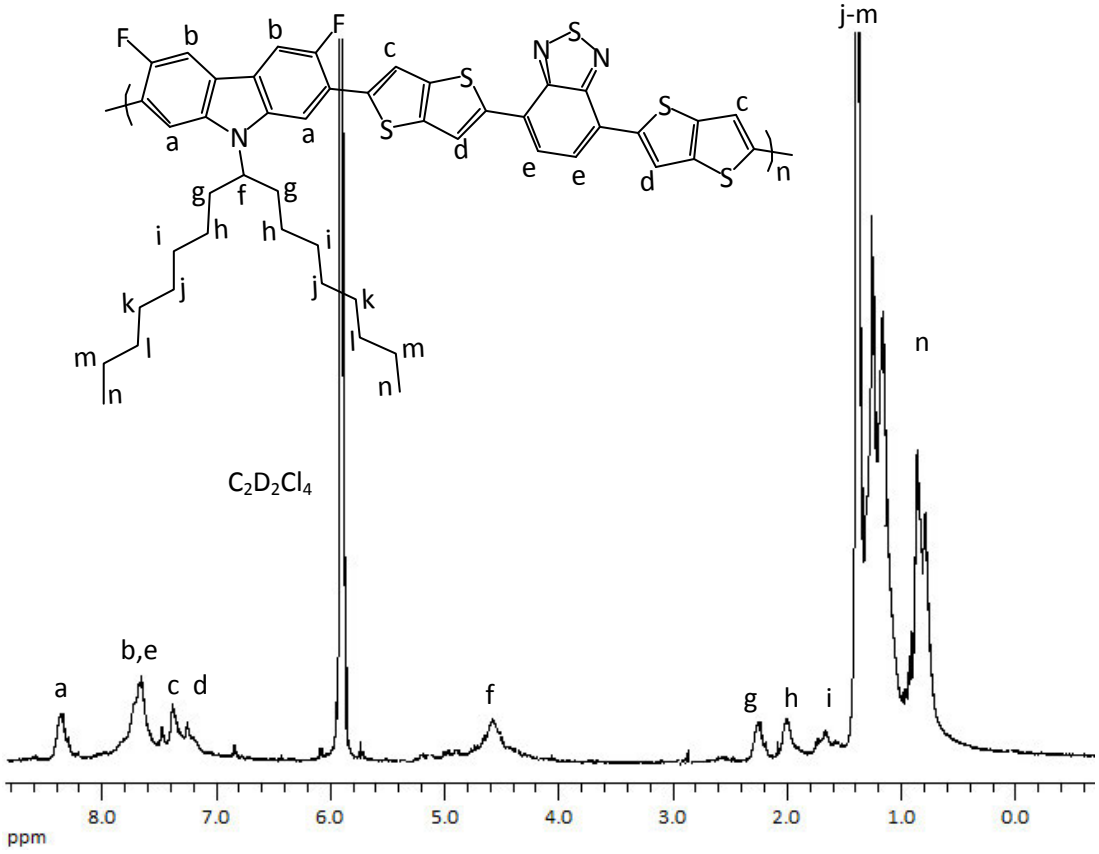

Figure 5.12: The ^{1}H-NMR spectra of **P5** in $C_2D_2Cl_4$ at 100 °C.

The peak at 7.77 ppm corresponds to the protons on the carbon atoms that are connected to the benzothiadiazole units and overlap with carbazole proton in position b. The two protons on the thienothiophene repeat units are observed at broad peak 7.41 ppm and 7.32 ppm assigned to protons c and d respectively. The broad peak at 4.52 ppm corresponds to the proton on the carbon atom at position f. Other peaks correspond to alkyl chains which are connected to carbazole units.

^{1}H-NMR studies conducted at 100 °C in 1,1,2,2-tetrachloroethane-d_2 on **P6** confirmed its assigned structure. The ^{1}H-NMR spectrum of **P6** is shown in **Figure 5.13**, it reveals in the aromatic region the proton of the carbazole hydrogen with multiplet signal at 8.44 ppm, 8.06 ppm and 7.77 ppm assigned to protons a, b and c respectively.

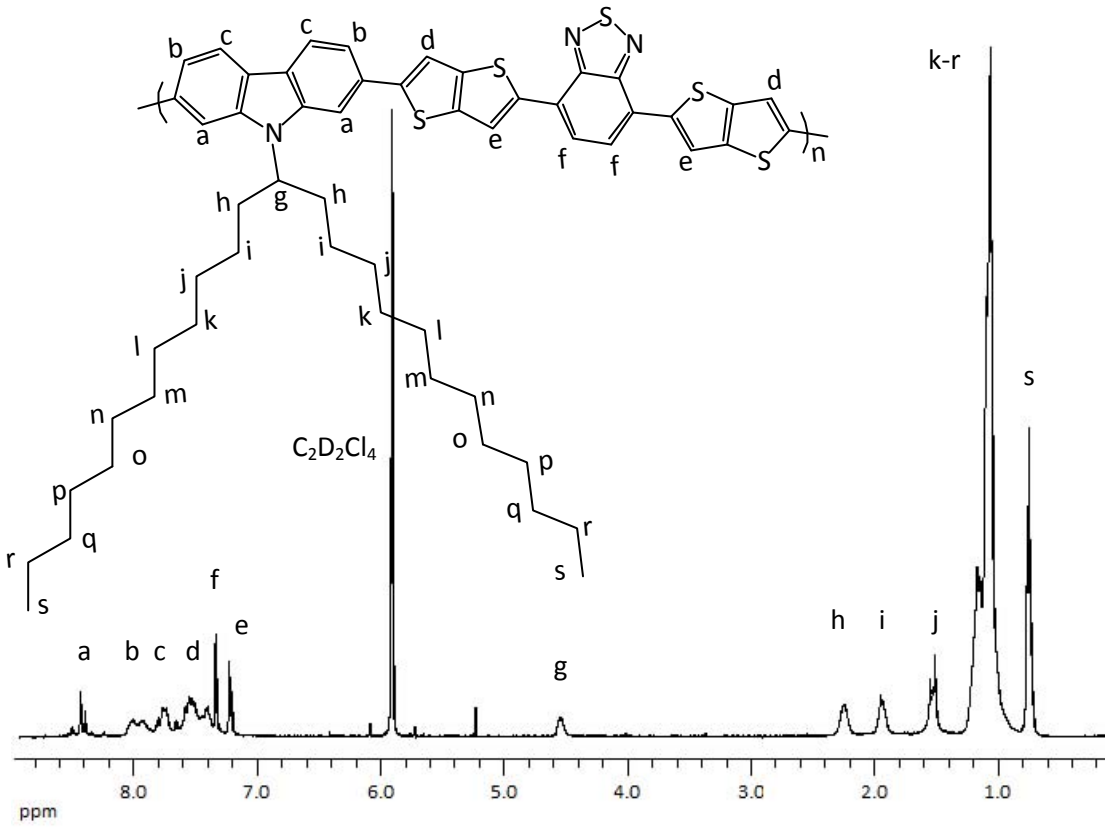

Figure 5.13: The ^{1}H-NMR spectra of **P6** in $C_2D_2Cl_4$ at 100 °C.

The peak at 7.35 ppm corresponds to the protons on the carbon atoms that are connected to the benzothiadiazole units in position f. The two protons on the thienothiophene repeat units are observed at broad peak 7.51 ppm and 7.21 ppm assigned to protons d and e respectively. The broad peak at 4.57 ppm corresponds to the proton on the carbon atom at position g. Other peaks correspond to alkyl chains which are connected to carbazole units.

^{1}H-NMR studies conducted at 100 °C in 1,1,2,2-tetrachloroethane-d_2 on **P7** confirmed its assigned structure. The ^{1}H-NMR spectrum of **P7** is shown in **Figure 5.14**, it reveals in the aromatic region the proton of the carbazole hydrogen with multiplet signal at 8.51 ppm and 7.91 ppm assigned to protons a and b respectively.

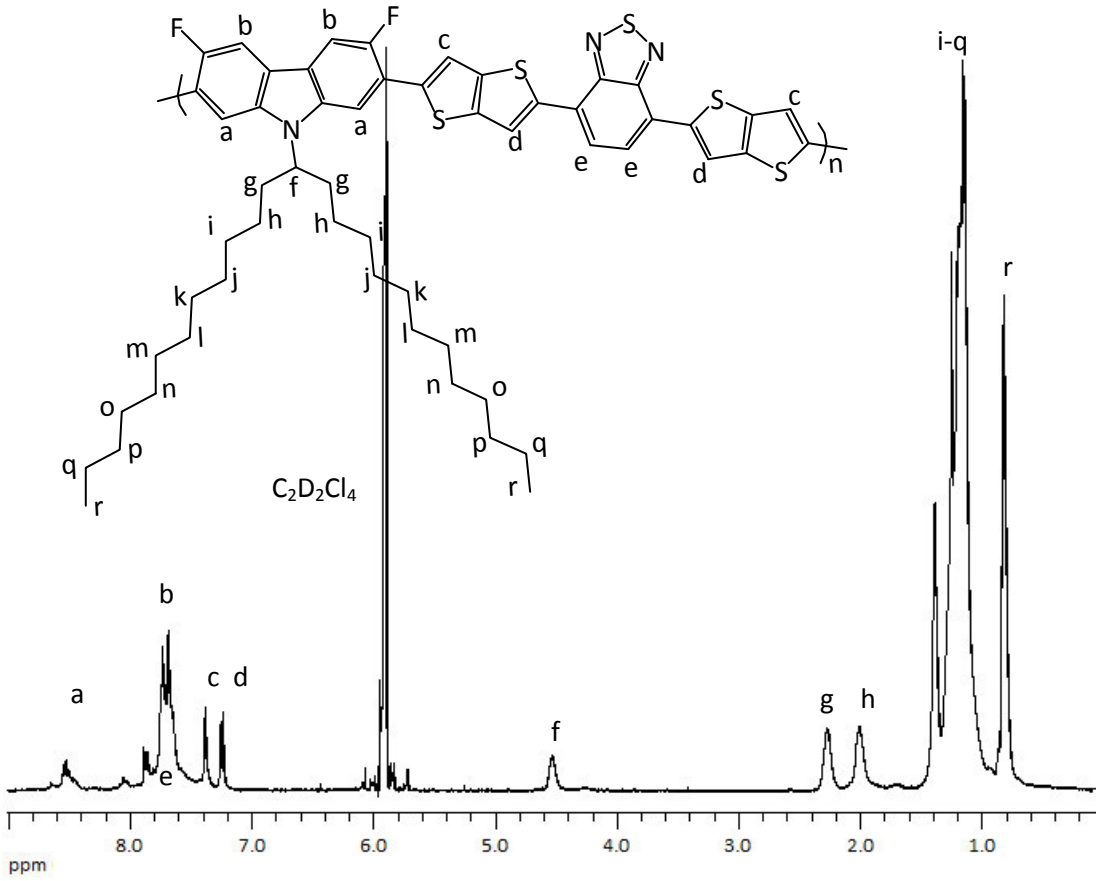

Figure 5.14: The proton NMR spectra of **P7** in $C_2D_2Cl_4$ at 100 °C.

The peak at 7.42 ppm corresponds to the protons on the carbon atoms that are connected to the benzothiadiazole units in position e. The two protons on the thienothiophene repeat units are observed at broad peak 7.37 ppm and 7.28 ppm assigned to protons c and d respectively. The broad peak at 4.57 ppm corresponds to the proton on the carbon atom at position g. Other peaks correspond to alkyl chains which are connected to carbazole units.

5.2.3 Infrared spectroscopy (FT-IR) analysis of P4, P5, P6 and P7

The IR spectrum of **P4** had similar patterns to those of its constituent monomers with some assignments of different bands/peaks. It can be seen the characterizing peak at 3082 cm^{-1} and 3013 cm^{-1} which falls in relation to aromatic benzene groups =C–H stretch. The characteristic peaks at 2930 cm^{-1}, 2920 cm^{-1} and 2849 cm^{-1} are assigned to the alkyl stretching frequencies of the methylene groups.

The characteristic overtones are seen from about 2159-1977 cm^{-1}. The assignment of different peaks compare to monomer **(37)** was observed at 1452 cm^{-1} and 1328 cm^{-1} and its has a mixture of peaks related to the combination bands and also the deformations bands of the aromatic –CH groups and methylene $–CH_2-$ groups.

The peak originally at 1037 cm^{-1}, attributed to $C_{aromatic}$-Br linkage in the spectrum of monomer **(34)** disappeared from the spectrum of **P4** due to the consumption of the corresponding functional groups in the direct arylation polymerisation reaction.

The IR spectrum of **P5** had similar patterns to those of its constituent monomers with some assignments of different bands/peaks. It can be seen the characterizing peak at 3081 cm^{-1} which falls in relation to aromatic benzene groups =C–H stretch. The characteristic peaks at 2950 cm^{-1}, 2919 cm^{-1} and 2849 cm^{-1} are assigned to the alkyl stretching frequencies of the methylene groups.

The characteristic overtones are seen from about 2155-1975 cm^{-1}. The assignment of different peaks compare to monomer **(39)** was observed at 1470 cm^{-1}, 1452 cm^{-1} and 1390 cm^{-1} and its has a mixture of peaks related to the combination bands and also the deformations bands of the aromatic –CH groups and methylene $–CH_2-$ groups. Peaks at 1230 cm^{-1} are characteristic to the C-N bond and a peak at 1174 cm^{-1} and 1108 cm^{-1} is assigned to the C-F bonds.

The peak originally at 1020 cm^{-1}, attributed to $C_{aromatic}$-Br linkage in the spectrum of monomer **(34)** disappeared from the spectrum of **P5** due to the consumption of the corresponding functional groups in the direct arylation polymerisation reaction.

The IR spectrum of **P6** had similar patterns to those of its constituent monomers with some assignments of different bands/peaks. It can be seen the characterizing peak at 3082 cm^{-1} which falls in relation to aromatic benzene groups =C–H stretch. The characteristic peaks at 2950 cm^{-1}, 2918 cm^{-1} and 2848 cm^{-1} are assigned to the alkyl stretching frequencies of the methylene groups.

The characteristic overtones are seen from about 2158-1969 cm^{-1}. The assignment of different peaks compare to monomer **(38)** was observed at 1454 cm^{-1} and 1431 cm^{-1} and its has a mixture of peaks related to the combination bands and also the deformations bands of the aromatic –CH groups and methylene $–CH_2-$ groups.

The peak originally at 1037 cm^{-1}, attributed to $C_{aromatic}$-Br linkage in the spectrum of monomer **(34)** disappeared from the spectrum of **P6** due to the consumption of the corresponding functional groups in the direct arylation polymerisation reaction.

The IR spectrum of **P7** had similar patterns to those of its constituent monomers with some assignments of different bands/peaks. It can be seen the characterizing peak at 3105 cm^{-1} and 3035 cm^{-1} which falls in relation to aromatic benzene groups =C–H stretch. The characteristic peaks at 2957 cm^{-1}, 2920 cm^{-1} and 2849 cm^{-1} are assigned to the alkyl stretching frequencies of the methylene groups.

The characteristic overtones are seen at 2155 cm^{-1}, 2033 cm^{-1} and 1973 cm^{-1}. The assignment of different peaks compare to monomer **(40)** was observed at 1494 cm^{-1}, 1472 cm^{-1} and 1457 cm^{-1} and its has a mixture of peaks related to the combination bands and also the deformations bands of the aromatic –CH groups and methylene $–CH_2-$ groups. Peaks at 1310 cm^{-1} are characteristic to the C-N bond and a peak at 1120 cm^{-1} and 1097 cm^{-1} is assigned to the C-F bonds.

The peak originally at 1020 cm^{-1}, attributed to $C_{aromatic}$-Br linkage in the spectrum of monomer **(34)** disappeared from the spectrum of **P7** due to the consumption of the corresponding functional groups in the direct arylation polymerisation reaction.

5.2.4 Gel Permeation Chromatography (GPC) analysis of P4, P5, P6 and P7

GPC results from the polymerization for polymers **P4, P5, P6** and **P7** by using polystyrene standards are shown in **Table 5.6**. The yields of the different fractions polymers from the Soxhlet extraction are also shown. Gel permeation chromatography measurements were taken in 1, 2, 4-trichloror'benzene (TCB) at 100 °C as at lower temperatures it was not possible to solubilise all the higher molecular weight polymers to obtain the true molecular weights.

Table 5.6: GPC data of **P4**, **P5**, **P6** and **P7**

Polymer	Soxhlet Fraction	Yield (%)	M_w	M_n	PDI
P4	Toluene	29	10600	6200	1.7
	Chloroform	45	30600	13200	2.3
P5	Toluene	41	13700	5200	2.6
	Chloroform	27	83400	34100	2.4
P6	Chloroform	87	25100	10000	2.5
P7	Toluene	38	11200	4600	2.4
	Chloroform	27	30600	13300	2.3

Polymer **P4** was obtained as red solid in a 74 % overall yield. GPC analysis of the fraction of polymer **P4** which was extracted by toluene gave an M_w = 10600 and M_n = 6200 with a polydispersity of 1.7. The chloroform fraction GPC analysis of the polymer **P4** gave the M_w = 30600 and M_n = 13200 with a polydispersity of 2.3.

Polymer **P5** was obtained as red solid in a 68 % overall yield. GPC analysis of the polymer **P5** which was extracted by toluene gave an M_w = 13700 and M_n = 5200 with a polydispersity of 2.6. The chloroform ($CHCl_3$) fraction GPC analysis of the polymer **P5** gave the M_w = 83400 and M_n = 34100 with a polydispersity of 2.4.

Polymer **P6** was obtained as a red solid in 87 % overall yield. GPC analysis of the polymer **P6** which was extracted by chloroform gave the M_w = 25100 and M_n = 10000 with a polydispersity of 2.5.

Polymer **P7** was obtained as a red solid in 65 % yield. GPC analysis of polymer **P7** which was extracted by toluene gave the M_w = 11200 and M_n = 4600 with a polydispersity of 2.4. The chloroform fraction GPC analysis of the polymer **P7** gave the M_w = 30600 and M_n = 13300 with a polydispersity of 2.3.

One of the main reason why different solubilizing groups were used in this series of polymers is to investigate whether the use of longer alkyl substituent in these polymers could where their solubility and hence allow them to be easily processed in making films in devices. The use of branched-$C_{17}H_{35}$ and $–C_{25}H_{51}$ groups was hence studied for polymers **P4-P7**.

An observation of the GPC results obtained from these different polymers does not clearly show or marked increase in the molecular weight of the polymers with longer alkyl chains **P4** *vs* **P6** and **P5** *vs* **P7**.

5.2.5 Elemental analysis of P4, P5, P6 and P7

Elemental analysis was used to check if a sample is consistent with a given molecular formula by using qualitative analysis technique. **Table 5.7** showed no bromine content, indicating that the terminal groups were end-capped with during the polymerization of the **P4** and **P5**.

Table 5.7: Elemental analysis data of **P4 - P7.**

Polymers	Formula Weight	Molecule Weight		Elemental analysis (%)			
				C	H	N	Br
P4	$(C_{47}H_{47}N_3S_5)_n$	$(814.21)_n$	Calculated	69.33	5.82	5.16	0
			Found	72.03	7.88	8.03	0
P5	$(C_{47}H_{47}F_2N_3S_5)_n$	$(850.19)_n$	Calculated	66.40	5.33	4.94	0
			Found	73.02	7.77	6.65	0
P6	$(C_{55}H_{63}N_3S_5)_n$	$(926.43)_n$	Calculated	71.30	6.85	4.54	0
			Found	77.11	8.75	6.22	0
P7	$(C_{55}H_{63}F_2N_3S_5)_n$	$(962.41)_n$	Calculated	68.64	6.39	4.37	0
			Found	71.87	9.03	7.00	0

* n = repeating unit

The elemental analysis of the other elements of polymers **P4** - **P7** did give some differences between the calculated percentages of carbon, hydrogen and nitrogen and those found experimentally. This could be explained by problems in the combustions sample during analysis and formation of elements as is often seen for some conjugated polymers.

5.2.6 UV-Visible absorption spectroscopy (UV-Vis) analysis of P4, P5, P6 and P7

The UV-Vis absorption spectra of the polymers were measured in chloroform and in solid state as thin films. UV-Vis analysis of **P4** in **Figure 5.15** shows two absorption band at $\lambda_{max\ 1}$ = 386 nm and $\lambda_{max\ 2}$ = 509 nm in chloroform solution, and at $\lambda_{max\ 1}$ = 404 nm and $\lambda_{max\ 2}$ = 534 nm in solid state.

The optical band gap of polymer **P4** as determined from the onset of its absorption spectra in the solid state has a value E_g = 1.95 eV.

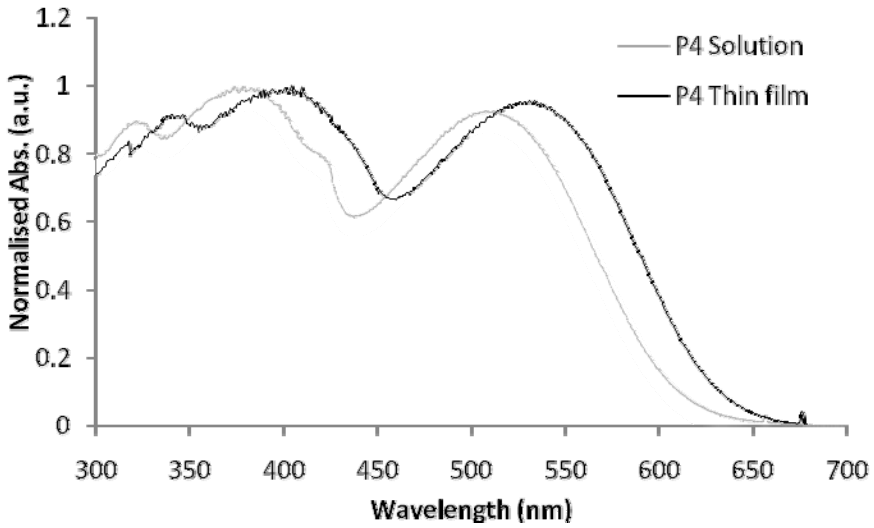

Figure 5.15: Normalised UV-Vis spectra of **P4** in chloroform (grey line) and a thin film (black line).

The UV-Vis absorption spectra of the polymer were measured in chloroform and in solid state as thin films. UV-Vis analysis of **P5** in **Figure 5.16** shows two absorption band at $\lambda_{max\ 1}$ = 404 nm and $\lambda_{max\ 2}$ = 537 nm in chloroform solution, and at $\lambda_{max\ 1}$ = 418 nm and $\lambda_{max\ 2}$ = 550 nm in solid state.

The optical band gap of polymer **P5** as determined from the onset of its absorption spectra in the solid state has a value E_g = 1.92 eV.

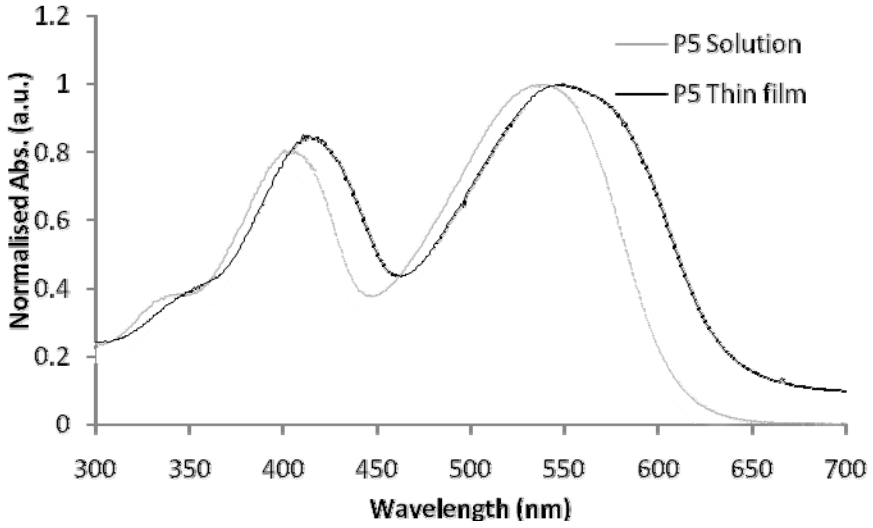

Figure 5.16: Normalised UV-Vis spectra of **P5** in chloroform (grey line) and a thin film (black line).

The UV-Vis absorption spectra of the polymer were measured in chloroform and in solid state as thin films. UV-Vis analysis of **P6** in **Figure 5.17** shows two absorption band at $\lambda_{max\ 1}$ = 393 nm and $\lambda_{max\ 2}$ = 519 nm in chloroform solution, and at $\lambda_{max\ 1}$ = 397 nm and $\lambda_{max\ 2}$ = 534 nm in solid state. The optical band gap of polymer **P6** as determined from the onset of its absorption spectra in the solid state has a value E_g = 1.86 eV.

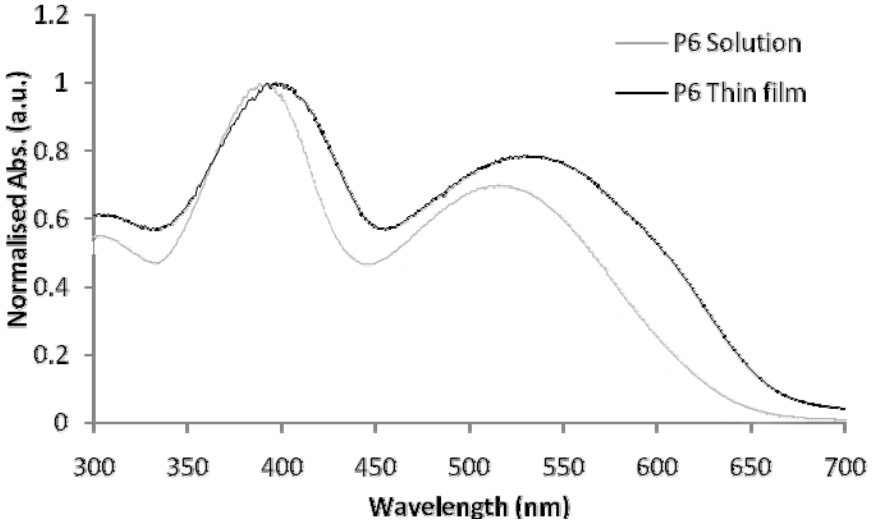

Figure 5.17: Normalised UV-Vis spectra of **P6** in chloroform (grey line) and a thin film (black line).

The UV-Vis absorption spectra of the polymer were measured in chloroform and in solid state as thin films. UV-Vis analysis of **P7** in **Figure 5.18** shows two absorption band at $\lambda_{max\ 1}$ = 400 nm and $\lambda_{max\ 2}$ = 519 nm in chloroform solution, and at $\lambda_{max\ 1}$ = 407 nm and $\lambda_{max\ 2}$ = 552 nm in solid state.

This slight red shift in the solid state for the same polymer was again observed in all polymers and this is because of the structure of polymers in solid state is more planar, thus more conjugation and lower band gap. Therefore, all calculations and comparisons will be based on the solid state results.

The optical band gaps were calculated from the onset of absorption of the polymers in the solid state The optical band gap of polymer **P7** as determined from the onset of its absorption spectra in the solid state has a value E_g = 1.85 eV.

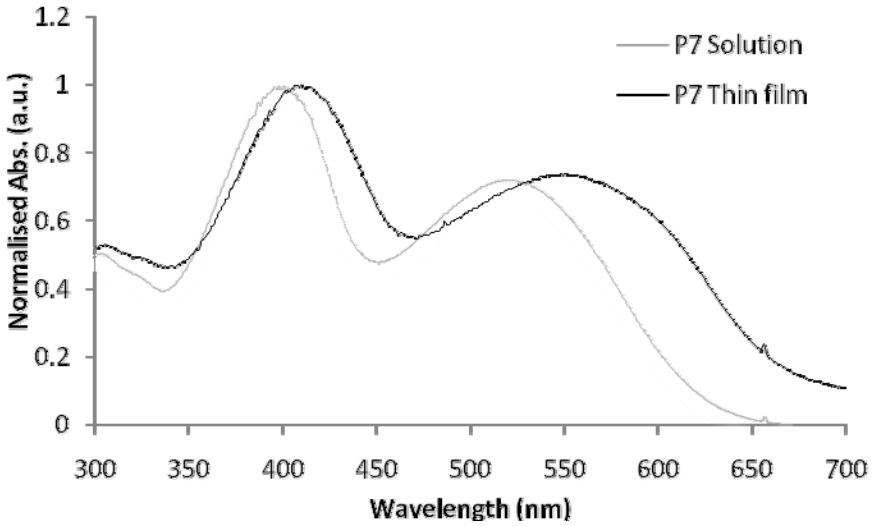

Figure 5.18: Normalised UV-Vis spectra of **P7** in chloroform (grey line) and a thin film (black line).

Table 5.8 below shown the optical band gap for the polymers **P4, P5, P6** and **P7.** All the polymers have two λ_{max} in chloroform solution and solid state form.

Table 5.8: UV-Vis data of **P4, P5, P6** and **P7.**

Polymers	λ_{max} Solution (nm)		λ_{max} Thin film (nm)		λ Onset Abs. (nm)	E_g Optical (eV)
	1	2	1	2		
P4	386	509	404	534	635	1.95
P5	404	537	418	550	645	1.92
P6	393	519	397	534	665	1.86
P7	400	519	407	552	670	1.85

Analysis of the absorption spectrum of all polymers indicate a little difference in the electronic delocalisation of polymers upon changing the length and size of their alkyl-substituents. The absorption maximum of **P4** *vs* **P6** are comparable (534 nm in films for both **P4** and **P6**) and (550 nm *vs* 552 nm in films for **P5** and **P7**, respectively). This is an expected result as the alkyl-substituents placement along the polymer chains does not interfere with their polarity.

The effect of fluorine substitution at the 3, 6-positions of carbazole repeat units has however an effect on the electronic delocalisation.

Polymer **P5** which has fluorine-substituents at the 3,6-positions of its carbazole repeat unit is more conjugated than the equivalent polymer **P4** (λ_{max} = 550 nm for **P5** vs λ_{max} = 534 nm for P4).

The some case when comparing the absorption maximum in films of **P6** vs **P7,** where the polymer with fluorine substituents has or more extended electronic delocalisation. These results point to the presence of interactions between the fluorine substituents on carbazole repeat units on P5 and P7 and either the sulphur or hydrogens of the adjacent thienothiophene repeat units along the polymer chains.

5.2.7 Cyclic Voltammetry (CV) analysis of P4, P5, P6 and P7

Investigations of the electrochemical properties of polymers **P4** and **P5** were also undertaken in cyclic voltammetry (CV) performed on drop-cast polymer films in acetonitrile with tetrabutylammonium perchlorate as the electrolyte. The LUMO level and the HOMO level were calculated from the onset reduction and oxidation respectively.

Then, the electrochemical band gap (E_g) can be calculated from the difference between them. The cyclic voltammogram of the polymers **P4** and **P5** are shown in **Figure 5.19** and **Table 5.9**.

Polymer **P4** exhibits an oxidation wave at E_{pa} = 1.09 V and a reduction wave at E_{pa} = -1.52 V, and their associated reduction and oxidation waves at E_{pc} = 0.72 V and E_{pc} = -1.74 V, respectively.

From the onset of oxidation (0.72 V) and the onset of reduction (-1.66 V), the HOMO level is at -5.52 eV and the LUMO level is at -3.14 eV for the polymer backbone (on the basis that ferrocene/ferrocenium has an IP of 4.8 eV below the vacuum level and the oxidation occurs at 0.082 V relative to Ag/Ag^+), therefore the electrochemical band gap of the polymer is 2.38 eV.

Polymer **P5** exhibits an oxidation wave at E_{pa} = 0.99 V and a reduction wave at E_{pa} = -1.60V, and their associated reduction and oxidation waves at E_{pc} = 0.68 V and E_{pc} = -1.78 V, respectively.

From the onset of oxidation (0.60 V) and the onset of reduction (-1.50 V), the HOMO level is at -5.40 eV and the LUMO level is at -3.30 eV for the polymer backbone (on the basis that ferrocene/ferrocenium has an IP of 4.8 eV below the vacuum level and the oxidation occurs at 0.082 V relative to Ag/Ag^+), therefore the electrochemical band gap of the polymer is 2.10 eV.

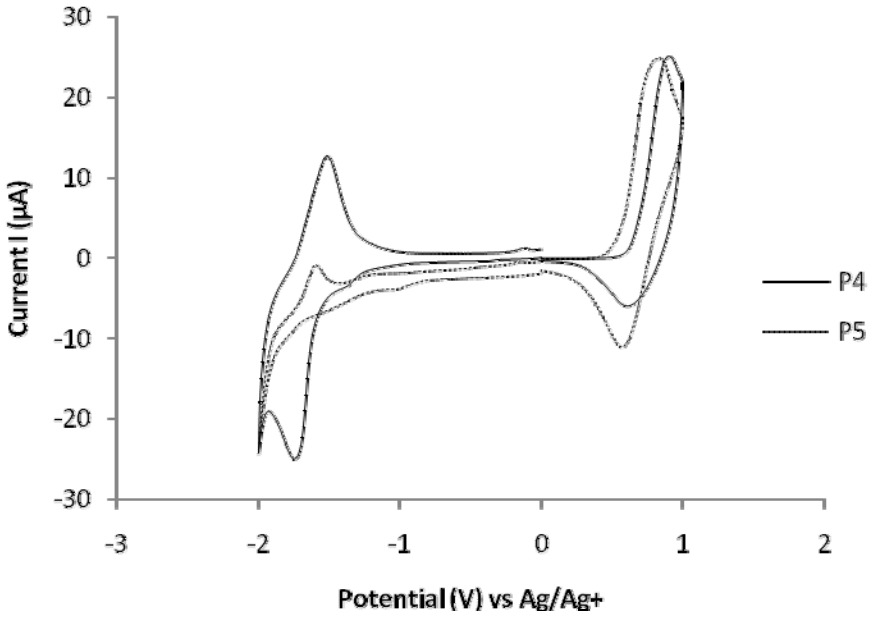

Figure 5.19: Normalised cyclic voltammogram of **P4** and **P5**.

Table 5.9: Voltammetry results and band gaps of **P4** and **P5.**

Polymers	*E*onset, $_{ox}$ (V)[a)]	*E*onset, $_{red}$ (V) [a)]	HOMO (eV)	LUMO (eV)	Band gap (eV)
P4	0.72	-1.66	-5.52	-3.14	2.38
P5	0.60	-1.50	-5.40	-3.30	2.10

[a)] *vs*. Ag/Ag^+

Investigations of the electrochemical properties of polymers **P6** and **P7** were also undertaken in cyclic voltammetry (CV) performed on drop-cast polymer films in acetonitrile with tetrabutylammonium perchlorate as the electrolyte. The LUMO level and the HOMO level were calculated from the onset reduction and oxidation respectively. Then, the electrochemical band gap (E_g) can be calculated from the difference between them. The cyclic voltammogram of the polymers **P6** and **P7** are shown in **Figure 5. 20** and **Table 5.10**.

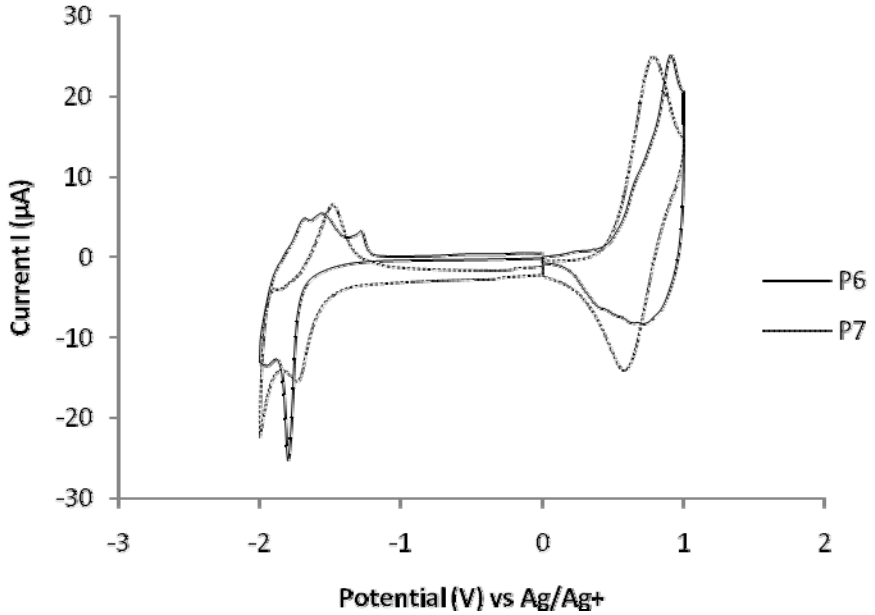

Figure 5.20: Normalised cyclic voltammogram of **P6** and **P7**.

Polymer **P6** exhibits an oxidation wave at E_{pa} = 0.90 V and a reduction wave at E_{pa} = -1.29 V, and their associated reduction and oxidation waves at E_{pc} = 0.69 V and E_{pc} = -1.79 V, respectively. From the onset of oxidation (0.39 V) and the onset of reduction (-1.80 V), the HOMO level is at -5.19 eV and the LUMO level is at -3.00 eV for the polymer backbone (on the basis that ferrocene/ferrocenium has an IP of 4.8 eV below the vacuum level and the oxidation occurs at 0.082 V relative to Ag/Ag^+), therefore the electrochemical band gap of the polymer is 2.19 eV.

Polymer **P7** exhibits an oxidation wave at E_{pa} = 0.92 V and a reduction wave at E_{pa} = -1.48 V, and their associated reduction and oxidation waves at E_{pc} = 0.67 V and E_{pc} = -1.72 V, respectively. From the onset of oxidation (0.52 V) and the onset of reduction (-1.62 V), the HOMO level is at -5.32 eV and the LUMO level is at -3.18 eV for the polymer backbone (on the basis that ferrocene/ferrocenium has an IP of 4.8 eV below the vacuum level and the oxidation occurs at 0.082 V relative to Ag/Ag^+), therefore the electrochemical band gap of the polymer is 2.14 eV.

Table 5.10: Voltammetry results and band gaps of **P6** and **P7.**

Polymers	*E*onset, $_{ox}$ (V)[a)]	*E*onset, $_{red}$ (V) [a)]	HOMO (eV)	LUMO (eV)	Band gap (eV)
P6	0.39	-1.80	-5.19	-3.00	2.19
P7	0.52	-1.62	-5.32	-3.18	2.14

[a)] *vs*. Ag/Ag^{+}

5.2.8 Thermogravimetric Analysis (TGA) of P4, P5, P6 and P7

The thermal stability of **P4** and **P5** were investigated in this study. The thermogram of **P4** and **P5** is shown in **Figure 5.21** and the details of the TGA results are shown in **Table 5.12**.

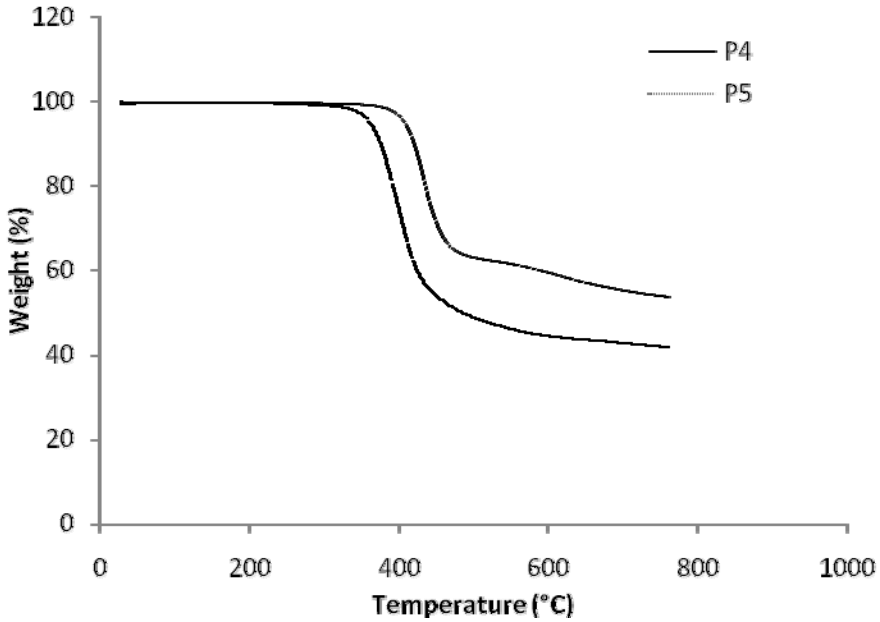

Figure 5.21: The TGA thermogram of **P4** and **P5**.

Figure 5.22 shows the TGA curves for of the thermal degradation of the polymer **P4**, the onset of the degradation occurs at 323 °C, the onset of second degradation is 433 °C with a weight loss of 46.1 %. The percentage of residual weight 28.9 % is consistent with percentage weight and polymer backbone.

Thermal gravimetry analysis measurements revealed the remarkable stability of the polymer up to 433 °C, which indicated that these polymers are thermally very stable. The subsequent degradation and weight loss of the polymer beyond 433 °C was proportional to the mass of its a alkyl-group substituents. The polymer did not show any further weight loss up to a temperature of 800 °C.

Figure 5.22 shows the TGA curves for of the thermal degradation of the polymer **P5**, the onset of the degradation occurs at 345 °C, the onset of second degradation is 452 °C with a weight **loss of 72.9 %. The** percentage of residual **weight 27.1 % is** consistent with percentage weight and polymer backbone. Thermal gravimetry analysis measurements revealed the remarkable stability of the polymer up to 452 °C, which indicated that these polymers are thermally very stable. The subsequent degradation and weight loss of the polymer beyond 452 °C was proportional to the mass of its a alkyl-group substituents. The polymer did not show any further weight loss up to a temperature of 800 °C.

The thermal stability of **P6** and **P7** were investigated in this study. The thermogram of **P6** and **P7** is shown in **Figure 5.22** and the details of the TGA results are shown in **Table 5.11**.

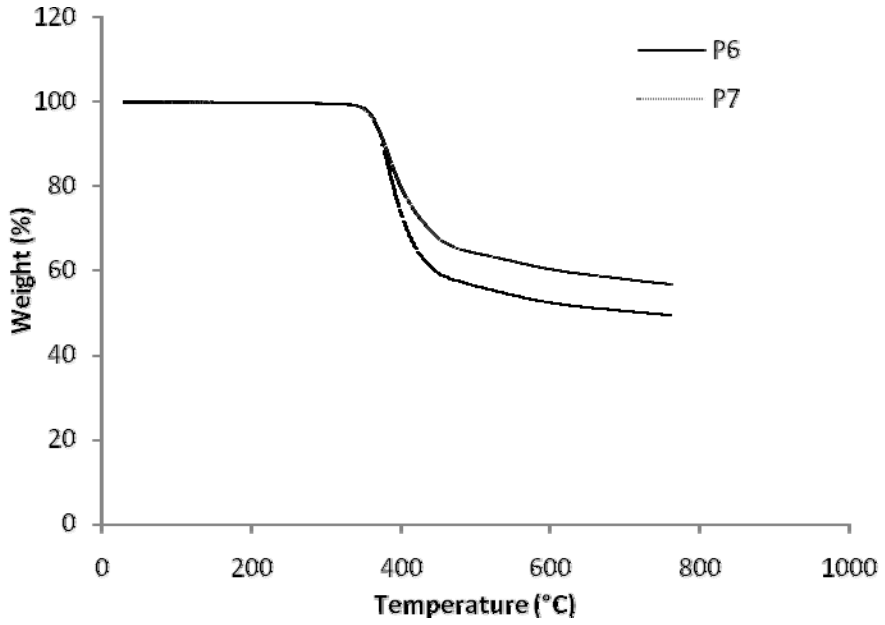

Figure 5.22: The TGA thermogram of **P6** and **P7**.

Figure 5.22 shows the TGA curves for of the thermal degradation of the polymer **P6**, the onset of the degradation occurs at 355 °C, the onset of second degradation is 443 °C with a

weight loss of **72.6 %.** The percentage of residual weight **27.4 %** is consistent with percentage weight and polymer backbone. Thermal gravimetry analysis measurements revealed the remarkable stability of the polymer up to 443 °C, which indicated that these polymers are thermally very stable. The subsequent degradation and weight loss of the polymer beyond 443 °C was proportional to the mass of its a alkyl-group substituents. The polymer did not show any further weight loss up to a temperature of 800 °C.

Figure 5.22 shows the TGA curves for of the thermal degradation of the polymer **P7**, the onset of the degradation occurs at 342 °C, the onset of second degradation is 438 °C with a weight loss **of 69.1 %.** The percentage of residual weight **30.9 %** is consistent with percentage weight and polymer backbone. Thermal gravimetry analysis measurements revealed the remarkable stability of the polymer up to 438 °C, which indicated that these polymers are thermally very stable. The subsequent degradation and weight loss of the polymer beyond 438 °C was proportional to the mass of its a alkyl-group substituents. The polymer did not show any further weight loss up to a temperature of 800 °C.

5.2.9 Differential Scanning Calorimetry (DSC) analysis of P4, P5, P6 and P7

Table 5.12 summarises the results from the thermo gravimetric analysis (TGA) and the differential scanning calorimetry (DSC). In applications that can experience temperature extremes, it is important to know what will happen when these polymers are exposed to variants in temperature and how they will affect the mechanical behaviour of the polymer.

Table 5.11: The TGA and DSC data of **P4, P5, P6** and **P7**.

Polymers	TG Analysis			DSC Analysis
	Onset degradation temp. / °C		Weight loss at 800 °C (wt. %)	T_g / °C
	1st degradation	2nd degradation		
P4	323	433	71.1	64
P5	345	452	72.9	67
P6	355	443	72.6	66
P7	342	438	69.1	68

The glass transition (T_g) is obtained from the DSC trace and it is a function of polymer backbone flexibility. The polymers were subjected to a first heating run, cooling run followed by further heating run, at the scan rate 10 °C/ min, and when no T_g was seen, 20 up to 100 °C/ min rates was applied. The glass transitions (T_g) value were estimated and obtained from the first scans as broad peaks, they were above 50 °C indicating that all polymers have good tolerance to the stages required in making devices.

Based on the table the T_g of **P4, P5, P6** and **P7** were 64 °C, 67 °C, 66 °C and 68 °C, respectively. All the T_g results of the polymers are similar to each other, due to the present of thienothiophene-benzothiadiazole substituents, which provide more flexibility for the polymer backbones.

5.3 Thienothiophene-bis(octyloxy) substituted benzothiadiazole-based Copolymer: P8, P9 and P10

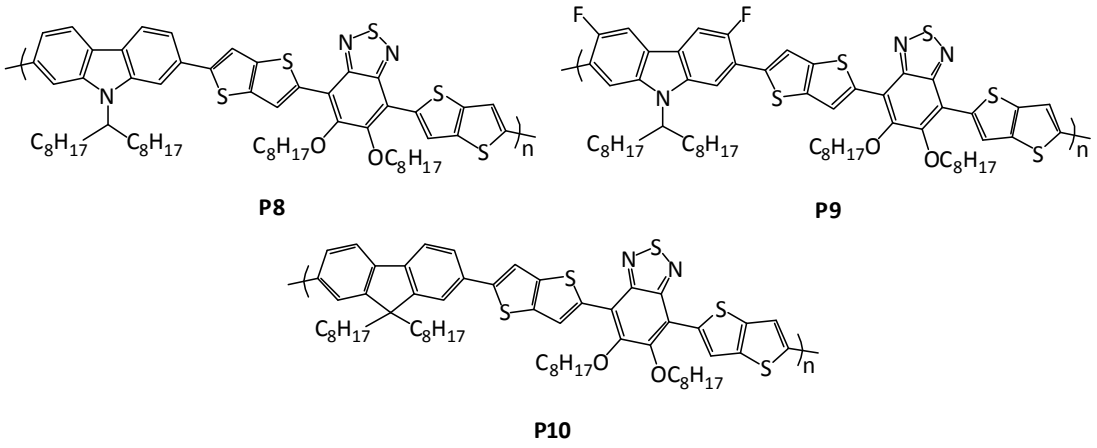

Figure 5.23: Structures of copolymers **P8**, **P9** and **P10**.

5.3.1 Synthesis of P8, P9 and P10

Figure 5.23 shows a series of copolymer, two of them are carbazole based poly(9-(heptadecan-9-yl)-*9H*-carbazole-*alt*-5,6-bis(octyloxy)-4,7-di(thieno[3,2-*b*]thiophen-2-yl)benzo[*c*][1,2,5]thiadiazole) **(P8)** and poly(3,6-difluoro-9-(heptadecan-9-yl)-*9H*-carbazole-*alt*-5,6-bis(octyloxy)-4,7-di(thieno[3,2-*b*]thiophen-2-yl)benzo[c][1,2,5]thiadiazole) **(P9),** and one is fluorine based poly(9,9-dioctyl-*9H*-fluorene-*alt*-5,6-bis(octyloxy)-4,7-di(thieno[3,2-*b*]thiophen-2-yl)benzo[*c*][1,2,5]thiadiazole) **(P10)**.

Polymers **P8-P10** were prepared using Suzuki cross-coupling polymerization as shown in the **Scheme 5.3** below.

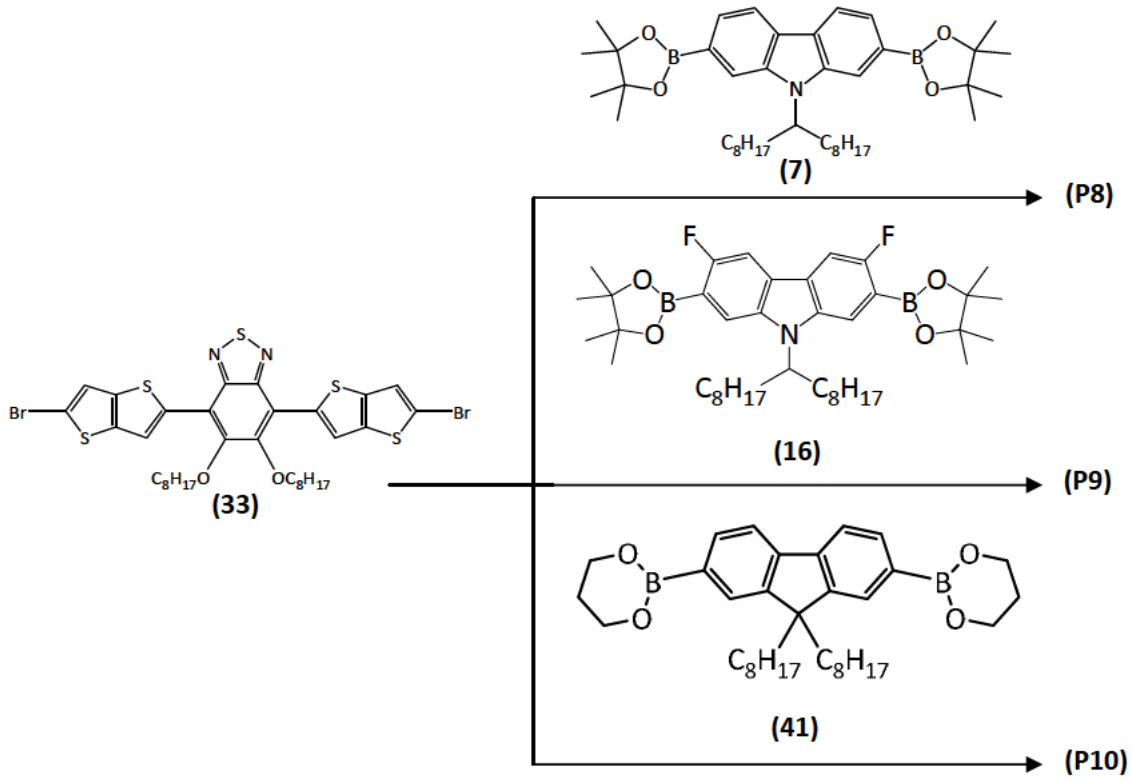

Scheme 5.3: Synthesis route to **P8-P10**.

All of them contain the same thienothiophene-bisoctyloxy substituted benzothiadiazole-based repeat units. All synthesis of copolymers were performed using a modified procedure by Iraqi *et al.*[103] These polymers were chosen due to similarities in their composition with polymers made previously by the Iraqi group, and also in the literature.[82, 83, 86, 189]

These copolymers were synthesized using Suzuki cross coupling reactions, in presence of $Pd(OAc)_2$ and tri(o-tolyl)phosphine (1:2) as catalysts. A proposed mechanism for the polymerization is shown in **Scheme 5.4**. The first step involves an oxidative addition of palladium (0) to the aryl bromide to form a palladium (II). The second step involves reaction with the base to produce an intermediate complex, which in the third step forms the organopalladium via transmetallation with the boronic ester in the second monomer. Finally, the polymer is obtained by reductive elimination, which restores the original palladium (0) and then the catalytic cycle starts again.

The polymerizations of **P8, P9** and **P10** were performed in different conditions, either in THF as solvent and $NaHCO_3$ as base, or in toluene solvent and tetraethylammonium hydroxide as base, due to the high boiling point of toluene, the average molecular weight of the polymers obtained from these polymerizations was higher than these using THF.

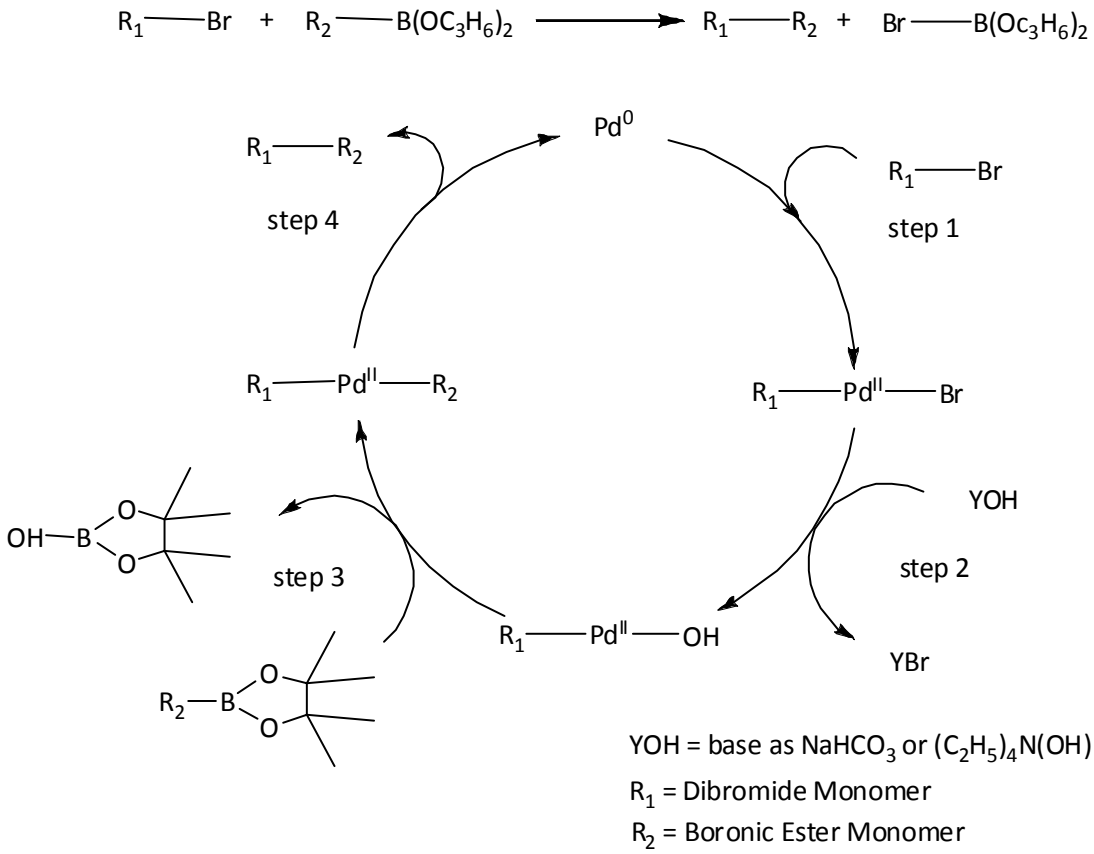

Scheme 5.4: The catalytic cycle of Suzuki cross coupling reaction for polymerization of polymers **P8, P9** and **P10**.

All polymerization were performed under argon and in degassed systems, and they stopped when the solutions became viscous. Then another portion of solvent was added to solubilise the formed polymers, and then the end-capping reagents (bromobenzene and phenyl boronic acid) could be added to the polymer solutions to increase the stability of the polymer in device operation and to remove bromine and boronic ester end groups from the polymer. Then the polymer solutions were stirred with ammonia to remove catalyst remnants and other impurities.

To remove palladium impurities, oligomers and unreacted monomers, all the crude polymers were purified by using several methods. After washing the polymers solutions with water to remove the ammonia and then concertrating the solutions to approximately 50 ml, the polymers were precipitated in methanol to remove end-capping reagents, organic palladium species and unreacted comonomers.

The obtained crude polymers were then collected through filtration on micropore membranes then transferred to fiber glass thimbles and cleaned with different solvents using a Soxhlet apparatus.

The first solvent was methanol to remove the palladium residues from the copolymer, followed by acetone and hexane, to clean off the low molecular weight oligomers.

Then the purified polymers were extracted with toluene, chloroform and chlorobenzene and the solutions precipitated separately in methanol to obtain the different fractions of polymers as dark purple powders. The elemental analysis of all fractions did not show any traces of bromine and they gave satisfactory results.

5.3.2 Nuclear Magnetic Resonance (NMR) spectroscopy analysis of P8, P9 and P10

^{1}H-NMR studies conducted at 100 °C in 1,1,2,2-tetrachloroethane-d_2 ($C_2D_2Cl_4$) on **P8** confirmed its assigned structure. The ^{1}H-NMR spectrum of **P8** is shown in **Figure 5.24**, it reveals in the aromatic region the protons of the carbazole hydrogen with multiplet signal at 8.76 ppm, 8.16 ppm and 7.82 ppm assigned to protons a, b and c respectively.

The two protons on the thienothiophene repeat units are observed at broad peak 7.61 ppm and 7.58 ppm assigned to protons d and e respectively. The broad peak at 4.71 ppm corresponds to the proton on the carbon atom at position f. The peak at 4.25 ppm corresponds to the protons on the carbon atoms that are connected to the oxygen atoms in the octyloxy chains (position g). Other peaks correspond to alkyl chains which are connected to carbazole and benzothiadiazole units.

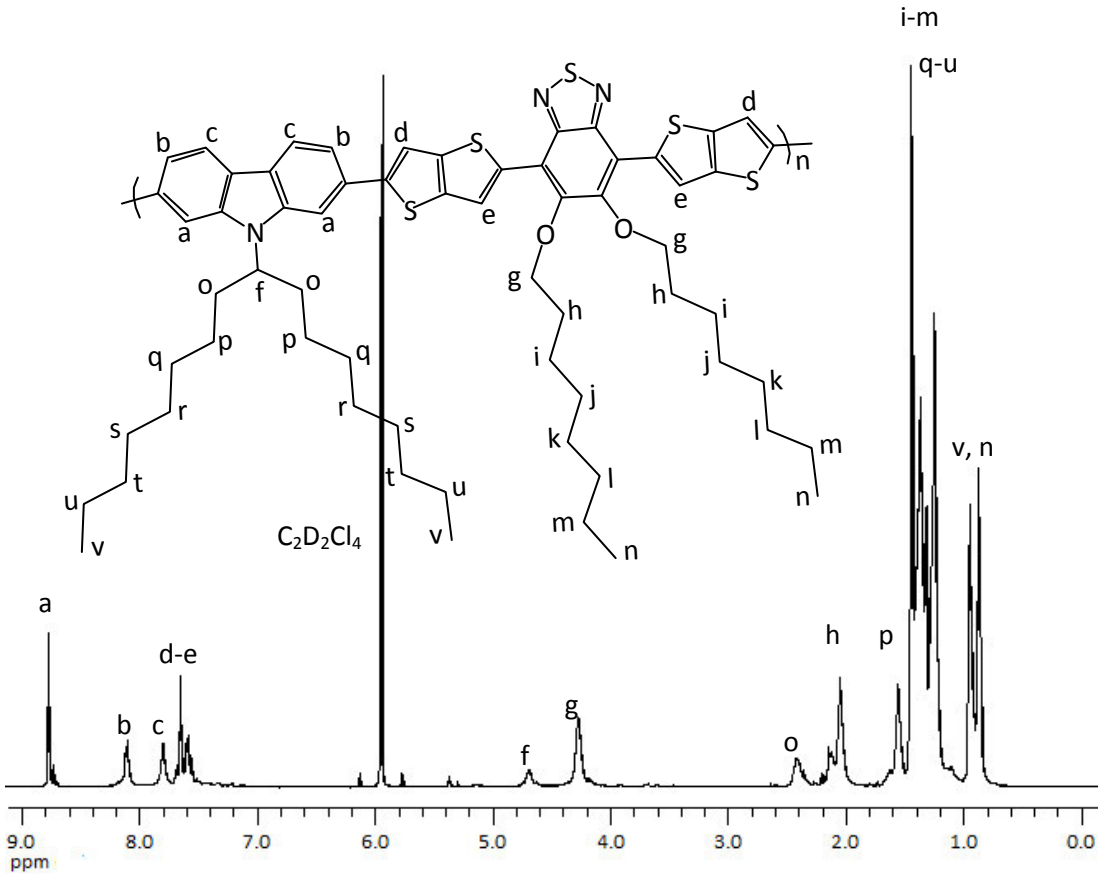

Figure 5.24: The proton NMR spectra of **P8** in $C_2D_2Cl_4$ at 100 °C.

^{1}H-NMR studies conducted at 100 °C in 1,1,2,2-tetrachloroethane-d_2 on **P9** confirmed its assigned structure. The ^{1}H-NMR spectrum of **P9** is shown in **Figure 5.25**, it reveals in the aromatic region the proton of the carbazole hydrogen with multiplet signal at 8.76 ppm, and 8.62 ppm assigned to protons a and b respectively.

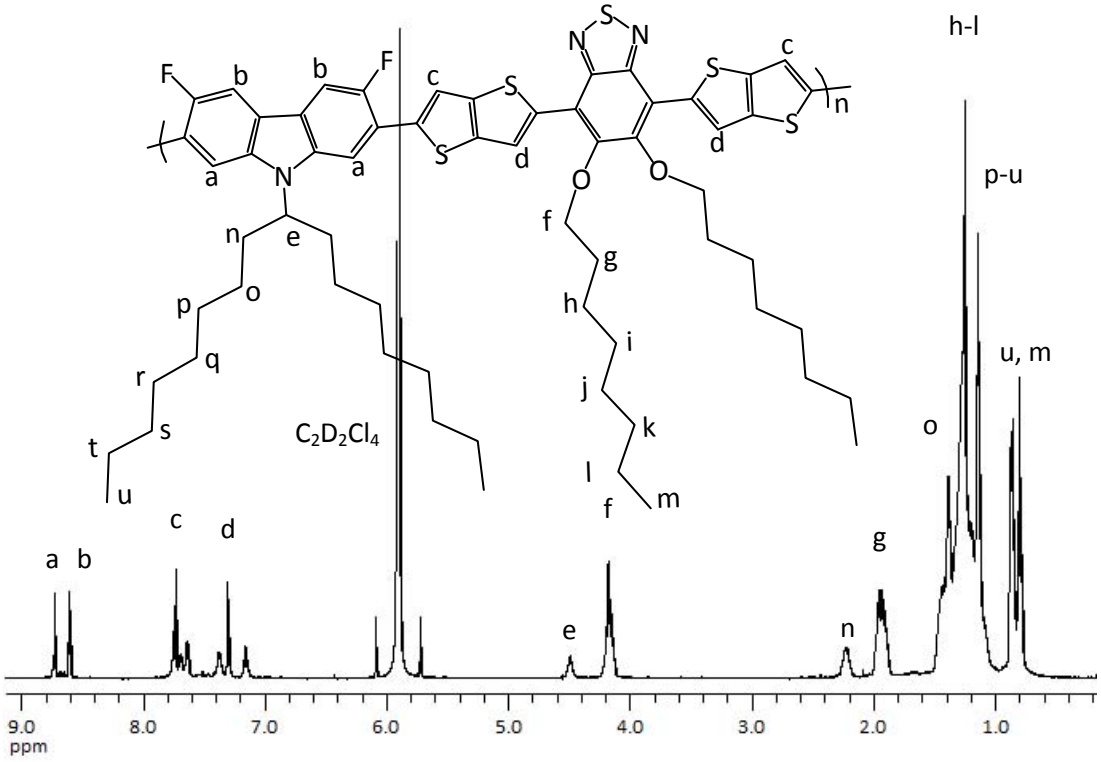

Figure 5.25: The proton NMR spectra of **P9** in $C_2D_2Cl_4$ at 100 °C.

The two protons on the thienothiophene repeat units are observed at broad peak 7.73 ppm and 7.33 ppm assigned to protons d and e respectively. The broad peak at 4.56 ppm corresponds to the proton on the carbon atom at position e. The peak at 4.18 ppm corresponds to the protons on the carbon atoms that are connected to the oxygen atoms in the octyloxy chains (position f). Other peaks correspond to alkyl chains which are connected to carbazole and benzothiadiazole units.

^{1}H-NMR studies conducted at 100 °C in 1,1,2,2-tetrachloroethane-d_2 on **P10** confirmed its assigned structure. The ^{1}H-NMR spectrum of **P10** is shown in **Figure 5.26**, it reveals in the aromatic region the proton of the fluorene hydrogen with multiplet signal at 8.78 ppm, and 7.77 ppm assigned to protons a and b respectively.

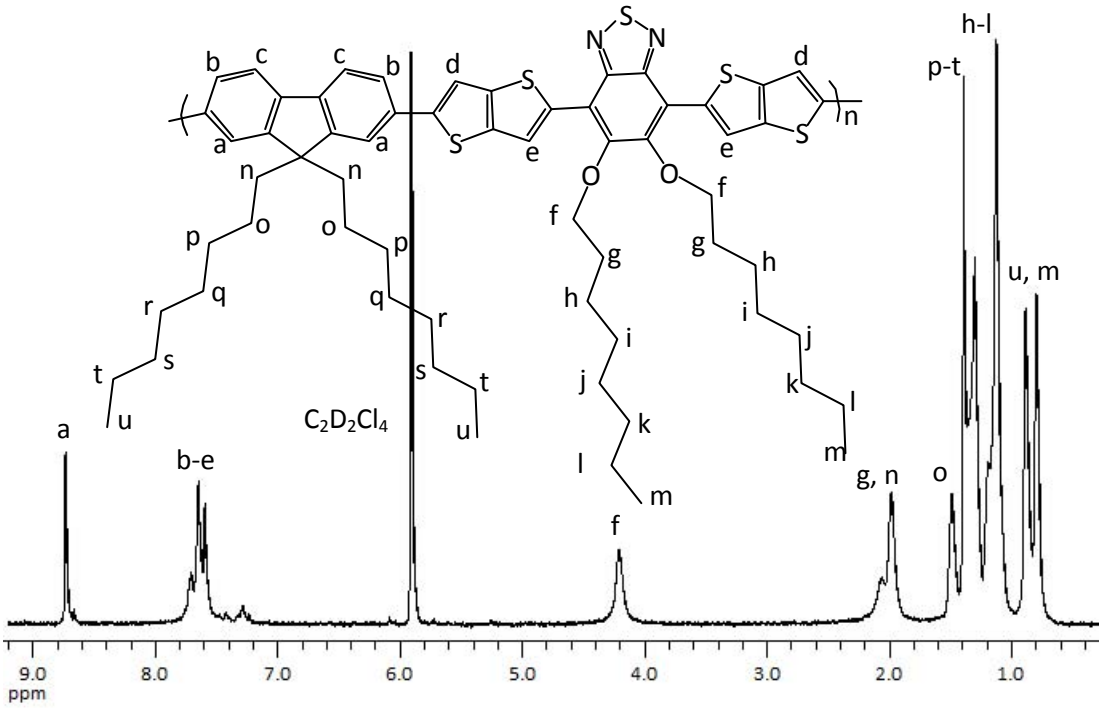

Figure 5.26: The proton NMR spectra of **P10** in $C_2D_2Cl_4$ at 100 °C.

The two protons on the thienothiophene repeat units are observed at broad peak 7.77 ppm assigned to protons d and e. Other peaks on the aromatic region which overlap with others are coming from protons on pheneylene end groups. The peak at 4.22 ppm corresponds to the protons on the carbon atoms that are connected to the oxygen atoms in the octyloxy chains (position f). Other peaks correspond to alkyl chains which are connected to fluorene and benzothiadiazole units.

5.3.3 Infrared spectroscopy (FT-IR) analysis of P8, P9 and P10

The IR spectrum of the **P8** showed similar patterns to those of its constituent monomers with some assignments of different bands/peaks. The characterizing peaks at 3079 cm^{-1} and 3009 cm^{-1} due to aromatic benzene groups =C–H stretch can be observed. The characteristic peaks at 2949 cm^{-1}, 2920 cm^{-1} and 2853 cm^{-1} are assigned to the alkyl stretching frequencies of the methylene groups.

The characteristic overtones are seen from about 2159-1977 cm^{-1}. The assignment of different peaks compare to monomer **(7)** was observed at 1471 cm^{-1}, 1410 cm^{-1} and 1310 cm^{-1} and its has a mixture of peaks related to the combination bands and also the deformations bands of the aromatic –CH groups and methylene $–CH_2-$ groups.

The peak originally at 1037 cm^{-1}, attributed to $C_{aromatic}$-Br linkage in the spectrum of monomer **(33)** disappeared. And also peaks at 1327 cm^{-1} and 1296 cm^{-1} (B-O stretch), and 1140 cm^{-1} (B-C stretch) present in the spectrum of **(7)** did also disappear from the spectrum of **P8** due to the consumption of the corresponding functional groups in the Suzuki cross-coupling reaction.

The IR spectrum of the **P9** had similar patterns to those of its constituent monomers with some assignments of different bands/peaks. It can be seen the characterizing peak at 3113 cm^{-1} which falls in relation to aromatic benzene groups =C–H stretch. The characteristic peaks at 2949 cm^{-1}, 2923 cm^{-1} and 2849 cm^{-1} are assigned to the alkyl stretching frequencies of the methylene groups.

The characteristic overtones are seen from about 2159-1977 cm^{-1}. The assignment of different peaks compare to monomer (**16)** was observed at 1477 cm^{-1}, 1428 cm^{-1} and 1350 cm^{-1} and its has a mixture of peaks related to the combination bands and also the deformations bands of the aromatic –CH groups and methylene $–CH_2-$ groups. Peaks at 1280 cm^{-1} are characteristic to the C-N bond and a peak at 1050 cm^{-1} and 1008 cm^{-1} is assigned to the C-F bonds.

The peak originally at 1020 cm^{-1}, attributed to $C_{aromatic}$-Br linkage in the spectrum of monomer **(33)** disappeared. And also peaks at 1327 cm^{-1} and 1296 cm^{-1} (B-O stretch), and 1140 cm^{-1} (B-C stretch) present in the spectrum of **(16)** did also disappear from the spectrum of **P9** due to the consumption of the corresponding functional groups in the Suzuki cross-coupling reaction.

The IR spectrum of the **P10** had similar patterns to those of its constituent monomers with some assignments of different bands/peaks. It can be seen the characterizing peak at 3118 cm^{-1} and 3081 cm^{-1} which falls in relation to aromatic benzene groups =C–H stretch. The

characteristic peaks at 2953 cm^{-1}, 2921 cm^{-1} and 2851 cm^{-1} are assigned to the alkyl stretching frequencies of the methylene groups.

The characteristic overtones are seen from about 2158-1887 cm^{-1}. The assignment of different peaks compare to monomer **(41)** was observed at 1456 cm^{-1}, 1424 cm^{-1} and 1375 cm^{-1} and its has a mixture of peaks related to the combination bands and also the deformations bands of the aromatic –CH groups and methylene $–CH_2-$ groups.

The peak originally at 1037cm^{-1}, attributed to $C_{aromatic}$-Br linkage in the spectrum of monomer **(33)** disappeared. And also peaks at 1327 cm^{-1} and 1296 cm^{-1} (B-O stretch), and 1140 cm^{-1} (B-C stretch) presents in the spectrum of **(41)** did also disappear from the spectrum of **P10** due to the consumption of the corresponding functional groups in the Suzuki cross-coupling reaction.

5.3.4 Gel Permeation Chromatography (GPC) analysis of P8, P9 and P10

GPC results from the polymerization for polymers **P8, P9** and **P10** by using polystyrene standards as shown in **Table 5.12**.

The yields of the different fractions of the polymers after Soxhlet extraction are also shown. Gel permeation chromatography measurements were taken in 1, 2, 4-trichlororbenzene (TCB) at 100 °C as at lower temperatures it was not possible to solubilise all the higher molecular weight polymers to obtain the true molecular weights.

Table 5.12: GPC data of **P8**, **P9** and **P10**

Polymer	Fraction	Yield (%)	M_w	M_n	PDI
P8	Toluene	13	20000	8500	2.4
	Chloroform	60	63000	27000	2.3
P9	Toluene	28	4600	1900	2.4
	Chloroform	32	62900	26200	2.4
P10	Chloroform	34	20000	7600	2.6

Polymer **P8** was obtained as a red solid in 73 % overall yield. GPC analysis of polymer **P8** which was extracted by toluene gave as M_w = 20000 and M_n = 8500 with a polydispersity of 2.4. The chloroform fraction GPC analysis of **P8** gave the M_w = 63000 and M_n = 27000 with a polydispersity of 2.3.

Polymer **P9** was obtained as a red solid in 60 % overall yield. GPC analysis of **P9** which was extracted by toluene gave an M_w = 4600 and M_n = 1900 with a polydispersity of 2.4. The chloroform fraction GPC analysis of **P9** gave an M_w = 62900 and M_n = 26200 with a polydispersity of 2.4. Polymer **P10** was obtained as a red solid in 34 % yield. GPC analysis of the polymer **P10** which was extracted by chloroform gave the M_w = 20000 and M_n = 7600 with a polydispersity of 2.6.

These GPC results indicate that by attaching octyloxy-substituents on the benzothiadiazole repeat units, polymers with greater molecular weights are obtained when compound to polymers which did not have such substituent. Such or result could be due to the higher solubility of these polymers which allows them to grow and stay in solution during the polymerization as opposed to other polymers.

Hence, **P8** has a higher M_w and M_n than those of **P4** and **P6** discussed earlier. The some result is true for **P9** when its GPC data is compound to polymers **P5** and **P7**. The GPC data of **P10** provide however lower molecular weight polymers with lower yields of polymers obtained. This is due to the fact that the solubility of such polymers was quite lower.

5.3.5 Elemental analysis of P8, P9 and P10

Elemental analysis was used to check if a sample is consistent with a given molecular formula by using qualitative analysis technique. **Table 5.13** showed no bromine content, indicating that the terminal groups were end-capped with bromobenzene and phenylboronic acid during the polymerization of the **P8, P9** and **P10**. The elemental analysis of the other elements of polymers **P8** and **P9** while **P10** was not in or very good agreement with it calculated values perhaps as a result of formation of during the combustion process during the analysis. **P9** and **P10** did also give a satisfactory agreement with its proposed structure.

Table 5.13: Elemental analysis data of **P8, P9** and **P10**.

Polymers	Formula Weight	Molecule Weight		Elemental analysis (%)			
				C	H	N	Br
P8	$(C_{63}H_{79}N_3O_2S_5)_n$	$(1070.64)_n$	Calculated	70.67	7.44	3.92	0
			Found	70.82	7.52	3.74	0
P9	$(C_{63}H_{77}F_2N_3O_2S_5)_n$	$(1106.62)_n$	Calculated	68.38	7.01	3.80	0
			Found	70.10	6.66	3.11	0
P10	$(C_{63}H_{78}N_2O_2S_5)_n$	$(1055.63)_n$	Calculated	71.68	7.45	2.65	0
			Found	79.01	12.18	4.11	0

* n = repeating unit

5.3.6 UV-Visible absorption spectroscopy (UV-Vis) analysis of P8, P9 and P10

The UV-Vis absorption spectra of the polymer were measured in chloroform and in solid state as thin films. UV-Vis analysis of **P8** in **Figure 5.27** and **Table 5.14** shows two absorption band at $\lambda_{max\ 1}$ = 373 nm and $\lambda_{max\ 2}$ = 466 nm in chloroform solution, and at $\lambda_{max\ 1}$ = 410 nm and $\lambda_{max\ 2}$ = 545 nm in solid state.

This slight red shift in the solid state for the same polymer was again observed in all polymers and this is because of the structure of polymers in solid state is more planar, thus more conjugation and lower band gap. Therefore, all calculations and comparisons will be based on the solid state results.

The optical band gaps were calculated from the onset of absorption of the polymers in the solid state The optical band gap of polymer **P8** as determined from the onset of its absorption spectra in the solid state has a value E_g = 1.89 eV.

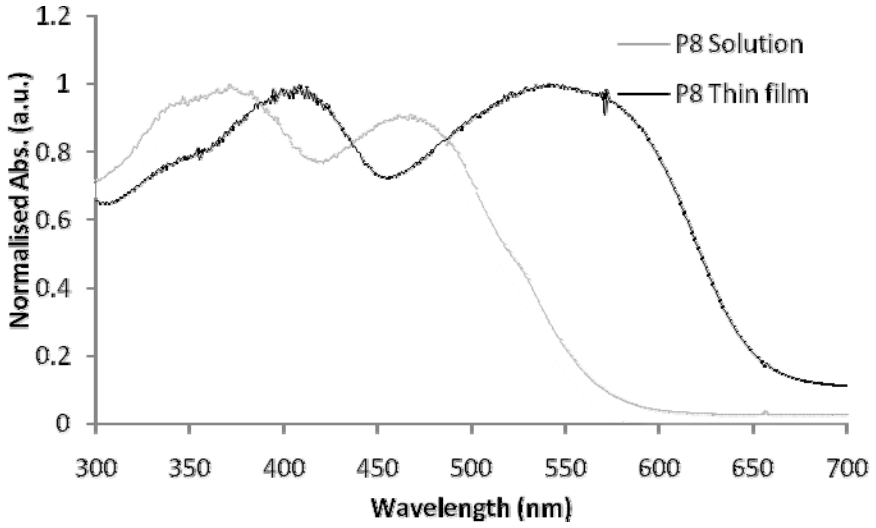

Figure 5.27: Normalised UV-Vis spectra of **P8** in chloroform (grey line) and a thin film (black line).

The UV-Vis absorption spectra of the polymer were measured in chloroform and in solid state as thin films. UV-Vis analysis of **P9** in **Figure 5.28** shows two absorption band at $\lambda_{max\ 1}$ = 344 nm and $\lambda_{max\ 2}$ = 486 nm in chloroform solution, and at $\lambda_{max\ 1}$ = 390 nm and $\lambda_{max\ 2}$ = 512 nm in solid state.

This slight red shift in the solid state for the same polymer was again observed in all polymers and this is because of the structure of polymers in solid state is more planar, thus more conjugation and lower band gap. Therefore, all calculations and comparisons will be based on the solid state results.

The optical band gaps were calculated from the onset of absorption of the polymers in the solid state The optical band gap of polymer **P9** as determined from the onset of its absorption spectra in the solid state has a value E_g = 2.03 eV.

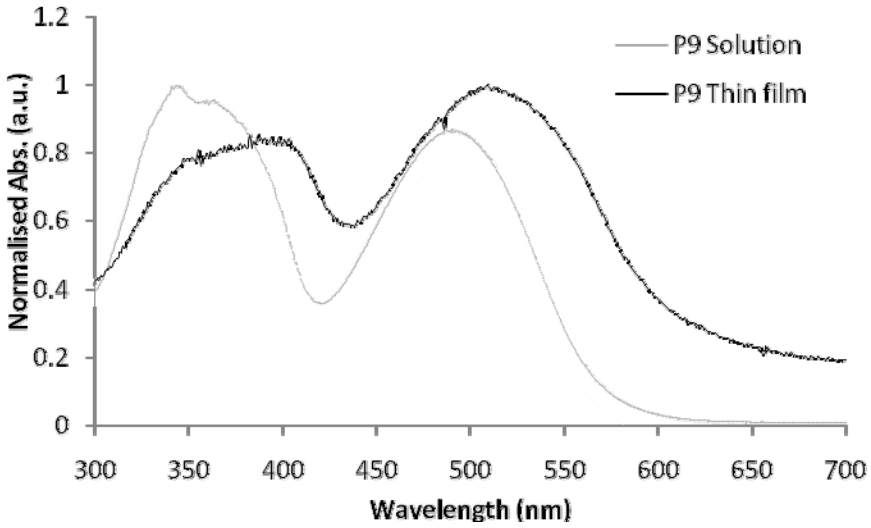

Figure 5.28: Normalised UV-Vis spectra of **P9** in chloroform (grey line) and a thin film (black line).

The UV-Vis absorption spectra of the polymer were measured in chloroform and in solid state as thin films. UV-Vis analysis of **P10** in **Figure 5.29** shows two absorption band at $\lambda_{max\ 1}$ = 355 nm and $\lambda_{max\ 2}$ = 487 nm in chloroform solution, and at $\lambda_{max\ 1}$ = 380 nm and $\lambda_{max\ 2}$ = 519 nm in solid state.

This slight red shift in the solid state for the same polymer was again observed in all polymers and this is because of the structure of polymers in solid state is more planar, thus more conjugation and lower band gap. Therefore, all calculations and comparisons will be based on the solid state results. The optical band gaps were calculated from the onset of absorption of the polymers in the solid state The optical band gap of polymer **P10** as determined from the onset of its absorption spectra in the solid state has a value E_g = 1.98 eV.

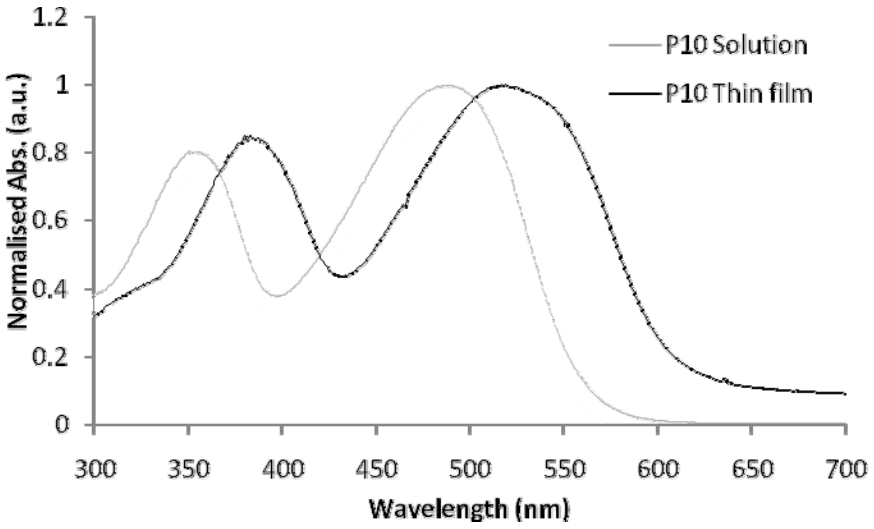

Figure 5.29: Normalised UV-Vis spectra of **P10** in chloroform (grey line) and a thin film (black line).

Table 5.14: UV-Vis data of **P8**, **P9** and **P10.**

Polymers	λ_{max} Solution (nm)		λ_{max} Thin film (nm)		λ Onset Abs. (nm)	E_g Optical (eV)
	1	2	1	2		
P8	373	466	410	545	655	1.89
P9	344	486	390	512	610	2.03
P10	355	487	380	519	625	1.98

5.3.7 Cyclic Voltammetry (CV) analysis of P8, P9 and P10

Investigations of the electrochemical properties of polymers **P8, P9 and P10** were also undertaken in cyclic voltammetry (CV) performed on drop-cast polymer films in acetonitrile with tetrabutylammonium perchlorate as the electrolyte. The LUMO level and the HOMO level were calculated from the onset reduction and oxidation respectively. Then, the electrochemical band gap (E_g) can be calculated from the difference between them. The cyclic voltammogram of the polymers **P8, P9** and **P10** are shown in **Figure 5.30** and **Table 5.15**.

To assess the electrochemical stability of the polymers cyclic voltametry measurements on drop-cast polymer films were conducted in acetonitrile with tetrabutylammonium perchlorate as an electrolyte. The ionization potential (I_p), electron affinities (E_a) and band gap were estimated from the onset potential of oxidation and reduction from the curves.
All values were taken relative to the reference electrode Ag/Ag+, on the basis that the energy level of the ferrocene/ ferrocenium is 4.8 eV below the vacuum level and oxidation occurs at 0.082 V data from the spectra were adjusted to give the polymers relative to these values.

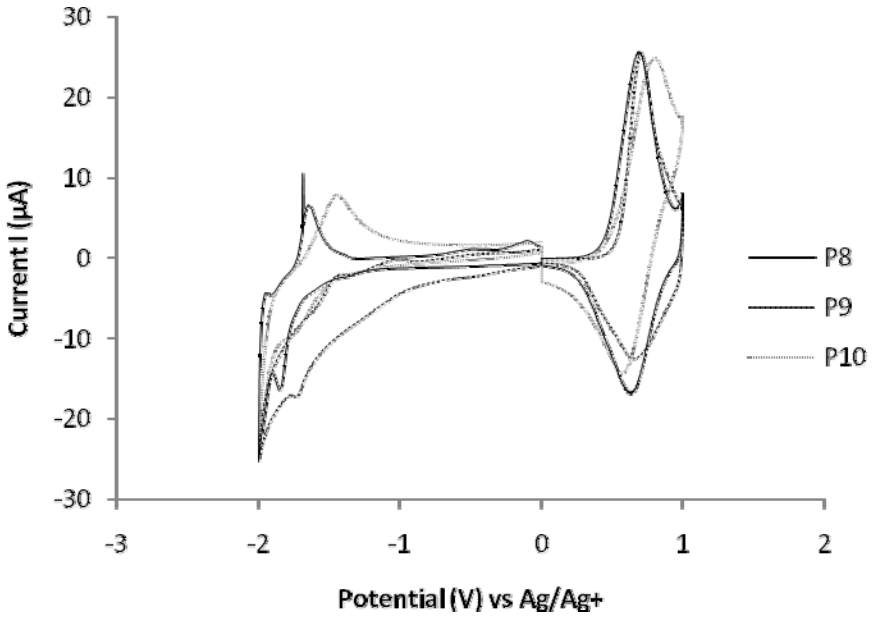

Figure 5.30: Normalised cyclic voltammogram of **P8, P9** and **P10**.

Polymer **P8** exhibits an oxidation wave at E_{pa} = 0.82 V and a reduction wave at E_{pa} = -1.65 V, and their associated reduction and oxidation waves at E_{pc} = 0.76 V and E_{pc} = -1.85 V, respectively. From the onset of oxidation (0.47 V) and the onset of reduction (-1.80 V), the HOMO level is at -5.27 eV and the LUMO level is at -3.01 eV for the polymer backbone (on the basis that ferrocene/ferrocenium has an IP of 4.8 eV below the vacuum level and the oxidation occurs at 0.082 V relative to Ag/Ag^+), therefore the electrochemical band gap of the polymer is 2.26 eV.

Polymer **P9** exhibits an oxidation wave at E_{pa} = 0.70 V and a reduction wave at E_{pa} = -1.36 V, and their associated reduction and oxidation waves at E_{pc} = 0.64 V and E_{pc} = -1.81 V, respectively. From the onset of oxidation (0.47 V) and the onset of reduction (-1.64 V), the HOMO level is at -5.27 eV and the LUMO level is at -3.16 eV for the polymer backbone (on the basis that ferrocene/ferrocenium has an IP of 4.8 eV below the vacuum level and the oxidation occurs at 0.082 V relative to Ag/Ag^+), therefore the electrochemical band gap of the polymer is 2.11 eV.

Table 5.15: Voltammetry results and band gaps of **P8**, **P9** and **P10**.

Polymers	*E*onset, $_{ox}$ (V)[a)]	*E*onset, $_{red}$ (V) [a)]	HOMO (eV)	LUMO (eV)	Band gap (eV)
P8	0.47	-1.79	-5.27	-3.01	2.26
P9	0.47	-1.64	-5.27	-3.16	2.11
P10	0.52	-1.51	-5.32	-3.29	2.03

[a)] *vs*. Ag/Ag^+

Polymer **P10** exhibits an oxidation wave at E_{pa} = 0.95 V and a reduction wave at E_{pa} = -1.45 V, and their associated reduction and oxidation waves at E_{pc} = 0.70 V and E_{pc} = -1.71 V, respectively. From the onset of oxidation (0.52 V) and the onset of reduction (-1.51V), the HOMO level is at -5.32 eV and the LUMO level is at -3.29 eV for the polymer backbone (on the basis that ferrocene/ferrocenium has an IP of 4.8 eV below the vacuum level and the oxidation occurs at 0.082 V relative to Ag/Ag^+), therefore the electrochemical band gap of the polymer is 2.03 eV.

5.3.8 Thermogravimetric Analysis (TGA) of P8, P9 and P10

The thermal stability of **P8, P9** and **P10** were investigated in this study. The thermogram of **P8, P9** and **P10** is shown in **Figure 5.31** and the details of the TGA results are shown in **Table 5.17**.

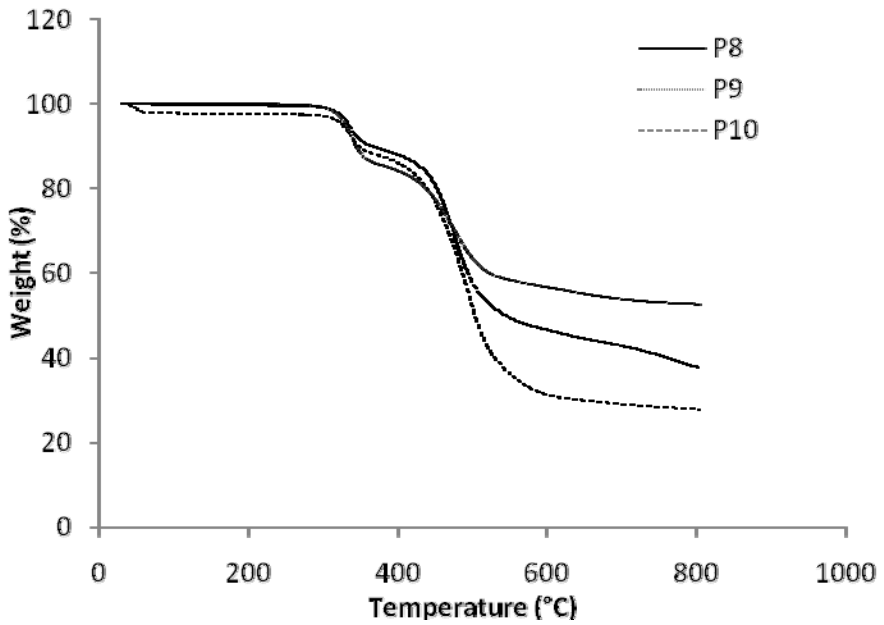

Figure 5.31: The TGA thermogram of **P8, P9** and **P10**.

Figure 5.30 shows the TGA curves for of the thermal degradation of the polymer **P8**, the onset of the degradation occurs at 444 °C, the onset of second degradation is 566 °C with a weight loss of 73.8 %. The percentage of residual weight 26.2 % is consistent with percentage weight of PDI units and polymer backbone.

Thermal gravimetry analysis measurements revealed the remarkable stability of the polymer up to 566 °C, which indicated that these polymers are thermally very stable. The subsequent degradation and weight loss of the polymer beyond 566 °C was proportional to the mass of its a alkyl-group substituents. The polymer did not show any further weight loss up to a temperature of 800 °C.

Figure 5.31 shows the TGA curves for of the thermal degradation of the polymer **P9**, the onset of the degradation occurs at 324 °C, the onset of second degradation is 442 °C with a weight loss of 52.3 %. The percentage of residual weight 47.7 % is consistent with percentage weight of PDI units and polymer backbone.

Thermal gravimetry analysis measurements revealed the remarkable stability of the polymer up to 442 °C, which indicated that these polymers are thermally very stable. The subsequent degradation and weight loss of the polymer beyond 442 °C was proportional to

the mass of its a alkyl-group substituents. The polymer did not show any further weight loss up to a temperature of 800 °C.

Figure 5.31 shows the TGA curves for of the thermal degradation of the polymer **P10**, the onset of the degradation occurs at 321 °C, the onset of second degradation is 433 °C with a weight loss of 71.1 %. The % of residual weight 28.9 % is consistent with percentage weight of PDI units and polymer backbone.

Thermal gravimetry analysis measurements revealed the remarkable stability of the polymer up to 433 °C, which indicated that these polymers are thermally very stable. The subsequent degradation and weight loss of the polymer beyond 433 °C was proportional to the mass of its a alkyl-group substituent. The polymer did not show any further weight loss up to a temperature of 800 °C.

5.3.9 Differential Scanning Calorimetry (DSC) analysis of P8, P9 and P10

Table 5.16 summarises the results from the thermo gravimetric analysis (TGA) and the differential scanning calorimetry (DSC). In applications that can experience temperature extremes, it is important to know what will happen when these polymers are exposed to variants in temperature and how they will affect the mechanical behaviour of the polymer.

Table 5.16: The TGA and DSC data for **P8, P9** and **P10**.

Polymers	TGA Analysis			DSC Analysis
	Onset degradation temp. / °C		Weight loss at 800 °C (wt. %)	T_g / °C
	1st degradation	2nd degradation		
P8	444	566	73.8	75
P9	324	442	52.3	71
P10	321	433	71.1	71

The glass transition (T_g) is obtained from the DSC trace and it is a function of polymer backbone flexibility. The polymers were subjected to a first heating run, cooling run followed by further heating run, at the scan rate 10 °C/ min, and when no T_g was seen, 20 up to 100 °C/ min rates was applied. The glass transitions (T_g) value were estimated and

obtained from the first scans as broad peaks, they were above 50 °C indicating that all polymers have good tolerance to the stages required in making devices. Based on the table the T_g of **P8, P9** and **P10** were 75 °C, 71 °C and 71 °C, respectively. All the T_g results of the polymers are similar to each other, due to the present of thienothiophene-bisoctyloxy substituted benzothiadiazole , which provide more flexibility for the polymers backbones.[209, 210]

CHAPTER 6 - CONCLUSIONS AND FUTURE WORK

6.1 Conclusions

All polymers **P1-P10** were successfully obtained in yields ranging from 32 % to 87 %. The structure of the polymers have been confirmed by NMR spectroscopy, FT-IR and elemental analysis, and their weight-average molecular weights were estimated using gel permeation chromatography (GPC). The optical and electronic properties of the polymers were investigated by UV-Vis absorption spectroscopy. Cyclic voltammetry measurements were used to investigate their electrochemical properties. The thermal properties of the materials were investigated by thermal gravimetric analysis (TGA) and differential scanning calorimetry (DSC) measurements.

A range of different polymers were prepared in this work. These polymers were designed for use as electron donors to fullerenes as active layers in bulk heterojunction solar cells.[127]

Three main classes of such polymers were described. The first class of polymers **P1 - P3** consisted of alternating co-polymers comprising thienothiophene repeat units and either 2,7-linked 9-alkyl carbazole units **P1**, or 2, linked-9-alkyl carbazole repeat units with fluorine substituents of their 3,6-positions **P2**, or 2,7-linked-9,9-diolkylfluorene **P3**.

Poly(9-(heptadecan-9-yl)-9H-carbazole-alt-thieno[3,2-b]thiophene) **(P1)** composed of alternating carbazole and thienothiophene were successfully prepared. The polymer was synthesised by Suzuki cross coupling, in order to investigate its suitability for application in photovoltaic cell. GPC results from polymerisation have shown that **P1** had a weight average molecular weight values M_w of 6500 Da with a polydispersity of 2.3.

UV-Vis analysis showed the polymer absorbed at high wavelengths λ_{max} 435 nm in solution and 442 nm in the solid state and the band gap of **P1** in solid state is 2.46 eV. CV measurements estimated the band gap as 2.18 eV from the onset of oxidation and reduction. The HOMO and LUMO levels can be estimated as -5.45 eV and -3.27 eV respectively. TGA of **P1** showed good stability, the thermal stability, up to 430 °C. DSC analysis of **P1** exhibited T_g peak at 70 °C. These results are in agreement with the design procedures for the use of these materials in photovoltaic applications.

Poly(3,6-difluoro-9-(heptadecan-9-yl)-9H-carbazole-alt-thieno[3,2-b]thiophene) **(P2)** composed of alternating carbazole and thienothiophene unit were successfully prepared. The polymer was synthesised by Suzuki cross coupling, in order to investigate its suitability for application in photovoltaic cell. GPC results from polymerisation have shown that **P2** had a weight average molecular weight values M_w of 7100 Da with a polydispersity of 2.4.

UV-Vis analysis showed the polymer **P2** absorbed at high wavelengths λ_{max} 405 nm in solution and 419 nm in the solid state and the band gap of P2 in solid state is 2.36 eV. CV measurements estimated the band gap as 2.33 eV from the onset of oxidation and reduction. The HOMO and LUMO levels can be estimated as -5.50 eV and -3.17 eV respectively. TGA of P2 showed good stability, the thermal stability, up to 432 °C. DSC analysis of **P2** exhibited Tg peak at 78 °C. These results are in agreement with the design procedures for the use of these materials in photovoltaic applications.

Polyfluorene poly(9,9-dioctyl-9H-fluorene-alt-thieno[3,2-b]thiophene) **(P3)** composed of alternating carbazole donor unit and acceptor unit were successfully prepared. The polymer was synthesised by Suzuki cross coupling, in order to investigate its suitability for application in photovoltaic cell. GPC results from polymerisation have shown that **P3** had a weight average molecular weight values M_w of 4600 Da with a polydispersity of 2.2.

UV-Vis analysis showed the polymer **P3** absorbed at high wavelengths λ_{max} 395 nm in solution and 400 nm in the solid state and the band gap of **P3** in solid state is 2.47 eV. CV measurements estimated the band gap as 2.44 eV from the onset of oxidation and reduction. The HOMO and LUMO levels can be estimated as -5.64 eV and -3.20 eV respectively. TGA of **P3** showed good stability, the thermal stability, up to 425 °C. DSC analysis of **P3** exhibited T_g peak at 76 °C.

These results are in agreement with the design procedures for the use of these materials in photovoltaic applications. The optical band gap, E_g of polymers **P1, P2** and **P3** were 2.46 eV, 2.36 eV and 2.47 eV respectively. The photophysical properties of these polymers show that **P2** has the narrowest optical band gap due to the electrostatic interaction between the hydrogens at the 4-position on thienothiophene rings and the fluorine substituents on the neighbouring carbazole repeat units.

All polymers in this first class of materials **P1 - P3** have fairly low molecular weights as a result of their low solubility and their precipitation out of solution during the polymerisation reaction.

The presence of fluorine substitutes at the 3,6-position of carbazole repeat units on **P2** has led into a monomer band gap in the polymer when it is composed to that of the equivalent polymer without fluorine substituent **P1**. This indicates the present of fluorine interactions of **P2** with neighboring sulfur or hydrogen atoms of the thienothiophene repeat units along the polymer backbone.

The second class of materials consisted of alternating copolymers comprising benzothiadiazole repeat units and 2,7-linked carbazole repeat units flanked by thienothiophene repeat unit with or without fluorine-substituents at the 3,6-positions on the carbazole repeat unit polymers **P4 - P7**. These materials have low energy bandgaps in view of their alternating electron donors and acceptors along their polymer backbones which to intermolecular change transfer and more extended electronic delocalisation along the polymer backbone.

Poly(9-(heptadecan-9-yl)-9H-carbazole-atl-4,7-di(thieno[3,2-b]thiophen-2-yl)benzo [c][1,2,5]thiadiazole), **(P4)** composed of alternating carbazole donor unit and acceptor unit were successfully prepared. The polymer was synthesised by direct arylation polymerization, in order to investigate its suitability for application in photovoltaic cell. GPC results from polymerisation have shown that P4 had a weight average molecular weight values M_w of 30600 Da with a polydispersity of 2.3.

UV-Vis analysis showed the polymer absorbed at high wavelengths λ_{max} 509 nm in solution and 534 nm in the solid state and the band gap of **P4** in solid state is 1.95 eV. CV measurements estimated the band gap as 2.38 eV from the onset of oxidation and reduction. The HOMO and LUMO levels can be estimated as -5.52 eV and -3.14 eV respectively. TGA of **P4** showed good stability, the thermal stability, up to 433 °C. DSC analysis of P4 exhibited T_g peak at 64 °C. These results are in agreement with the design procedures for the use of these materials in photovoltaic applications.

poly(3,6-difluoro-9-(heptadecan-9-yl)-9H-carbazole-atl-4,7-di(thieno[3,2-b]thiophen -2-yl)benzo[c][1,2,5]thiadiazole), **(P5)** composed of alternating carbazole donor unit and acceptor unit were successfully prepared. The polymer was synthesised by direct arylation polymerization, in order to investigate its suitability for application in photovoltaic cell. GPC results from polymerisation have shown that P5 had a weight average molecular weight values M_w of 83400 Da with a polydispersity of 2.4.

UV-Vis analysis showed the polymer absorbed at high wavelengths λ_{max} 537 nm in solution and 550 nm in the solid state and the band gap of **P5** in solid state is 1.92 eV. CV measurements estimated the band gap as 2.10 eV from the onset of oxidation and reduction. The HOMO and LUMO levels can be estimated as -5.40 eV and -3.30 eV respectively. TGA of **P5** showed good stability, the thermal stability, up to 452 °C. DSC analysis of **P5** exhibited Tg peak at 67 °C. These results are in agreement with the design procedures for the use of these materials in photovoltaic applications.

Poly(9-(pentacosan-13-yl)-9H-carbazole-atl-4,7-di(thieno[3,2-b]thiophen-2-yl)benzo [c][1,2,5]thiadiazole) **(P6)** composed of alternating carbazole donor unit and acceptor unit were successfully prepared. The polymer was synthesised by direct arylation polymerization, in order to investigate its suitability for application in photovoltaic cell. GPC results from polymerisation have shown that **P6** had a weight average molecular weight values M_w of 25100 Da with a polydispersity of 2.5. UV-Vis analysis showed the polymer absorbed at high wavelengths λ_{max} 519 nm in solution and 534 nm in the solid state and the band gap of **P6** in solid state is 1.86 eV.

CV measurements estimated the band gap as 2.19 eV from the onset of oxidation and reduction. The HOMO and LUMO levels can be estimated as -5.19 eV and -3.00 eV respectively. TGA of **P6** showed good stability, the thermal stability, up to 443 °C. DSC analysis of **P6** exhibited T_g peak at 66 °C. These results are in agreement with the design procedures for the use of these materials in photovoltaic applications.

Poly(3,6-difluoro-9-(pentacosan-13-yl)-9H-carbazole-atl-4,7-di(thieno[3,2-b]thiophen-2-yl)benzo[c][1,2,5]thia diazole) **(P7)** composed of alternating carbazole donor unit and acceptor unit were successfully prepared. The polymer was synthesised by direct arylation polymerization, in order to investigate its suitability for application in photovoltaic cell.[211]

GPC results from polymerisation have shown that **P7** had a weight average molecular weight values M_w of 30600 Da with a polydispersity of 2.3. UV-Vis analysis showed the polymer absorbed at high wavelengths λ_{max} 519 nm in solution and 552 nm in the solid state and the band gap of **P7** in solid state is 1.85 eV.

CV measurements estimated the band gap as 2.14 eV from the onset of oxidation and reduction. The HOMO and LUMO levels can be estimated as -5.32 eV and -3.18 eV respectively. TGA of **P7** showed good stability, the thermal stability, up to 438 °C. DSC analysis of **P7** exhibited T_g peak at 68 °C. These results are in agreement with the design procedures for the use of these materials in photovoltaic applications.

The optical band gap, E_g a series of carbazole and the fluorene based co-polymers containing thienothiophene and benzothiadiazole units copolymers **P4, P5, P6** and **P7** were 1.95 eV, 1.92 eV, 1.86 eV and 1.85 eV respectively. The obtained M_w and M_n of the polymers **P4, P5, P6** and **P7,** were relatively low to **P1, P2,** and **P3** due to their low solubility.

The presence of fluorine substituents at the 3,6-position of carbazole repeat units on **P5** and **P7** has led into a monomer band gap in the polymer series. The band gap was also effect to the polymer series without fluorine substituent **P4** and **P6**. This indicates the presece of fluorine interactions of P5 and P7 with neighboring sulfur or hydrogen atoms of the co-polymers containing thienothiophene and benzothiadiazole units along the polymer backbone.

The third class of materials consisted of alternating down acceptor conjugated polymers which are similar to the second class of materials but have octyloxy-substituents on the benzothiadiazole repeat units **P8 - P10**. The presence of octyloxy-substituents units on the benzothiadiazole electron accepting units along the polymer chains reduce the intramolecular charge transfer and provides materials with wider band gaps then those of the second class of materials pepared and hence have lower electronic delocalisation.

In order to solve this problem, two octyloxy solubilising groups were attached to the benzothiadiazole units to obtain another series of three copolymers **P8, P9** and **P10**.

Poly(9-(heptadecan-9-yl)-9H-carbazole-alt-5,6-bis(octyloxy)-4,7-di(thieno[3,2-b]thiophen-2-yl)benzo[c][1,2,5]thiadiazole) **(P8)** composed of alternating carbazole donor unit and acceptor unit were successfully prepared. The polymer was synthesised by Suzuki cross coupling, in order to investigate its suitability for application in photovoltaic cell. GPC results from polymerisation have shown that **P8** had a weight average molecular weight values M_w of 63000 Da with a polydispersity of 2.3.

UV-Vis analysis showed the polymer absorbed at high wavelengths λ_{max} 466 nm in solution and 545 nm in the solid state and the band gap of **P8** in solid state is 1.89 eV. CV measurements estimated the band gap as 2.26 eV from the onset of oxidation and reduction. The HOMO and LUMO levels can be estimated as -5.27 eV and -3.01 eV respectively.

TGA of **P8** showed good stability, the thermal stability, up to 566 °C. DSC analysis of **P8** exhibited T_g peak at 75 °C. These results are in agreement with the design procedures for the use of these materials in photovoltaic applications.

Poly(3,6-difluoro-9-(heptadecan-9-yl)-9H-carbazole-alt-5,6-bis(octyloxy)-4,7-di(thieno[3,2-b]thiophen-2-yl)benzo[c][1,2,5]thiadiazole) **(P9)** composed of alternating carbazole donor unit and acceptor unit were successfully prepared. The polymer was synthesised by Suzuki cross coupling, in order to investigate its suitability for application in photovoltaic cell. GPC results from polymerisation have shown that P9 had a weight average molecular weight values M_w of 62900 Da with a polydispersity of 2.4.

UV-Vis analysis showed the polymer absorbed at high wavelengths λ_{max} 486 nm in solution and 512 nm in the solid state and the band gap of **P9** in solid state is 2.03 eV. CV measurements estimated the band gap as 2.11 eV from the onset of oxidation and reduction. The HOMO and LUMO levels can be estimated as -5.27 eV and -3.16 eV, respectively.

TGA of **P9** showed good stability, the thermal stability, up to 442 °C. DSC analysis of **P9** exhibited T_g peak at 71 °C. These results are in agreement with the design procedures for the use of these materials in photovoltaic applications.

Poly(9,9-dioctyl-9H-fluorene-alt-5,6-bis(octyloxy)-4,7-di(thieno[3,2-b]thiophen-2-yl)benzo[c][1,2,5]thiadiazole) **(P10)** composed of alternating carbazole donor unit and acceptor unit were successfully prepared. The polymer was synthesised by Suzuki cross coupling, in order to investigate its suitability for application in photovoltaic cell. GPC results from polymerisation have shown that P10 had a weight average molecular weight values M_w of 20000 Da with a polydispersity of 2.6.

UV-Vis analysis showed the polymer absorbed at high wavelengths λ_{max} 487 nm in solution and 519 nm in the solid state and the band gap of **P10** in solid state is 1.98 eV. CV measurements estimated the band gap as 2.03 eV from the onset of oxidation and reduction. The HOMO and LUMO levels can be estimated as -5.32 eV and -3.29 eV respectively.

TGA of **P10** showed good stability, the thermal stability, up to 433 °C. DSC analysis of **P10** exhibited T_g peak at 71 °C. These results are in agreement with the design procedures for the use of these materials in photovoltaic applications.

The optical band gap, E_g of polymer **P8, P9** and **P10** were 1.89 eV, 2.03 eV and 1.98 eV respectively. These copolymers were prepared successfully via Suzuki cross coupling reactions. The photophysical and electrochemical properties of these polymers are higher than those of their analogous polymers **P4, P5, P6** and **P7**, due to the presence of bisoctyloxy substituents that act as electron donor groups, reducing the electron acceptor properties of benzothiadiazole units. The photophysical properties of these polymers show that **P8** has the narrowest optical band gap compared to **P9** and **P10**.

All the co-polymers based containing thienothiophene and benzothiadiazole **P4 - P10** showed a remarkable decrease in the band gap compared to their analogous thienothiophene -based copolymers, which makes these materials very promising for use in solar cell applications.

It would therefore be reasonable to enlarge this family of copolymers and find whether the use of alkyl substituents of different sizes could influence their efficiency when used in bulk heterojunction solar cell devices.[134] In addition, the use of other electron donor comonomers such as anthracene derivatives with selenophene-based comonomers should

also be investigated to probe any possible improvements of the photophysical properties of this series of selenophene-based materials.

6.2 Future Work

Based on the development of the solar cells polymers , device studies which will include the use of polymers P4-P7 in bulk heterojunction solar cells as electron donors to PCBM (a C60 derivative) should be tested. All four polymers show great promise for use in this area, as all of these polymers are low band gap polymers and should be able to absorb a large portion of light from the solar spectrum.

Further work in this area should also be directed at preparing a processable polymer analogue to P4 in order to be able to investigate its properties in bulk heterojunction solar cell applications. The use of different polymerisation conditions should allow an increase of the molecular weight of these materials which in turn should provide a better performance in devices.

In addition, further work is necessary to fine-tune the combination of these carbazole systems with other conjugated systems in order to produce polymers with desirable properties to fabricate more efficient and stable devices which will ultimately be used in commercial solar cells.

REFERENCES

1. Baek, M.-J., Lee, S.-H., Kim, D., and Lee, Y.-S. *Macromolecular Research* **2012**, 20, 147-154.
2. Cheng, Y.-J., Yang, S.-H., and Hsu, C.-S. *Chemical Reviews* **2009**, 109, 5868-5923.
3. Coakley, K. M. and Mcgehee, M. D. *Chemistry of Materials* **2004**, 16, 4533-4542.
4. Dennler, G., Scharber, M. C., and Brabec, C. J. *Advanced Materials* **2009**, 21, 1323-1338.
5. Friend, R. H. *Pure Appl. Chem.* **2001**, 73, 425-430.
6. Schwartz, B. J. *Annu. Rev. Phys. Chem.* **2003**, 54, 141-172.
7. Günes, S., Neugebauer, H., and Sariciftci, N. S. *Chemical Reviews* **2007**, 107, 1324-1338.
8. Xie, H., Zhang, K., Duan, C., Liu, S., Huang, F., and Cao, Y. *Polymer* **2012**, 53, 5675-5683.
9. Nozik, A. J. and Miller, J. *Chemical Reviews* **2010**, 110, 6443-6445.
10. Yang, L., Yan, L., and You, W. *The Journal of Physical Chemistry Letters* **2013**, 4, 1802-1810.
11. Po, R., Maggini, M., and Camaioni, N. *The Journal of Physical Chemistry C* **2009**, 114, 695-706.
12. Hoppe, H. and Sariciftci, N. S. *J. Mater. Res.* **2004**, 19, 1924-1945.
13. Liang, Y. and Yu, L. *Accounts of Chemical Research* **2010**, 43, 1227-1236.
14. Deng, X.-Y. *International Journal of Molecular Sciences* **2011**, 12, 1575-1594.
15. Li, J. and Grimsdale, A. C. *Chemical Society Reviews* **2010**, 39, 2399-2410.
16. Michinobu, T., Osako, H., and Shigehara, K. *Polymers* **2010**, 2, 159-173.
17. Qin, R., Li, W., Li, C., Du, C., Veit, C., Schleiermacher, H.-F., Andersson, M., Bo, Z., Liu, Z., InganäS, O., Wuerfel, U., and Zhang, F. *Journal of the American Chemical Society* **2009**, 131, 14612-14613.
18. Zhou, H., Yang, L., and You, W. *Macromolecules* **2012**, 45, 607-632.
19. Xiao, S., Stuart, A. C., Liu, S., Zhou, H., and You, W. *Advanced Functional Materials* **2010**, 20, 635-643.
20. Gendron, D. and Leclerc, M. *Energy & Environmental Science* **2011**, 4, 1225-1237.
21. Boudreault, P.-L. T., Beaupre, S., and Leclerc, M. *Polymer Chemistry* **2010**, 1, 127-136.
22. Sharma, G. D., Singh, M., Kurchania, R., Koukaras, E. N., and Mikroyannidis, J. A. *RSC Advances* **2013**, 3, 18821-18834.
23. Zhang, G., Fu, Y., Xie, Z., and Zhang, Q. *Macromolecules* **2011**, 44, 1414-1420.
24. Xia, Y., Luo, J., Deng, X., Li, X., Li, D., Zhu, X., Yang, W., and Cao, Y. *Macromolecular Chemistry and Physics* **2006**, 207, 511-520.
25. Winder, C. and Sariciftci, N. S. *Journal of Materials Chemistry* **2004**, 14, 1077-1086.
26. Wakim, S., Alem, S., Li, Z., Zhang, Y., Tse, S.-C., Lu, J., Ding, J., and Tao, Y. *Journal of Materials Chemistry* **2011**, 21, 10920-10928.
27. Wlosnewski, J., Piyakulawat, P., Keawprajak, A., Saekung, C., and Asawapirom, U. *Thammasat Int. J. Sc. Tech.* **2010**, 15.
28. Tuncel, D. and Demir, H. V. *Nanoscale* **2010**, 2, 484-494.
29. Duan, C., Huang, F., and Cao, Y. *Journal of Materials Chemistry* **2012**, 22, 10416-10434.
30. Yao, Y., Dong, H., and Hu, W. *Polymer Chemistry* **2013**, 4, 5197-5205.
31. Cravino, A. and Sariciftci, N. S. *Journal of Materials Chemistry* **2002**, 12, 1931-1943.
32. Chabinyc, M. L. *Journal of Vacuum Science & Technology B* **2008**, 26, 445-457.
33. Voit, B. I. and Lederer, A. *Chemical Reviews* **2009**, 109, 5924-5973.
34. Chen, J.-T. and Hsu, C.-S. *Polymer Chemistry* **2011**, 2, 2707-2722.

35. Reiss, P., Couderc, E., De Girolamo, J., and Pron, A. *Nanoscale* **2011**, 3, 446-489.
36. Blouin, N., Michaud, A., Gendron, D., Wakim, S., Blair, E., Neagu-Plesu, R., Belletête, M., Durocher, G., Tao, Y., and Leclerc, M. *Journal of the American Chemical Society* **2008**, 130, 732-742.
37. Burroughes, J. H., Bradley, D. D. C., Brown, A. R., Marks, R. N., Mackay, K., Friend, R. H., Burns, P. L., and Holmes, A. B. *Nature* **1990**, 347, 539-541.
38. Kim, H. U., Mi, D., Kim, J.-H., Park, J. B., Yoon, S. C., Yoon, U. C., and Hwang, D.-H. *Solar Energy Materials and Solar Cells* **2012**, 105, 6-14.
39. Shi, H.-P., Shi, L.-W., Dai, J.-X., Xu, L., Wang, M.-H., Wu, X.-H., Fang, L., Dong, C., and Choi, M. M. F. *Tetrahedron* **2012**, 68, 9788-9794.
40. Lipomi, D. J., Chong, H., Vosgueritchian, M., Mei, J., and Bao, Z. *Solar Energy Materials and Solar Cells* **2012**, 107, 355-365.
41. Mabkhot, Y. N., Barakat, A., and Alshahrani, S. *Journal of Molecular Structure* **2012**, 1027, 15-19.
42. Lim, Y., Ihn, S.-G., Bulliard, X., Yun, S., Chung, Y., Kim, Y., Chang, H., and Choi, Y. S. *Polymer* **2012**, 53, 5275-5284.
43. Ewbank, P. C., Laird, D., and Mccullough, R. D., *Regioregular Polythiophene Solar Cells: Material Properties and Performance*, in *Organic Photovoltaics*2009, Wiley-VCH Verlag GmbH & Co. KGaA. p. 1-55.
44. Hoppe, H. and Sariciftci, N. S. *Journal of Materials Chemistry* **2006**, 16, 45-61.
45. Pron, A. and Rannou, P. *Prog. Polym. Sci.* **2002**, 27, 135-190.
46. Subramaniyan, S., Xin, H., Kim, F. S., and Jenekhe, S. A. *Macromolecules* **2011**, 44, 6245-6248.
47. He, X. and Baumgartner, T. *RSC Advances* **2013**, 3, 11334-11350.
48. Brédas, J.-L., Norton, J. E., Cornil, J., and Coropceanu, V. *Accounts of Chemical Research* **2009**, 42, 1691-1699.
49. Sworakowski, J. and Ulanski, J. *Annual Reports Section "C" (Physical Chemistry)* **2003**, 99, 87-125.
50. Zhan, X. and Zhu, D. *Polymer Chemistry* **2010**, 1, 409-419.
51. Shirakawa, H., Louis, E. J., Macdiarmid, A. G., Chiang, C. K., and Heeger, A. J. *Journal of the Chemical Society, Chemical Communications* **1977**, 0, 578-580.
52. Edelmann, M. J., Raimundo, J.-M., Utesch, N. F., Diederich, F., Boudon, C., Gisselbrecht, J.-P., and Gross, M. *Helvetica Chimica Acta* **2002**, 85, 2195-2213.
53. Long, Y.-Z., Li, M.-M., Gu, C., Wan, M., Duvail, J.-L., Liu, Z., and Fan, Z. *Progress in Polymer Science* **2011**, 36, 1415-1442.
54. Ince, F. G., Ozbek, S. Z., Goktas, H., Oze, M. E., and Capan, R. *Journal of Optoelectronics and Advanced Materials* **2009**, 11, 1182-1185.
55. Printz, A. D., Savagatrup, S., Burke, D. J., Purdy, T. N., and Lipomi, D. J. *RSC Advances* **2014**, 4, 13635-13643.
56. Hou, J., Chen, H.-Y., Zhang, S., Li, G., and Yang, Y. *Journal of the American Chemical Society* **2008**, 130, 16144-16145.
57. Kim, Y., Choulis, S. A., Nelson, J., Bradley, D. D. C., Cook, S., and Durrant, J. R. *Journal of Materials Science* **2005**, 40, 1371-1376.
58. Levi, M. D. and Aurbach, D. *Journal of Power Sources* **2008**, 180, 902-908.
59. Shi, F., Fang, G., Liang, F., Wang, L., Mua, Z., Zhang, X., Xie, Z., and Su, Z. *European Polymer Journal* **2010**, 46, 1770-1777.
60. Ashraf, R. S., Gilot, J., and Janssen, R. a. J. *Solar Energy Materials and Solar Cells* **2010**, 94, 1759-1766.
61. Niu, H., Kang, H., Cai, J., Wang, C., Bai, X., and Wang, W. *Polymer Chemistry* **2011**, 2, 2804-2817.
62. Raj, M. R. and Anandan, S. *RSC Advances* **2013**, 3, 14595-14608.

63. Dovgolevsky, E., Kirmayer, S., Lakin, E., Yang, Y., Brinker, C. J., and Frey, G. L. *Journal of Materials Chemistry* **2008**, 18, 423-436.
64. Yu, C.-Y., Chen, C.-P., Chan, S.-H., Hwang, G.-W., and Ting, C. *Chemistry of Materials* **2009**, 21, 3262-3269.
65. Nguyen, T. Q., Yee, R. Y., and Schwartz, B. J. *Journal of Photochemistry and Photobiology A: Chemistry* **2001**, 144, 21-30.
66. Bao, Z., Rogers, J. A., Dodabalapur, A., Lovinger, A. J., Katz, H. E., Raju, V. R., Peng, Z., and Galvin, M. E. *Optical Materials* **1999**, 12, 177-182.
67. Mitchell, W. J., Pena, C., and Burn, P. L. *Journal of Materials Chemistry* **2002**, 12, 200-205.
68. Chen, Y.-C., Yu, C.-Y., Fan, Y.-L., Hung, L.-I., Chen, C.-P., and Ting, C. *Chemical Communications* **2010**, 46, 6503-6505.
69. Weder, C. *Chemical Communications* **2005**, 5378-5389.
70. El-Khouly, M. E., Lee, S.-H., Kay, K.-Y., and Fukuzumi, S. *New Journal of Chemistry* **2013**, 37, 3252-3260.
71. Campos, L. M., Tontcheva, A., Günes, S., Sonmez, G., Neugebauer, H., Sariciftci, N. S., and Wudl, F. *Chemistry of Materials* **2005**, 17, 4031-4033.
72. Xin, H., Subramaniyan, S., Kwon, T.-W., Shoaee, S., Durrant, J. R., and Jenekhe, S. A. *Chemistry of Materials* **2012**, 24, 1995-2001.
73. Ding, P., Chu, C.-C., Liu, B., Peng, B., Zou, Y., He, Y., Zhou, K., and Hsu, C.-S. *Macromolecular Chemistry and Physics* **2010**, 211, 2555-2561.
74. Yang, J., You, J., Chen, C.-C., Hsu, W.-C., Tan, H.-R., Zhang, X. W., Hong, Z., and Yang, Y. *ACS Nano* **2011**, 5, 6210-6217.
75. Wu, F.-C., Hsu, S.-W., Cheng, H.-L., Chou, W.-Y., and Tang, F.-C. *The Journal of Physical Chemistry C* **2013**, 117, 8691-8696.
76. Sun, J., Zhu, Y., Xu, X., Lan, L., Zhang, L., Cai, P., Chen, J., Peng, J., and Cao, Y. *The Journal of Physical Chemistry C* **2012**, 116, 14188-14198.
77. Gong, W.-L., Zhong, F., Aldred, M. P., Fu, Q., Chen, T., Huang, D.-K., Shen, Y., Qiao, X.-F., Ma, D., and Zhu, M.-Q. *RSC Advances* **2012**, 2, 10821-10828.
78. Sun, J., Jiang, H.-J., Zhang, J.-L., Tao, Y., and Chen, R.-F. *New Journal of Chemistry* **2013**, 37, 977-985.
79. Chou, H.-H., Hsu, C.-Y., Hsu, Y.-C., Lin, Y.-S., Lin, J. T., and Tsai, C. *Tetrahedron* **2012**, 68, 767-773.
80. Stanislovaityte, E., Simokaitiene, J., Raisys, S., Al-Attar, H., Grazulevicius, J. V., Monkman, A. P., and Jankus, V. *Journal of Materials Chemistry C* **2013**, 1, 8209-8221.
81. Lee, J.-Y., Shin, W.-S., Haw, J.-R., and Moon, D.-K. *Journal of Materials Chemistry* **2009**, 19, 4938-4945.
82. Staniec, P. A., Parnell, A. J., Dunbar, A. D. F., Yi, H., Pearson, A. J., Wang, T., Hopkinson, P. E., Kinane, C., Dalgliesh, R. M., Donald, A. M., Ryan, A. J., Iraqi, A., Jones, R. a. L., and Lidzey, D. G. *Advanced Energy Materials* **2011**, 1, 499-504.
83. Wang, T., Pearson, A. J., Dunbar, A. D. F., Staniec, P. A., Watters, D. C., Yi, H., Ryan, A. J., Jones, R. a. L., Iraqi, A., and Lidzey, D. G. *Advanced Functional Materials* **2012**, 22, 1399-1408.
84. Moet, D. J. D., Koster, L. J. A., De Boer, B., and Blom, P. W. M. *Chem Mater* **2007**, 19, 5856-5861.
85. Masresha, T. *MSc Thesis* **2006**.
86. Mohamad, D. K., Fischereder, A., Yi, H., Cadby, A. J., Lidzey, D. G., and Iraqi, A. *Journal of Materials Chemistry* **2011**, 21, 851-862.
87. Voortman, T. P., De Gier, H. D., Havenith, R. W. A., and Chiechi, R. C. *Journal of Materials Chemistry C* **2014**, 2, 3407-3415.

88. Xie, L.-H., Yin, C.-R., Lai, W.-Y., Fan, Q.-L., and Huang, W. *Progress in Polymer Science* **2012**, 37, 1192-1264.
89. Chuen, C. C., Lai, M. H., Tsai, J. H., Wang, C. F., and Chen, W. C. *Journal of Polymer Science Part A: Polymer Chemistry* **2010**, 48, 74-81.
90. Yang, L., Tumbleston, J. R., Zhou, H., Ade, H., and You, W. *Energy & Environmental Science* **2013**, 6, 316-326.
91. Zhuang, J., Su, W., Li, W., Zhou, Y., Shen, Q., and Zhou, M. *Organic Electronics* **2012**, 13, 2210-2219.
92. Lv, J., Liu, Q., Tang, J., Perdih, F., and Kranjc, K. *Tetrahedron Letters* **2012**, 53, 5248-5252.
93. Bian, L., Zhu, E., Tang, J., Tang, W., and Zhang, F. *Progress in Polymer Science* **2012**, 37, 1292-1331.
94. Lee, W.-Y., Cheng, K.-F., Wang, T.-F., Chueh, C.-C., Chen, W.-C., Tuan, C.-S., and Lin, J.-L. *Macromolecular Chemistry and Physics* **2007**, 208, 1919-1927.
95. Yang, P.-C., Sun, J.-Y., Ma, S.-Y., Shen, Y.-M., Lin, Y.-H., Chen, C.-P., and Lin, C.-F. *Solar Energy Materials and Solar Cells* **2012**, 98, 351-356.
96. Schmid, S. A., Yim, K. H., Chang, M. H., Zheng, Z., Huck, W. T. S., Friend, R. H., Kim, J. S., and Herz, L. M. *Physical Review B* **2008**, 77, 115338.
97. Kong, F.-T., Dai, S.-Y., and Wang, K.-J. *Advances in OptoElectronics* **2007**, 2007.
98. Nguyen, L. H., Günes, S., Neugebauer, H., Sariciftci, N. S., Banishoeib, F., Henckens, A., Cleij, T., Lutsen, L., and Vanderzande, D. **2006**, 61921T-61921T.
99. Bundgaard, E. and Krebs, F. C. *Solar Energy Materials and Solar Cells* **2007**, 91, 954-985.
100. Yu, Z. G., Wu, M. W., Rao, X. S., Sun, X., and Bishop, A. R. *Journal of Physics: Condensed Matter* **1996**, 8, 8847.
101. Reyes-Reyes, M., Kim, K., and Carroll, D. L. *Applied Physics Letters* **2005**, 87, 083506-083506-3.
102. Chen, C.-P., Chan, S.-H., Chao, T.-C., Ting, C., and Ko, B.-T. *Journal of the American Chemical Society* **2008**, 130, 12828-12833.
103. Yi, H., Al-Faifi, S., Iraqi, A., Watters, D. C., Kingsley, J., and Lidzey, D. G. *Journal of Materials Chemistry* **2011**, 21, 13649-13656.
104. Wu, J.-S., Cheng, Y.-J., Dubosc, M., Hsieh, C.-H., Chang, C.-Y., and Hsu, C.-S. *Chemical Communications* **2010**, 46, 3259-3261.
105. Chen, H.-Y., Hou, J., Zhang, S., Liang, Y., Yang, G., Yang, Y., Yu, L., Wu, Y., and Li, G. *Nat Photon* **2009**, 3, 649-653.
106. Chu, T.-Y., Lu, J., Beaupré, S., Zhang, Y., Pouliot, J.-R., Wakim, S., Zhou, J., Leclerc, M., Li, Z., Ding, J., and Tao, Y. *Journal of the American Chemical Society* **2011**, 133, 4250-4253.
107. Liang, Y., Xu, Z., Xia, J., Tsai, S.-T., Wu, Y., Li, G., Ray, C., and Yu, L. *Advanced Materials* **2010**, 22, E135-E138.
108. Yamanari, T., Taima, T., Sakai, J., and Saito, K. *Solar Energy Materials and Solar Cells* **2009**, 93, 759-761.
109. Xiang, N., Liu, Y., Zhou, W., Huang, H., Guo, X., Tan, Z., Zhao, B., Shen, P., and Tan, S. *Eur Polym J* **2010**, 46, 9-9.
110. Pei, J., Wen, S., Zhou, Y., Dong, Q., Liu, Z., Zhang, J., and Tian, W. *New Journal of Chemistry* **2011**, 35, 385-393.
111. Hollenbeck, T. P. E., Siuzdak, G., and Blackledge, R. D. *Journal of Forensic Sciences* **1998**, 783-787.
112. Baghbanzadeh, M., Pilger, C., and Kappe, C. O. *The Journal of Organic Chemistry* **2011**, 76, 8138-8142.
113. Yu, D., Yang, Y., Durstock, M., Baek, J.-B., and Dai, L. *ACS Nano* **2010**, 4, 5633-5640.

114. Kim, K., Liu, J., Namboothiry, M. a. G., and Carroll, D. L. *Applied Physics Letters* **2007**, 90, 163511.
115. Chen, M., Perzon, E., Andersson, M. R., Marcinkevicius, S., Jonsson, S. K. M., Fahlman, M., and Berggren, M. *Applied Physics Letters* **2004**, 84, 3570-3572.
116. Pina, J., Burrows, H. D., and Sergio Seixas De Melo, J., *Excited state dynamics in [small pi]-conjugated polymers*, in *Photochemistry: Volume 39*2011, The Royal Society of Chemistry. p. 30-64.
117. Helgesen, M., Sondergaard, R., and Krebs, F. C. *Journal of Materials Chemistry* **2010**, 20, 36-60.
118. Biniek, L., Chochos, C. L., Leclerc, N., Hadziioannou, G., Kallitsis, J. K., Bechara, R., Leveque, P., and Heiser, T. *Journal of Materials Chemistry* **2009**, 19, 4946-4951.
119. Luo, J., Liu, Y., Shi, D., Wang, Y., Zhang, Z., Yu, J., Lei, G., Chen, Q., Li, J., Deng, X., and Zhu, W. *Dalton Transactions* **2012**, 41, 1074-1081.
120. Cai, W., Gong, X., and Cao, Y. *Solar Energy Materials and Solar Cells* **2010**, 94, 114-127.
121. Jørgensen, M., Norrman, K., and Krebs, F. C. *Solar Energy Materials and Solar Cells* **2008**, 92, 686-714.
122. Son, H. J., Carsten, B., Jung, I. H., and Yu, L. *Energy & Environmental Science* **2012**, 5, 8158-8170.
123. Lee, J. U., Jung, J. W., Jo, J. W., and Jo, W. H. *Journal of Materials Chemistry* **2012**, 22, 24265-24283.
124. Chen, L., Yang, L., Shi, M., and Chen, H. *Solar Energy Materials and Solar Cells* **2010**, 94, 2244-2250.
125. Výprachtický, D., Kmínek, I., Pokorná, V., and Cimrová, V. *Tetrahedron* **2012**, 68, 5075-5080.
126. Ji, G., Zhang, B., and Wu, Y. *Journal of Hazardous Materials* **2012**, 225–226, 1-7.
127. Brenner, T. J. K., Li, Z., and Mcneill, C. R. *The Journal of Physical Chemistry C* **2011**, 115, 24435-24435.
128. Tang, C. W. *Applied Physics Letters* **1986**, 48, 183-185.
129. Fang, Q., Xu, B., Jiang, B., Fu, H., Zhu, W., Jiang, X., and Zhang, Z. *Synthetic Metals* **2005**, 155, 206-210.
130. Brabec, C. J., Gowrisanker, S., Halls, J. J. M., Laird, D., Jia, S., and Williams, S. P. *Advanced Materials* **2010**, 22, 3839-3856.
131. Brabec, C. J. and Sariciftci, S. N. *Monatshefte für Chemie / Chemical Monthly* **2001**, 132, 421-431.
132. Chu, T.-Y., Alem, S., Verly, P. G., Wakim, S., Lu, J., Tao, Y., Beaupre, S., Leclerc, M., Belanger, F., Desilets, D., Rodman, S., Waller, D., and Gaudiana, R. *Applied Physics Letters* **2009**, 95, 063304.
133. Wlosnewski, J., Piyakulawat, P., Keawprajak, A., Saekung, C., and Asawapirom, U. *Thammasat Int. J. Sc. Tech.* **2010**, 15, 26-31.
134. Dennler, G., Scharber, M. C., Ameri, T., Denk, P., Forberich, K., Waldauf, C., and Brabec, C. J. *Advanced Materials* **2008**, 20, 579-583.
135. Paul, A. L., *Solid State Organic Solar Cells*, in *Organic Thin Films for Photonic Applications*2010, American Chemical Society. p. 185-198.
136. Topp, K., Borchert, H., Johnen, F., Tunc, A. V., Knipper, M., Von Hauff, E., Parisi, J., and Al-Shamery, K. *The Journal of Physical Chemistry A* **2009**, 114, 3981-3989.
137. Shengqiang, X., Samuel, C. P., Huaxing, Z., and Wei, Y., *Recent Progress on Highly Efficient Bulk Heterojunction Polymer Solar Cells*, in *Functional Polymer Nanocomposites for Energy Storage and Conversion*2010, American Chemical Society. p. 71-80.

138. Song, D., Cho, W., Lee, J. H., and Kang, Y. S. *The Journal of Physical Chemistry Letters* **2014**, 5, 1249-1258.
139. Pelley, J. *Environmental Science & Technology* **2005**, 39, 151A-152A.
140. Baek, M.-J., Lee, S.-H., Zong, K., and Lee, Y.-S. *Synthetic Metals* **2010**, 160, 1197-1203.
141. Chen, J. and Cao, Y. *Accounts of Chemical Research* **2009**, 42, 1709-1718.
142. Chochos, C. L. and Choulis, S. A. *Progress in Polymer Science* **2011**, 36, 1326-1414.
143. Kim, K. H., Han, Y.-K., and Jung, J. *Theoretical Chemistry Accounts* **2005**, 113, 233-237.
144. Zhang, Z.-B., Fujiki, M., Tang, H.-Z., Motonaga, M., and Torimitsu, K. *Macromolecules* **2002**, 35, 1988-1990.
145. Chi, S. H., Hales, J. M., Cozzuol, M., Ochoa, C., Fitzpatrick, M., and Perry, J. W. *Optics Exoress* **2009**, 17, 22062-22072.
146. Guo, X., Zhang, M., Huo, L., Cui, C., Wu, Y., Hou, J., and Li, Y. *Macromolecules* **2012**, 45, 6930-6937.
147. Sun, Y., Lin, B., Yang, H., and Gong, X. *Polymer* **2012**, 53, 1535-1542.
148. Fernández, G., Sánchez, L., Veldman, D., Wienk, M. M., Atienza, C., Guldi, D. M., Janssen, R. a. J., and Martín, N. *The Journal of Organic Chemistry* **2008**, 73, 3189-3196.
149. Kowalski, S., Allard, S., and Scherf, U. *ACS Macro Letters* **2012**, 1, 465-468.
150. Liang, D., Tang, S., Liu, J., Liu, J., and Kang, L. *Journal of Molecular Structure: THEOCHEM* **2009**, 908, 102-106.
151. Min, J., Peng, B., Wen, Y., Zhang, Z.-G., Zhang, M., Zhang, J., Xie, Q., Liu, Y., and Li, Y. *Synthetic Metals* **2011**, 161, 1832-1837.
152. Ding, P., Chu, C.-C., Zou, Y., Xiao, D., Pan, C., and Hsu, C.-S. *Journal of Applied Polymer Science* **2012**, 123, 99-107.
153. Bubnova, O. and Crispin, X. *Energy & Environmental Science* **2012**, 5, 9345-9362.
154. Yang, L., Zhou, H., Price, S. C., and You, W. *Journal of the American Chemical Society* **2012**, 134, 5432-5435.
155. Kamat, P. V. *The Journal of Physical Chemistry Letters* **2010**, 1, 3147-3148.
156. He, M., Li, J., Sorensen, M. L., Zhang, F., Hancock, R. R., Fong, H. H., Pozdin, V. A., Smilgies, D.-M., and Malliaras, G. G. *Journal of the American Chemical Society* **2009**, 131, 11930-11938.
157. Earmme, T., Hwang, Y.-J., Murari, N. M., Subramaniyan, S., and Jenekhe, S. A. *Journal of the American Chemical Society* **2013**, 135, 14960-14963.
158. He, F. and Yu, L. *The Journal of Physical Chemistry Letters* **2011**, 2, 3102-3113.
159. Kurniawan, M., Salim, T., Tai, K. F., Sun, S., Sie, E. J., Wu, X., Yeow, E. K. L., Huan, C. H. A., Lam, Y. M., and Sum, T. C. *The Journal of Physical Chemistry C* **2012**, 116, 18015-18022.
160. Friend, R. H., Gymer, R. W., Holmes, A. B., Burroughes, J. H., Marks, R. N., Taliani, C., Bradley, D. D. C., Santos, D. a. D., Bredas, J. L., Logdlund, M., and Salaneck, W. R. *Nature* **1999**, 397, 121-128.
161. Prim, D. and Kirsch, G. *J. Chem. Soc., Perkin Trans. 1* **1994**, 2603-2606.
162. Feast, W. J., Tsibouklis, J., Pouwer, K. L., Groenendaal, L., and Meijer, E. W. *Polymer* **1996**, 37, 5017-5047.
163. Ding, J., Zhang, B., Lü, J., Xie, Z., Wang, L., Jing, X., and Wang, F. *Advanced Materials* **2009**, 21, 4983-4986.
164. Henssler, J. T., Zhang, X., and Matzger, A. J. *The Journal of Organic Chemistry* **2009**, 74, 9112-9119.

165. Pelkey, E. T., *Chapter 5.1 Five-membered ring systems: Thiophenes & Se, Te analogs*, in *Progress in Heterocyclic Chemistry*, Gordon, W.G. and Thomas, L.G., Editors. 2002, Elsevier. p. 90-113.
166. Rahman, M., Kumar, P., Park, D.-S., and Shim, Y.-B. *Sensors* **2008**, 8, 118-141.
167. Lee, W. S., Park, J. H., Baek, M.-J., Lee, Y.-S., Lee, S.-H., Pyo, M., and Zong, K. *Synthetic Metals* **2010**, 160, 1368-1371.
168. Bronstein, H., Chen, Z., Ashraf, R. S., Zhang, W., Du, J., Durrant, J. R., Shakya Tuladhar, P., Song, K., Watkins, S. E., Geerts, Y., Wienk, M. M., Janssen, R. a. J., Anthopoulos, T., Sirringhaus, H., Heeney, M., and Mcculloch, I. *Journal of the American Chemical Society* **2011**, 133, 3272-3275.
169. Yamamoto, T., Imai, T., Shimada, M., Suzuki, N., Maeno, M., Konoshima, S., Fujii, T., Uehara, K., Nagashima, T., Funahashi, A., and Fujisawa, N. *Physical Review Letters* **1980**, 45, 716-719.
170. Amir, E. and Rozen, S. *Angewandte Chemie International Edition* **2005**, 44, 7374-7378.
171. Corriu, R. J. P. and Masse, J. P. *Journal of the Chemical Society, Chemical Communications* **1972**, 144a-144a.
172. Tamao, K., Sumitani, K., and Kumada, M. *Journal of the American Chemical Society* **1972**, 94, 4374-4376.
173. Adrio, J. and Carretero, J. C. *ChemCatChem* **2010**, 2, 1384-1386.
174. Frey, J., Bond, A. D., and Holmes, A. B. *Chemical Communications* **2002**, 0, 2424-2425.
175. Rutherford, D. R., Stille, J. K., Elliott, C. M., and Reichert, V. R. *Macromolecules* **1992**, 25, 2294-2306.
176. Miyaura, N., Yamada, K., and Suzuki, A. *Tetrahedron Letters* **1979**, 20, 3437-3440.
177. Facchetti, A., Vaccaro, L., and Marrocchi, A. *Angewandte Chemie International Edition* **2012**, 51, 3520-3523.
178. Duan, C., Chen, K.-S., Huang, F., Yip, H.-L., Liu, S., Zhang, J., Jen, A. K. Y., and Cao, Y. *Chemistry of Materials* **2010**, 22, 6444-6452.
179. Lee, W., Cho, N., Kwon, J., Ko, J., and Hong, J.-I. *Chemistry – An Asian Journal* **2012**, 7, 343-350.
180. Kim, J., Yun, M. H., Anant, P., Cho, S., Jacob, J., Kim, J. Y., and Yang, C. *Chemistry – A European Journal* **2011**, 17, 14681-14688.
181. Zhang, Z.-G., Liu, Y.-L., Yang, Y., Hou, K., Peng, B., Zhao, G., Zhang, M., Guo, X., Kang, E.-T., and Li, Y. *Macromolecules* **2010**, 43, 9376-9383.
182. Kun, H., Yi, H., Johnson, R. G., and Iraqi, A. *Polymers for Advanced Technologies* **2008**, 19, 299-307.
183. Bugge, A. *Acta Chemica Scandinavicaes* **1968**, 22, 63-69.
184. Dhanabalan, A., Van Duren, J. K. J., Van Hal, P. A., Van Dongen, J. L. J., and Janssen, R. a. J. *Advanced Functional Materials* **2001**, 11, 255-262.
185. Svensson, M., Zhang, F., Inganas, O., and Andersson, M. R. *Synthetic Metals* **2003**, 135-136, 137-138.
186. Svensson, M., Zhang, F., Veenstra, S. C., Verhees, W. J. H., Hummelen, J. C., Kroon, J. M., Inganäs, O., and Andersson, M. R. *Advanced Materials* **2003**, 15, 988-991.
187. Bulman, M. J. *Tetrahedron* **1969**, 25, 1433-1439.
188. Pickup, D. F., Yi, H., Kun, H., Iraqi, A., Stevenson, M., and Lidzey, D. G. *Thin Solid Films* **2009**, 517, 2840-2844.
189. Pickup, D., Yi, H., and Iraqi, A. *Journal of Materials Science* **2009**, 44, 3172-3178.
190. Gritzner, G. *Pure and Applied Chemistry* **1990**, 62, 1839-58.
191. Blouin, N. and Leclerc, M. *Accounts of Chemical Research* **2008**, 41, 1110-1119.
192. Dierschke, F., Grimsdale, A. C., and Müllen, K. *Synthesis* **2003**, 2003, 2470-2472.

193. Yamato, T., Hideshima, C., Suehiro, K., Tashiro, M., Prakash, G. K. S., and Olah, G. A. *J. Org. Chem.* **1991**, 56, 6248-6250.
194. Sonntag, M. and Strohriegl, P. *Chemistry of Materials* **2004**, 16, 4736-4742.
195. Fuller, L., Iddon, B., and Smith, K. *Journal of the Chemical Society, Perkin Transactions 1* **1997**, 3465-3470.
196. Henssler, J. T. and Matzger, A. J. *Organic Letters* **2009**, 11, 3144-3147.
197. Gooßen, L. J., Thiel, W. R., Rodríguez, N., Linder, C., and Melzer, B. *Advanced Synthesis & Catalysis* **2007**, 349, 2241-2246.
198. Liu, P., Wu, Y., Pan, H., Li, Y., Gardner, S., Ong, B. S., and Zhu, S. *Chemistry of Materials* **2009**, 21, 2727-2732.
199. Helgesen, M., Gevorgyan, S. A., Krebs, F. C., and Janssen, R. a. J. *Chemistry of Materials* **2009**, 21, 4669-4675.
200. Ku, S.-Y., Liman, C. D., Burke, D. J., Treat, N. D., Cochran, J. E., Amir, E., Perez, L. A., Chabinyc, M. L., and Hawker, C. J. *Macromolecules* **2011**, 44, 9533-9538.
201. Jo, J., Chi, C., Höger, S., Wegner, G., and Yoon, D. Y. *Chemistry – A European Journal* **2004**, 10, 2681-2688.
202. Ishiyama, T., Murata, M., and Miyaura, N. *The Journal of Organic Chemistry* **1995**, 60, 7508-7510.
203. Choy, N., Russell, K. C., Alvarez, J. C., and Fider, A. *Tetrahedron Letters* **2000**, 41, 1515-1518.
204. Parham, W. E., Wynberg, H. *Org. Syn.* **1955**, 35, 51-52.
205. Torun, L., Liu, S., Madras, B. K., and Meltzer, P. C. *Tetrahedron Letters* **2006**, 47, 599-603.
206. Bouffard, J. and Swager, T. M. *Macromolecules* **2008**, 41, 5559-5562.
207. Abd El Haleem, S. M. and Ateya, B. G. *Journal of Electroanalytical Chemistry and Interfacial Electrochemistry* **1981**, 117, 309-319.
208. Fujinami, Y., Kuwabara, J., Lu, W., Hayashi, H., and Kanbara, T. *ACS Macro Letters* **2011**, 1, 67-70.
209. Chang, S.-W., Waters, H., Kettle, J., Kuo, Z.-R., Li, C.-H., Yu, C.-Y., and Horie, M. *Macromolecular Rapid Communications* **2012**, n/a-n/a.
210. Lee, J. Y., Heo, S. W., Choi, H., Kwon, Y. J., Haw, J. R., and Moon, D. K. *Solar Energy Materials and Solar Cells* **2009**, 93, 1932-1938.
211. Gledhill, S. E., Scott, B., and Gregg, B. A. *J. Mater. Res.* **2005**, 20, 3167-3179.